UNIVERSITAT POLITÈCNICA DE VALÈNCIA

Departamento de Máquinas y Motores Térmicos

Doctoral Thesis

Study of Organic Rankine Cycles for Waste Heat Recovery in Transportation Vehicles

---

Presented by: MS. LUCÍA ROYO PASCUAL
Supervised by: DR. VICENTE DOLZ RUIZ

in fulfillement of the requisites for the degree of

Doctor of Philosophy

Valencia, May 2017

Ph.D. Thesis

Study of Organic Rankine Cycles (ORC) for Waste Heat Recovery in Transportation Vehicles

AUTHORS

Presented by: Ms. Lucía Royo Pascual
Supervised by: Dr. Vicente Dolz Ruiz

PhD ASSESSORS

Dr. Vincent Lemort
Dr. Apostolos Pesiridis
Dr. Francisco Javier Royo Herrer

DEFENSE COMMITTEE

Chairman: Dr. José Ramón Serrano Cruz
Secretary: Dr. Francisco Vera García
Member: Dr. Vincent Lemort

Valencia, May 2017

Study of Organic Rankine Cycles for Waste Heat Recovery in Transportation Vehicles

Lucía Royo Pascual

Abstract

Regulations for ICE-based transportation in the EU seek carbon dioxide emissions lower than 95 g CO_2/km by 2020. In order to fulfill these limits, improvements in vehicle fuel consumption have to be achieved. One of the main losses of ICEs happens in the exhaust line. Internal combustion engines transform chemical energy into mechanical energy through combustion; however, only about 15–32% of this energy is effectively used to produce work, while most of the fuel energy is wasted through exhaust gases and coolant. Therefore, these sources can be exploited to improve the overall efficiency of the engine. Between these sources, exhaust gases show the largest potential of Waste Heat Recovery (WHR) due to its high level of exergy. Regarding WHR technologies, Rankine cycles are considered as the most promising candidates for improving Internal Combustion Engines. However, the implementation of this technology in modern passenger cars requires additional features to achieve a compact integration and controllability in the engine. While industrial applications typically operates in steady state operating points, there is a huge challenge taking into account its impact in the engine during typical daily driving profiles.

This thesis contributes to the knowledge and characterization of an Organic Rankine Cycle coupled with an Internal Combustion Engine using ethanol as working fluid and a swash-plate expander as expansion machine. The main objective of this research work is to obtain and quantify the potential of Organic Rankine Cycles for the use of residual energy in automotive engines. To do this, an experimental ORC test bench was designed and built at CMT (Polytechnic University of Valencia), which can be coupled to different types of automotive combustion engines. Using these results, an estimation of the main variables of the cycle was obtained both in stationary and transient operating points. A potential of increasing ICE mechanical efficiency up to 3.7% could be reached at points of high load installing an ORC in a conventional turbocharged gasoline engine. Regarding transient conditions, a slightly simple and robust control based on adaptive PIDs, allows the control of the ORC in realistic driving profiles. High loads and hot conditions should be the starting ideal conditions to test and validate the control of the ORC in order to achieve high exhaust temperatures that justify the feasibility of the system.

In order to deepen in the viability and characteristics of this particular application, some theoretical studies were done. A 1D model was developed using LMS Imagine.Lab Amesim platform. A potential improvement of 2.5% in fuel conversion efficiency was obtained at the high operating points as a direct consequence of the 23.5 g/kWh reduction in bsfc. To conclude, a thermo-economic study was developed taking into account the main elements of the installation costs and a minimum Specific Investment Cost value of 2030 €/kW was obtained. Moreover, an exergetic study showed that a total amount of 3.75 kW, 36.5% of exergy destruction rate, could be lowered in the forthcoming years, taking account the maximum efficiencies considering technical restrictions of the cycle components.

Resumen

Las normativas anticontaminantes para el transporte propulsado por motores de combustión interna alternativos en la Unión Europea muestran límites de emisión menores a 95 g CO_2/km para el año 2020. Con el fin de cumplir estos límites, deberán ser realizadas mejoras en el consumo de combustible en los vehículos. Una de las principales pérdidas en los Motores de Combustión Interna Alternativos (MCIA) ocurre en la línea de escape. Los MCIA transforman la energía química en energía mecánica a través de la combustión; sin embargo, únicamente el 15-32% de esta energía es eficazmente usada para producir trabajo, mientras que la mayor parte es desperdiciada a través de los gases de escape y el agua de refrigeración del motor. Por ello, estas fuentes de energía pueden ser utilizadas para mejorar la eficiencia global del vehículo. De estas fuentes, los gases de escape muestran un potencial mayor de recuperación de energía residual debido a su mayor contenido exergético. De todos los tipos de Sistemas de Recuperación de Energía Residual, los Ciclos Rankine son considerados como los candidatos más prometedores para mejorar la eficiencia de los MCIA. Sin embargo, la implementación de esta tecnología en los vehículos de pasajeros modernos requiere nuevas características para conseguir una integración compacta y una buena controlabilidad del motor. Mientras que las aplicaciones industriales normalmente operan en puntos de operación estacionarios, en el caso de los vehículos con MCIA existen importantes retos teniendo en cuenta su impacto en el modo de conducción cotidianos.

Esta Tesis contribuye al conocimiento y caracterización de un Ciclo Rankine Orgánico acoplado con un Motor de Combustión Interna Alternativo utilizando etanol como fluido de trabajo y un expansor tipo Swash-plate como máquina expansora. El principal objetivo de este trabajo de investigación es obtener y cuantificar el potencial de los Ciclos Rankine Orgánicos (ORC) para la recuperación de la energía residual en motores de automoción. Para ello, una instalación experimental con un Ciclo Rankine Orgánico fue diseñada y construida en el Instituto Universitario “CMT - Motores Térmicos" (Universidad Politécnica de Valencia), que puede ser acoplada a diferentes tipos de motores de combustión interna alternativos. Usando esta instalación, una estimación de las principales variables del ciclo fue obtenida tanto en puntos estacionarios como en transitorios. Un potencial de mejora en torno a un 3.7 % puede ser alcanzada en puntos de alta carga instalando un ORC en un motor gasolina turboalimentado. Respecto a las condiciones transitorias, un control sencillo y robusto basado en PIDs adaptativos permite el control del ORC en perfiles de conducción reales. Las condiciones ideales para testear y validar el control del ORC son alta carga en el motor comenzando con el motor en caliente para conseguir altas temperaturas en el escape que justifiquen la viabilidad de estos ciclos.

Para tratar de profundizar en la viabilidad y características de esta aplicación particular, diversos estudios teóricos fueron realizados. Un modelo 1D fue desarrollado usando el software LMS Imagine.Lab Amesim. Un potencial de mejora en torno a un 2.5% en el rendimiento efectivo del

motor fue obtenido en condiciones transitorias en los puntos de alta carga como una consecuencia directa de la reducción de 23.5 g/kWh del consumo específico. Para concluir, un estudio termo-económico fue desarrollado teniendo en cuenta los costes de los principales elementos de la instalación y un valor mínimo de 2030 €/kW fue obtenido en el parámetro de Coste Específico de inversión. Además, el estudio exergético muestra que un total de 3.75 kW, 36.5 % de la tasa de destrucción total de exergía, podría ser reducida en los años futuros, teniendo en cuenta las máximas eficiencias considerando restricciones técnicas en los componentes del ciclo.

Resum

Les normatives anticontaminants per al transport propulsat per motors de combustió interna alternatius a la Unió Europea mostren límits d'emissió menors a 95 g·CO2/km per a l'any 2020. Per tal d'acomplir aquests límits, s'hauran de realitzar millores al consum de combustible dels vehicles. Una de les principals pèrdues als Motors de combustió interna alternatius (MCIA) ocorre a la línia d'escapament. Els MCIA transformen l'energia química en energia mecànica a través de la combustió; però, únicament el 15-32% d'aquesta energia és usada per produir treball, mentre que la major part és desaprofitada a través dels gasos d'escapament i l'aigua de refrigeració del motor. Per això, aquestes fonts d'energia poden ser utilitzades per millorar l'eficiència global del vehicle. Considerant aquestes dues fonts d'energia, els gasos d'escapament mostren un potencial major de recuperació d'energia residual debut al seu major contingut exergètic. De tots els tipus de Sistemes de Recuperació d'Energia Residual, els Cicles Rankine són considerats com els candidats més prometedors per millorar l'eficiència dels MCIA. No obstant, la implementació d'aquesta tecnologia en els vehicles de passatgers moderns requereix un desenvolupament addicional per aconseguir una integració compacta i una bona controlabilitat del motor. Mentre que les aplicacions industrials normalment operen en punts d'operació estacionaris, en el cas dels vehicles amb MCIA hi han importants reptes a solucionar tenint en compte el funcionament en condicions variables del motor i el seu impacte en la manera de conducció quotidiana del usuari.

Aquesta Tesi contribueix al coneixement i caracterització d'un Cicle Rankine Orgànic (ORC) acoblat amb un motor de combustió interna alternatiu (MCIA) utilitzant etanol com a fluid de treball i un expansor tipus Swash-plate com a màquina expansora. El principal objectiu d'aquest treball de recerca és obtenir i quantificar el potencial dels ORCs per a la recuperació de l'energia residual en motors d'automoció. Per aconseguir-ho, una instal·lació experimental amb un ORC va ser dissenyada i construïda a l'Institut "CMT- Motores Térmicos" (Universitat Politècnica de València). Esta instal·lació pot ser acoblada a diferents tipus de MCIAs. Mitjançant assajos experimentals en aquesta instal·lació, una estimació de les principals variables del cicle va ser obtinguda tant en punts estacionaris com en punts transitoris. Un potencial de millora al voltant d'un 3.7% pot ser aconseguida en punts d'alta càrrega instal·lant un ORC acoblat a un motor gasolina turboalimentat. Pel que fa a les condicions transitòries, un control senzill i robust basat en PIDs adaptatius permet el control del ORC en perfils de conducció reals. Les condicions ideals per a testejar i validar el control de l'ORC són alta càrrega al motor començant amb el motor en calent per aconseguir altes temperatures d'escapament que justifiquen la viabilitat d'aquests cicles.

Per tractar d'aprofundir en la viabilitat i característiques d'aquesta aplicació particular, diversos estudis teòrics van ser realitzats. Un model 1D va ser desenvolupat usant el programari LMS Imagine.Lab Amesim. Un potencial de millora al voltant d'un 2.5% en el rendiment efectiu del

motor va ser obtingut en condicions transitòries en els punts d'alta càrrega com una conseqüència directa de la reducció de 23.5 g/kWh al consum específic. Per concloure, un estudi termo-econòmic va ser desenvolupat tenint en compte els costos dels principals elements de la instal·lació i un valor mínim de 2030 €/kW va ser obtingut en el paràmetre del Cost Específic d'Inversió. A més, l'estudi exergètic mostra que un total de 3.75 kW, 36.5% de la taxa de destrucció total d'exergia, podria ser recuperat en un pròxim, considerant restriccions tècniques en els components del cicle i tenint en compte les màximes eficiències que es poden aconseguir.

List of publications

The following papers form the basis of this thesis have been published:

- "Experimental and thermodynamic analysis of a bottoming Organic Rankine Cycle (ORC) of gasoline engine using swash-plate expander" by Galindo, Ruiz, Dolz, Royo-Pascual, Haller, Nicolas, and Glavatskaya [1].
- "Study of a volumetric expander suitable for waste heat recovery from an automotive IC engine using an ORC with ethanol" by Galindo, Dolz, Royo-Pascual, Haller, and Melis [2].
- "Advanced exergy analysis for a bottoming organic rankine cycle coupled to an internal combustion engine" by Galindo, Ruiz, Dolz, and Royo-Pascual [3].
- "Dynamic tests and adaptive control of a bottoming organic Rankine cycle of IC engine using swash-plate expander" by Torregrosa, Galindo, Dolz, Royo-Pascual, Haller, and Melis [4].
- "Modeling and Experimental Validation of a Volumetric Expander Suitable for Waste Heat Recovery from an Automotive Internal Combustion Engine Using an Organic Rankine" by Galindo, Dolz, Royo-Pascual, Haller, and Melis [5].
- "Multi-objective optimization of a bottoming Organic Rankine Cycle (ORC) of gasoline engine using swash-plate expander" by Galindo, Climent, Dolz, and Royo-Pascual [6].

Division of work between authors

These publications have been produced in collaboration with other researchers, being the author signatures in order of seniority. The author of this Thesis helped with the experimental measurements development, results post-processing and developed the models presented here. Methodologies and results discussions were conducted in collaboration with my supervisor, Assist. Prof. Dolz, as well as with the rest of co-authors.

Other publications

The following list presents other publications in which the author of this thesis was involved during the researches leading to the present work. Although not directly present in this document, they have provided a deeper insight into Waste Heat recovery.

- “Thermodynamic analysis of an absorption refrigeration system used to cool down the intake air in an Internal Combustion Engine” by Novella, Dolz, Martín, and Royo-Pascual [7].

To my family,
with love and affection.

Work hard. Have fun. And make it happen.
(Rafael Nadal)

Acknowledgements

First of all, my most sincere acknowledgement to the whole CMT-Motores Térmicos team for giving me the opportunity of being part of it and to the “Apoyo para la investigación y Desarrollo (PAID)” grant for doctoral studies (FPI S2 2015 1067). All the students, technicians, researchers, professors and the rest of the staff have contributed in one way or another to the successful completion of my research, and I truly thank them for that.

Specially, I would like to thank my fellow grad students (and the ones that have successfully obtained their PhD title during these years), specially Miguel Andrés López, Jaime Sánchez, Luis Miguel García-Cuevas, Yuly Tatiana Rodríguez and Petar Kleut.

Also, my special acknowledgements are for Raúl Luján and Rafael Carrascosa for their contribution in the experimental process and their patience with my testing demands.

My sincere gratitude to professor José Galindo, who has done all the best to guide me during my Thesis. And, above all, I wish to express my sincere gratitude to my thesis supervisor, professor Vicente Dolz, for his support, advices, guidance, valuable comments and suggestions who had helped me with the completion and success of this Thesis and also because of his care and shelter in doing this research.

Besides my supervisor, I would also like to thank people from Siemens PLM Software, where I spent three months working in the Thermal Team with Aldrik Brizard and his team. I learnt a lot of things during this period in Lyon.

Also, I feel emotionally in debt with my school friends (particularly Paloma Sampedro and Beatriz Paúl), my "CPS" friends and "Somaeneros" friends for their conversations during long hours and advices, which motivates me and give me strength to follow with this Thesis.

Finally, I would like to thank my whole family, specially my mother and my father, for supporting and encouraging me throughout this experience, and give me good advices during my whole life.

And, of course, I owe all to my partner, David, for his patience and love through all these years of hard work and for the understanding that the PhD was a great opportunity to improve my career, although we have to sacrifice long time of being together.

Contents

List of Figures

List of Tables

Nomenclature

$\dot{E}$	Exergy [kW]
$\dot{W}$	Power [kW]
$\dot{m}$	Mass flow rate [kg/s]
$\dot{V}$	Volumetric flow [m^3/s]
A	Area [m^2]
B	Cylinder bore [m]
$bsfc$	Brake Specific Fuel consumption [g/kWh]
C	Cost [€]
C_p	Specific heat at constant pressure [kJ/kgK]
C_v	Specific heat at constant volume [kJ/kgK]
D	Total displacement of the expander [m^3]
d	Diameter [m]
D_h	Hydraulic diameter [m]
e	Specific exergy [kJ/kg]
f	Friction factor [-]
f_c	Fuel consumption [kg/h]
G	Mass flow velocity [kg/m^2s]
h	Specific Enthalpy [kJ/kg]
h_r	Hours
I_l	Current [A]
K	Thermal conductivity [W/mK]
L	Length [m]
N	Speed [rpm]
n	Number of cylinders
N_{pl}	Number of plates
P	Power [kW]
P_e	Electric power [kW]
P_i	State Point i
Q_{fuel}	Total fuel power [kW]
r	Discount rate [%]
R_{swash}	Radius of the swash-plate [m]
S	Saving [kg/s]
s	Specific entropy [kJ/kgK]
SH	Superheating [°C]
T	Temperature [°C]
t	Number of periods [-]

U	Heat transfer coefficient [W/m^{2}K]
U_l	Voltage [V]
V	Volume covered by the piston [m^3]
v	Specific volume [m^3/kg]
V_d	Dead volume [m^3]
Vol	Reservoir volume [l]
W	Work [J]
Wi	Width [m]
X	Displacement covered by the piston [m]
X_m	Average gas mass fraction
X_{tt}	Martinelli parameter [-]
y	Exergy destruction ratio
ASHRAE	American Society of Heating, Refrigeration, and Air-Conditioning Engineers
BDC	Bottom Dead Center
CFC	Chlorofluorocarbon
CMT	Centro de Motores Térmicos
E	Experimental
EGR	Exhaust Gas Recirculation
FS	Full Scale
GA	Genetic Algorithm
GHG	Green House Gases
GWP	Global warming potential
HCFC	Hydrochlorofluorocarbon
HDV	Heavy Duty Vehicle
HFC	Hydrofluorocarbons
ICE	Internal Combustion Engine
Kpf	Kinetic power flow
LDV	Light Duty Vehicle
LMTD	Logarithmic Mean Temperature Difference
M	Modelled
MDV	Medium Duty Vehicle
NEDC	New European Driving Cycle
NFPA	National Fire Protection Association
NPV	Net Present Value
ODP	Ozone depletion potential
ORC	Organic Rankine Cycle
P-V	Pressure-Volume
PB	Payback
PID	Proportional Integral Derivative Controller
SFC	Specific Fuel Consumption
SIC	Specific Investment Cost
SM	Steady Map
TCC	Total Component Costs
TDC	Top Dead Center
TEG	Thermoelectric generator

TOPSIS Technique for Order Preference by Similarity to an Ideal Solution

TPF Two Phase Flow

Tpf Thermal power flow

VC Volume Coefficient

WHR Waste Heat Recovery

WLTC Worldwide harmonized Light vehicles Test Procedures

Greek Symbols

Δ Increment

η Efficiency

μ Dynamic viscosity [Pa s]

ϕ Power factor

ρ Density [kg/m^3]

τ Torque [Nm]

ε Exegetic efficiency

Overbar and others

AV Avoidable

EN Endogenous

EX Exogenous

UN Unavoidable

Subscripts

$1-8$ State points

A Zone A

ave Average

B Zone B

b Boiler

C Zone C

$cond$ Condenser

cp Components

cs Consumption

cv Convective boiling

cyl Cylinder

D Refers to exergy destruction (internal exergy loss)

e Effective

EG Exhaust Gases

eng Engine

eq Equivalent

ET Ethanol

exp Expander

fg Liquid to gas

$fuel$ Fuel

GE Gasoline Engine

in Inlet

ind Indicated

iso Isentropic

k Kth component

L Refers to exergy loss (external exergy loss)

l Lower temperature level in the cycle

lab Labour

m	Average
mec	Mechanical
NcB	Nucleate Boiling
$ORC-GE$	Organic Rankine Cycle-Gasoline Engine
out	Outlet
P	Product
$ploss$	Pressure loss
pp	Pinch point
$pump$	Pump
rr	Rolling resistance
sat	Saturation conditions
sh	Shaft
sp	Set point
st	Steady
th	Thermal
tot	Refers to the total system
tp	Two Phase
u	Higher temperature level in the cycle
v	Vapour
ve	Vehicle
vol	Volumetric
W	Water
$wall$	Wall

CHAPTER 1

Introduction

Contents

Figures

1.1 Background

Due to increasingly environmental restrictions and rising fuel prices, higher efficiencies are imposed upon our actual powertrains [8]. Turbocharging technology have CO_2 emissions reduction potential of downsizing engines up to 12% for diesel engines and 14% for gasoline engines [9]. The objective of the turbocharger is to increase engine torque and the specific power output with no or slight bsfc reductions less than 1% [10]. Indeed, a turbocharged diesel engine still rejects 35–40% of input energy through the exhaust gas [11]. Therefore, WHR applications can also be found in turbocharged engines. Moreover, new future homologation cycles (such as Worldwide harmonized Light vehicles Test Procedures), will focus on CO_2 emissions, requiring higher driveline efficiencies. In this type of cycles, different driving situations on the WLTC are already covered by the hybrid technology: stop and start mode when the vehicle is stopped (13% of the time) and regenerative breaking system when the vehicle is slowed down (42% of the time). However, the exhaust heat recovery may offer a solution for the remaining time of the cycle (45%) when the engine is loaded. New advanced engine technologies [12], such as, electrical and mechanical turbocompounding, thermoelectrical materials (TEG), Heat-to-heat and organic Rankine cycles (ORC) are expected to grow strongly in the coming years [9]. They are considered as a promising source of improvement in modern internal combustion engines (ICE).

Among these technologies, Organic Rankine Cycles promise high potential [13], therefore, this technology is most widely used in small-scale energy production and industrial applications, i.e. geothermal, biomass, solar thermal power and waste heat recovery (WHR) on industrial processes.

The Rankine cycle is named after William John Macquorn Rankine (1820-1872), a Scottish engineer and professor at Glasgow University. In its simplest configuration this cycle consists of a pump, an evaporator, a condenser and an expander. Since its introduction, it has produced more energy than any other cycle and is widely used in power generation plants generally utilizing water as working fluid. Many fluids have been proposed and studied to be applied in Rankine cycles in order to suit the different heat sources. In the 1960's the first organic Rankine cycle was developed Harry Zvi Tabor and Lucien Bronicki [14]. With this improvement Rankine cycles are able to achieve higher efficiencies with lower grade heat sources avoiding extreme pressures.

However, the implementation of this technology in modern passenger cars requires additional features to achieve a compact integration and controllability in the engine [15]. While industrial applications typically operate in steady state conditions, there is a huge challenge taking into account its impact in the engine during typical daily driving profiles [16].

1.2 Motivation

Waste Heat Recovery (WHR) has proved to be a path to increase the overall efficiency of automotive vehicles. Recovery potential of up to 7% are showed in several works in the literature, however most of them are theoretical estimations, and only in some of them there are results from prototypes fed not with actual engine exhaust gases but steady flow generated in an auxiliary gas tank. This fact raises doubts on the system feasibility, especially regarding the expander as there are no commercial expanders for this application.

This thesis contributes to the knowledge and characterization of an Organic Rankine Cycle coupled with an Internal Combustion Engine using ethanol as working fluid and a swash-plate expander as expansion machine. The thesis is based on experimental and modelling works carried out on a mock-up coupled to a gasoline engine using swash-plate as expander.

The expander efficiency is one of the main drawbacks for this system to be advantageous over other systems. Most investigations are focused on achieving a relatively high expander efficiency to increase the output to weight ratio. This study contributes to the analysis and development of Organic Rankine Cycles in internal combustion engines, characterizing the conditions that maximize the expander efficiency.

This work is part of a research project named “Evaluation of bottoming cycles in IC engines to recover waste heat energies” funded by a National Project of the Spanish Government with reference TRA2013-46408-R and by two international private companies, called Valeo Systèmes Thermiques and Exoès. In this work several tests were performed to evaluate ORC global performance and viability of its implementation in the vehicle.

1.3 Objectives

The main objective of this research work is to obtain and quantify the potential of Organic Rankine Cycles for the use of residual energy in automotive engines. The purpose of this system is to achieve an improvement in the overall efficiency of the automotive engine and a subsequent reduction in fuel consumption and pollutant emissions. Therefore, the main objective can be divided in two partial objectives:

Experimental evaluation of the cycle In order to quantify the potential of this system, an experimental ORC test bench was designed and built at CMT - Motores Térmicos, which can be coupled to different types of automotive combustion engines. Using these results, an estimation of the main variables of

the cycle were obtained. In order to fulfil this partial objective two types of tests were performed:

- Stationary tests: To estimate the global impact that an ORC cycle has on ICE performance in different engine operating points.
- Transient tests: To understand the transient behaviour of the cycle and validate the ORC control at realistic dynamic engine conditions.

Theoretical evaluation of the cycle To deepen the viability and characteristics of this particular application, some theoretical studies are presented. Four types of theoretical studies were developed:

- Simulation model: To help the understanding of those physical phenomena difficult to observe by means of experimentation. To estimate the behaviour of the cycle without the need of experimental tests under dangerous operating conditions to the installation and / or people.
- Thermodynamic studies: To understand the operating conditions and cycle limitations and the main working fluids for this type of application.
- Economic studies: To obtain estimations regarding the main economic parameters (Payback, Net Present Value, Specific Investment Cost) and sizing parameters (Volume Coefficient and A_{tot}) in Organic Rankine Cycles for WHR applications.
- ORC impact on the engine: To acquire a quantitative value of improvement in engine performance at real driving conditions.

1.4 Method employed

The methodology used in this work has been firstly focused on the literature review of Organic Rankine Cycles to recover Waste Heat Energy for vehicle applications. The main heat sources, operating conditions, cycle components and working fluids are reviewed in Chapter 2. Subsequently, the methodology is split, as in the objectives, into two different parts: the former based on an experimental basis and the latter based on a theoretical one.

The aim of the experimental methodology presented in Chapter 3 is to obtain an experimental understanding of Organic Rankine Cycles as a path to improve ICE efficiency. Two main tasks are performed:

- Using the information obtained from the literature review, an experimental mock-up is built to evaluate the feasibility of such cycles. The experimental mock-up is an innovative facility, which is able to control all

the variables and measure pressures, temperatures and mass flows in all the cycle components.

- Both steady-state and transient experimental tests are performed. The results analysis are focused on the Pressure-Volume diagram computation. An estimation of the indicated work and the performance of the cycle under different engine operating points are presented. These tasks enable to fulfil the first objective described in the previous section.

The aim of the theoretical methodology is focused on the understanding of the thermodynamic characteristics of the Organic Rankine Cycles in vehicle applications. Four main tasks will be performed:

- Develop a 1D simulation expander model and the Organic Rankine Cycle to achieve a deep understanding of all the variables of the system that cannot be measured by experimental testing. Amesim software was used to simulate both models. This will be presented in Chapter 4.

- Analyse the theoretical features of the cycle. For that, a study of the different available working fluids will be presented in the first part of Chapter 5. Results of 6 working fluids will be compared in terms of expander power, pinch point and volume flow rate. The second part of Chapter 5 will be focused on an advanced exergy analysis to understand the main exergy losses of the cycle by means of a mathematical model.

- Develop a methodology to optimize a multiobjective problem using a Genetic Algorithm taking into account economic and sizing parameters. This will be presented in the first part Chapter 6.

- Analyse the impact that the ORC has on the engine by taking into account the drawbacks of this system in the engine performance (increase of back pressure and increase of weight) and the advantages of this system (increase of net power output of the system). This will be presented in the last part of Chapter 6.

1.5 References

[8] F. Payri, J. M. Luján, C. Guardiola, and B. Pla. "A Challenging Future for the IC Engine: New Technologies and the Control Role". In: *Oil & Gas Science and Technology – Revue d'IFP Energies nouvelles* 70 (2014), pp. 15–30. ISSN: 1294-4475. DOI: 10.2516/ogst/2014002. URL: http://ogst.ifpenergiesnouvelles.fr/10.2516/ogst/2014002 (cit. on p. 2).

[9] R. Berger. "Trends in ICE-Technologies Besides Electrification , improvements in conventional powertrain technologies will play a major role looking forward". In: *Automotive megatrends*. 2013, pp. 1–13 (cit. on p. 2).

[10] J. B. Heywood. *Internal combustion engine fundamentals*. 1988, pp. 1–930. ISBN: 007028637X. URL: http://books.google.es/books/about/Internal{_}combustion{_}engine{_}fundamentals.html?id=u9FSAAAAMAAJ{\&}pgis=1 (cit. on pp. 2, 15, 126).

[11] S. N. Hossain and S. Bari. "Waste heat recovery from the exhaust of a diesel generator using Rankine Cycle". In: *Energy Conversion and Management* 75 (2013), pp. 141–151. ISSN: 01968904. DOI: 10.1016/j.enconman.2013.06.009. URL: http://dx.doi.org/10.1016/j.enconman.2013.06.009 (cit. on p. 2).

[12] R. Saidur, M. Rezaei, W. K. Muzammil, M. H. Hassan, S. Paria, and M. Hasanuzzaman. "Technologies to recover exhaust heat from internal combustion engines". In: *Renewable and Sustainable Energy Reviews* 16.8 (2012), pp. 5649–5659. ISSN: 13640321. DOI: 10.1016/j.rser.2012.05.018. URL: http://dx.doi.org/10.1016/j.rser.2012.05.018 (cit. on p. 2).

[13] M. Bianchi and A. De Pascale. "Bottoming cycles for electric energy generation: Parametric investigation of available and innovative solutions for the exploitation of low and medium temperature heat sources". In: *Applied Energy* 88.5 (2011), pp. 1500–1509. ISSN: 03062619. DOI: 10.1016/j.apenergy.2010.11.013. URL: http://linkinghub.elsevier.com/retrieve/pii/S0306261910004769 (cit. on p. 2).

[14] L. Bronicki and Z. Harry. *Vapor turbines*. US Patent 3,040,528. 1962. URL: https://www.google.com/patents/US3040528 (cit. on p. 2).

[15] A. Hernandez, A. Desideri, C. Ionescu, and S. Quoilin. "Towards the optimal operation of an Organic Rankine Cycle unit by means of model predictive control". In: *3rd International Seminar on ORC Power Systems* (2015), pp. 1–10 (cit. on p. 2).

[16] M. C. Robertson, A. W. Costall, P. J. Newton, and R. F. Martinez-botas. “Transient duty cycle analysis for mobile Organic Rankine Cycle applications”. In: *3rd International Seminar on ORC Power Systems* (2015), pp. 1–10 (cit. on p. 2).

CHAPTER 2

Literature review

Contents

Figures

2.1 Current energetic situation

Transportation represents approximately 25% of world energy demand (61.5% of all the used oil each year), so that, an improvement in efficiency could result in an important saving in the amount of energy consumed [17]. Despite global alerts regarding to the use of fossil fuels, it might be said that global energy demand in following years is projected to be 50-60% more than current levels [18], thus energy efficiency and vehicle performance improvements could play an essential role in reducing GHG emissions. According to the Eurostat [19], the GHG emission from transportation has increased up to 22.2 % from the 14.9 % of 1990, which is shown in Figure 2.1.

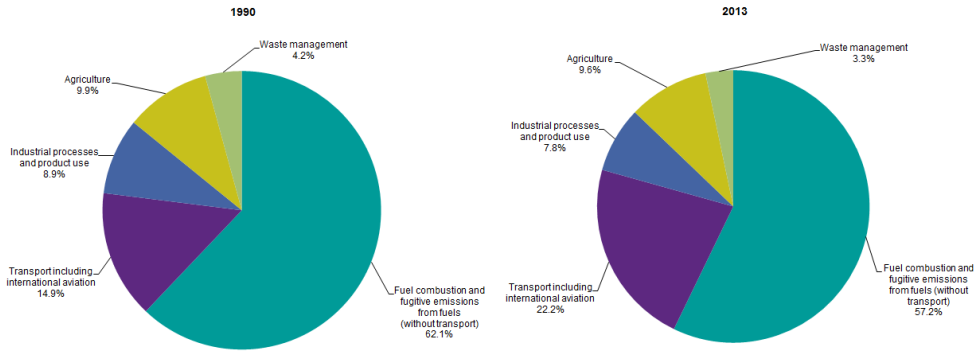

Figure 2.1: Greenhouse gas (CO_2, CH_4 and N_2O) emissions by economic activity, EU-27, 1990 and 2013 [19]

Upcoming CO_2 regulations will result in introducing different technologies, increasing the overall powertrain efficiency without raising GHG emissions. While some hybrid systems, such as start-stop mode and regenerative breaking system, try to optimize the vehicle when it is stopped and slowed down respectively, it will not be enough to reach future CO_2 demands, especially when the engine is loaded. According to the International Council on Clean Transportation (Figure 2.2), the target for CO_2 emissions in passenger cars was reduced until 2007 an average of 1 % per year, however from 2008 more restrictive targets were imposed with an average of 4 % per year. In 2020 the target of CO_2 emissions in passenger cars and light-commercial vehicles will be reduced from 2012 up to 28% and 18%, reaching values of 95 g/km and 147 g/km respectively. Therefore, waste heat recovery technologies seem to assume an essential role in the CO_2 reductions of the forthcoming decade [20].

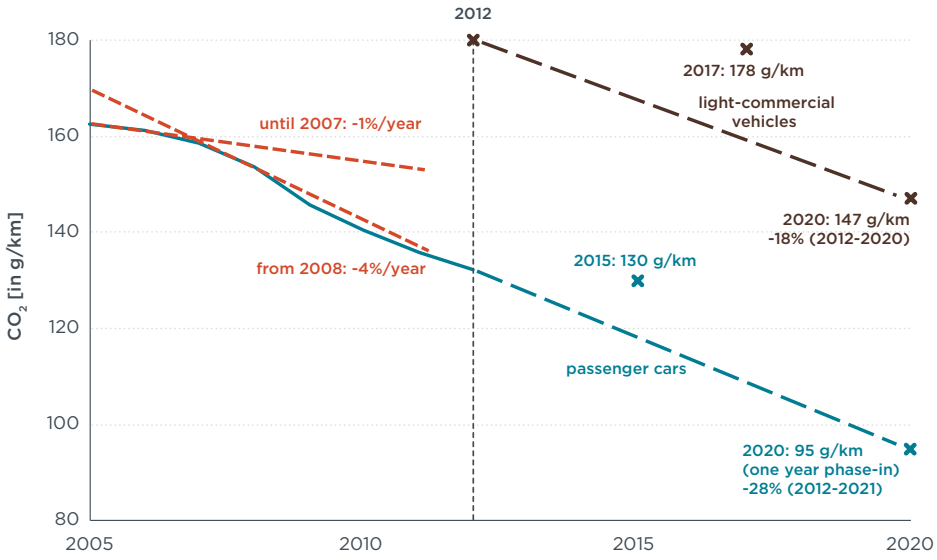

Figure 2.2: Historical development and future targets for CO_2 emission levels of new passenger cars and light-commercial vehicles in the EU [21]

Recent findings of climate change on the potentially catastrophic impacts on ecosystems and biodiversity in Europe confirm the ongoing importance of developing new technologies which can improve energy efficiency. As shown in Figure 2.3, the global annual mean temperature has already increased by 0.6 °C since 1850. According to Eurostat [22], the mean temperature rise will have an effect on the weather severity (such as coastal erosion, flooding due to sea level rise, storms and heat waves), as well as on human and animal health.

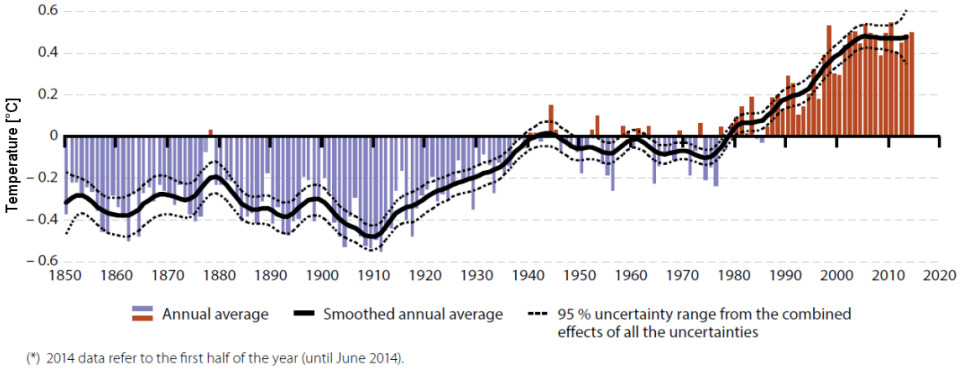

Figure 2.3: Global annual mean temperature deviations, 1850–2014 [22]

Since the ICE invention, there have been some attempts to increase the effective power using Waste Heat Recovery sources. Nowadays, different WHR technologies applied in ICE are under research in order to generate electrical or mechanical energy for the vehicle or to heat specific elements during its warm-up process. According to Figure 2.4, these technologies can be classified in thermal (Tpf) and kinetic power flow (Kpf):

- Heat to heat (Tpf), this technique consists of installing a heat exchanger in the exhaust line in order to heat up critical engine areas during its warm up process. It is relatively easy to implement, however it has only potential during cold starting processes [23].

- Heat to cool (Tpf), in this case, the heat energy released from the exhaust gas is used to cool the intake air of an IC engine. Consequently, the engine efficiency and reduction of pollutant emissions improve by means of tri-thermal cooling systems (ejector cycles [24, 25] and absorption cycles [26, 7]).

- Rankine cycle (Tpf), where the working fluid is vaporized using the exhaust gases thermal energy from an evaporator. Then, this vapour is expanded and mechanical power is produced. Particularly, Organic Rankine Cycles, based on the use of organic fluids, are especially suited to recover energy from exhaust gases at low temperatures [1, 27].

- Other thermodynamic cycles (Tpf), as Ericsson, Brayton and Stirling. These technologies are less mature than the ORC and they are focused on reducing the ORC complexity and generate an additional mechanical power [28].

- Thermal electricity (Tpf), which consist of thermoelectric materials installed in the exhaust pipe. It generates electricity by Seebeck effect, providing at least some of the powertrain electric power requirements. Nowadays, these materials are expensive and low-efficient, so it might be a promising technology when these materials will be improved [29, 30].

- Electrical turbocompounding (Kpf), which consists of an electric generator coupled to a turbocharger. The generator extracts surplus power from the turbine, and the excess produced electricity is used to run a motor coupled to the engine crankshaft [31, 32].

- Mechanical turbocompounding (Kpf), in this case, the engine is equipped with an additional power turbine. This turbine is placed in the exhaust line and is mechanically coupled to the engine crankshaft via a gearbox [31, 32].

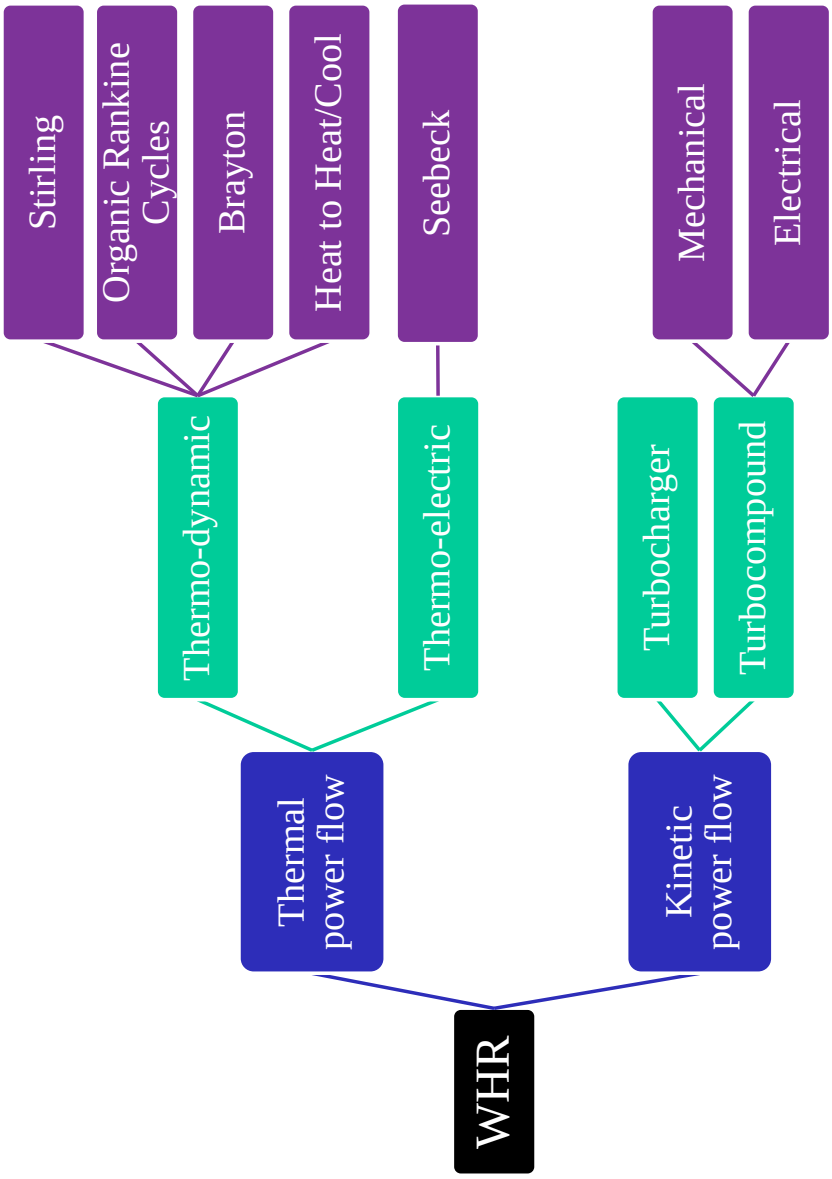

Figure 2.4: Waste Heat Recovery Systems

2.2 Energetic evaluation of Internal Combustion Engines

Internal combustion engines transform chemical energy into mechanical energy through combustion; however, only about 15-35% of this energy is effectively used to produce work [10]. The remaining 60 to 70% of the fuel energy is rejected as waste heat to the environment through exhaust gases (22 to 46%) and the radiator (18 to 42%) [33], which evacuates the heat from the Charge Air Cooler (CAC), Exhaust Gas Recirculation (EGR) and cooling loop.

Exhaust gases. A large part of energy (and exergy) is contained in exhaust gas in the form of heat. Duparchy et al. [34] indicated that exhaust gases represent the greatest recovery potential due to large differences in the thermodynamic properties of the two fluids and lower mass flow rates in comparison to other ICE heat sources (cooling loop). Chammas et al. [35] tested a 1.4 liter Spark Ignition internal combustion engine, achieving, as result, exhaust waste heat ranges from 4.6 to 120 kW depending on operating conditions (25 % load and 1500 rpm and 100% and 4500 rpm) using a reference temperature of 20 °C. From these results, the calculated maximum work of an Ideal Rankine Cycle varied from 1.7 to 45 kW. Similar results were found by Macián et al. [36] and Dolz et al. [37].

Exhaust Gas Recirculation. Most modern diesel engines recirculate exhaust gases back into the combustion chamber in order to reduce the amount of NOx liberated during the combustion process. The EGR flow rate depends on the employed strategy used by the engine manufacturer to reduce nitrogen oxides emissions NOx. The temperature is around 100 °C higher than in the exhaust line but the recirculated mass flow rate is lower by more than 70% compared to the exhaust gas mass flow rate. In order to minimize the recirculation impact in the volumetric efficiency of the engine, these gases should be cooled down by a heat exchanger. According to Teng et al. [38], high EGR rates strategies can be employed considering the EGR a very attractive heat source for WHR. Hountalas et al. [39] studied the EGR contribution in a diesel engine. An engine speed of 1700 rpm and 4 loads (25-50-75 and 100 %) were studied, concluding that the EGR implies approximately the 15-20 % of the global waste heat energy produced by an engine. Despite of this, there is a current trend to increase the efficiency of the NOx aftertreatment system. As a result, high EGR rates (that reduce the engine efficiency) are becoming less interesting to manufacturers [40].

Charge Air Cooling. Due to the turbocharger implementation in ICEs, the intake manifold air temperature increases, specially in high load engine operating points. The main turbocharger objective is to increase the air density at the inlet of the cylinder, in order to rise the mass flow with the same air-fuel ratio. Therefore, the engine power output increases although the displacement is maintained constant. It means that the efficiency increases due to the reduction in the engine friction losses. The compression causes a temperature increase in the intake air, therefore the CAC is needed to reduce the temperature and maintain a high air density value. However, due to the low thermal power and temperature level, this source cannot be used as a the main WHRS heat input. It can only be used as additional power to the one recovered from other heat sources in the engine [37, 41]. Teng et al. [42] assessed that this percentage can be up to 10 % of the global waste heat power in an engine.

Cooling loop (engine block and lubricating system). Coolant heat is one of the primary targets of thermal management. The amount of energy cooled down in the lubricating system and in the engine block represents a high waste energy percentage, specially in medium and low engine vehicle speeds (low engine speed and load) [43]. However, this source shows a much lower recovery potential in terms of exergy compared to the other sources available in the engine. Coolant water exits the engine block at about 110 °C and is cooled down in the radiator to about 80 °C. The high mass flow and low temperature strategy makes heat transfer almost impossible as the temperatures are too low and the conversion efficiency is not very high [44]. Chammas et al. [45] obtained similar results, in the 1500 rpm and 25 % load, the available exhaust gases power percentage was 21% compared to 42 % in the cooling line. By contrast, in the engine operating point of 4500 rpm and 18 %, the available exhaust gas power was 44 % compared to the 18 % of cooling water.

2.3 Rankine Cycles in IC engines

The first study concerning Rankine Cycles to an automotive application was reported in 1970s [46], and since then huge work has been done to investigate the feasibility of applying this technology to vehicles. In ICE applications, size and weight restrictions are greater than in industrial installations, which greatly hinders their adaptation. On the other hand, thermal power available and the level of temperature in the engines for WHR is lower than in industrial processes. Therefore, the optimized Rankine cycle configuration, cycle components (expander machine and boiler) and the working fluid characteristics can be different from the options considered in other applications.

2.3.1 Working fluid

2.3.1.1 Characteristics of the working fluid

The working fluid selection is one of the most important parameters in order to optimize the ORC behaviour in ICEs. No universal optimal fluid is indicated since the choice is highly dependent on the target application. The main optimal working fluid characteristics should be:

1. Slope of the saturation vapor curve: A working fluid can be classified as a dry, isotropic or wet fluid depending on the slope of the saturation vapor curve on a T–s diagram (dT/ds). The inverse of the slope (ds/dT), is used to express how dry or wet a fluid is. Wet fluids have a negative vapour slope line and produce droplets at the end of the expansion. The vapour must be superheated at the expander inlet to avoid internal damages. Therefore, isentropic or dry fluids were suggested for Organic Rankine Cycle applications. However, if the fluid is too dry, the expanded vapour will leave the turbine with substantial superheat, which increase the cooling requirements in the condenser.

2. Density: High vapour density is of key importance, especially for fluids showing a very low condensing pressure. Low density leads to a higher volume flow rate. Moreover, pressure drop in the heat exchangers increases and the size of the expander will therefore increase. This fact has a non-negligible impact on the cost of the system [47].

3. Viscosity: Low viscosity in both phases (liquid and vapor) is required to maintain low friction losses and high heat transfer coefficients in the heat exchangers.

4. Conductivity: High conductivity is required to obtain a high heat transfer coefficient in the heat exchangers.

5. Heat of vaporization: A fluid with high latent heat will absorb more energy from the source in the evaporator. Thus, the required flow rate, the size of the facility and the pump consumption will be reduced.

6. Acceptable evaporating pressures: High pressures usually result in higher cycle complexity and investment costs.

7. Condensing gauge pressure: Low pressure should be higher than the atmospheric pressure in order to avoid air infiltration in the cycle.

8. Stability temperature: The stability temperature should be as high as possible in order to avoid chemical deteriorations and decomposition at high temperatures. Unlike water, the maximum heat source temperature in organic fluids is limited by the chemical stability of the working fluid [48].

9. Critical temperature: It is the temperature at and above which vapour of the substance cannot be liquefied, no matter how much pressure is applied. In subcritical cycles, the evaporation temperature is limited by the critical temperature, and the fluids can be divided into three categories based on the critical temperature [49]:

    - High temperature fluids: Critical temperatures are above 250 °C.
    - Medium temperature fluids: Critical temperatures are in the range 150–250 °C.
    - Low temperature fluids: The critical temperatures are below 150 °C.

10. Freezing point: Fluid melting point should be lower than the lowest ambient temperature through the year to avoid the working fluid freezing.

11. Other thermodynamic properties: Both the ORC efficiency and the output expander power should be as high as possible for a given input heat source and heat sink power. This performance depends on a high number of interdependent thermodynamic properties of the working fluid: Critical point, acentric factor, molecular complexity, etc. It is not easy to define a thermodynamic optimum for each specific property independently.

    - Molecular mass: A fluid with high molecular mass shows small enthalpy drops in expansion but also a low speed of sound. This helps the machine design and results in compact and relatively cheap machines.
    - Molecular complexity: The higher the molecular complexity is, the higher the volume ratio across the expansion is for a fixed pressure ratio.

12. Safety level: Safety includes two main parameters: the toxicity and the flammability. The ASHRAE Standard 34 [50] classifies refrigerants in safety groups and can be used for the fluid evaluation.

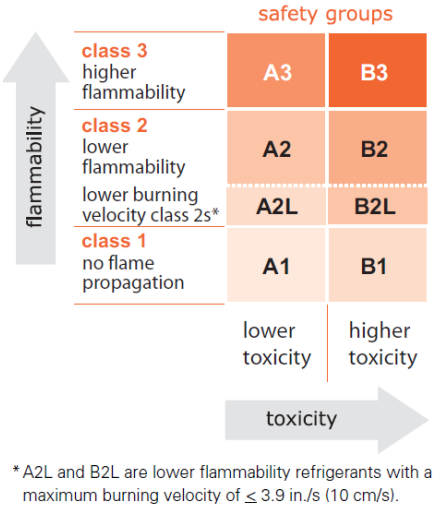

Figure 2.5: ASHRAE Standard 34-2013 safety classifications [51]

13. Ozone Depleting Potential (ODP): The ozone depleting potential is measured with comparison to the R11 ODP value, set to the unity. The current refrigerants ODP value (defined by US Environmental Protection Agency) is null or very close to zero. The refrigerants with high ODP levels have progressively been phased out by the Montreal Protocol [52].

14. Greenhouse Warming Potential (GWP): GWP (defined by US Environmental Protection Agency) is measured with comparison to the CO_2 GWP value, set to the unity. Due to the new F-gas regulation of the European Union applied from 1st January 2015 this limit will be reduced until 150 at 2030 [53].

15. Good availability and low cost: Fluids already used in refrigeration or in the chemical industry are easier to obtain and more cost-effective.

Figure 2.6 shows a summary with the main desirable characteristics of the working fluid.

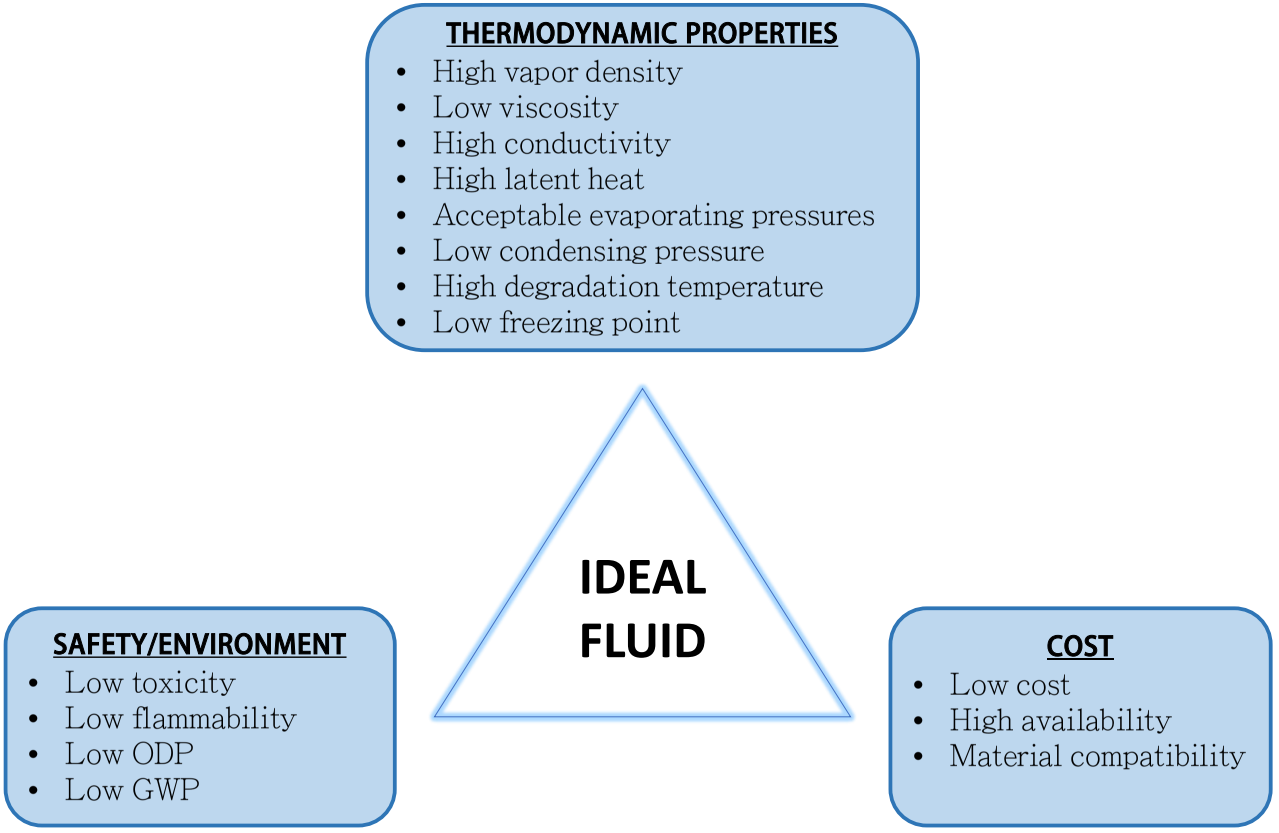

Figure 2.6: Desirable characteristics of the working fluid

2.3.1.2 Selection of working fluids

Trying to optimize the cycle, both in thermodynamic and economic aspects, different working fluids have been used in automotive applications. There are an array of potential working fluids, inorganics refrigerants (water, CO_2 and ammonia), synthetic refrigerants (CFCs, HCFs, HCFCs, PFCs, HCFOs and HFOs), ethers, amines, siloxanes, hydrocarbons, alcohols, and mixtures.

Water is a very convenient fluid because the low cost and high availability, non-toxicity, non-flammability, environmentally friendly, chemical stability and low viscosity [54] characteristics. However, it is not the ideal working fluid in terms of recovering low heat sources, particularly waste heat recovery in ICEs, due to the high operating boiling pressures, low condensing pressures, excessively high vaporization heat and high triple-point temperature. For this reason, using water as the working fluid will result in larger systems, increasing weight and cost of the global vehicle [35]. Ammonia (R717) is widely used as a refrigerant in industrial systems due to its efficiency. However, it is both flammable and toxic, which is deemed less suitable for ICE applications [55]. CO_2 (R744) is a good fluid in terms of flammability and toxicity properties, however it is not efficient enough and is normally used in transcritical systems. Boccardi et al. [56] tested a commercial cooling application using CO_2.

Synthetic refrigerants have been identified as suitable candidates for recovering moderate to low temperature (between 120 °C and 150 °C) waste energy [38, 57, 58, 59, 60, 61]. Between synthetic refrigerants Chlorofluorocarbons (CFC) and perfluorocarbons (PFC) are no longer used since the Montreal Protocol regulation [52] due to its high level of ODP and GWP. Hydrochlorofluorocarbons (HCFC) and hydrofluorocarbons (HFC) were used as substitutes of CFC, because its lower level of ODP, however the index of GWP was still high. Moreover, due to the new F-gas regulation in the EU, the total amount of fluorinated refrigerants (HFC and HCFC) that can be sold in the EU will be gradually phased down up to two thirds of 2010 emissions by 2030 [53]. Hydrochlorofluoroolefin (HCFO) and Hydrofluoroolefine (HFO), among which R1233zde [62] and R1234ze [63] are highlighted respectively, are considered as the main candidates to substitute the previous refrigerants in the forthcoming years for low-grade heat applications.

Ethers present another concern around reactivity and stability; amines have been shown to have major toxicological effects, therefore these components were not considered by Juhasz et al. [64] in the scope of good working fluids.

Siloxanes (or siliconic oils) were proposed by Fernández et al. [65] as compounds that have the desired characteristics that can reach high working temperatures (between 250 °C and 300 °C). They are promising working fluids in high-temperature applications, specially, in waste heat recovery from industrial processes. Their characteristics are low/non toxicity, limited flammability, good material compatibility, good thermal stability and good thermodynamic properties with respect to the cycle design [66]. However, according to Preißinger [67] the film temperature at the heat exchanger surface, hot-spots within the heat exchanger and the failure mode have to be kept in mind.

Hydrocarbons presents good thermal performance (with low levels of GWP and ODP) and non-toxic characteristics. Therefore, they are possible candidates for this type of application. However, they are classified as A3 class according to ASHRAE Standard 34. Song et al. [68] showed good thermal performance in high-temperature ORCs for engine waste heat recovery (greater than 250 °C).

Several authors consider ethanol as a promising fluid due to its good features in the vehicle application temperature range (100-450 °C). Ethanol has been taken into account for its environmental, thermo-physical (high expansion ratios, condensation temperatures at atmospheric pressure and low freezing point) and cost features properties. Although ethanol is positively evaluated taking into account previous characteristics, it has been classified as serious hazard by NFPA due to its high flammability. Seher et. al [69] concluded that ethanol is one of the most favourable solutions using a piston machine fo high temperature applications (greater than 250 °C) and thermal power between 100 kW and 300 kW. Gibble et. al [70] selected ethanol as the best working fluid for a successful ORC in a HD truck.

Zeotropic ethanol and water mixtures have been considered by Zhang et al. [71] and Andersson et al. [72] in order to reduce irreversibilities in the heat exchangers. Mixtures of hydrocarbons and non-inflammable refrigerants are proposed by Shu et al. [73] to reduce the flammability and GWP level of hydrocarbons and extend its application range. According to Zhao [74], 5-15% improvement in the thermal efficiency might be achieved using an appropriately selected binary-mixture working fluid in comparison to the pure working fluid with a heat source temperature below 120 °C.

Supercritical cycles have been considered by Teng et al. [75]. Due to the supercritical state of the working fluid, the high-cost evaporator will be reduced and it can be replaced by a regular heat exchanger [76]. Moreover, the supercritical cycles can potentially achieve better thermodynamic performance than subcritical cycles [77]. By contrast, there is a huge trade-off between the

expansion ratio, the weight and the performance of the expander machines in these type of cycles.

2.3.2 Cycle Components

2.3.2.1 Expander machine

The expander is the component that have a greater impact on the overall efficiency and feasibility of the system. This is due to the relatively low efficiency of the expander prototypes (around 40-70% [1]) compared to other elements that constitute the Rankine cycle. In the case of the pump, its performance has a small effect on the global Rankine efficiency. Moreover, expander isentropic efficiency cannot be easily improved. This remains one of the main challenges in order to improve the cycle power output and therefore to become more attractive to engine manufacturers.

The expander output can be mechanical or electrical depending on the waste heat recovery system objective. The expander shaft can be directly connected to the engine drive belt in the case of volumetric expanders with a clutch, to avoid power losses when the ORC cycle power output is too low. Moreover, this system is preferred by truck manufacturers because it can be used all the time and not only at particular times. The main disadvantage of this configuration is the imposed expander speed because this speed is directly related with the engine speed by a fixed ratio and is not necessarily the optimal speed for maximizing cycle efficiency. In the case of electricity generation, the turbines can be coupled to an alternator, used to recharge the batteries or supply auxiliary equipments such as the air conditioning, thus making it a practical solution to Hybrid Vehicles [78]. It should be noted that current vehicle alternators show a quite low efficiency (about 50 to 60%), which reduces the ORC output power. Regarding the pump, it can be directly connected to the drive belt, to the expander shaft, or to an electrical motor. In the latter case, the working fluid flow rate can be independently controlled, which makes the regulation of such a system much easier.

Many publications evaluate and test different types of expanders including volumetric expanders (scroll, screw and rotary vane piston) and turbines (radial and axial). Other types of expander have been tested or analysed but offered even lower efficiencies and were discarded as an alternative to the ones here discussed.

In the following paragraphs several expanders are examined to highlight the advantages and drawbacks of each design type and to understand were each state of the art stands.

Volumetric Expanders. Volumetric expanders are characterized by a built-in volume ratio, which corresponds to the volumetric expansion of an internal pocket. In this pocket, the working fluid is expanded. Therefore, it is obtained effective work that could be harnessed to improve ICE mechanical efficiency [79]. The volumetric expansion ratio, defined as the ratio of the discharge volume to the swept volume, should fit into the actual working fluid expansion ratio in order to avoid under-expansion and over-expansion losses [80].

Displacement expanders run at lower rotational speeds, which involve less cost-intensive technologies than turbines [81]. Moreover, expander speed range is similar to the engine one, which is considered one of the main advantages regarding adaptability to actual vehicles. Lower flow rates and higher expansion ratios could be reached, making displacement expanders the main technology for recovering waste heat from low temperature sources and low expander power in vehicle applications. Some examples of these expanders are:

- **Scroll expander.** Expanders with this geometry are discussed and tested in several articles and publications [82, 83, 84] supposedly offering efficiencies close to positive displacement expanders. This type of expander has advantages over other machines such as low rotational speeds, having no valves and robustness. The reduced number of moving parts grants this type of expander reliability and low wear. Mechanical efficiency is relatively low because of mechanical losses in the bearings, crank mechanisms as well as friction between fixed and orbiting scrolls. Internal leakages are characteristic of this type of expander [85], which reduces the volumetric efficiency achievable. This effect combined with the expected low isentropic efficiency yield a low global efficiency. However, scroll expanders designed specifically to this type of applications are not commercially available. So, prototypes are usually scroll compressors working as expanders [86, 87].

- **Screw expander.** Screw expanders operate by inletting the working fluid on the intake side, trapping the fluid between the blades and the housing as it moves forward, which expands and rotates the screws on the way to the exhaust side. The fluid is then expelled through the exhaust. This type of expander is a good solution for heavy industrial systems. For automotive vehicles, screw expanders are turned down because of their size, weight and power.

- **Piston expander.** The reciprocating-type expander seems to be considered more appropriate for combining mechanical energy output directly to the crankshaft, in particular for on-road vehicle applications where the condition for waste heat is variable, because of its flexibility [88]. This type of expanders are preferred because they are suitable for higher pressure ratios comparing to scroll, screw and rotary vane expanders. These higher pressure ratios imply a better efficiency of the global ORC. They have high resistance to water droplets, tolerate high working fluid pressures and work well under large volumetric expansion ratios. The drawbacks are the friction losses at higher pressures and possible sealing problems on the piston contact with the cylinder wall [89]. Reciprocating machines are considered by Glavatskaya et al. [90] as the most promising technology for a waste heat recovery applications. Between reciprocating expanders, crank drives are often used in high power applications, despite the vibrations problems. By contrast, swash-plate expanders are increasingly taking into account due to its versatility, compactness, robustness, good specific power and lower vibrations.

Turbines. Turbines are typically chosen when the packaging of the waste-heat recovery system is the most important issue. Despite of that, the efficiency of turbines drops under off-design operating conditions, and small drops in the expanded vapor can erode the turbine blades due to its high speed [76]. This speed varies between 30000-120000 rpm [91]. Therefore, turbines present huge coupling challenges because of the difference between engine and turbine speed. Moreover, its highly dynamic behaviour during most of the time increases the complexity of the control.

According to Sauret [92] axial turbines handle higher flow rates than radial turbines, but radial turbines achieve higher pressure ratios. In summary, for small-scale applications (lower than 10 kW), turbines should rotate at very high speeds in order to maintain optimal performance. Single-stage turbines have low pressure ratios, therefore the expander mass flow rate to obtain a fix output power increases. Impulse turbines (Laval turbine) can work under higher expansion rates. Considering an expansion ratio smaller than 50, they can achieve efficiencies higher than 80% with single stage only [89]. They are precision machines that are expensive. The solution to round the low pressure ratio problem is to select multiple-stage turbines, which increases even more their cost, size and weight.

Table 2.1: Advantages and drawbacks of the expander machines in ORC applications

Type of expander	Manufacturers	Advantages	Drawback
Scroll	Sanden [JP]	High robustness	Poor compactness
		Low Cost	Lubrication issues
		Few moving parts	High leakages
		High reliability	Low capacity
		Low rotary speed	Low efficiency
Screw	Eaton [US]	High robustness	Adopted in RC plants
		High off-design efficiency	Seal to prevent leakage
		Low rotary speed	Lubrication issues
		Compact	Efficiency
Piston	Amovis & Voith [DE]	High robustness	Many moving parts
		Large built-in volume ratio	Heavy weight
		High achievable T and P	Valves and torque impulse
	Exoès [FR]	Low Cost	Lubrication issues
		Low rotary speed	
Turbine	Barber Nichols [US]	Compact	Erosion with droplets
		Light weight	Design and fabrication
	Bosch [DE]	High Efficiency	High cost
		Mature manufacturability	Low off-design efficiency

2.3.2.2 Heat exchangers

Several heat exchanger technologies can be found, however, most of them are still prototypes in the automotive application (due to its high pressure range, compactness and working fluids). They are divided in two main categories: Plate-Heat and Shell-Tubes heat exchangers.

The heat exchanger (boiler and condenser) dimensions and costs depend on the thermal sources characteristics: type of fluid (liquid, gas and vapour), temperature, mass flow rate, density and flow direction. Some of the desirable characteristics are: low pressure drops, small mass, small volume, high heat transfer efficiency and low cost. The heat exchanger dimensions are directly related to the mass flow rates in the installation. Thus, higher mass flow rates require large pipes and flow passages in order to avoid excessive pressure drop. Operating pressures affect the plate (or tube) thickness and thus the heat exchanger mass.

Shell and tubes heat exchangers are used for a wide range of operating conditions, however they are not commonly found in small-scale applications due to the higher size and weight compared to other technologies. Despite of that, some prototypes are presented in automotive applications, i.e. Thesys [93]. Plate heat exchangers are used in the vast majority of the systems, particularly with low or medium temperature heat sources. In addition, this technology is preferred when both compactness and low pressure drop are the main requirements of the system. This heat exchanger type was used by Haller et al. [94] in an ORC mock-up.

2.3.3 Experimental studies

Recovery potential cuts in brake specific fuel consumption and emissions of up to 5% [95] are showed in several works in the literature, however most of them are theoretical estimations, and only in some of them there are results from prototypes fed not with actual engine exhaust gases but steady flow generated in an auxiliary gas tank. Table 2.2 shows a summary of the main experimental results using ORCs in automotive applications.

Table 2.2: Summary of main experimental tests in ORC cycles in automotive applications

Expander type	Researcher	Heat Sources	Application	Working fluid	P_{source} (kW)	P_{exp} (kW)	$\eta_{Rankine}$ (%)	η_{iso} (%)
Scroll	Oomori [96]	CW [1]	Passenger car	R123	12.5	0.4	3.2%	58%
	Kosmadakis [97]	EH [2]	Truck engine	R404a	46	3.2	6.9%	85%
Screw	Zhang [71]	EG [3]	Truck engine	R123	160	10.4	6.5%	57.9 %
Vane-cell	Freymann [98]	EG + CW	SI engine	Water - HT [5]	52	9	10%	No data
				Ethanol - LT [6]	35			No data
Piston expander	Endo [99]	EG	SI engine	Water	30.8	4	13%	10 %
	Daccord [100]	EG	SI engine	Ethanol	No data	3.6	No data	65%
	Galindo [1]	EG	SI engine	Ethanol	30	1.8	6.1%	38.5%
	Seher [69]	EG + EGR [4]	Truck engine	Water	275	14	5.1%	65%
	Latz [101]	EGR	Truck engine	Water	38	1.5	3.9%	10%
Impulse Turbine	Freymann [102]	EG + CW	SI engine	Water	27	2	7.4%	40%
	Cipollone [103]	EG	Truck engine	R245fa	55	2.8	4%	48%
Radial Turbine	Seher [69]	EG + EGR	Truck engine	Water	209	9	4.3%	48.4%
	Park [104]	EG + EGR	Truck engine	Ethanol	55	9.1	16.5%	No data
	Guillaume [105]	EH	Truck engine	R1233zd	85	2.8	3.3%	32%
				R245fa	88	2.5	2.8%	31%

[1] Cooling Water [2] Electric Heater [3] Exhaust gases [4] Exhaust Gas Recirculation [5] High Temperature [6] Low Temperature

2.4 Summary

A deep literature review has been done, focusing on Organic Rankine Cycles for automotive applications. In these publications, the optimization of Rankine Cycles has been done considering the following points:

- Cycle configuration
- Operating conditions of the cycle
- Working fluid
- Expander machine and boiler

Regarding the working fluid, water was considered as the preferred fluid due to its low cost and high availability, non-toxicity, non-flammability, environmentally friendly, chemical stability and low viscosity. However, it is not the ideal working fluid in terms of recovering low heat sources, particularly waste heat recovery in ICEs, due to the high operating boiling pressures, low condensing pressures, high heat of vaporization, high triple-point temperature and negative temperature-entropy slope. Synthetic refrigerants have been identified as suitable candidates for recovering moderate to low temperature waste energy. However, due to the forecoming regulations regarding low ODP and GWP, only Hydrochlorofluoroolefin (HCFO) and Hydrofluoroolefine (HFO) will be available. By contrast, several authors consider ethanol as a promising fluid due to its good features in the vehicle application temperature range (100-450 °C). Ethanol has been taken into account for its environmental, thermo-physical properties (high expansion ratios, condensation temperatures at atmospheric pressure and low freezing point) and cost features. However, the main ethanol drawback is related with flammability.

Regarding the expander technology, there are two main types of expanders, turbines and volumetric expanders. The expander is one of the main challenges in this type of cycles due to the low efficiency of this component compared to other elements that constitute the Rankine cycle. Experimental tests have been done using both type of expanders, with similar results regarding isentropic efficiency of the machine in the operating points tested.

Regarding the cycle configuration, the exhaust gases represent the greater recovery potential. The use of other engine heat sources (Exhaust Gas Recirculation, Charge Air Cooling and Cooling loop in the engine block and lubricating system) increase the thermal power recovered by the cycle, however, this type of installations are more complex and heavier.

To sum up, there is not optimal configuration of the cycle, working fluid, expander technology for automotive applications because the ideal cycle depends on the boundary conditions defined in the case study and the objectives of the ORC system (steady or transient, coupled to the engine or coupled to an alternator,...).

2.5 References

[1] J. Galindo, S. Ruiz, V. Dolz, L. Royo-Pascual, R. Haller, B. Nicolas, and Y. Glavatskaya. "Experimental and thermodynamic analysis of a bottoming Organic Rankine Cycle (ORC) of gasoline engine using swash-plate expander". In: *Energy Conversion and Management* 103 (2015), pp. 519–532. ISSN: 01968904. DOI: 10.1016/j.enconman.2015.06.085. URL: http://linkinghub.elsevier.com/retrieve/pii/S0196890415006470 (cit. on pp. vii, 13, 23, 28, 115, 116, 181).

[7] R. Novella, V. Dolz, J. Martín, and L. Royo-Pascual. "Thermodynamic analysis of an absorption refrigeration system used to cool down the intake air in an Internal Combustion Engine". In: *Applied Thermal Engineering* 111 (2017), pp. 257–270. ISSN: 13594311. DOI: 10.1016/j.applthermaleng.2016.09.084. URL: http://linkinghub.elsevier.com/retrieve/pii/S1359431116316921 (cit. on pp. viii, 13).

[10] J. B. Heywood. *Internal combustion engine fundamentals*. 1988, pp. 1–930. ISBN: 007028637X. URL: http://books.google.es/books/about/Internal{_}combustion{_}engine{_}fundamentals.html?id=u9FSAAAAMAAJ{\&}pgis=1 (cit. on pp. 2, 15, 126).

[17] J. P. Rodrigue, C. Comtois, and B. Slack. *The Geography of Transport Systems*. 2006, p. 297 (cit. on p. 11).

[18] Holditch, Stephen. "Factors That Will Influence Oil and Gas Supply and Demand in the 21st Century". In: *MRS Bulletin* 33 (2010), pp. 317–323 (cit. on p. 11).

[19] Eurostat. *Energy, transport and environment indicators*. 2007. ISBN: 978-92-79-07044-0. DOI: 10.2785/547816 (cit. on p. 11).

[20] T. A. Horst, W. Tegethoff, P. Eilts, and J. Koehler. "Prediction of dynamic Rankine Cycle waste heat recovery performance and fuel saving potential in passenger car applications considering interactions with vehicles' energy management". In: *Energy Conversion and Management* 78 (2014), pp. 438–451. ISSN: 01968904. DOI: 10.1016/j.enconman.2013.10.074. URL: http://linkinghub.elsevier.com/retrieve/pii/S0196890413007097 (cit. on p. 11).

[21] P. Mock. "EU CO2 standards for passenger cars and light-commercial vehicles". In: *Policy update* January (2014). URL: http://www.theicct.org/eu-co2-standards-passenger-cars-and-lcvs (cit. on p. 12).

[22] Eurostat. *Smarter, greener, more inclusive?* 2015. ISBN: 9789279400797 (cit. on p. 12).

[23] A. J. Torregrosa, A. Broath, P. Olmeda, and C. Romero. “Assessment of the influence of different cooling system configurations on engine warm-up, emissions and fuel consumption”. In: *International Journal of Automotive Technology* 9.4 (2008), pp. 447–458. DOI: 10.1007/s12239âĹŠ008âĹŠ0054âĹŠ1 (cit. on p. 13).

[24] T. Zegenhagen and F. Ziegler. “Experimental investigation of the characteristics of a jet-ejector and a jet-ejector cooling system operating with R134a as a refrigerant”. In: *International Journal of Refrigeration* 56 (2015), pp. 173–185. ISSN: 01407007. DOI: 10.1016/j.ijrefrig.2015.01.001. URL: http://linkinghub.elsevier.com/retrieve/pii/S0140700715000031 (cit. on p. 13).

[25] M. Zegenhagen and F. Ziegler. “Feasibility analysis of an exhaust gas waste heat driven jet-ejector cooling system for charge air cooling of turbocharged gasoline engines”. In: *Applied Energy* 160 (2015), pp. 221–230. ISSN: 03062619. DOI: 10.1016/j.apenergy.2015.09.057. URL: http://linkinghub.elsevier.com/retrieve/pii/S0306261915011629 (cit. on p. 13).

[26] A. Rêgo, S. Hanriot, A. Oliveira, P. Brito, and T. Rêgo. “Automotive exhaust gas flow control for an ammonia–water absorption refrigeration system”. In: *Applied Thermal Engineering* 64.1-2 (2014), pp. 101–107. ISSN: 13594311. DOI: 10.1016/j.applthermaleng.2013.12.018. URL: http://linkinghub.elsevier.com/retrieve/pii/S1359431113008958 (cit. on p. 13).

[27] M. Bailey. “Comparative Evaluation of Three Alternative Power Cycles for Waste Heat Recovery from the Exhaust of Adiabatic Diesel Engines”. In: *DOE NASA, United Technologies Research Center* 86953 (1985). ISSN: 04999320 (cit. on pp. 13, 191).

[28] J. Galindo, J. Serrano, V. Dolz, and P. Kleut. “Brayton cycle for internal combustion engine exhaust gas waste heat recovery”. In: *Advances in Mechanical Engineering* 7.6 (2015), pp. 1–9. ISSN: 1687-8140. DOI: 10.1177/1687814015590314. URL: http://ade.sagepub.com/lookup/doi/10.1177/1687814015590314 (cit. on p. 13).

[29] J. Liebl, S. Neugebauer, A. Eder, and M. Linde. “The Thermoelectric Generator from BMW is Making Use of Waste Heat”. In: *MTZ* 70 (2009), pp. 4–11 (cit. on p. 13).

[30] A. Kushch, J. Bass, S. Ghamaty, and N. Eisner. “Thermoelectric development at Hi-Z technology”. In: *Proceedings ICT2001. 20 International Conference on Thermoelectrics (Cat. No.01TH8589)* (2001), pp. 1–9. ISSN: 1094-2734. DOI: 10.1109/ICT.2001.979922 (cit. on p. 13).

[31] H. Aghaali and H.-E. Ångström. “A review of turbocompounding as a waste heat recovery system for internal combustion engines”. In: *Renewable and Sustainable Energy Reviews* 49 (2015), pp. 813–824. ISSN: 13640321. DOI: 10.1016/j.rser.2015.04.144. URL: http://linkinghub.elsevier.com/retrieve/pii/S1364032115004141 (cit. on p. 13).

[32] W. Weerasinghe, R. Stobart, and S. Hounsham. “Thermal efficiency improvement in high output diesel engines a comparison of a Rankine cycle with turbo-compounding”. In: *Applied Thermal Engineering* 30.14-15 (2010), pp. 2253–2256. ISSN: 13594311. DOI: 10.1016/j.applthermaleng.2010.04.028. URL: http://linkinghub.elsevier.com/retrieve/pii/S1359431110001912 (cit. on p. 13).

[33] R. Stobart and R. Weerasinghe. “Heat Recovery and Bottoming Cycles for SI and CI engines”. In: *SAE Technical Paper* 2006.724 (2006). DOI: 10.4271/2006-01-0662. URL: http://sro.sussex.ac.uk/15122/ (cit. on p. 15).

[34] A. Duparchy, P. Leduc, G. Bourhis, and C. Ternel. “Heat Recovery for next Generation of Hybrid Vehicles : Simulation and Design of a Rankine Cycle System”. In: *World Electric Vehicle Journal Vol.3* 3 (2009), pp. 1–17 (cit. on pp. 15, 46).

[35] R. E. Chammas and D. Clodic. “Combined Cycle for Hybrid Vehicles”. In: *SAE International* 1 (2012), p. 10 (cit. on pp. 15, 21).

[36] V. Macián, J. Serrano, V. Dolz, and J. Sánchez. “Methodology to design a bottoming Rankine cycle, as a waste energy recovering system in vehicles. Study in a HDD engine”. In: *Applied Energy* 104 (2013), pp. 758–771. ISSN: 03062619. DOI: 10.1016/j.apenergy.2012.11.075. URL: http://linkinghub.elsevier.com/retrieve/pii/S0306261912008859 (cit. on p. 15).

[37] V. Dolz, R. Novella, A. García, and J. Sánchez. “HD Diesel engine equipped with a bottoming Rankine cycle as a waste heat recovery system. Part 1: Study and analysis of the waste heat energy”. In: *Applied Thermal Engineering* 36 (2012), pp. 269–278. ISSN: 13594311. DOI: 10.1016/j.applthermaleng.2011.10.025. URL: http://linkinghub.elsevier.com/retrieve/pii/S1359431111005631 (cit. on pp. 15, 16).

[38] H. Teng and G. Regner. “Improving Fuel Economy for HD Diesel Engines with WHR Rankine Cycle Driven by EGR Cooler Heat Rejection”. English. In: *SAE International* 1 (2009), pp. 1–11. DOI: 10.4271/2009-01-2913. URL: http://papers.sae.org/2009-01-2913/ (cit. on pp. 15, 21).

[39] D. T. Hountalas, G. C. Mavropoulos, C. Katsanos, and W. Knecht. "Improvement of bottoming cycle efficiency and heat rejection for HD truck applications by utilization of EGR and CAC heat". In: *Energy Conversion and Management* 53.1 (2012), pp. 19–32. ISSN: 01968904. DOI: 10.1016/j.enconman.2011.08.002. URL: http://dx.doi.org/10.1016/j.enconman.2011.08.002 (cit. on p. 15).

[40] N. Espinosa, L. Tilman, V. Lemort, S. Quoilin, and B. Lombard. "Rankine cycle for waste heat recovery on commercial trucks: approach, constraints and modelling". en. In: *Diesel International Conference and Exhibition* 1 (2010), pp. 1–10. URL: http://orbi.ulg.ac.be/handle/2268/62995 (cit. on p. 15).

[41] J. R. Serrano, V. Dolz, R. Novella, and A. García. "HD Diesel engine equipped with a bottoming Rankine cycle as a waste heat recovery system. Part 2: Evaluation of alternative solutions". In: *Applied Thermal Engineering* 36.1 (2012), pp. 279–287 (cit. on p. 16).

[42] H. Teng, G. Regner, and C. Cowland. "Achieving High Engine Efficiency for Heavy-Duty Diesel Engines by Waste Heat Recovery Using Supercritical Organic-Fluid Rankine Cycle". In: 724 (2010) (cit. on p. 16).

[43] J. Ringler, M. Seifert, V. Guyotot, and W. Hübner. "Rankine Cycle for Waste Heat Recovery of IC Engines". In: *SAE International* 2.1 (2012), pp. 67–76 (cit. on p. 16).

[44] M. He, X. Zhang, K. Zeng, and K. Gao. "A combined thermodynamic cycle used for waste heat recovery of internal combustion engine". In: *Energy* 36.12 (2011), pp. 6821–6829. ISSN: 03605442. DOI: 10.1016/j.energy.2011.10.014. URL: http://linkinghub.elsevier.com/retrieve/pii/S0360544211006736 (cit. on p. 16).

[45] R. El Chammas, D. Clodic, and R. E. Chammas. "Combined Cycle for Hybrid Vehicles". English. In: *SAE International* 1.724 (2005), pp. 1–10. ISSN: 0148-7191. DOI: 10.4271/2005-01-1171. URL: http://papers.sae.org/2005-01-1171/ (cit. on p. 16).

[46] D. Morgan, P. Patel, E. Doyle, R. Raymond, R. Sakhuja, and K. Barber. "Laboratory test results low emission rankine-cycle engine with organic-based working fluid and reciprocating expander for automobiles". In: *Proceedings of the 8th Intersociety energy conversion engineering conference*. Philadelphia, PA, USA, 1973 (cit. on p. 17).

[47] H. Chen, D. Y. Goswami, and E. K. Stefanakos. "A review of thermodynamic cycles and working fluids for the conversion of low-grade heat". In: *Renewable and Sustainable Energy Reviews* 14.9 (2010), pp. 3059–

3067. ISSN: 13640321. DOI: 10.1016/j.rser.2010.07.006. URL: http://dx.doi.org/10.1016/j.rser.2010.07.006 (cit. on p. 17).

[48] P. Colonna, E. Casati, C. Trapp, T. Mathijssen, J. Larjola, T. Turunen-Saaresti, and A. Uusitalo. "Organic Rankine Cycle Power Systems: From the Concept to Current Technology, Applications, and an Outlook to the Future". In: *Journal of Engineering for Gas Turbines and Power* 137.10 (2015), p. 100801. ISSN: 0742-4795. DOI: 10.1115/1.4029884. URL: http://gasturbinespower.asmedigitalcollection.asme.org/article.aspx?doi=10.1115/1.4029884 (cit. on p. 18).

[49] B. F. Tchanche, G. Lambrinos, A. Frangoudakis, and G. Papadakis. "Low-grade heat conversion into power using organic Rankine cycles - A review of various applications". In: *Renewable and Sustainable Energy Reviews* 15.8 (2011), pp. 3963–3979. ISSN: 13640321. DOI: 10.1016/j.rser.2011.07.024. URL: http://dx.doi.org/10.1016/j.rser.2011.07.024 (cit. on p. 18).

[50] W. J. Brock, J. M. Calm, and R. G. Richard. *Designation and Safety Classifications of Refrigerants*. 2000, pp. 1–15 (cit. on p. 19).

[51] I. Rand. "Considerations for Next Generation HVAC Refrigerants". In: *Engineers Newsletter* (2015), pp. 1–4 (cit. on p. 19).

[52] E. Comission. *The Montreal Protocol*. Tech. rep. 2005, p. 24. DOI: 10.1093/0199286094.003.0008. URL: http://www.oxfordscholarship.com/view/10.1093/0199286094.001.0001/acprof-9780199286096 (cit. on pp. 19, 21).

[53] E. Comission. *Proposal for a Regulation on fluorinated greenhouse gases*. Tech. rep. 2012, p. 45 (cit. on pp. 19, 21).

[54] S. Quoilin, M. V. D. Broek, S. Declaye, P. Dewallef, and V. Lemort. "Techno-economic survey of Organic Rankine Cycle (ORC) systems". In: *Renewable and Sustainable Energy Reviews* 22 (2013), pp. 168–186. ISSN: 13640321. DOI: 10.1016/j.rser.2013.01.028. URL: http://linkinghub.elsevier.com/retrieve/pii/S1364032113000592 (cit. on p. 21).

[55] A. Pearson. "Refrigeration with ammonia". In: *International Journal of Refrigeration* 31.4 (2008), pp. 545–551. ISSN: 01407007. DOI: 10.1016/j.ijrefrig.2007.11.011 (cit. on p. 21).

[56] G. Boccardi, N. Calabrese, G. P. Celata, R. Mastrullo, A. W. Mauro, A. Perrone, and R. Trinchieri. "Experimental performance evaluation for a carbon dioxide light commercial cooling application under transcritical and subcritical conditions". In: *Applied Thermal Engineering* 54.2 (2013), pp. 528–535. ISSN: 13594311. DOI: 10.1016/j.applthermaleng.2013

.02.026. URL: http://dx.doi.org/10.1016/j.applthermaleng.2013.02.026 (cit. on p. 21).

[57] D. Ziviani and A. Beyene. "Advances and challenges in ORC systems modeling for low grade thermal energy recovery". In: *Applied Energy* 121 (2014), pp. 79–95 (cit. on p. 21).

[58] Y. Dai, J. Wang, and L. Gao. "Parametric optimization and comparative study of organic Rankine cycle (ORC) for low grade waste heat recovery". In: *Energy Conversion and Management* 50.3 (2009), pp. 576–582. ISSN: 01968904. DOI: 10.1016/j.enconman.2008.10.018. URL: http://linkinghub.elsevier.com/retrieve/pii/S0196890408004342 (cit. on p. 21).

[59] B. Saleh, G. Koglbauer, M. Wendland, and J. Fischer. "Working fluids for low-temperature organic Rankine cycles". In: *Energy* 32.7 (2007), pp. 1210–1221. ISSN: 03605442. DOI: 10.1016/j.energy.2006.07.001. URL: http://linkinghub.elsevier.com/retrieve/pii/S0360544206001812 (cit. on p. 21).

[60] H. Tian, G. Shu, H. Wei, X. Liang, and L. Liu. "Fluids and parameters optimization for the organic Rankine cycles (ORCs) used in exhaust heat recovery of Internal Combustion Engine (ICE)". In: *Energy* 47.1 (2012), pp. 125–136. ISSN: 03605442. DOI: 10.1016/j.energy.2012.09.021. URL: http://linkinghub.elsevier.com/retrieve/pii/S0360544212006998 (cit. on p. 21).

[61] E. H. Wang, H. G. Zhang, Y. Zhao, B. Y. Fan, Y. T. Wu, and Q. H. Mu. "Performance analysis of a novel system combining a dual loop organic Rankine cycle (ORC) with a gasoline engine". In: *Energy* 43.1 (2012), pp. 385–395. ISSN: 03605442. DOI: 10.1016/j.energy.2012.04.006 (cit. on p. 21).

[62] S. Eyerer, C. Wieland, A. Vandersickel, and H. Spliethoff. "Experimental study of an ORC (Organic Rankine Cycle) and analysis of R1233zd-E as a drop-in replacement for R245fa for low temperature heat utilization". In: *Energy* 103 (2016), pp. 660–671. ISSN: 03605442. DOI: 10.1016/j.energy.2016.03.034. URL: http://linkinghub.elsevier.com/retrieve/pii/S036054421630278X (cit. on p. 21).

[63] A. Mota-Babiloni, J. Navarro-Esbrí, F. Molés, Á. B. Cervera, B. Peris, and G. Verdú. "A review of refrigerant R1234ze(E) recent investigations". In: *Applied Thermal Engineering* 95 (2016), pp. 211–222. ISSN: 13594311. DOI: 10.1016/j.applthermaleng.2015.09.055. URL: http://linkinghub.elsevier.com/retrieve/pii/S1359431115009758 (cit. on p. 21).

[64] J. R. Juhasz and L. D. Simoni. “A Review of Potential Working Fluids for Low Temperature Organic Rankine Cycles in Waste Heat Recovery”. In: *3rd International Seminar on ORC Power Systems*. 2015, pp. 1–10 (cit. on p. 21).

[65] F. J. Fernández, M. M. Prieto, and I. Suárez. “Thermodynamic analysis of high-temperature regenerative organic Rankine cycles using siloxanes as working fluids”. In: *Energy* 36.8 (2011), pp. 5239–5249. ISSN: 03605442. DOI: 10.1016/j.energy.2011.06.028. URL: http://dx.doi.org/10.1016/j.energy.2011.06.028 (cit. on p. 22).

[66] P. Colonna, N. R. Nannan, A. Guardone, and E. W. Lemmon. “Multiparameter equations of state for selected siloxanes”. In: *Fluid Phase Equilibria* 244.2 (2006), pp. 193–211. ISSN: 03783812. DOI: 10.1016/j.fluid.2006.04.015 (cit. on p. 22).

[67] M. Preißinger and D. Brüggemann. “Thermal stability of hexamethyldisiloxane (MM) for high-temperature Organic Rankine Cycle (ORC)”. In: *Energies* 9.3 (2016). ISSN: 19961073. DOI: 10.3390/en9030183 (cit. on p. 22).

[68] J. Song and C. W. Gu. “Analysis of ORC (Organic Rankine Cycle) systems with pure hydrocarbons and mixtures of hydrocarbon and retardant for engine waste heat recovery”. In: *Applied Thermal Engineering* 89 (2015), pp. 693–702. ISSN: 13594311. DOI: 10.1016/j.applthermaleng.2015.06.055. URL: http://dx.doi.org/10.1016/j.applthermaleng.2015.06.055 (cit. on p. 22).

[69] D. Seher, T. Lengenfelder, J. Gerhardt, N. Eisenmenger, M. Hackner, and I. Krinn. “Waste Heat Recovery for Commercial Vehicles with a Rankine Process”. In: *21 st Aachen Colloquium Automobile and Engine Technology*. 2012, pp. 1–15 (cit. on pp. 22, 28).

[70] T. Howell and J. Gibble. “Development of an ORC system to improve HD truck fuel efficiency”. In: *Deer Conference*. Vol. 1. 2011, pp. 1–21 (cit. on p. 22).

[71] Y.-Q. Zhang, Y.-T. Wu, G.-D. Xia, C.-F. Ma, W.-N. Ji, S.-W. Liu, K. Yang, and F.-B. Yang. “Development and experimental study on organic Rankine cycle system with single-screw expander for waste heat recovery from exhaust of diesel engine”. In: *Energy* 77.0 (2014), pp. 499–508. ISSN: 03605442. DOI: http://dx.doi.org/10.1016/j.energy.2014.09.034. URL: http://www.sciencedirect.com/science/article/pii/S0360544214010901 (cit. on pp. 22, 28).

[72] G. Latz, S. Andersson, and K. Munch. “Comparison of Working Fluids in Both Subcritical and Supercritical Rankine Cycles for Waste-Heat Recovery Systems in Heavy-Duty Vehicles”. In: *SAE International* 1 (2012), pp. 1–18. DOI: 10.4271/2012-01-1200. URL: http://www.sae.org/technical/papers/2012-01-1200 (cit. on p. 22).

[73] G. Shu, L. Liu, H. Tian, H. Wei, and G. Yu. “Parametric and working fluid analysis of a dual-loop organic Rankine cycle (DORC) used in engine waste heat recovery”. In: *Applied Energy* 113 (2014), pp. 1188–1198. ISSN: 03062619. DOI: 10.1016/j.apenergy.2013.08.027. URL: http://linkinghub.elsevier.com/retrieve/pii/S0306261913006624 (cit. on p. 22).

[74] L. Zhao and J. Bao. “The influence of composition shift on organic Rankine cycle (ORC) with zeotropic mixtures”. In: *Energy Conversion and Management* 83 (2014), pp. 203–211. ISSN: 01968904. DOI: 10.1016/j.enconman.2014.03.072. URL: http://linkinghub.elsevier.com/retrieve/pii/S0196890414002830 (cit. on p. 22).

[75] H. Teng, G. Regner, and C. Cowland. “Waste Heat Recovery of Heavy-Duty Diesel Engines by Organic Rankine Cycle Part II : Working Fluids for WHR-ORC”. In: *SAE Technical Paper* 724 (2012), pp. 1–12 (cit. on p. 22).

[76] H. Teng, G. Regner, and C. Cowland. “Waste Heat Recovery of Heavy-Duty Diesel Engines by Organic Rankine Cycle Part I: Hybrid Energy System of Diesel and Rankine Engines”. English. In: *SAE International* 1.724 (2007), pp. 1–13. DOI: 10.4271/2007-01-0537. URL: http://papers.sae.org/2007-01-0537/ (cit. on pp. 22, 25).

[77] G. Shu, L. Liu, H. Tian, H. Wei, and X. Xu. “Performance comparison and working fluid analysis of subcritical and transcritical dual-loop organic Rankine cycle (DORC) used in engine waste heat recovery”. In: *Energy Conversion and Management* 74 (2013), pp. 35–43. ISSN: 01968904. DOI: 10.1016/j.enconman.2013.04.037. URL: http://linkinghub.elsevier.com/retrieve/pii/S0196890413002343 (cit. on p. 22).

[78] T. Wang, Y. Zhang, Z. Peng, and G. Shu. “A review of researches on thermal exhaust heat recovery with Rankine cycle”. In: *Renewable and Sustainable Energy Reviews* 15.6 (2011), pp. 2862–2871. ISSN: 13640321. DOI: 10.1016/j.rser.2011.03.015. URL: http://linkinghub.elsevier.com/retrieve/pii/S1364032111001158 (cit. on p. 23).

[79] J. Bao and L. Zhao. “A review of working fluid and expander selections for organic Rankine cycle”. In: *Renewable and Sustainable Energy Reviews* 24 (2013), pp. 325–342. ISSN: 13640321. DOI: 10.1016/j.rser.2013.0

3.040. URL: http://linkinghub.elsevier.com/retrieve/pii/S1364032113001998 (cit. on p. 24).

[80] S. Quoilin and C. Sart-tilman. "Expansion Machine and Fluid Selection for the Organic Rankine Cycle". In: *7th International Conference on Heat Transfer, Fluid Mechanics and Thermodynamics*. July. 2010, pp. 1–7 (cit. on p. 24).

[81] G. Latz, S. Andersson, and K. Munch. "Selecting an Expansion Machine for Vehicle Waste-Heat Recovery Systems Based on the Rankine Cycle". In: *SAE International* 1 (2013), pp. 1–15. DOI: 10.4271/2013-01-0552. URL: http://www.sae.org/technical/papers/2013-01-0552 (cit. on p. 24).

[82] S. Declaye, S. Quoilin, L. Guillaume, and V. Lemort. "Experimental study on an open-drive scroll expander integrated into an ORC (Organic Rankine Cycle) system with R245fa as working fluid". In: *Energy* 55 (2013), pp. 173–183. ISSN: 03605442. DOI: 10.1016/j.energy.2013.04.003. URL: http://linkinghub.elsevier.com/retrieve/pii/S0360544213003034 (cit. on pp. 24, 81).

[83] A. Legros, L. Guillaume, V. Lemort, M. Diny, I. Bell, and S. Quoilin. "Investigation on a scroll expander for waste heat recovery on internal combustion engines". In: *International conference on compressors and their systems* 1 (2013), p. 10 (cit. on p. 24).

[84] S. Quoilin, V. Lemort, and J. Lebrun. "Experimental study and modeling of an Organic Rankine Cycle using scroll expander". In: *Applied Energy* 87.4 (2010), pp. 1260–1268. ISSN: 03062619. DOI: 10.1016/j.apenergy.2009.06.026. URL: http://linkinghub.elsevier.com/retrieve/pii/S030626190900258X (cit. on p. 24).

[85] V. Lemort, S. Declaye, and S. Quoilin. "Experimental characterization of a hermetic scroll expander for use in a micro-scale Rankine cycle". In: *Proceedings of the Institution of Mechanical Engineers, Part A: Journal of Power and Energy* 226.1 (2011), pp. 126–136. ISSN: 0957-6509. DOI: 10.1177/0957650911413840. URL: http://pia.sagepub.com/lookup/doi/10.1177/0957650911413840 (cit. on p. 24).

[86] B. Aoun and D. F. Clodic. "Theoretical and Experimental Study of an Oil-Free Scroll Vapor Expander". In: *International Compressor Engineering Conference* (2008), p. 1925. DOI: http://docs.lib.purdue.edu/icec/1925 (cit. on p. 24).

[87] V. Lemort, S. Quoilin, C. Cuevas, and J. Lebrun. "Testing and modeling a scroll expander integrated into an Organic Rankine Cycle". In: *Applied Thermal Engineering* 29.14-15 (2009), pp. 3094–3102. ISSN: 13594311. DOI: 10.1016/j.applthermaleng.2009.04.013. URL: http://linkinghub.elsevier.com/retrieve/pii/S1359431109001173 (cit. on p. 24).

[88] J. Lopes, R. Douglas, G. McCullough, R. O'Shaughnessy, A. Hanna, C. Rouaud, and R. Seaman. "Review of Rankine Cycle Systems Components for Hybrid Engines Waste Heat Recovery". In: *SAE International* 1 (2012), pp. 1–14. DOI: 10.4271/2012-01-1942. URL: http://www.sae.org/technical/papers/2012-01-1942 (cit. on p. 25).

[89] H. Santos, S. Pinheiro, and M. Costa. "Expander Selection for Internal Combustion Engines Bottoming with steam and Organic Rankine Cycle". In: 1 (2012), pp. 1–12 (cit. on p. 25).

[90] Y. Glavatskaya, P. Podevin, V. Lemort, O. Shonda, and G. Descombes. "Reciprocating Expander for an Exhaust Heat Recovery Rankine Cycle for a Passenger Car Application". In: *Energies* 5.12 (2012), pp. 1751–1765. ISSN: 1996-1073. DOI: 10.3390/en5061751. URL: http://www.mdpi.com/1996-1073/5/6/1751/ (cit. on p. 25).

[91] H. Kunte and J. Seume. "Partial Admission Impulse Turbine for Automotive ORC Application". In: *SAE Technical Papers* 6 (2013). DOI: 10.4271/2013-24-0092. URL: http://www.scopus.com/inward/record.url?eid=2-s2.0-84890407668{\&}partnerID=tZOtx3y1 (cit. on pp. 25, 152).

[92] E. Sauret and A. S. Rowlands. "Candidate radial-inflow turbines and high-density working fluids for geothermal power systems". In: *Energy* 36.7 (2011), pp. 4460–4467. ISSN: 03605442. DOI: 10.1016/j.energy.2011.03.076. URL: http://dx.doi.org/10.1016/j.energy.2011.03.076 (cit. on p. 25).

[93] P. Ambros. "Twin-Round-Tube Evaporator for Waste Heat Recovery". In: *MTZ* 4 (2014), pp. 44–49 (cit. on p. 27).

[94] R. Haller, B. Nicolas, S. Hammi, A. Taklanti, and Y. Glavatskaya. "Comparison of High and Low Temperature Working Fluids for Automotive Rankine Waste Heat Recovery Systems". In: (2014), pp. 1–9 (cit. on p. 27).

[95] T. Töpfer, O. Dingel, I. Friedrich, and J. Seebode. "Use of Route Information for Predictive ORC Control". In: *MTZ* (2015), pp. 14–17 (cit. on p. 27).

[96] H. Oomori and S. Ogino. “Waste Heat Recovery of Passenger Car Using a Combination of Rankine Bottoming Cycle and Evaporative Engine Cooling System”. In: *SAE International* 930880 (1993). DOI: 10.4271/930880. URL: http://papers.sae.org/930880/ (cit. on p. 28).

[97] G. Kosmadakis, D. Manolakos, and G. Papadakis. “Experimental investigation of a low-temperature organic Rankine cycle (ORC) engine under variable heat input operating at both subcritical and supercritical conditions”. In: *Applied Thermal Engineering* 92 (2016), pp. 1–7. ISSN: 1359-4311. DOI: 10.1016/j.applthermaleng.2015.09.082. URL: http://www.sciencedirect.com/science/article/pii/S1359431115010078$\backslash$nhttp://www.sciencedirect.com/science/article/pii/S1359431115010078/pdfft?md5=07e1aaf4e5a0479ffff5611536d75123{\&}pid=1-s2.0-S1359431115010078-main.pdf (cit. on p. 28).

[98] R. Freymann. “The Turbosteamer : A System Introducing the Principle of Cogeneration in Automotive Applications”. In: *MTZ* 69.5 (2008), pp. 20–27 (cit. on p. 28).

[99] T. Endo, S. Kawajiri, Y. Kojima, K. Takahashi, T. Baba, S. Ibaraki, T. Takahashi, and M. Shinohara. “Study on Maximizing Exergy in Automotive Engines”. In: *SAE International* 1 (2007), pp. 1–12 (cit. on pp. 28, 78).

[100] R. Daccord, A. Darmedru, and J. Melis. “Oil-free axial piston expander for waste heat recovery”. English. In: *SAE International* 1 (2014), pp. 1–12. ISSN: 0148-7191. DOI: 10.4271/2014-01-0675.Copyright. URL: http://papers.sae.org/2014-01-0675/ (cit. on pp. 28, 214).

[101] G. Latz, O. Erlandsson, T. Skåre, and A. Contet. “Water-based Rankine-cycle waste heat recovery systems for engines: challenges and opportunities”. In: *Asme Orc 2015* 2013 (2015), pp. 1–10 (cit. on p. 28).

[102] R. Freyman, J. Ringler, M. Seifert, and T. Horst. “The Second Generation T urbosteamer”. In: *MTZ* 73 (2012), pp. 18–23 (cit. on p. 28).

[103] R. Cipollone, D. Di Battista, A. Perosino, and F. Bettoja. “Waste Heat Recovery by an Organic Rankine Cycle for Heavy Duty Vehicles”. In: *SAE International* 234 (2016), pp. 1–9. DOI: 10.4271/2016-01-0234. URL: http://papers.sae.org/2016-01-0234/ (cit. on p. 28).

[104] T. Park, H. Teng, G. L. Hunter, B. van der Velde, and J. Klaver. “A Rankine Cycle System for Recovering Waste Heat from HD Diesel Engines - Experimental Results”. In: *SAE International* 1 (2011), pp. 1–9. DOI: 10.4271/2011-01-1337. URL: http://papers.sae.org/2011-01-1337/ (cit. on p. 28).

[105] L. Guillaume, A. Legros, A. Desideri, and V. Lemort. "Performance of a radial-inflow turbine integrated in an ORC system and designed for a WHR on truck application: An experimental comparison between R245fa and R1233zd". In: *Applied Energy* (2016). ISSN: 03062619. DOI: 10.1016/j.apenergy.2016.03.012. URL: http://linkinghub.elsevier.com/retrieve/pii/S0306261916303233 (cit. on p. 28).

CHAPTER 3

Experimental tests

Contents

Figures

Tables

3.1 Introduction

FROM previous chapters, it has been shown that the exhaust gases are the main heat losses in an ICE [34]. Moreover, it represents the greater recovery potential compared to other heat sources (CAC, EGR and cooling loop) due to the large difference in temperature gradients and lower mass flow rates. Furthermore, ethanol seems to improve the ORC thermal characteristics in the temperature range of the ICE [106]. Therefore, an experimental mock-up is built and tested in order to show the potential of this technology in the automotive applications. The present chapter contains four parts:

- section 3.2 corresponds to the experimental setup description, both the ICE and the ORC (boiler, expander, condenser, pump, expander vessel and ethanol tank).
- section 3.3 corresponds to the detailed description of sensors installed in the experimental mock-up.
- section 3.4 focuses on the experimental results obtained in Steady-State Tests. The operating points and the control during this tests is presented. Moreover, the theoretical and experimental results of energy balances and cycle efficiencies are shown. Additional sensitivity analysis is performed to determine the main parameters affecting cycle efficiencies.
- section 3.5 presents the transient tests. In this section, the P-V diagram analysis is shown with the aim of understanding the behaviour of the expander machine during these transients. Furthermore, NEDC cycle is tested in the experimental facility to validate the control of the ORC in realistic dynamic conditions of the engine.

3.2 Experimental setup

3.2.1 General description of the WHRS

An experimental facility of an Organic Rankine Cycle coupled to an Internal Combustion Engine is tested in order to estimate the amount of energy obtained from this system and to compare cycle performances. The WHRS is presented in Figure 3.1.

It consists of two main components, both installed in the test bench. The components are: the internal combustion engine (ICE) and the Organic Rankine Cycle (ORC).

The ORC is installed downstream of the aftertreatment system in the gasoline engine using a by-pass valve to regulate the exhaust flow through the ORC evaporator. The main function of this system is to avoid further load-blocking problems in the exhaust line caused by the ORC and to be able to test different engine operating points. The ORC is detailed described in subsection 3.2.3. Temperature and pressure sensors are installed at the inlet and the outlet of the main cycle components. They are connected to the Data Adquisition System.

The gasoline engine characteristics are presented in subsection 3.2.2. The most interesting engine variables are: engine torque, engine speed, fuel consumption and air flow at the inlet. Temperature and pressure sensors are installed in the main elements of the engine. The engine is placed in a test bench with a asynchronous dynamometer. It is connected to the control chest using a specific software (STARS). Different driving cycles and vehicles can be simulated in the dynamometer. Moreover, the software let the control of the remainder sensors and actuators in the engine through the Electronic Control Unit (ECU) and the recording of them using the Data Collection Device.

The engine cooling circuit is connected to the intercooling circuit and the dynamometer with butterfly valves. Using the cooling tower, the temperature is reduced. The cooling tower is used to control the water temperature in the test benches. In the ORC both the brake and the condenser dissipate energy to the ambient using cooling water, which is cooled down in the cooling tower.

A flowmeter measured the compressor intake air mass flow, which is cooled in the intercooler. The exhaust gases at the engine outlet flows into the turbine of the turbocompressor, through the aftertreatment system and finally into the ORC.

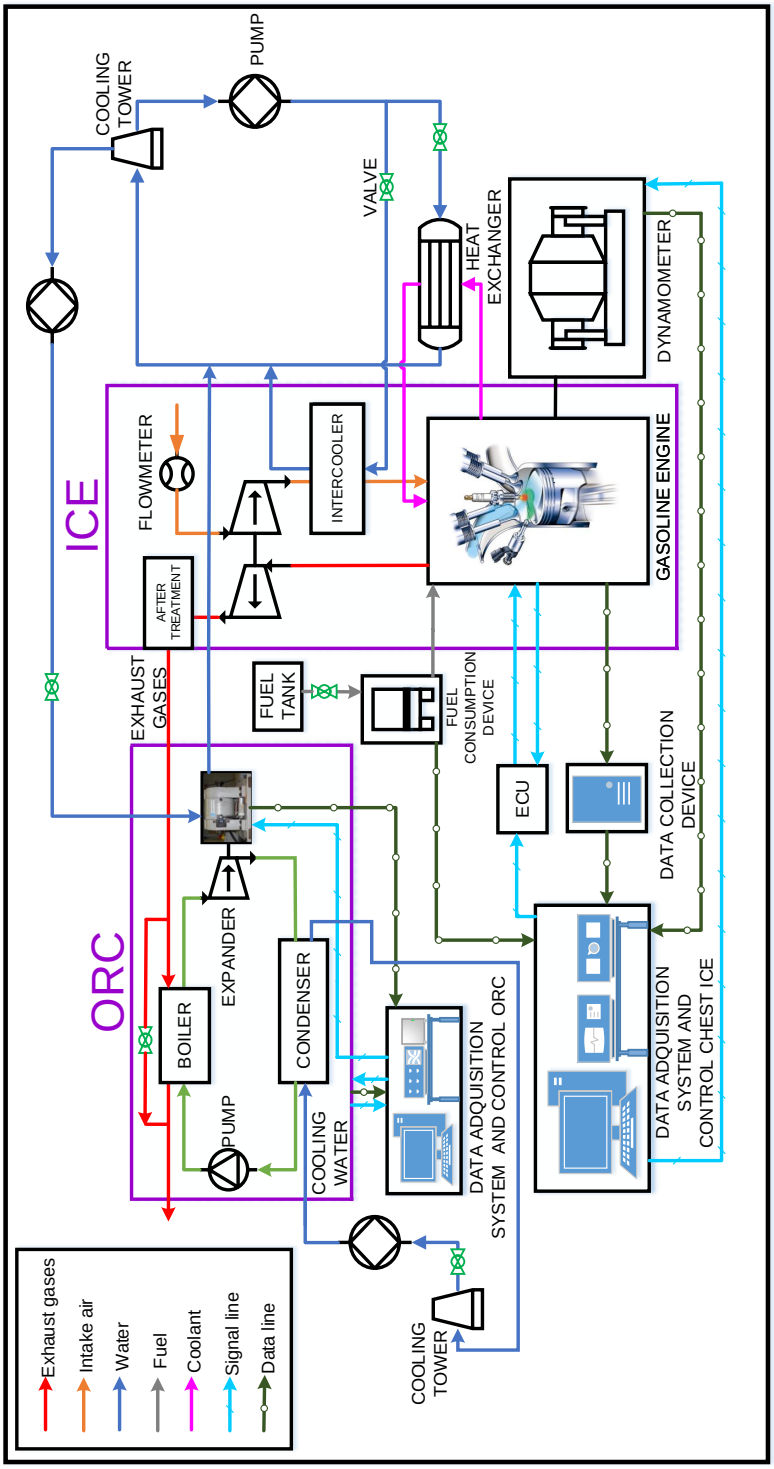

Figure 3.1: Waste Heat Recovery System diagram

3.2.2 Description of the gasoline engine

The gasoline engine used in these tests is an inline four-cylinder turbocharged engine with a volumetric capacity of 2 liter. The maximum engine torque is 308 Nm at 3000 rpm and 100% load. The maximum engine power is 153 kW at 5500 rpm and 100% load.

The engine is placed in a test bench and is instrumented to measure torque, speed, temperature in the exhaust line (before and after the catalyzer), injected mass of fuel and mass flow in the intake line. The exhaust gas power of each engine operating point is calculated from the temperature measurements and the exhaust mass flow estimation (obtained from the sum of intake air and injected fuel mass flow). The ambient conditions (25 °C and 1.013 atm) are considered as the reference state to compute the exhaust energy. It is presented in Figure 3.2. The Kriging interpolation method is used to plot the contour lines of Figure 3.2. It shows that the available exhaust gas energy increases with engine speed and engine load. The highest point corresponds to 5500 rpm and full load, with a value of 153 kW, whereas the lowest point corresponds to 1000 rpm where the engine generates almost any waste heat.

Additional blue lines plotted in Figure 3.2 indicate the ratio of the exhaust gases power to the total fuel power obtained from the injected fuel calorific value. It shows that although the greater exhaust gas power is reached at high engine speed and torque, the biggest recovery potential from the input fuel power is obtained at medium torque and engine speeds. At low engine speed, heat losses to the ambient increase. By contrast, at high engine speed, mechanical losses increase. Therefore, the power available in exhaust gases is maximized at medium speed and torque operating points.

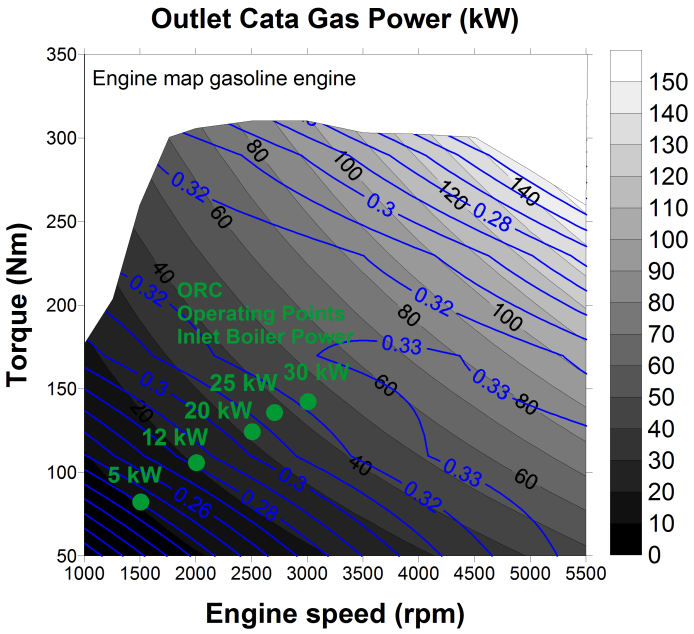

Figure 3.2: Exhaust gases power and percentage of exhaust gases power to the input fuel power in the engine

Five operating points, listed in Table 3.1 and plotted in Figure 3.2, have been chosen for design and simulations. These points belong to five vehicle operating points of Ford Explorer 2.0 EcoBoost gasoline direct injection engine at steady state simulation conditions. Every engine operating point has an equivalent boiler power of 5, 12, 20, 25 and 30 kW and throughout the whole document, references to them will be made. The more frequent engine operating points depend on the size of the engine and the passenger driving mode.

Figure 3.3 shows the NEDC cycle using the Ford Explorer (with Ecoboost 2 l engine) and the points tested in the ORC. As shown in this figure, points 1, 2 and 3, which corresponds to a boiler released power of 5, 12 and 20 kW respectively are ordinary engine operating points, thus it is justified its assessment. NEDC cycle is characterized by smooth acceleration and gradient of 0%. Waste Heat Recovery systems improve their efficiencies when the heat source power increases. Therefore, two points (4 and 5), which corresponds with ordinary engine operating points in highways, have been added, in order to estimate maximum WHR system efficiencies. They will be essential to evaluate the system viability.

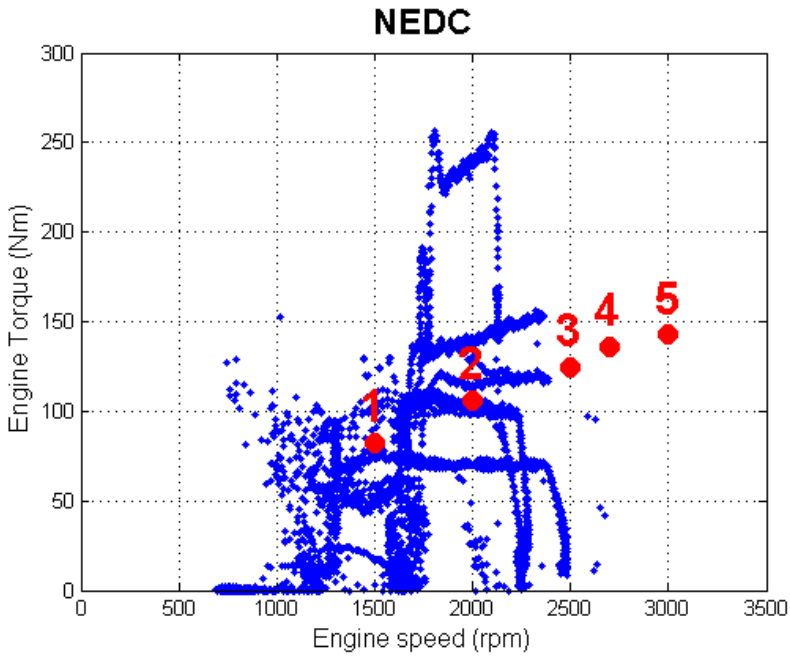

Figure 3.3: NEDC and engine operating points

Under these five conditions, the exhaust gas temperature is within 429-673 °C and the exhaust gases mass flow varies from 15 to 48 g/s. Differences between outlet catalyzer gas power and inlet boiler power are produced due to heat losses in the exhaust line.

Table 3.1: Engine operating points chosen for design and simulations bottoming cycle

	Op. point 1	**Op. point 2**	**Op. point 3**	**Op. point 4**	**Op. point 5**
Vehicle speed (km/h)	63	84	106	114	126
Gear position demand	5	5	5	5	5
Gradient	0.60%	0.90%	0.80%	0.90%	0.70%
Engine speed (rpm)	1500	2000	2500	2700	3000
Engine torque (Nm)	82.4	106	124.5	136	142.6
Fuel power (kW)	40.5	69.6	100.5	119.1	140.8
Engine power output (kW)	12.9	22.2	32.5	38.5	44.8
EG Inlet Temperature (°C)	429	526	602	646	673
EG Mass flow (g/s)	15	24	35	41	48
EG power (kW)	5	12	20	25	30

Figure 3.4 shows the exhaust gas temperature at the boiler inlet and the exhaust gas mass flow for the five engine operating points. It should be noticed that these points correspond to low operating points in the engine map. Temperature is measured after the catalytic converter.

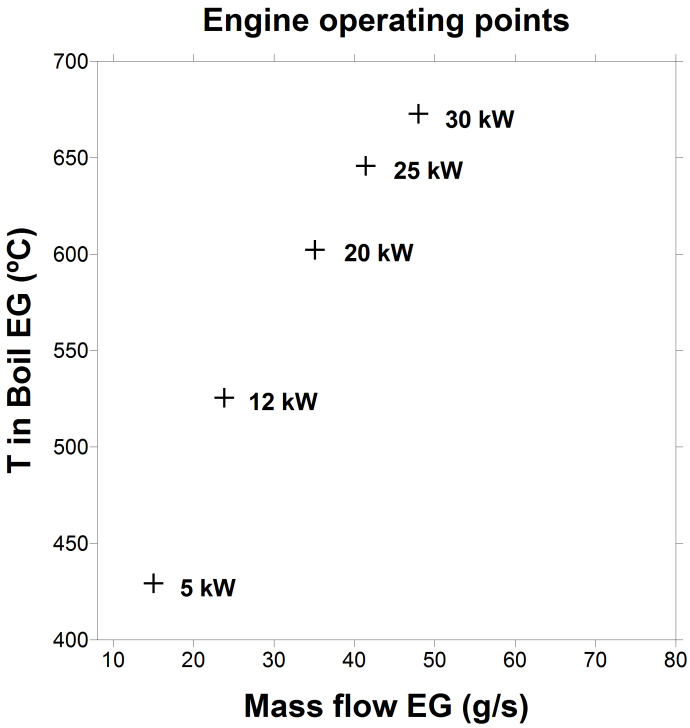

Figure 3.4: Measured exhaust gas temperature at the boiler inlet with exhaust gas mass flow

3.2.3 Description of the ORC mock-up

In this section, a brief description of the ORC system is given, which explains the main characteristics of the ORC. Figure 3.5 shows a picture of the experimental ORC set up system used in this study.

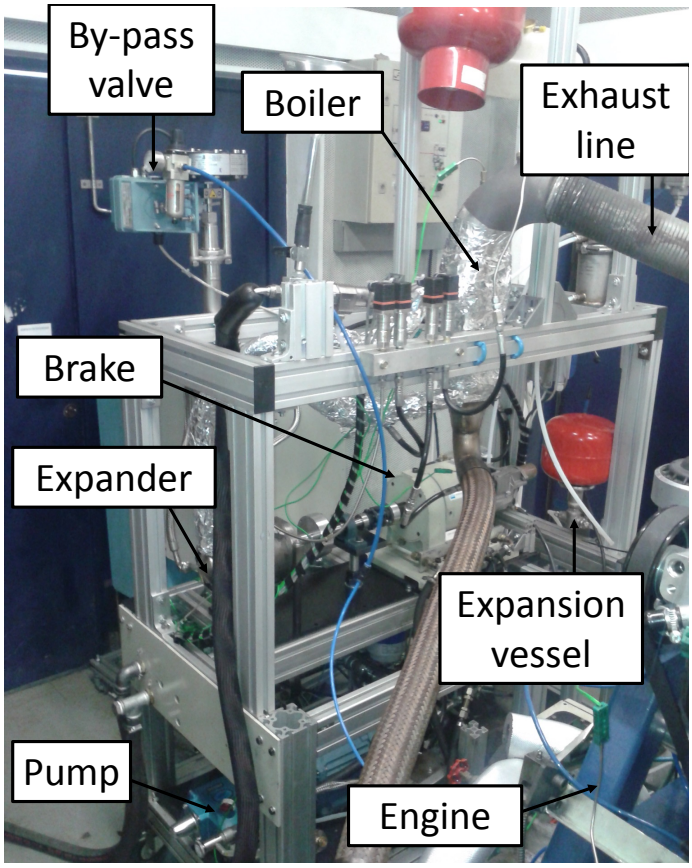

Figure 3.5: Experimental ORC installation

The ORC operating principle is as follows: heat from engine exhaust gases are transferred through the boiler to the working fluid, in this case, ethanol. Then, it is pumped into the high pressure loop and then it is evaporated in the boiler and slightly superheated. After that, the vapour flows into the expander where enthalpy is converted into effective power measured by a torque measuring unit. Low pressure vapour was expanded passaging through the expander and flows to the condenser, reducing its temperature by cooling water and producing condensed ethanol.

Therefore, the cycle starts again. Figure 3.6 shows the ORC cycle schematic diagram. This facility can be coupled to different types of automotive combustion engines (an automotive diesel engine, a Heavy Duty diesel engine and an automotive petrol engine).

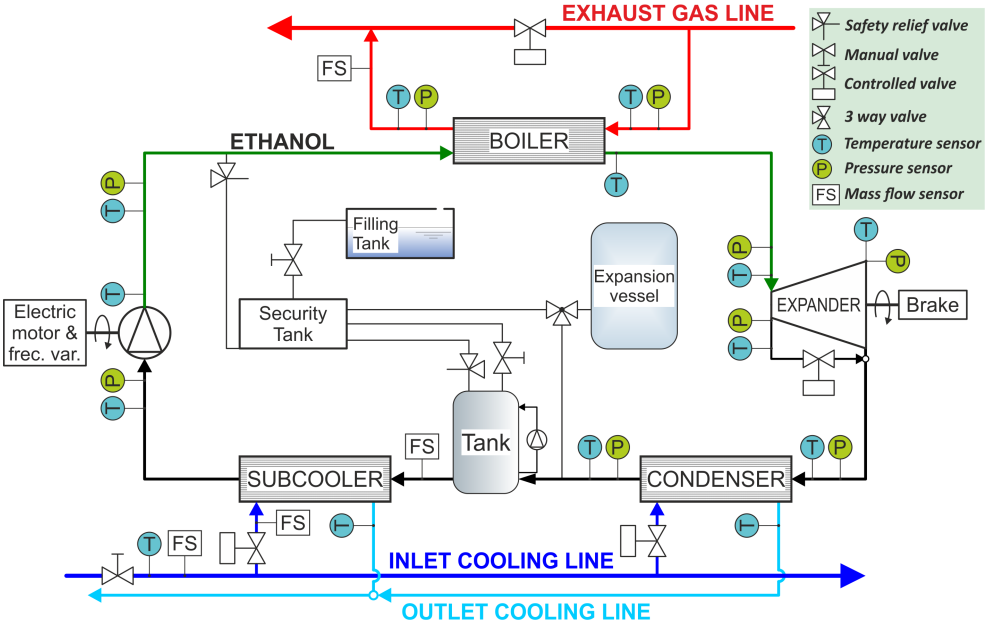

Figure 3.6: Experimental ORC installation diagram

To sum up, the main components of the cyle are the boiler, the expander, the condenser, the pump, the expander vessel and the ethanol tank.

Boiler. The boiler allows the heat transfer from exhaust gas to the working fluid. It is based upon plate and fin technology and it is specifically designed and supplied by Valeo Systèmes Thermiques. This is a countercurrent heat exchanger, designed to withstand a maximum pressure of 40 bar. Therefore, a complex design is done in order to avoid premature failures. It is presented in Figure 3.7. Plate and fin exchangers allow compact and efficient boilers due to their high surface to volume ratio so makes them appropriate for automotive applications. This heat exchanger has two different fin profiles: for the ethanol section and the exhaust gas section. The exhaust gas section is made of consecutive alternate thin fin profiles which are disposed lengthwise to enhance the heat transfer between the fluids. For the ethanol section a simpler continuous profile is used to divide the ethanol into two sections, each one against a thin plate. These curved profiles also contribute to the stiffness of the plate as they

restrain the vertical displacement of the plates. The stiffer the plate the better, as the vertical displacement will limit the pressure this kind of exchanger may withstand. Belts are welded surrounding the exchanger to reduce the displacement on the top and bottom channels which are the ones suffering greater displacement and therefore are expected to be damaged first. Ethanol inlet and outlet channels have different areas due to changes in volumetric flow . Two rectangular frames are also welded to the sides of the evaporator to be able to attach it safely to its position.

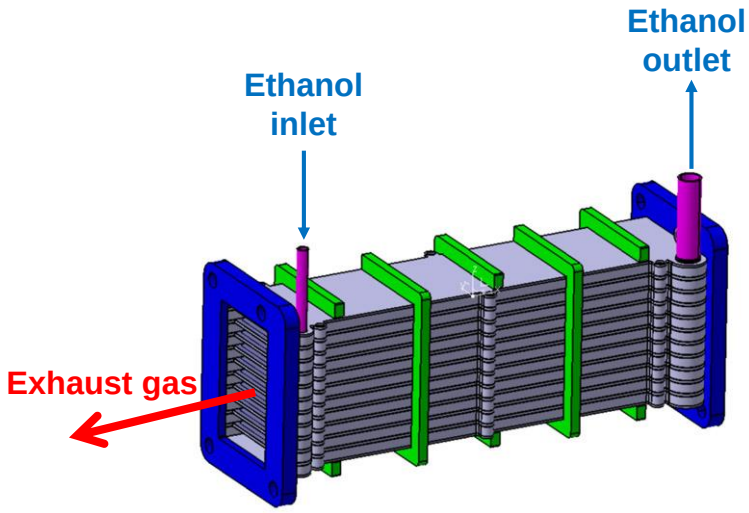

Figure 3.7: Boiler

Expander. The expander prototype is a piston swash-plate. Lower flow rates and higher expansion ratios could be expanded with this machine. Expander speed range is similar to the engine one. Therefore, the expander shaft can be directly connected to the engine drive belt with a clutch, to avoid power losses when the ORC cycle power output is too low. Moreover, this system is preferred by truck manufacturers because it can be used all the time and not only at particular times. Thus, displacement expanders are considered the main technology for recovering waste heat from low temperature sources in vehicle applications using ethanol as a working fluid. The geometrical features of the expander are listed in Table 3.2 and Figure 3.8 shows a picture of the Swash-plate expander delivered by Exoès.

Table 3.2: Swash-plate characteristics

Swash-plate characteristics	
Number of pistons	3
Bore (mm)	40
Stroke (mm)	31
Maximum expander speed (rpm)	4500
Swash-plate angle (°)	20

Figure 3.8: Swash-plate Expander

A swash-plate expander is a positive displacement machine. It works as a two-stroke machine, which means that during one revolution the piston moves from the Top Dead Center (TDC) to the Bottom Dead Center (BDC) and back again and thus, one working cycle is completed. The superheated vapour flows through the intake port into the cylinder whose piston is near top dead center. Moving the piston downwards, the vapour is expanded and led out by exhaust ports in the cylinder (slits) situated near the bottom dead center. Finally, the upmoving piston closes the exhaust ports and compresses the vapour remained in the cylinder and the cycle starts again.

Condenser. The condenser used in the experimental setup is a fin plate exchanger with ethanol as the hot source and water as the cold sink. It is a stainless steel heat exchanger chosen among industrial residential products. The exchanger is set up in counter current configuration .This is a practical solution to ensure saturated liquid leaves the condenser so that the pump can operate properly. As the operating pressures of this component are relatively low, around 2 bar on both sides, no special attention is required. It is a stainless steel heat exchanger. The condenser has a section of 74mm x 465mm and thickness of 160mm. The inlet diameter of tubes both in the ethanol and water side are 40mm. Figure 3.9 shows the Condenser tested in the ORC installation.

Figure 3.9: Condenser

Pump. The pump used to pressurize the high pressure loop is a stainless steel direct drive plunger pump supplied by CAT PUMPS (3CP1231). Therefore, the mass flow can be directly estimated considering the pump speed. At the pump inlet, the condenser and subcooler lines are connected to provide the pump with saturated liquid in low pressure conditions. As long as the working fluid is saturated in the inlet and the pressure is high enough to ensure no cavitation, the pump will operate properly. It is connected to an electrical motor with a maximum speed of 1725 rpm. At this speed, the pump delivers 8.7 l/min and a range of pressures between 7 and 140 bar. Its size is 246 x 223 x 136 mm. It is presented in Figure 3.10.

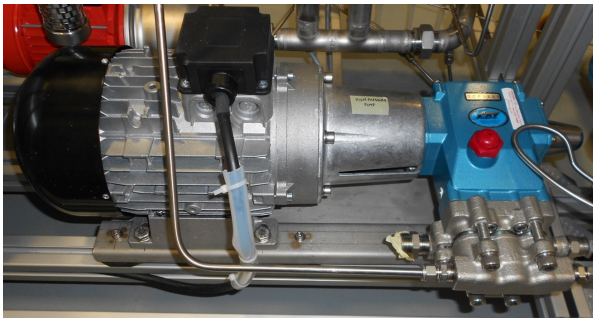

Figure 3.10: Pump

Expansion Vessel. The condenser is followed by an expander vessel to regulate the low pressure in the installation. Figure 3.11 shows the expander vessel used in the test bench.

Figure 3.11: Expansion Vessel

Ethanol tank and security tank. In closed loop systems with volumetric machines, it is needed the existence of tanks, in order to ensure the proper disponibility of working fluid in all operating points and to avoid pressure pulses in the inlet of the expander. The ethanol tank is connected with the security tank. The security tank is used to absorb the working fluid in case the level is increased above the ethanol tank due to pressure pulses and to discharge the security valves if an overpressure value is reached during the operation of the facility. Moreover, this security tank is connected through a manual valve to an additional tank in order to fill the installation.

3.3 Sensors

Temperature and pressure sensors have been placed at the inlet and the outlet of the different elements (boiler, expander, condenser and pump). Measurements of temperatures in the ORC cycle are made through 14 K-type thermocouples (class 2) with an uncertainty of ±2.5°C installed in each element of the cycle (boiler, condenser, pump and expander) at the inlet and outlet. Piezoresistive pressure sensors made by Kistler are used at the inlet and the outlet of the main elements of the installation. Three types of pressure sensors are installed, depending on the expected pressure range. In the high pressure loop, the flow pressure (from the outlet of the pump and the inlet of the expander) is measured using the pressure sensor Kistler type 4260A750B7BD00Y1. The medium pressure flow (from the outlet of the expander to the inlet of the pump) is measured by different Kistler type 4260A075B7BD00Y1 sensor. The pressure drop through the boiler on the exhaust side is measured using a Kistler type 4260A030B7BD00Y1. This type of sensor has an uncertainty of ±0.05% in full scale range, which is 50, 5 and 2 bar respectively.

Regarding mass flow sensors, water is measured by an electromagnetic flow sensor made by ADMAG AE (AE 202 mg) with an uncertainty of ±0.5% FS. The flow rate of the working fluid is measured using a Coriolis measurement unit made by Emerson with an uncertainty that varies from ±0.273% to ±1.001% depending on the measured value. Exhaust gases mass flow is measured by adding to the air mass flow (measured by the Sensyflow FMT700-P) the fuel mass flow. This estimation is only applicable when the exhaust gases by-pass is closed.

Torque and expander speed are measured in order to compute the power delivered by the expander. The Torque measuring unit used is 4550A200S10N1KA0 model made by Kistler. Its uncertainty is ±0.05% in full scale (200 Nm). Range and uncertainty of sensors are summarized in Table 3.3.

Table 3.3: Range and uncertainty of sensors

	Measurement principle	**Range**	**Uncertainty**
EG Pressure	Piezoresistive	0-2 bar	±0.05% FS
ET High Pressure	Piezoresistive	0-50 bar	±0.05% FS
ET Low Pressure	Piezoresistive	0-5 bar	±0.05% FS
Temperatures	K-type thermocouples (class 2)	(-270)-(1,372)K	±2.5°C
ET Flow Meter	Coriolis flow meter	0-2,720 kg/h	±0.1%
W Flow Meter	Electromagnetic flow sensor	0.3-1 m/s	±0.5% of rate
EG Flow Meter	Sensyflow FMT700-P	0-500 kg/h	±1% of rate
Expander Speed	Optical tachymeter	0-20,000 rpm	±1 rpm
Expander Torque	Strain gauges	0-200 Nm	±0.05%FS

An AVL GU13P piezoelectric pressure sensor (Figure 3.12) is placed inside the cylinder of one piston to evaluate the pressure oscillations during filling and emptying processes. The piezoelectric transducer is connected to a Kistler 5015 charge amplifier. The Pressure-Volume diagram is used to describe changes of volume and pressure in a system. Furthermore, a TDC sensor (Figure 3.12) and an angle encoder measure the position of the BDC. TDC sensor is an eddy current-sensor, which delivers a signal correlating to the distance between sensor and the swashplate. The piezoelectric pressure signal has been referenced using low frequency measurement (piezoresistive sensor). LabVIEW software is used to record all these signals with a sampling frequency of 50 kHz. In order to measure the expander speed with an ordinary brake, a pulley system is installed. It allows to increase the expander speed to a brake feasible speed. The brake used in the installation is an Eddy-Current Dynamo (Vibrometer 1WB65). On the other hand, an exterior oil loop lubricate the swash-plate expander.

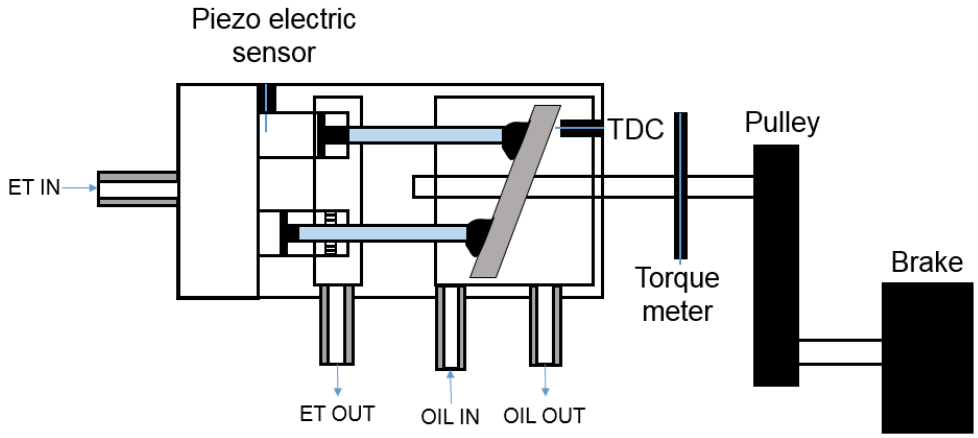

Figure 3.12: Swash-plate expander sensors

3.4 Stationary Tests

3.4.1 Operating points

A total of 28 steady-state points have been tested varying several parameters to evaluate cycle and expander efficiencies under a wide range of conditions. The global analysis of these points is presented in the sensitivity analysis, however, in order to evaluate the potential of this ORC only five operating points have been chosen for design and simulations. These points, listed Table 3.4, correspond to optimum points tested for each boiler power (5, 12, 20, 25 and 30 kW) of Figure 3.2.

Table 3.4: ORC operating points chosen for design and simulations bottoming cycle

	Op. Point 1	**Op. Point 2**	**Op. Point 3**	**Op. Point 4**	**Op. Point 5**
High pressure (bar)	14.8	15.7	18.7	24	24.8
Low pressure (bar)	2.3	1.9	2	2.5	2.5
Expansion ratio	6.4	8.3	9.2	9.4	9.5
Mass flow (kg/h)	16.67	39.95	64.95	82.01	102.87
Pump speed (rpm)	69	154	250	313	403
Expander speed (rpm)	1018	2527	3511	3021	3354
Expander torque (Nm)	2	2.7	3.5	5	5.2
Expander power (kW)	0.21	0.71	1.28	1.58	1.83
Boiler power (kW)	5	12	20	25	30

3.4.2 Steady State Control

The control of the installation at steady-state conditions has been made by following four states, which are presenting in Figure 3.13.

- STATE 0: Stop state
- STATE 1: HP, LP and ethanol mass flow of starting reference conditions. Boiler bypassed.
- STATE 2: The exhaust boiler conditions is at starting reference conditions. Vapor conditions into the expander. Expander bypassed.
- STATE 3: ORC cycle works at steady conditions.

All the states are connected by paths, which could prevent the installation from a dangerous situation during running conditions.

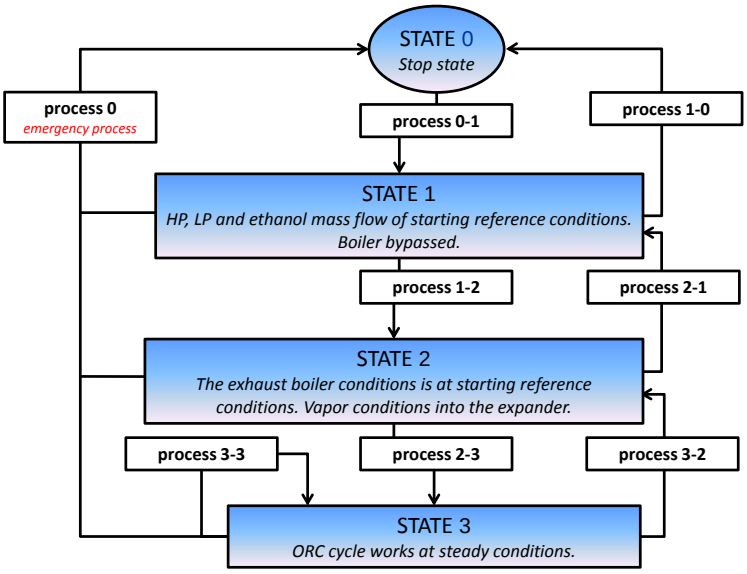

Figure 3.13: States of the electronic control

- **STATE 0: Stop state**
  The installation is filled with liquid ethanol at ambient conditions (Figure 3.14). The process 0-1 is activated manually. The setpoints are fixed as starting reference conditions ($\dot{m}_{ET}$ setpoint, HP setpoint, LP setpoint and $T_{in,pump}$ setpoint).

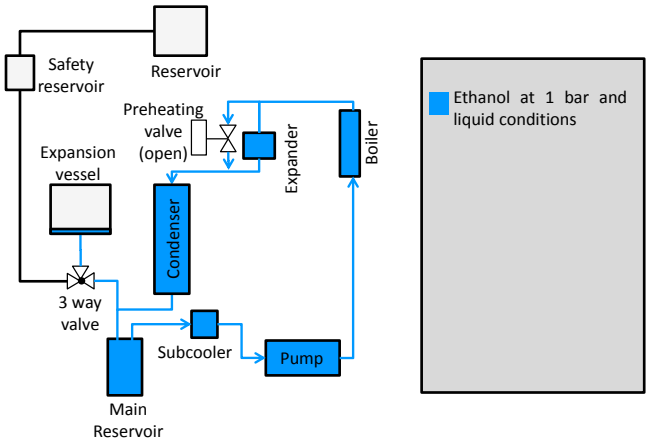

Figure 3.14: State 0

- **STATE 1: HP, LP and $\dot{m}_{ET}$ of starting reference conditions.**
  The ethanol flows in liquid state at the starting reference working point. The boiler bypass and preheating valve are open simultaneously (Figure 3.15). The process 1-2 is activated manually. The setpoints (ethanol mass flow setpoint, HP setpoint, LP setpoint and inlet expander temperature setpoint) are fixed using a control map from the exhaust gasses ($\dot{m}_{EG}$) and the inlet boiler temperature of exhaust gasses ($T_{in,b,EG}$).

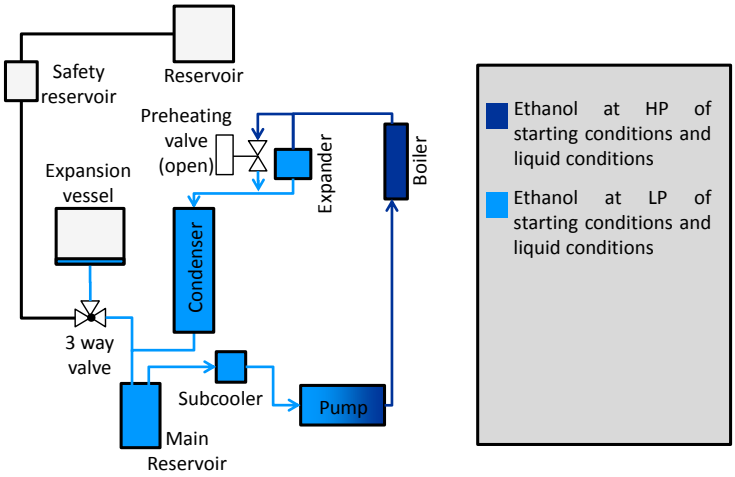

Figure 3.15: State 1

- **STATE 2: The exhaust boiler conditions is at starting reference conditions. Vapor conditions into the expander. Expander bypassed.**
  The ethanol flows at the starting reference working point with vapor conditions into the expander. The boiler bypass and preheating valve are closed simultaneously (Figure 3.16). The process 2-3 is activated manually. The setpoints (ethanol mass flow setpoint, HP setpoint, LP setpoint and inlet pump temperature setpoint) are fixed using a control map from the exhaust gasses ($\dot{m}_{EG}$) and the inlet boiler temperature of exhaust gasses ($T_{in,b,EG}$).

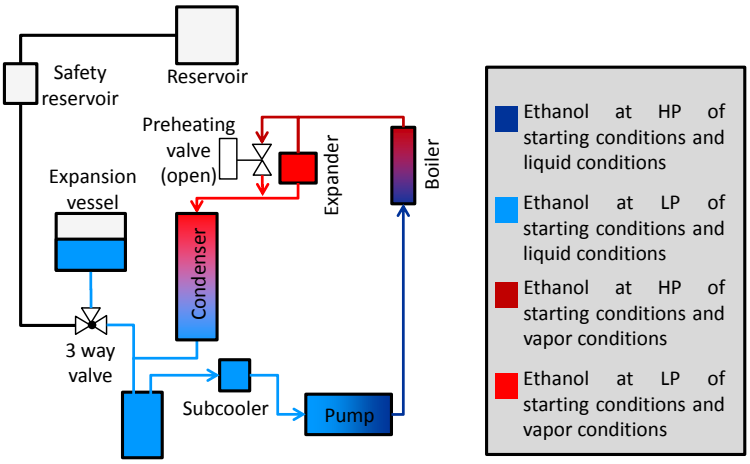

Figure 3.16: State 2

- **STATE 3: ORC cycle works at steady conditions.**
  The ethanol flows through the expander in the setpoint conditions. The boiler bypass and preheating valve are closed simultaneously. (Figure 3.17). The process 3-3 is activated manually. The setpoints (ethanol mass flow setpoint, HP setpoint, LP setpoint and inlet pump temperature setpoint) are fixed using a control map from the exhaust gasses ($\dot{m}_{EG}$) and the exhaust gasses inlet boiler temperature ($T_{in,b,EG}$).

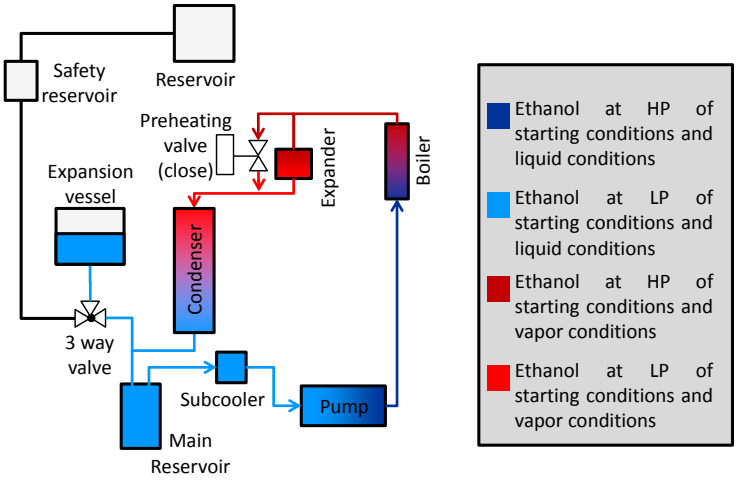

Figure 3.17: State 3

3.4.3 Energy Balances Analysis

Temperatures and pressures are measured at the inlet and outlet of the main elements of the system (boiler, expander, condenser and pump). Moreover, mass flow rates have been measured both in the ethanol, water and exhaust gases. Therefore, all the elements can be considered as black boxes with inlet power and outlet powers estimated using the following equations. Differences between inlet powers and outlet powers are the power losses of the different elements.

Boiler. The boiler inlet power is calculated from inlet and outlet measurements of exhaust gases temperatures and considering them as ideal gases, Equation 3.1.

$$P_{b,EG} = \dot{m}_{EG} \cdot (h_{in,b,EG} - h_{out,b,EG}) = \dot{m}_{EG} \cdot Cp_{EGt} \cdot (T_{in,b,EG} - T_{out,b,EG}) \quad (3.1)$$

Where Cp_{EGt} is the global specific heat at constant pressure for exhaust gases, $\dot{m}_{EG}$ is the exhaust gas mass flow through the installation, $T_{in,b,EG}$ and $T_{out,b,EG}$ are respectively the inlet and outlet exhaust gas temperature of the boiler in the exhaust gas side. Cp_{EGt} has been estimated considering the properties of the mixture (lean or rich) and Mayer's equation for ideal gases [107]. Depending on the ratio between fuel and air of each particular point a different equation is used, using Equation 3.2 when the mixture is rich and Equation 3.3 when the mixture is lean. Equation 3.4 and Equation 3.5 shows the correlation obtained for the specific heat at constant volume using the same methodology as Lapuerta [108] did for Diesel, but in this case for gasoline.

$$Cp_{EGt} = X_{gasoline} \cdot Cp_{gasoline} + X_{EG} \cdot Cp_{EG} \quad (3.2)$$

$$Cp_{EGt} = X_{air} \cdot Cp_{air} + X_{EG} \cdot Cp_{EG} \quad (3.3)$$

$$\begin{aligned} Cp_{EG} &= R + Cv_{EG} \\ &= R + (655.110 + 401.688 \times 10^{-3} \cdot T - 69.8091 \times 10^{-6} \cdot T^2 \\ &\quad - 9.31055 \times 10^{-9} \cdot T^3 + 2.53355 \times 10^{-12} \cdot T^4) \end{aligned} \quad (3.4)$$

$$\begin{aligned} Cp_{gasoline} &= R + Cv_{gasoline} \\ &= R + (-12.2910 \times 10^{6} \cdot T^{-2} + 227.580 \times 10^{3} \cdot T^{-1} - 1.54551 \times 10^{3} \\ &\quad + 10.8382 \cdot T - 8.37844 \times 10^{-3} \cdot T^2 + 3.25570 \times 10^{-6} \cdot T^3 \\ &\quad - 404.290 \times 10^{-12} \cdot T^4 - 72.7813) \end{aligned} \quad (3.5)$$

$$Cp_{air} = 226.527 \times 10^{-6} \cdot T + 977.898 \times 10^{-3} \tag{3.6}$$

Where Cp_{EG}, $Cp_{gasoline}$, Cp_{air} are the specific heat at constant pressure for exhaust gases, gasoline and air respectively. $X_{gasoline}$ is the fraction of additional gasoline respect to the stoichiometric mixture divided by the sum of fuel and air. X_{air} is the fraction of additional air respect to the stoichiometric mixture divided by the sum of fuel and air. X_{EG} is the remainder fraction of exhaust gases divided by the sum of fuel and air. Cv_{EG} is the specific heat at constant volume for exhaust gases. $Cv_{gasoline}$ is the specific heat at constant volume for gasoline. Cp_{air} is the specific heat at constant pressure for air and T is the temperature of exhaust gases. Cp_{EG} and $Cp_{gasoline}$ have been obtained using Mayer equation for ideal gases using Equation 3.4 and Equation 3.5. Cp_{air} is calculated by REFPROP develop by the National Institute of Standards and Technology of the United States. These correlations have been calculated using an average between inlet and outlet temperature. The outlet power of the boiler is calculated using inlet and outlet temperature and pressure measurements of ethanol in the boiler (Equation 3.7).

$$P_{b,ET} = \dot{m}_{ET} \cdot (h_{out,b,ET} - h_{in,b,ET}) \tag{3.7}$$

Where $h_{out,b,ET}$ and $h_{in,b,ET}$ can be obtained using temperature and pressure at the outlet and inlet of the boiler. The properties of ethanol are calculated by REFPROP develop by the National Institute of Standards and Technology of the United States.

Expander. The expansion power can be calculated based on Equation 3.8, Equation 3.9 and Equation 3.10 which corresponds to isentropic power, expansion power and shaft power respectively.

$$P_{exp,is} = \dot{m}_{ET} \cdot (h_{in,exp,ET} - h_{out,exp,ET,is}) \tag{3.8}$$

$$P_{exp,int} = \dot{m}_{ET} \cdot (h_{in,exp,ET} - h_{out,exp,ET}) \tag{3.9}$$

$$P_{exp,sh} = \tau_{exp} \cdot N_{exp} \cdot \frac{2 \cdot \pi}{60} \tag{3.10}$$

Where $h_{in,exp,ET}$ and $h_{out,exp,ET}$ have been calculated using temperature and pressures at the inlet and outlet of the expander. In Equation 3.8, $h_{out,exp,ET,is}$ is the isentropic enthalpy at the outlet of the expander, calculated from an isentropic expansion between the temperature and pressure inlet conditions and the pressure at the outlet of the expander in rpm. As regards shaft power, τ_{exp} is the expander torque and N_{exp} is the expander speed. In order to lubricate the

expander, a small quantity of oil has been added to the working fluid. It has been considered in the calculations, taking into account the percentage of oil and estimating its calorific capacity using its data sheet.

Condenser. The outlet power of the condenser is calculated using inlet and outlet conditions of water in the condenser, considering them as an incompressible fluid (Equation 3.11).

$$\begin{aligned} P_{cond,W} &= \dot{m}_W \cdot (h_{out,cond,W} - h_{in,cond,W}) \\ &= \dot{m}_W \cdot Cp_W \cdot (T_{out,cond,W} - T_{in,cond,W}) \end{aligned} \tag{3.11}$$

Where Cp_W is the specific heat at constant pressure for water, $\dot{m}_W$ is the water mass flow through the installation, $T_{in,cond,W}$ and $T_{out,cond,W}$ are respectively the inlet and outlet exhaust water temperature of the boiler in the condenser. Cp_W has been considerate 4.18 kJ/kgK for water. The inlet power of the condenser is calculated using inlet and outlet temperatures and pressures of ethanol in the condenser, Equation 3.12.

$$P_{cond,ET} = \dot{m}_{ET} \cdot (h_{in,cond,ET} - h_{out,cond,ET}) \tag{3.12}$$

Where $h_{in,cond,ET}$ and $h_{out,cond,ET}$ can be obtained using temperature and pressures at the inlet and outlet of the condenser.

Pump. The outlet power of the pump is calculated using inlet and outlet temperatures and pressures of ethanol in the pump. It is calculated using Equation 3.13. The assumption of incompressible fluid is imposed. It is defined using the isentropic efficiency.

$$\begin{aligned} P_{pump,ET} &= \dot{m}_{ET} \cdot (h_{out,pump,ET} - h_{in,pump,ET}) \\ &= \dot{m}_{ET} \cdot \frac{1}{\rho_m} \cdot (P_{out,pump,ET} - P_{in,pump,ET}) \end{aligned} \tag{3.13}$$

Where ρ_m is the average density considering inlet and outlet conditions, $P_{in,pump,ET}$ is the pressure at the inlet of the pump in bar and $P_{out,pump,ET}$ is the pressure at the outlet of the pump in bar. The pump electric power in kW can be calculated by Equation 3.14.

$$P_{pump,el} = \sqrt{3} \cdot U_l \cdot I_l \cdot \cos\varphi \tag{3.14}$$

Where U_l is the line voltage and I_l is the line current of the three-phase pump. In this particular case U_l corresponds to 400V and $\cos\varphi$ corresponds to 0.57.

3.4.4 Experimental results (Energy Balances)

Previous equations have been applied to calculate the power balances in the main components of the system: Boiler, condenser, swash-plate expander and pump. Table 3.5 shows the power balances in all the elements of the installation. The reduction of the engine load (from operating point 5 to 1) results in a decrease in the temperature and mass flow of the exhaust gases and, thus, the heat absorbed in the boiler, as shown the 1st and 2nd columns of Table 3.5. As expected, the greater power in the boiler is absorbed, the greater amount of energy in the shaft of the expander is produced, as shown in columns 5th, 6th and 7th of Table 3.5. Regarding the boiler heat efficiency (ratio of $P_{b,ET}$ and $P_{b,EG}$), it varies from 93% to 98% depending on the operating point. Regarding the boiler recovery effectiveness (ratio of the heat transferred and the maximum heat transfer rate), it varies from 95% to 99% depending on the operating point.

Table 3.5: Power balances in the system (kW)

Op.P	$P_{b,EG}$	$P_{b,ET}$	$P_{cond,ET}$	$P_{cond,W}$	$P_{exp,is}$	$P_{exp,int}$	$P_{exp,sh}$	$P_{pump,ET}$	$P_{pump,el}$
5	5.36	5.03	4.2	4.7	0.74	0.64	0.21	0.007	0.063
12	12.07	11.72	10.31	9.91	1.93	1.18	0.71	0.02	0.102
20	19.45	18.86	16.86	16.39	3.2	1.7	1.28	0.039	0.118
25	24.22	23.35	20.95	21.03	4.14	2.1	1.58	0.045	0.157
30	29.51	28.95	26.16	25.21	5.18	2.47	1.83	0.085	0.195

As shown also in Figure 3.18, the expansion power produced by the expander increases as the power absorbed by the boiler is magnified. It should be noted that the difference between boiler power and cooling water power does not remain constant, increasing with the power of the boiler. On the other hand, power in the pump can be neglected. As shown in Figure 3.18 the maximum expansion power is achieved under 30 kW (operating point number 5), reaching an expander power of 1.83 kW.

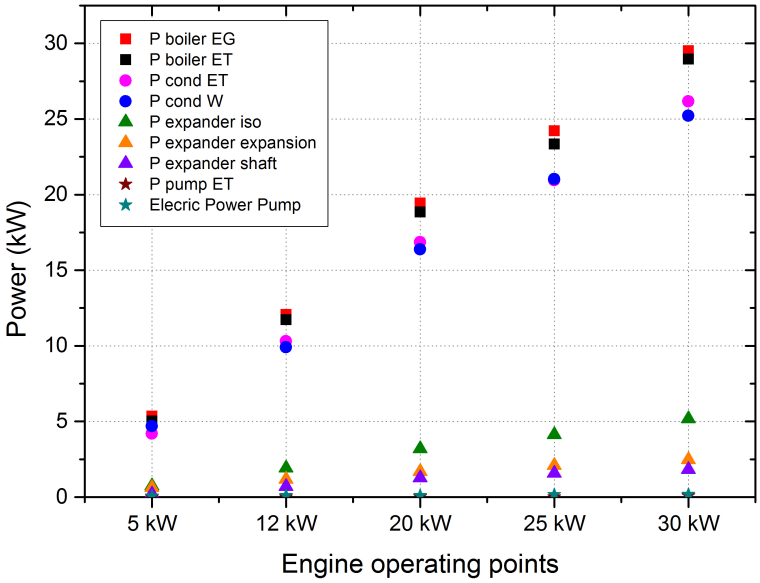

Figure 3.18: Power balances operating points

The energy balance is reflected in Figure 3.18. Under the five operating points, energy balances fit quite well and the maximum deviation is 0.91 kW at the point of 30 kW, which represents a relative deviation of 3%. Differences could be explained due to inaccuracies in specific calorific power estimations in both the water and the exhaust gases, and in the uncertainties of temperature measurement. On the contrary, although pipes are insulated, heat losses to the environment could appear. In order to estimate the global balance of the cycle the sum of $P_{b,ET}$ and $P_{pump,ET}$ has been compared with the sum of $P_{cond,ET}$ and $P_{exp,int}$ and the maximum deviation is 0.405 kW at 30 kW point.
The energy balances for 30 kW are gathered in Figure 3.19 using a Sankey Diagram. The Sankey Diagram is divided in two parts: The first one corresponds to the ICE energy balance, which results in 32% of brake power, 31% of exhaust gases energy and 37% in cooling water energy. In the exhaust line, a heat loss of 1% is released to the ambient. The 30 % remainder goes to the evaporator. An additional energy of 0.16 % comes from the pump to the evaporator. Considering that the temperature at the outlet of the boiler is not ambient temperature and heat losses to the ambient, 19 % of the energy goes to the expander. The last part shows the mechanical power delivered by the expander, which results in a global expander isentropic efficiency of approximately 38%. The remainder

power is released as heat to the environment and the condenser. Part of the energy in the condenser is transferred to the pump and the cycle starts again.

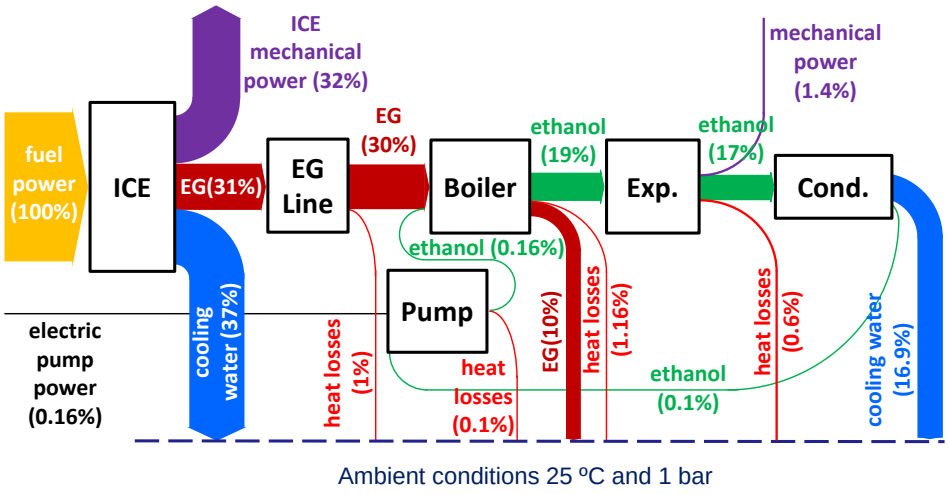

Figure 3.19: Sankey Diagram of 30kW

Similar tendencies are appreciated in the remaining boiler power Sankey diagrams, but 30 kW is represented due to its greater recovery potential and its lower level of uncertainty in measurements.

3.4.5 Cycle efficiencies

Engine-ORC efficiencies. Efficiency of the Gasoline engine (η_{eng}) is the ratio of the total engine brake power and the calorific fuel power:

$$\eta_{eng} = \frac{P_{eng}}{Q_{fuel}} \tag{3.15}$$

Where P_{eng} is the brake power of the gasoline engine (calculated using the engine torque, τ_{eng} and the engine speed, N_{eng}) and Q_{fuel} is the fuel calorific power.
Efficiency of the system ORC-engine ($\eta_{ORC,eng}$) is the ratio of the difference between mechanical expansion power ($P_{exp,sh}$) and the electric power consumed by the pump ($P_{pump,el}$) to the total power obtained from the calorific value of the injected fuel (Q_{fuel}). It is defined in Equation 3.16.

$$\eta_{ORC,eng} = \frac{P_{exp,sh} - P_{pump,el}}{Q_{fuel}} \tag{3.16}$$

Efficiency of the system ORC-engine-mechanical ($\eta_{ORC,eng,mec}$) is the ratio of the difference between mechanical expansion power ($P_{exp,sh}$) and the electric power consumed by the pump ($P_{pump,el}$) to the mechanical power of the engine (P_{eng}).

$$\eta_{ORC,eng,mec} = \frac{P_{exp,sh} - P_{pump,el}}{P_{eng}} \tag{3.17}$$

Where P_{eng} is the mechanical power of the gasoline engine defined in Equation 3.15. The available power of the exhaust gases can be expressed as Equation 3.18:

$$\eta_{EG} = \frac{P_{b,EG}}{Q_{fuel}} \tag{3.18}$$

Where $P_{b,EG}$ is the available power between inlet and outlet conditions of exhaust gases and Q_{fuel} is the total power obtained from the calorific value of the injected fuel.

Rankine and Carnot efficiencies. Three global efficiencies are taken into account: Carnot efficiency (Equation 3.19), the ideal Rankine efficiency (Equation 3.20) and real Rankine efficiency (Equation 3.21).

$$\eta_{carnot} = 1 - \frac{T_l}{T_u} \tag{3.19}$$

Where T_l and T_u are respectively, the average lower temperature and the average upper temperature of the cycle process.

$$\eta_{Rankine,ideal} = \frac{P_{exp,is} - P_{pump,ET}}{P_{b,ET}} \tag{3.20}$$

Where $P_{exp,is}$ is the expansion power delivered by the expander considering an isentropic process, $P_{pump,ET}$ is the power decrease between inlet and outlet conditions of ethanol in the pump and $P_{b,ET}$ is the power increase between inlet and outlet conditions of ethanol in the boiler.

$$\eta_{Rankine,real} = \frac{P_{exp,sh} - P_{pump,el}}{P_{b,EG}} \tag{3.21}$$

Where $P_{exp,sh}$ is the shaft power delivered by the expander, $P_{pump,el}$ is the electric power required to pressurize the ethanol in the pump and $P_{b,EG}$ is the power increase between inlet and outlet conditions of exhaust gases in the boiler. In later versions of this ORC cycle prototype, the ethanol pump will be coupled directly to the IC engine shaft, whereby the power consumed by the pump could be reduced.

Expander efficiencies. Two performance indexes are considered: The expander isentropic efficiency, presented in Equation 3.22, and the volumetric efficiency, presented in Equation 3.23.

$$\eta_{exp,is} = \frac{P_{exp,sh}}{P_{exp,is}} \tag{3.22}$$

$$\eta_{exp,vol} = \frac{\dot{m}_{ET}}{\rho_{ET} \cdot \frac{N_{exp}}{60} \cdot D} \tag{3.23}$$

Where $P_{exp,sh}$ and $P_{exp,is}$ are the mechanical power of the expander shaft and the isentropic expansion power respectively, $\dot{m}_{ET}$, ρ_{ET} are the mass flow through the expander and the density of the ethanol at the inlet of the expander. Moreover, N_{exp} and D are the expander speed and the volume displaced by the expander.

3.4.6 Experimental results (Cycle efficiencies)

A summary of the engine ORC efficiencies obtained for each operating point is presented in Table 3.6. These values are plotted in Figure 3.20.

Table 3.6: Engine ORC efficiencies

Op. Points (kW)	$\eta_{eng}(\%)$	$\eta_{ORC,eng,mec}(\%)$	$\eta_{ORC,eng}(\%)$	$\eta_{EG}(\%)$
5	30.56	1.19	0.36	13.06
12	31.24	2.79	0.87	17.22
20	32.07	3.61	1.16	19.41
25	32.3	3.7	1.19	20.29
30	31.86	3.65	1.16	20.96

Figure 3.20 shows engine ORC efficiencies for each operating point of the engine. The efficiency of the gasoline engine (η_{eng}) remains almost constant for all operating points, slightly increasing with operating points up to 25 kW and decreasing gradually with the highest engine operating point due to higher mechanical losses and engine optimization characteristics.

As regards recovery potential from exhaust gases (η_{EG}), it increases significantly with the engine operating point. The reason is that whilst the engine operating point keeps rising, fuel injected increases as well and consequently, large quantity of energy is available in the exhaust gases. Although the amount of fuel entered to the engine is high, this is lower than the power of the exhaust gases.

This efficiency (η_{EG}) represents the maximum energy that could be absorbed from the exhaust gases, which varies from 13.06% at lower loads and 20.96% at higher loads. Nevertheless, in the ORC there are several irreversibilities, such as friction losses, non isentropic processes and heat losses to the environment. Thus, the maximum efficiency that could be reached in the cycle decreases greatly regarding the exhaust gases efficiency (η_{EG}).

Similar tendencies are shown in the efficiency of the gasoline engine (η_{eng}) and the efficiencies concerning fuel input power ($\eta_{ORC,eng}$) and mechanical engine power ($\eta_{ORC,eng,mec}$). They both follow a similar tendency, reaching during the test with our bill of material based on prototype and not optimized, a maximum value of 1.19% and 3.7% respectively with 25 kW. Although higher recovery potential in the exhaust gases (η_{EG}) is observed with increasing operating points, different trends are shown in $\eta_{ORC,eng}$ and $\eta_{ORC,eng,mec}$. In both indexes the maximum value is obtained at 25 kW due to the fact that, as shown in Table 3.5, lower expander speeds are required at 25 kW comparing to 20 kW and 30 kW. Therefore, mechanical losses are minimized at this point.

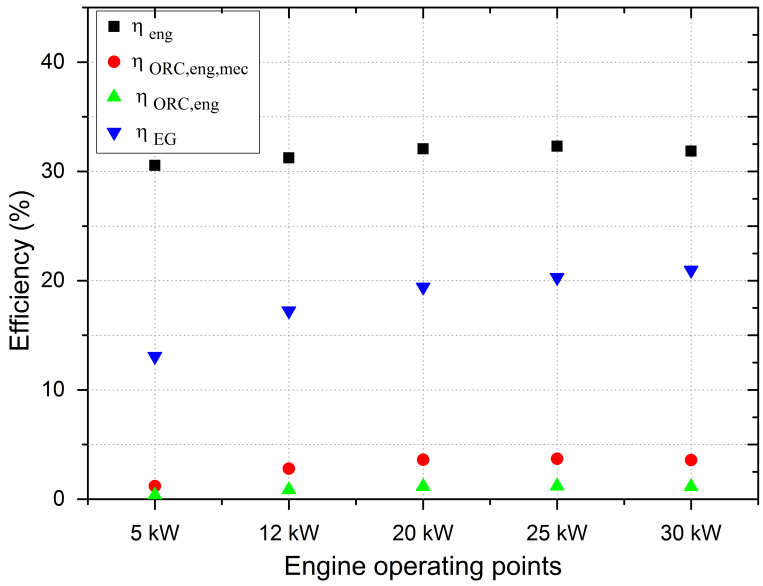

Figure 3.20: Engine ORC efficiencies for operating points

A summary of the Rankine (ideal and real) and Carnot efficiencies obtained for each operating point is presented in Table 3.7. Under these five conditions, the Carnot efficiency, η_{carnot}, decreases when the operating point increases, whereas, the efficiency of the Rankine cycle, $\eta_{Rankine,ideal}$, increases constantly with the increase of the operating point. As regards $\eta_{Rankine,real}$, it can be seen that it reaches its maximum value at 20 kW.

Table 3.7: Rankine and Carnot efficiencies

Op. Points (kW)	$\eta_{carnot}(\%)$	$\eta_{Rankine,ideal}(\%)$	$\eta_{Rankine,real}(\%)$
5	80.78	14.6	2.79
12	79.31	16.37	5.07
20	78.63	17.26	5.97
25	78.35	17.47	5.89
30	76.81	17.62	5.55

The Carnot efficiency is a theoretical efficiency estimation considering an ideal approach based on a cycle process made up by isentropic compression and expansion and isochoric supply and heat transfer. The evolution of Carnot efficiency shows a flat trend in all operating points. It can be seen that, it decreases slightly with the increasing operating point due to the increase in the lower level of temperature in the cycle for higher operating points. It reaches its maximum value of 80.78% at 5 kW operating point.
The Rankine ideal efficiency computes the ideal amount of energy available in the cycle, so that, it increases as the power of exhaust gases is magnified because higher quantity of energy is available at the exhaust gases and thus, the isentropic power of the expander is higher. Its reaches its maximum value of 17.62% at 30 kW operating point.
On the other hand, Rankine real efficiency takes into account irreversibilities of the expander, thus, its maximum is not obtained in the maximum boiler power, but at 20 kW with a value of 5.97%. Contrary to Rankine ideal efficiency, which keeps rising with increasing operating points, the Rankine real efficiency reach a peak at 20 kW due to, as it can be seen in Table 3.4, optimal expander conditions are fixed, using a expander speed of 3511 rpm and an expansion ratio of 9.2. These conditions seem to be the best ones where the working fluid expansion fits better with volumetric expansion ratio of this swash-plate expander.

To sum up, although there is a great recovery potential in the exhaust gases of ICE, the influence of adding an expansion machine is clearly visible comparing Carnot efficiency (approximately 80%) to ideal Rankine efficiency (approximately 17%), which takes into account an isentropic expansion machine, and to real Rankine efficiency (approximately 6%), which takes into account irreversibilities of the process, including heat losses to the environment and pressure drop.

3.4.7 Sensitivity Analysis

In this section 28 steady-state points are analyzed to evaluate cycle and expander efficiencies under different expander parameters, i.e. expansion ratio, expander speed and outlet pressure of the expander. For each boiler power (5, 12, 20, and 25 kW) two different outlet expander pressures are tested. Increasing operating points with higher mass flows are tested by changing pump speed. The lower pressure limit is imposed due to limitations of cooling temperature in the vehicle cooling system. It is controlled by the balloon pressure of the expansion vessel. Tests are performed changing expander speed from 1000 to 5000 rpm. High pressure is imposed by the expander speed regulation. Temperature at the inlet of the expander is fixed around 225°C in order to maintain a certain degree of superheating.

Engine ORC efficiencies. Figure 3.21 shows the variation of shaft power with expansion ratio for different boiler power. The expander shaft power appears to increase at first and then reaches a maximum of 0.213 kW, 0.677 kW, 1.171 kW and 1.57 kW at 5 kW, 12 kW, 20 kW and 25 kW respectively. Sequentially, the power delivered by the expander decreases with increasing expansion ratios (above the value of 6.4 with 5 kW, 7.6 with 12 kW and 9.4 with 20 and 25 kW). When the expansion ratio is lower than the optimum one, leakages effects and over-expansion losses appear, whereas, when the expansion ratio is above the optimum point, under expansion effects are shown. In both cases, the expander shaft power is reduced. The optimum value is performed when the working fluid expansion ratio matches with the built-in volumetric expansion ratio.

The same tendency could be noticed in every boiler power. The maximum shaft power is gained under the boiler operating point of 25 kW (30 kW studies are not performed) and running expander speed at 3000 rpm, with a shaft power value of 1.57 kW.

Variation of $\eta_{ORC,eng,mec}$ with expansion ratio are gathered in Figure 3.22. The reduction of engine operating load from operating point 5 to 1 results in a efficiency drop from 3.7% to 0.5%. Similar tendencies as Figure 3.21 are shown in Figure 3.22. It reveals that the maximum $\eta_{ORC,eng,mec}$ of each boiler power is obtained by increasing expansion ratios until a maximum value, i.e. 1.19% in 5kW, 2.59% in 12kW, 3.15% in 20kW and 3.7% in 25kW. It can be concluded that under high engine operating points a potential of improvement in engine mechanical efficiency could be made, by increasing it upon conventional engine at least in a 3.7%.

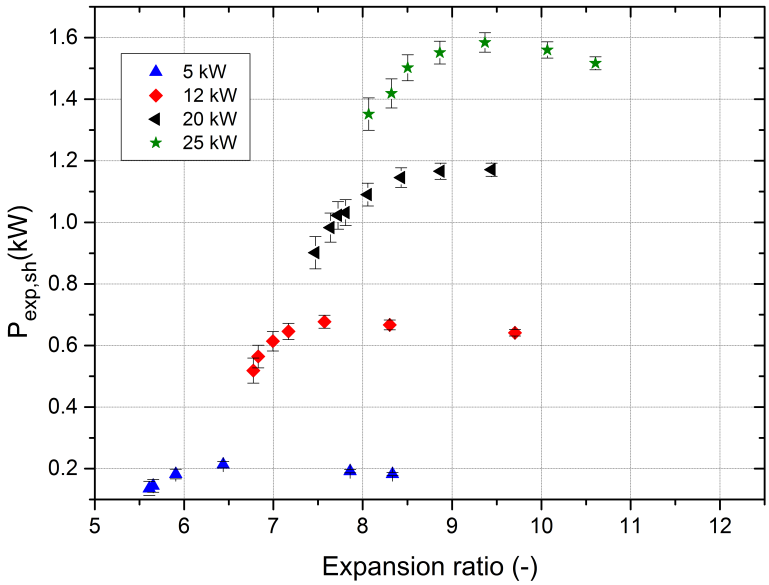

Figure 3.21: Variation of shaft power delivered by the expander with expansion ratio for different boiler power

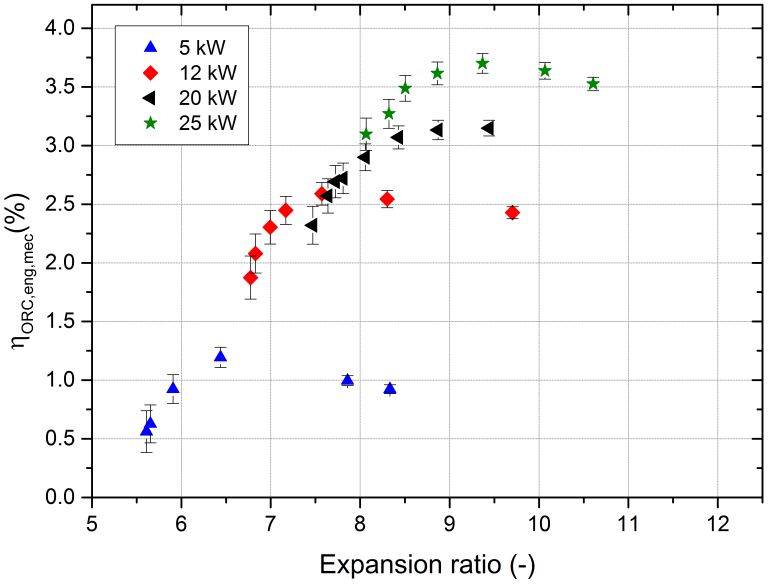

Figure 3.22: Variation of $\eta_{ORC,eng,mec}$ with expansion ratio

Similar tendencies in $\eta_{ORC,eng,mec}$ and the power delivered by the expander could be seen comparing Figure 3.21 and Figure 3.22, except for curves with 20 kW and 25 kW, which seems to collapse in a single curve at low expansion ratios. Uncertainty propagation of the measured values ($P_{exp,sh}$, $\eta_{ORC,eng,mec}$, $\eta_{Rankine,ideal}$ and $\eta_{Rankine,real}$) have been calculated as a function of one or more measured variables upon which they depend. This Method is described in NIST Technical Note 1297 [109]. They are shown from Figure 3.21 to Figure 3.24.

Rankine efficiencies. Figure 3.23 and Figure 3.24 present ideal and real Rankine efficiencies respectively.

Rankine ideal efficiency is calculated taking into account isentropic power and heat absorbed by the ethanol. As shown in Figure 3.23, ideal Rankine efficiency in the system increases with the expansion ratio (from 5.5 to 11), following a similar tendency in every boiler power. Increments in expansion ratios involved increments in the differences of high and low temperatures of the cycle and greater isentropic power delivered by the expansion process. Thus, in each boiler power, as the expansion ratio increases, the isentropic power enhances while the rest of the parameters that affect Rankine ideal efficiency, $P_{b,ET}$ and $P_{pump,ET}$, does not significantly change. Rankine ideal efficiency increases with expansion ratio because it is considered inlet (enthalpy) and outlet (pressure) conditions to calculate isentropic power. Ideal Rankine efficiencies varies from 14% to 19%. Similar values are reported in literature [99].

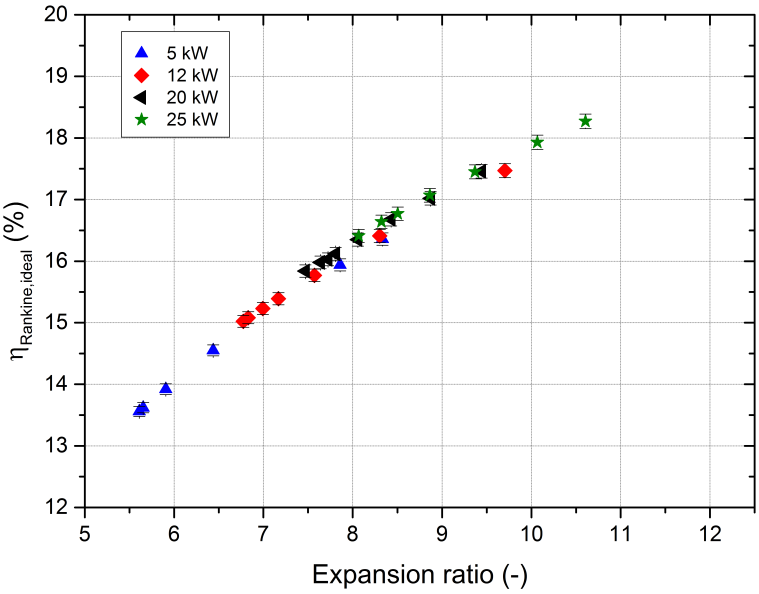

Figure 3.23: Variation of $\eta_{Rankine,ideal}$ with expansion ratio for different boiler power

In Figure 3.24 Rankine real efficiency is reported as a function of the expansion ratio, for different boiler power. It shows a global tendency similar to Figure 3.23. As stated before, the maximum Rankine real efficiency for each boiler power is obtained increasing expansion ratio with peaks at 6.4, 7.6 and 9.4 at 5, 12 and 20/25 kW respectively. Differences between ideal and real Rankine efficiency exist due to irreversibilities of the expansion machine and external irreversibilities in the boiler. Therefore, although a potential Rankine efficiency of 19% is obtained at high operating points using an ideal isentropic machine, indeed, a maximum real Rankine efficiency of 6% is achieved considering heat losses to the environment and real expansion and compression processes.

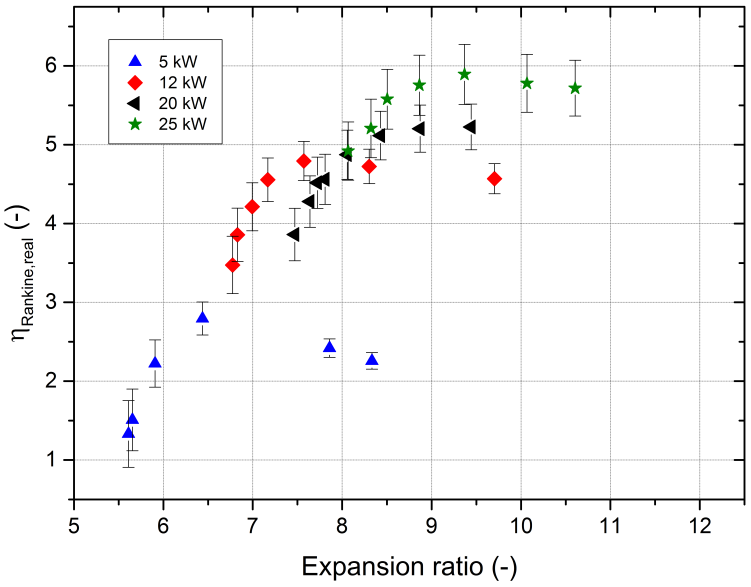

Figure 3.24: Variation of $\eta_{Rankine,real}$ with expansion ratio

Expander efficiencies. Volumetric efficiency could be used to compute engine performance in terms of movement of charge into and out of the cylinders. It is used to evaluate the intake process and to compare different intake technologies. Volumetric efficiency as a function of expander speed and expansion ratio is plotted in Figure 3.25 for the same points of previous figures.
As shown in Figure 3.25, volumetric efficiency is a monotonically decreasing function of expander speed and increasing with expansion ratio. In these points, a maximum value of 38.5% is reached at 5 kW. As the expander speed rises up, less time is available to introduce ethanol in the cylinders, which results in lower volumetric efficiencies, obtaining a lower value of 5% at the highest expander speed (5500 rpm). In terms of expansion ratio, the higher it is, the better volumetric efficiency is achieved because higher expansion rates involved higher inlet pressures, which will force the ethanol to enter the cylinders.

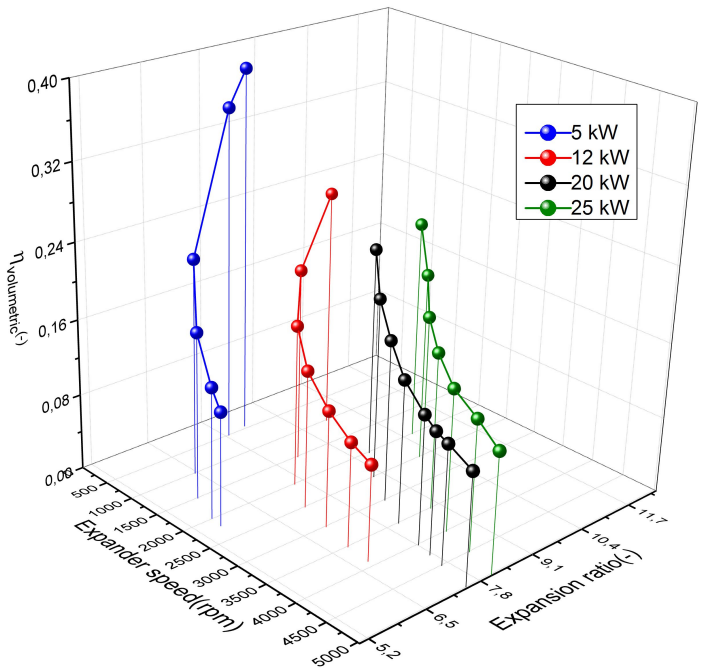

Figure 3.25: Variation of volumetric efficiency with expansion ratio and expander speed

The second important performance parameter of the expander is the isentropic efficiency calculated by Equation 3.22. As it is indicated in Figure 3.26, the isentropic efficiency reaches a maximum, which is different depending on the boiler power and the outlet pressure at the expander. Thus, the pressure ratio that maximizes the isentropic efficiency is not constant for all rotational speeds. Leakages, friction losses, pressure drop at the inlet and outlet processes and heat losses [82] could influence this peak of isentropic efficiency. The maximum value, 38.2%, is obtained with an expander speed of 3021 rpm and an expansion ratio of 9.4 at the point of 25 kW. For each boiler power it could be seen that lower expander speeds and higher pressure ratios lead to an expander performance drop due to the effect of leakages, whereas higher expander speed and lower pressure ratios lead to a sharply reduction in the expander isentropic efficiency due to the effect of mechanical losses and intake pressure drop. Therefore, there is an optimal expander speed and expansion ratio for each boiler power and outlet pressure. Peaks of isentropic efficiency corresponds to 28.8% (5 kW), 36.4% (12 kW), 34.6% (20 kW) and 38.3% (25 kW).

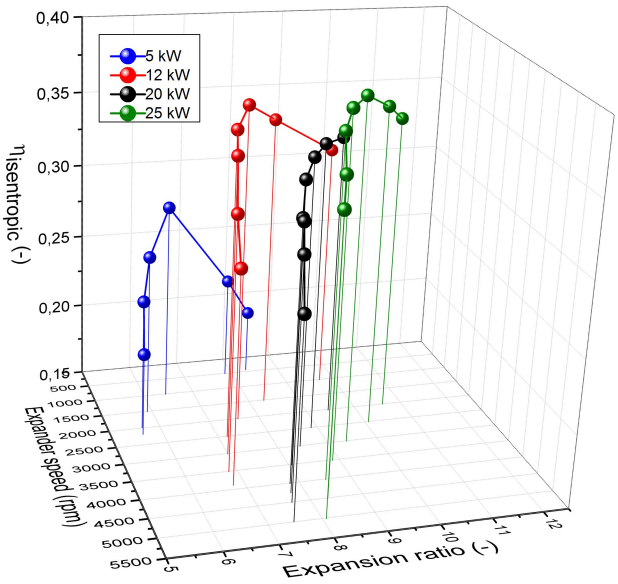

Figure 3.26: Variation of isentropic efficiency with expansion ratio and expander speed

To sum up, the pressure ratio that optimizes the isentropic efficiency is not constant for all boiler powers (Figure 3.26). The maximum value is fixed by the built-in volumetric expansion ratio, which for this particular expander corresponds to a value of 7.633. However, it only matches this value at low boiler powers. With low boiler power (5 kW), the ethanol mass flow pumped through the installation is lower than the one circulating in 25 kW. If the ethanol mass flow is low, lower expander speeds are required to fill in the cylinders and therefore, lower inlet pressures (and expansion ratios) are obtained. This behaviour can be observed in Figure 3.25, getting higher volumetric efficiencies with lower boiler power and lower expander speeds. Therefore, higher boiler powers implies higher ethanol mass flows and higher expander speeds. Consequently, higher pressure ratios are required during the intake and exhaust processes of the expander in order to enter the ethanol into the cylinders. Because of this, the optimal pressure ratio between the inlet and outlet of the expander increases as the power available to the expander increases. Volumetric and isentropic efficiencies have been correlated using points discussed in previous chapters in order to model the entire ORC system. It will allow developing an indispensable tool to simulate steady and transient points and for being able to identify the influence of the operating parameters and predict the behaviour of the system at critical operating points.

3.5 Transient Tests

3.5.1 Operating points

Three engine operating points have been chosen in this tests (12 kW, 20 kW and 25 kW) (Figure 3.2). The vehicle model within the test bench is the Ford Explorer. As Table 3.1 shows, these points correspond with 84 km/h (12 kW power in the boiler), 106 km/h (20 kW power in the boiler) and 114 km/h (25 kW power in the boiler). Transient tests are performed varying from 84 km/h to 114 km/h and from 106 km /h to 114 km/h to understand the behaviour and inertia of the system.

3.5.2 Dynamic control

The control of the installation on dynamic conditions has been made using five actuators: IC engine conditions (exhaust gases power), speed of the pump, expander speed, expander vessel pressure (low pressure in the cycle) and the cooling mass flow through the condenser. These actuators can change the behaviour of the ORC system:

- Exhaust gases power (P_{EG}), in order to estimate the engine operating point. In a real ORC system for WHR in a IC engine, this engine working point is not an actuator to control the system, it is a boundary condition which is imposed to the system. It is obtained from measuring the exhaust gases temperature at the inlet of the boiler ($T_{in,b,EG}$) and at the outlet ($T_{out,b,EG}$) and the exhaust gases mass flow ($\dot{m}_{EG}$).
- The speed of the pump (N_{pump}), in order to control the mass flow of ethanol flowing through the installation. It is affected by the exhaust gases power and the temperature at the outlet of the boiler ($T_{out,b,ET}$).
- The expander speed (N_{exp}), in order to control the high pressure at the inlet of the expander. A brake coupled to the expander shaft fixes this speed. The brake speed is obtained from the exhaust power released in the boiler. Depending on the exhaust gases power, the optimal expander speed is fixed by means of previous parametric studies in steady and optimal conditions for each particular power.
- The expander vessel pressure, in order to control the low pressure in the system.
- The cooling mass flow, in order to avoid cavitation in the pump.

Transient tests are performed changing the exhaust gases power from an initial to a final engine operating point. During the transient, low pressure of the cycle

is settled to 2 bar and the cooling mass flow to 672 l/h to avoid cavitation in the pump. The speed of the pump (N_{pump}) and the speed of the expander (N_{exp}) have been controlled by using an adaptive control, presenting in Figure 3.27. Red arrows correspond to inputs of the system, while blue ones correspond to outputs. Different steady-state maps, obtained from previous steady tests, are implemented in the control. Table 3.8 summarizes the inputs and outputs of the system.

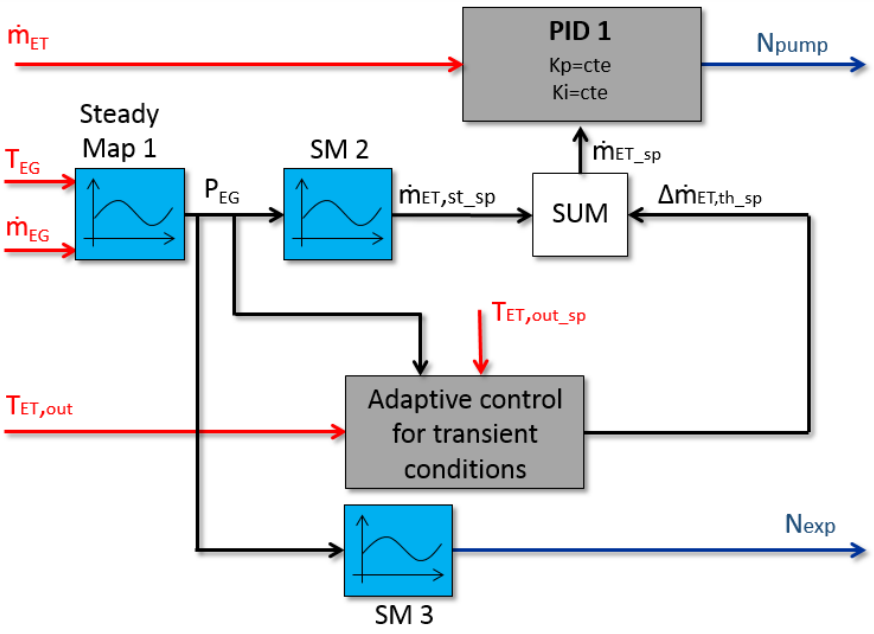

Figure 3.27: Dynamic control diagram

Table 3.8: Inputs and outputs of the ORC control

Variable name	Description	I/O
$\dot{m}_{ET}$	Ethanol mass flow	Input
$T_{in,b,EG}$	Inlet exhaust gases temperature	Input
$T_{out,b,EG}$	Outlet exhaust gases temperature	Input
$\dot{m}_{EG}$	Exhaust gases mass flow	Input
$T_{ET,out}$	Temperature at the outlet of the boiler	Input
$T_{ET,out,sp}$	Temperature at the outlet of the boiler set point	Input
N_{pump}	Pump speed	Output
N_{exp}	Expander speed	Output

The exhaust gases mass flow ($\dot{m}_{EG}$) and the temperatures at the inlet ($T_{in,b,EG}$) and outlet of the boiler ($T_{out,b,EG}$) in the exhaust gases side are measured; therefore, an estimation of the power released by the exhaust gases is obtained (P_{EG}) by using steady-state map (**SM 1**). In the ethanol side, both the ethanol mass flow ($\dot{m}_{ET}$) and the temperature at the outlet of the boiler ($T_{ET,out}$) are inputs of the control.

Using steady-state map (**SM 2**), an initial ethanol mass flow set point is specified ($\dot{m}_{ET,st,sp}$). However, in the steady tests, as the temperature vary smoothly, the control system does not take into account effects of transients.

During transient conditions, once the operating point is changed, the control should consider two interconnected phenomena: High inertia (temperatures) and low inertia (mass flows and pressures) thermodynamic variables. Therefore, the heating process (mainly produced in the heat exchangers) will be heavily affected by the low inertia thermodynamic variables (temperatures) and the expansion - compression processes (mainly produced in the expander and the pump respectively) will be heavily affected by the high inertia thermodynamic variables (pressures and mass flows). For this reason, in an ORC system, changes in the pump and expander speed have a fast time response (lower than 1 s), because they affect mainly to pressures and mass flows in the system. However, changes in the heat transferred by the heat exchangers (boiler and evaporator) have a higher time response (40 s) because its main function is to heat or cool down the ethanol, and therefore they affect mainly to the temperatures in the system. Thus, an adaptive part of the control corrects the ethanol mass flow set point of steady conditions to take into account the high inertia elements. The correction ($\Delta\dot{m}_{ET,th,sp}$) is applied to the initial ethanol mass flow ($\dot{m}_{ET,st,sp}$). The result signal ($\dot{m}_{ET,sp}$) is compared to the actual ethanol mass flow through the system (measured by a Coriolis mass flow meter) and using PID 1 the pump speed set point for transient conditions is obtained (N_{pump}).

The correction ($\Delta\dot{m}_{ET,th,sp}$) takes into account the dynamic conditions of the boiler and deviation between the temperature signal at the outlet of the boiler ($T_{ET,out}$) and the ethanol temperature reference of steady conditions, setting by an external threshold $T_{ET,out,sp}$. This temperature is fixed by the working fluid in order to avoid degradation. In these tests, the working fluid is ethanol; therefore, the maximum temperature is 240 °C. However, in these particular tests the temperature is 210 °C in order to ensure a stable operation of the working fluid. The adaptive control consists of two inputs (P_{EG} and ΔT) and two outputs corresponding to the proportional and integral constant of the PID (Kp and Ki). Depending on the exhaust power required and the difference of temperatures between the measurement ($T_{ET,out}$) and the set point

($T_{ET,out,sp}$) a specific value for Kp and Ki is obtained. Values of adaptive control are progressively adjusted from experimental tests. Different values of Kp and Ki are implemented in the control to avoid condensation at the expander inlet when the engine operating point changes from a lower to a higher exhaust power and superheating (and thus ethanol degradation due to high temperatures) in the opposite case. When the engine operating point changes from a lower to a high power, the ethanol mass flow should not change rapidly because the boiler is not hot enough and condensation could appear if there is not enough power to maintain the temperature at the outlet of the boiler. Regarding the expander, a steady state map (**SM 3**) is used to fix the optimum expander speed for each boiler power (P_{EG}).

3.5.3 Experimental results P-V Diagram

P-V Diagram Calculation. The expander performance has been characterized by the calculation of the indicated diagram Pressure-Volume (Figure 3.28). It is used to describe changes of volume and pressure of a system. Red and green crosses indicate the intake and exhaust valve closing angle (or volume) respectively. Red and green circles indicate the intake and exhaust valve opening angle (or volume) respectively. The area enclosed by the P-V curve represents the work delivered by one piston in each cycle.

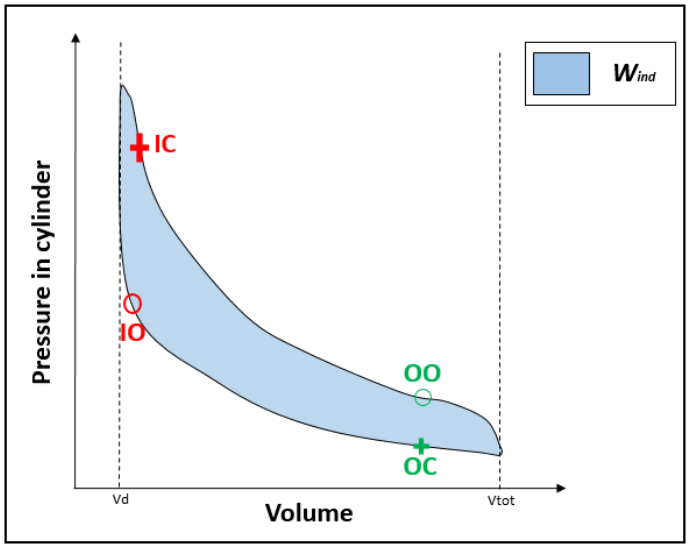

Figure 3.28: Pressure-Volume diagram

P-V diagram can be obtained using a piezoelectric sensor installed in one of the pistons and an angular encoder placed in the expander shaft.

Furthermore, a TDC is used to detect the position of the BDC. TDC is a sensor for axial piston expanders which delivers a signal correlated to the distance between sensor and a small magnet fixed to the piston bottom. Figure 3.29 shows the steps that should be followed in the data post-processing. Furthermore, the geometrical characteristics of each expander (pistons number, bore, stroke, swash-plate angle, dead volume and the intake and exhaust valve opening and closing angle) should be taken into account to complete this calculation. Using a high frequency acquisition data (50 kHz), both the TDC signal and the in cylinder pressure are recorded. Using a filter (convolution of the raw signal to a Gaussian window), the high frequency noise is eliminated. When the TDC sensor is installed in the same piston as the instantaneous pressure signal, it would give directly the position of the BDC. However, as shown in figures it is not in this case, so a delay in angle between TDC sensor and the instantaneous pressure sensor should be applied.

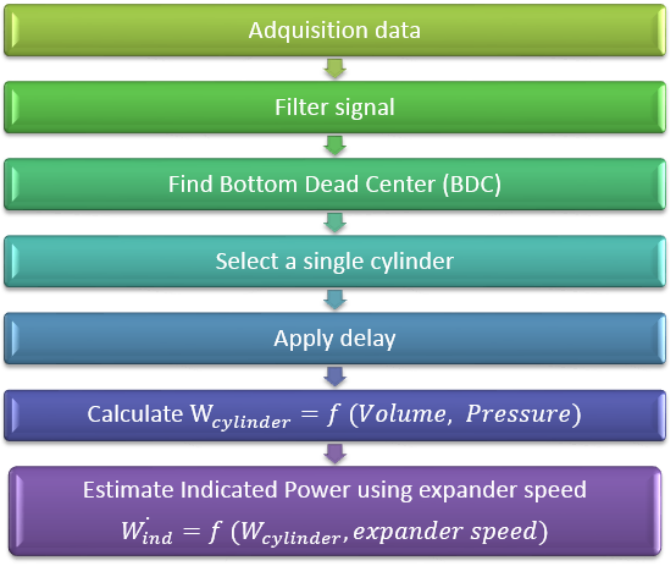

Figure 3.29: Steps in the data post process

Figure 3.30 shows an scheme of the procedure carried out to compute the variation of displacement in a Swash-plate piston.

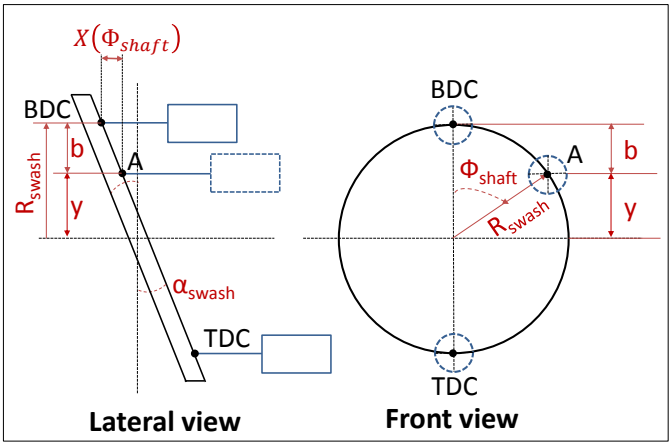

Figure 3.30: Calculation of displacement in a swash-plate expander

In figure Figure 3.30, point A is considered to explain the relation between angle and displacement of the swash-plate expander. Equation 3.24, Equation 3.25, Equation 3.26 and Equation 3.27 are the equations used to calculate the displacement as a function of swash-plate angle, angle covered by the swash-plate and swash-plate radius. The volume is calculated in Equation 3.28, using the dead volume, the stroke and the bore of the piston.

$$y = R_{swash} \cdot \cos(\Phi_{shaft}) \tag{3.24}$$

$$X(\Phi_{shaft}) = b \cdot \tan(\alpha_{shaft}) \tag{3.25}$$

$$R_{swash} = y + b = R_{swash} \cdot \cos(\Phi_{shaft}) + \frac{X(\Phi_{shaft})}{\tan(\alpha_{shaft})} \tag{3.26}$$

$$X(\Phi_{shaft}) = R_{swash} \cdot (1 - \cos(\Phi_{shaft})) \cdot \tan(\alpha_{shaft}) \tag{3.27}$$

$$V(\Phi_{shaft}) = V_d + \pi \cdot \frac{B^2}{4} \cdot X(\Phi_{shaft}) \tag{3.28}$$

Where R_{swash} is the radius of the Swash Plate, α_{shaft} is the Swash-plate angle, Φ_{shaft} is the angle covered by the piston, V_d is the dead volume, B is the bore of the piston and V_{swash} is the volume displaced by the piston. Once the pressure and volume are calculated, the indicated diagram could be plotted. The indicated power can be obtained using the indicated work, the number of pistons and the expander speed.

Transient 12-25 kW and 20-25 kW. Two transient tests are performed in the cycle measuring the instantaneous pressure inside the swash-plate cylinder, varying the vehicle speed from 84 km/h (12 kW power in the boiler) to 114 km/h (25 kW in the boiler) and from 106 km/h (20 kW) to 114 km/h (25 kW). The time step between the two engine operating points is set to 5 s in order to test the most severe conditions to the engine and ORC.

Transient 12-25 kW with 5 s

The main actuators of the system are presented in Figure 3.31. The first subplot (A) indicates the pressure in the expansion vessel ($P_{out,cond,ET}$). The second subplot (B) indicates the temperatures in the exhaust line: inlet boiler temperature ($T_{in,b,EG}$) in the left axis and outlet boiler temperature ($T_{out,b,EG}$) in the right axis. The third subplot (C) indicates the mass flows through the system: the exhaust gases mass flow ($\dot{m}_{EG}$) in the left axis and the cooling mass flow ($\dot{m}_W$) in the right axis. The last subplot (D) indicates the pump speed (N_{pump}) in the left axis and the expander speed (N_{exp}) in the right axis. In this transient test, the vehicle speed is shifted from 84 km/h to 114 km/h.

As it can be seen in Figure 3.31, exhaust gas mass flow increases from 100 kg/h to approximately 150 kg/h. The exhaust gas step starts approximately in second 15. The water mass flow remains constant with a value of 690 kg/h. Both expander and pump speed change according to the control presented in Figure 3.27. The coloured vertical lines correspond to particular times of the transient tests deeply analysed on next paragraphs.

The main output cycle variables are presented in Figure 3.32. The first subplot (A) indicates the pressures in the ORC: HP ($P_{in,exp,ET}$) in the left axis and LP ($P_{out,exp,ET}$) in the right axis. The second subplot (B) indicates the inlet temperature in the expander ($T_{in,exp,ET}$), the saturation temperature (T_{sat}) and the outlet temperature in the expander ($T_{out,exp,ET}$). The third subplot (C) indicates the ethanol mass flow through the system ($\dot{m}_{ET}$). The last subplot (D) indicates the torque (τ_{exp}) and the expander speed (N_{exp}).

As explained in subsection 3.5.2, the expander speed is optimized for each particular exhaust gas power. The engine operating point is shifted from 12 kW to 25 kW and the expander speed is varied from 2000 rpm to 2500 rpm. As higher power is released in the exhaust gases, the ethanol is vaporized into a higher level of pressure. Outlet temperature in the boiler remains almost constant due to the reference threshold of the control that fix 210 °C as a set point. Ethanol mass flow increases considering both dynamic effects: high and low inertia elements.

Expander torque increases with exhaust gases power, as a consequence of the rise in nominal ethanol mass flow. The isentropic efficiency remains constant because although the power delivered by the expander increases, the expansion ratio increases too. Thus, the relation between isentropic and shaft power remains almost constant. The expander speed varies from 2000 rpm to 2500 rpm.

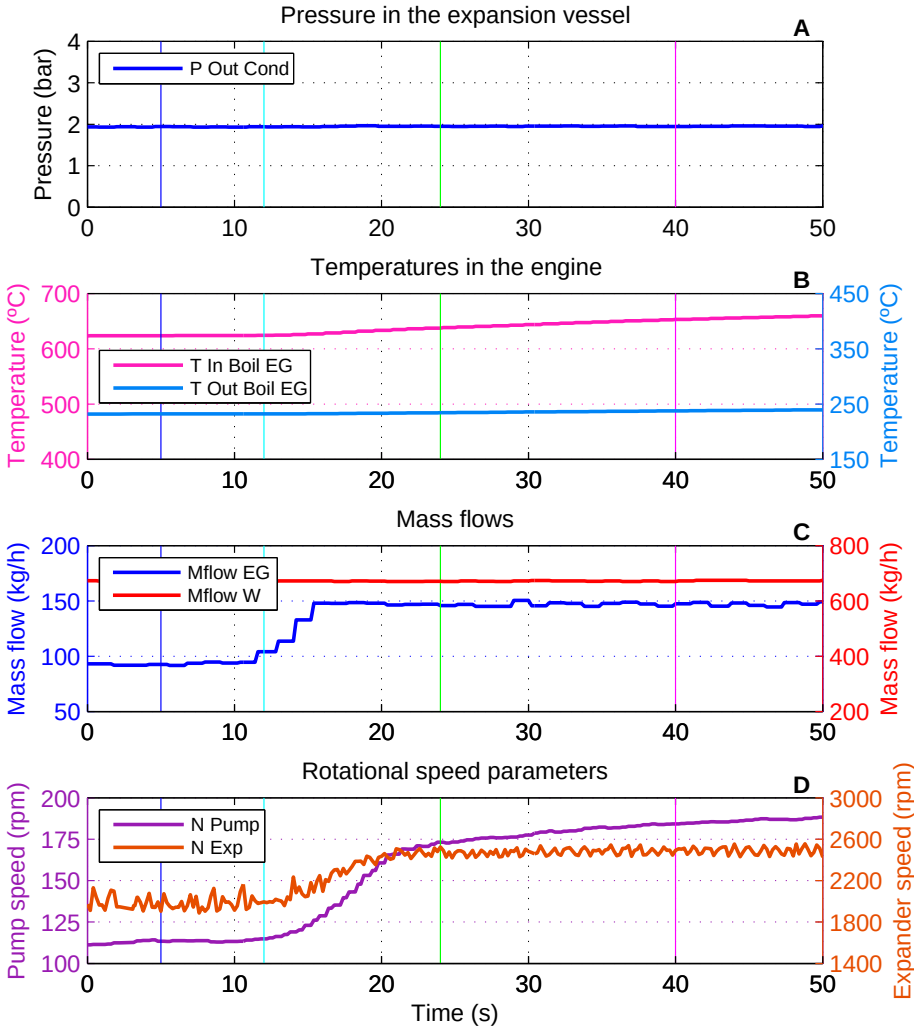

Figure 3.31: Actuators of the ORC transient 12-25 kW (5s)

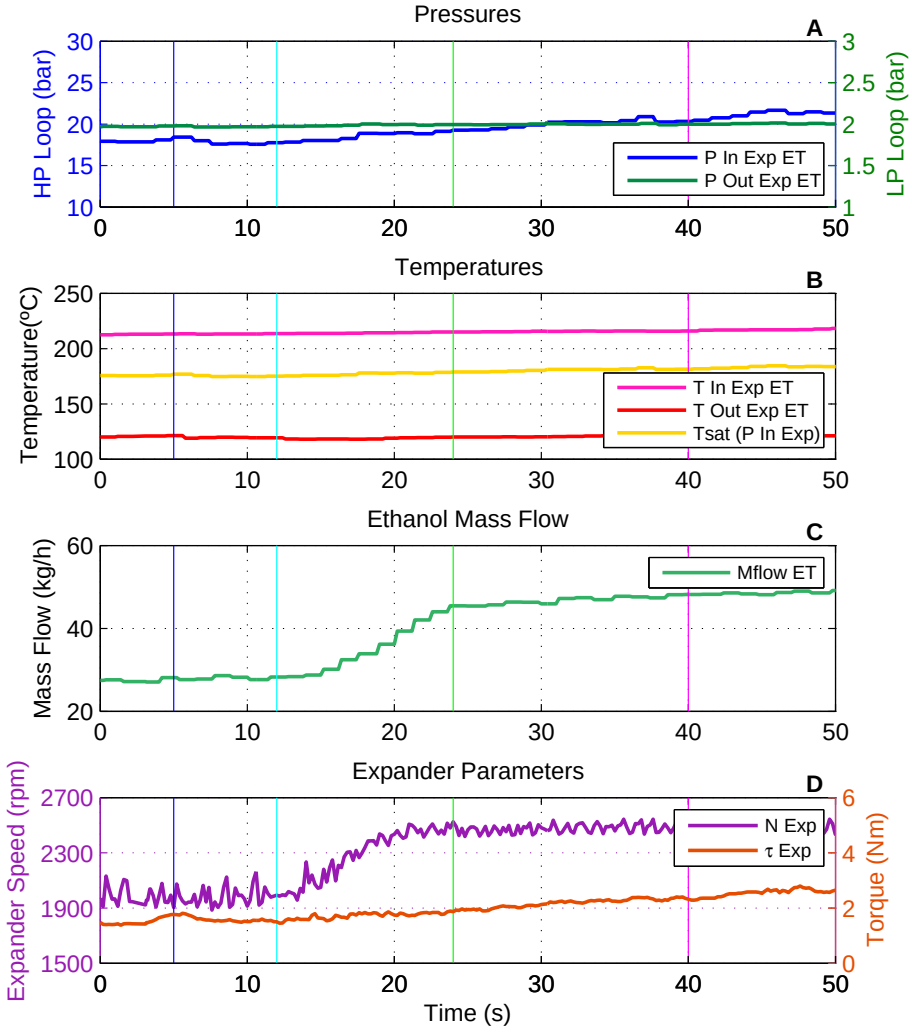

Figure 3.32: Main parameters in the ORC transient 12-25 kW (5s)

The PV diagram analysis during the transient is used to evaluate possible irreversibilities in the expansion machine. Thus, it has been computed at 4 specific instants of time during the transient. The instances are chosen to represent initial steady-state, start of transient, end of transient and final steady-state (5 s, 12 s, 24 s and 40 s):

- t=5 s: Initial steady state point at the lower engine operating point (12 kW). All the system variables remain constant and the expander speed value is 2000 rpm.
- t=12 s: Start of the transient test. The ethanol mass flow increases to adapt the ORC to the new engine operating point (25 kW). Pressures rise up and expander speed changes from 2000 rpm to 2500 rpm.
- t=24 s: End of the transient test. The ethanol mass flow has almost reached the new operating conditions. Pressure continues rising. Expander speed value is 2500 rpm.
- t=40 s: Steady state at the new engine operating conditions (25 kW). All the system variables remain almost constant and the expander speed value is 2500 rpm.

These points have been indicated in Figure 3.31 and Figure 3.32 using vertical lines with the same colors that the PV plots of Figure 3.34. In order to estimate the PV diagram at a specific time of the transient, an average of a finite number of cycles have been computed. On one hand, a low number of cycles will not be representative because of the deviation in measurements. On the other hand, if a high number of cycles are considered, the PV diagram area increases as a consequence of the change in the engine operating point. Therefore, a sensitivity study is performed to obtain the optimal number of cycles. An average of the PV diagram area during these cycles is computed. Figure 3.33 shows the result of this parametric study. The average indicated power remains constant in the range from 80 to 110 cycles. Thus, 80 cycles are elected to reduce the CPU calculation time. This parametric study is performed in the middle of the transient (t=18 s) to consider a high level of variability.

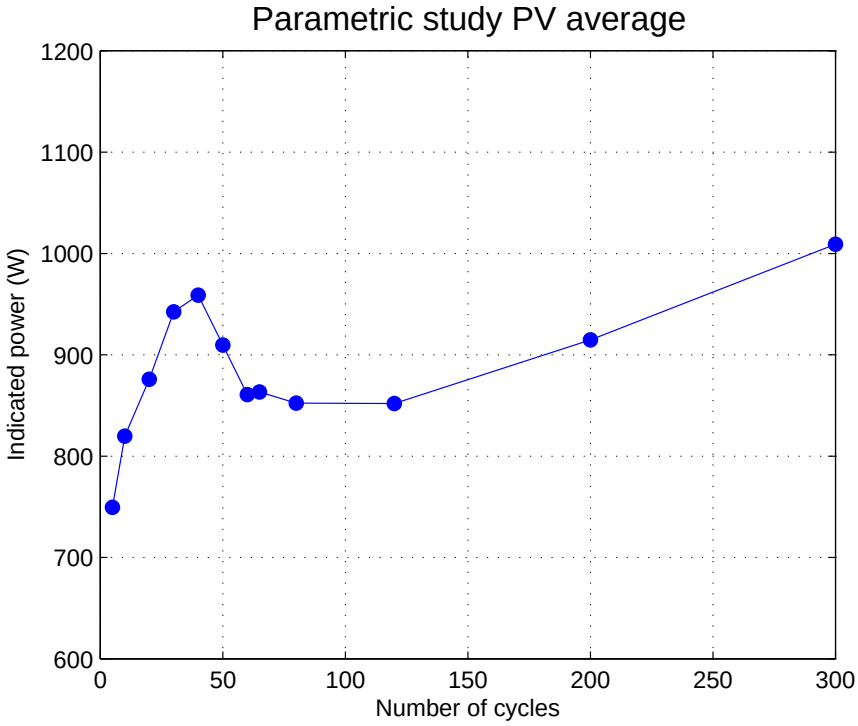

Figure 3.33: Parametric study PV average

Figure 3.34 shows the PV diagram in the previous time instances. Red and green crosses indicate the intake and exhaust valve closing angles (or volumes) respectively. Red and green circles indicate the intake and exhaust valve opening angles (or volumes) respectively. By comparing all the diagrams, it can be seen that the compression process in the piston (PV slope during compression process) is more isothermal at lower expander speeds (at time 5 s, 2000 rpm) than at higher expander speeds (at time 12 s, 24 s and 40 s, 2500 rpm). Lower expander speeds involve higher heat transfer rates, therefore more isothermal compression process. Focusing on the maximum pressure reached by the system (at time 12 s, 24 s and 40 s) it can be seen that higher exhaust power has a direct impact on the maximum pressure of the PV diagram. This effect justifies the increase on the high pressure of the cycle and the thermal behavior of the system. Once the engine operating point is shifted, the thermal delay of the boiler causes that although the mass flow transient is finished, the indicated diagram continues increasing to higher levels of pressure. This effect is visible comparing 24 s and 40 s indicated diagrams.

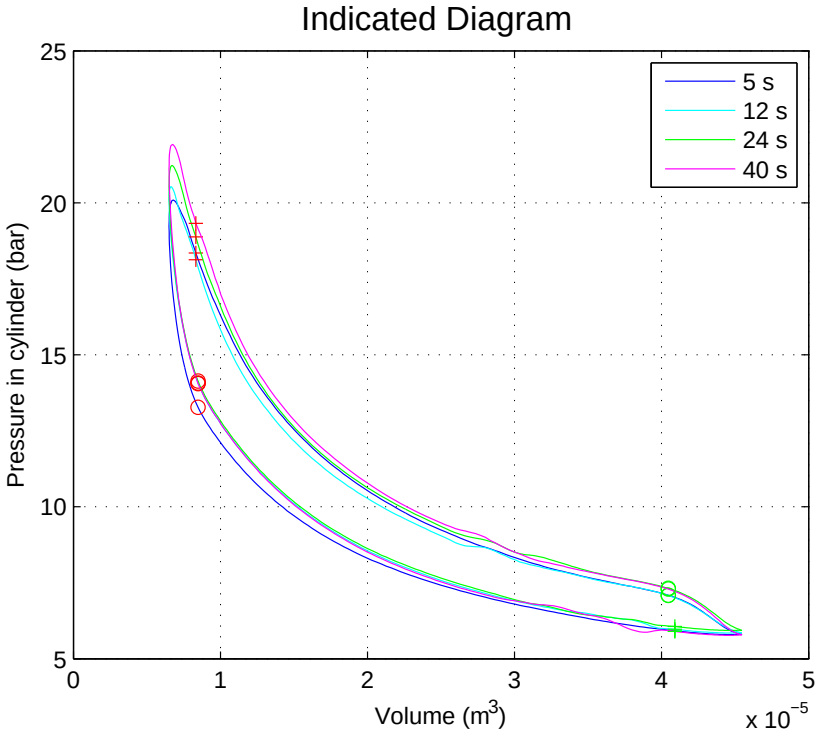

Figure 3.34: Diagram transient tests 12-25 kW (5s)

Transient 20-25 kW with 5 s

Figure 3.35 and Figure 3.36 show respectively the actuators and the main parameters of the cycle for the transient 20-25 kW. The first subplot (A) indicates the pressure in the expansion vessel ($P_{out,cond,ET}$). The second subplot (B) indicates the temperatures in the exhaust line: inlet temperature of the boiler ($T_{in,b,EG}$) in the left axis and outlet temperature of the boiler ($T_{out,b,EG}$) in the right axis. The third subplot (C) indicates the mass flow through the system: the exhaust gases mass flow ($\dot{m}_{EG}$) in the left axis and the cooling mass flow ($\dot{m}_W$) in the right axis. The last subplot (D) indicates the pump speed (N_{pump}) in the left axis and the expander speed (N_{exp}) in the right axis. In this transient test, the vehicle speed is shifted from 106 km/h to 114 km/h. As shown in Figure 3.35, the exhaust gas mass flow increases from 120 kg/h to approximately 150 kg/h. The exhaust gas step starts approximately in second 15. The water mass flow remains constant with a value of 690 kg/h. In this case, the expander speed is constant (2500 rpm).

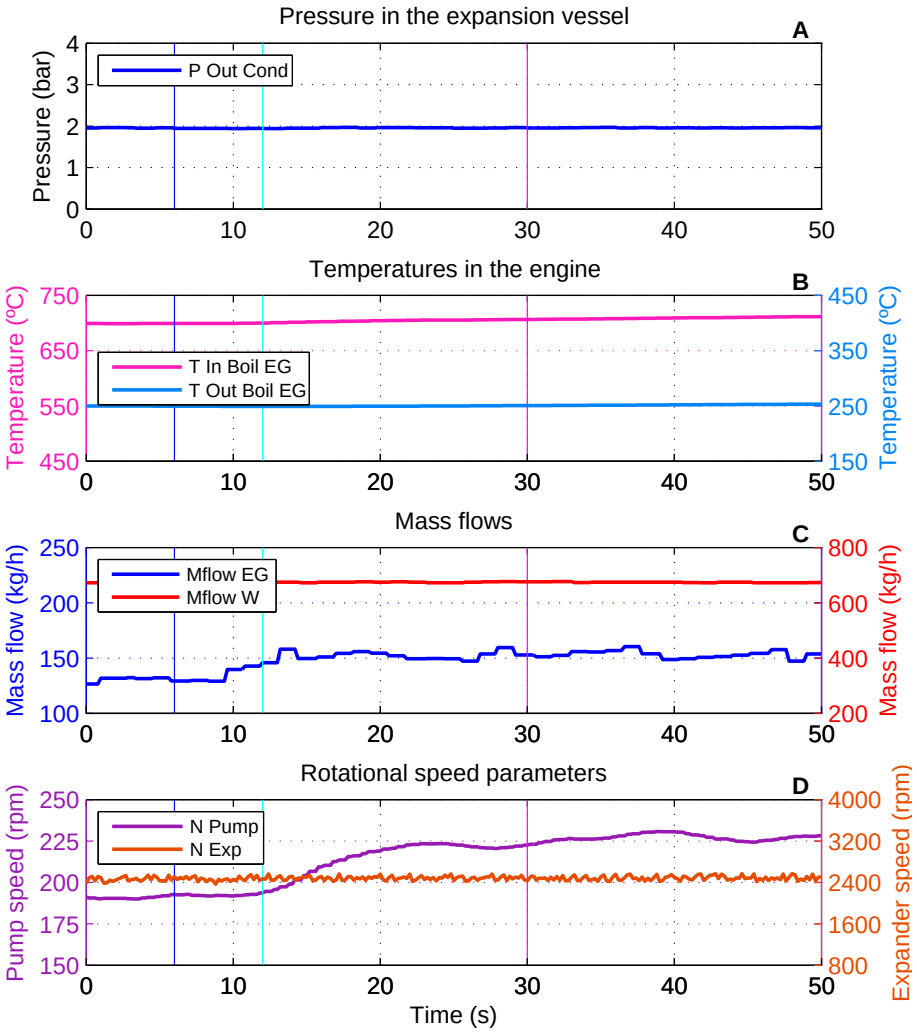

Figure 3.35: Actuators of the ORC transient 20-25 kW (5s)

The main output variables of the cycle are presented in Figure 3.36. The same outputs parameters have been used as in Figure 3.32. The expander is optimized at 2500 rpm in 20-25 kW. As higher power is released in the exhaust gases, the ethanol is vaporized into a slightly higher level of pressure. Changes are lower than in the previous transient due to lower differences in the boiler heat transferred during the transient. Outlet temperature in the boiler remains at the same level of 210 °C.

Ethanol mass flow increases considering both dynamic effects: high and low inertia elements. Torque delivered by the expander increases with exhaust gases power as a consequence of the ethanol mass flow increase.

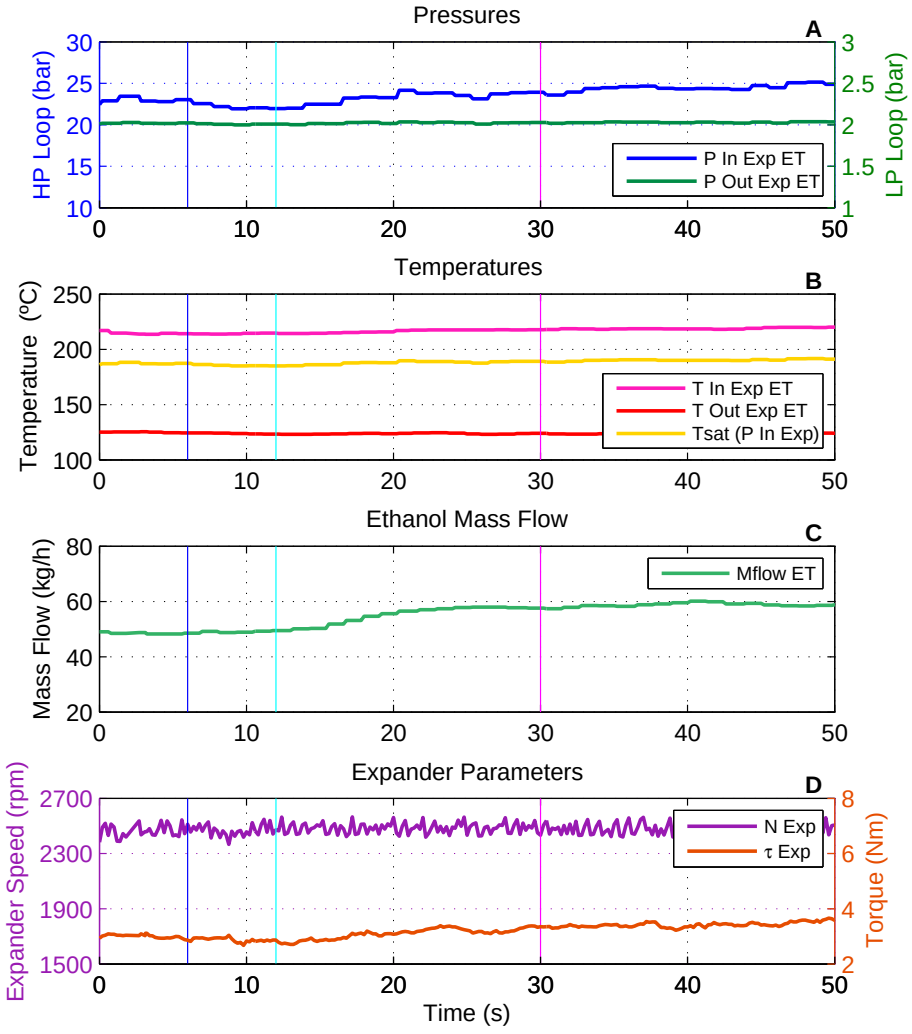

Figure 3.36: Main parameters in the ORC transient 20-25 kW (5s)

The PV diagram has been computed at 3 specific instants of time during the transient. The instances are chosen to represent initial steady-state, start of transient and the end of transient (6 s, 12 s and 30 s):

- t=6 s: Initial steady state point at the lower engine operating point (20 kW). All the variables of the system remain constant and the expander speed is 2500 rpm.
- t=12 s: Start of the transient test. The ethanol mass flow increases to adapt the ORC to the new engine operating point (25 kW). Pressures rise up while the expander speed remains constant.
- t=30 s: End of the transient test. The ethanol mass flow has almost reached the new operating conditions. Pressure continues increasing. Expander speed is 2500 rpm.

Figure 3.37 shows the PV diagram at different instants of time during the test. By comparing all the diagrams, it is observed that the compression process in the piston remains approximately unchanged (in second 6 s, 12 s and 30 s) due to the constant expander speed. As regards the maximum pressure reached by the system, it can be seen that higher exhaust power has a direct impact on the maximum PV diagram pressure. Therefore, the more power it is released on the boiler, the higher amount of indicated power it is produced. The expansion laws are approximately equal. However, the inlet valve closes at higher pressure level as time goes on and therefore, the area of the PV diagram increases.

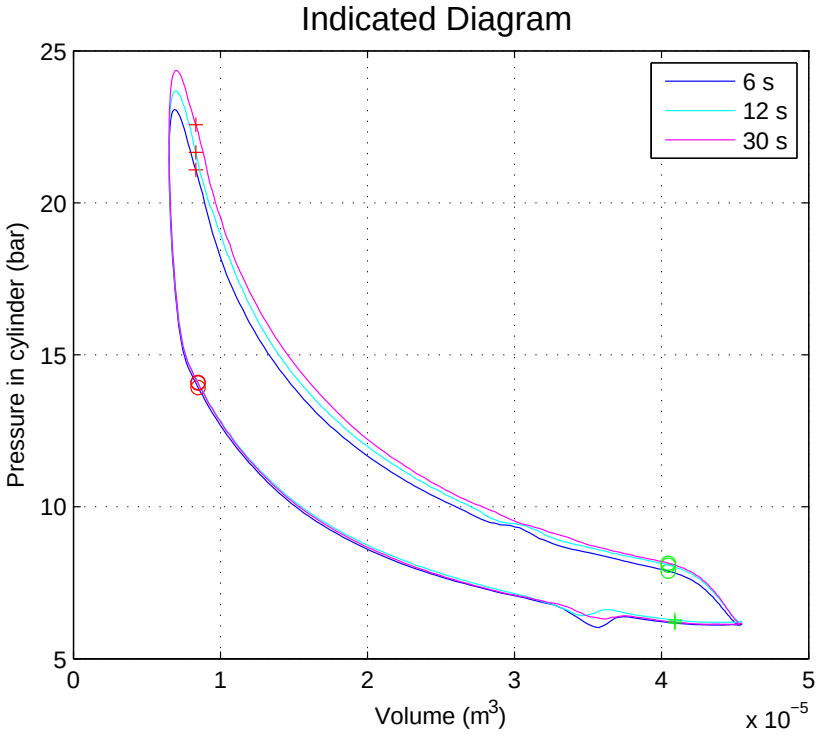

Figure 3.37: Diagram transient tests 20-25 kW (5s)

To sum up, taking into account the previous analysis, the control of the system should consider two phenomena, high inertia temperature effects (heating process in the heat exchangers) and low inertia pressure and mass flows effects (expansion-compression processes in the pump and the expander). A delay is visible analysing the PV diagram of the expander machine. The temperature at the outlet of the boiler is fixed to 210 °C. Therefore, the boiler delay is visible in the pressure signal. As a result, although the ethanol mass flow changes promptly, the thermal inertia of the system causes the cycle a delay in pressures. The final ORC control should consider both effects. Thus, the adaptive correction introduced in the control of the cycle is justified with previous analysis, as shown in Figure 3.27.

A statistical analysis of the work delivered by the expander in J during the transient 20-25 kW is presented in Table 3.9. In this table the average work delivered by the expander, the standard deviation, the maximum and the minimum values are shown in the same time previously analysed (6 s, 12 s and 24 s). The average work delivered by the expander increases from 11.101 J to

12.832 J as a result of the change in the engine operating point. Regarding the standard deviation, it remains approximately constant with a maximum value of 0.781 J in the second 12. Similar results are obtained with the transient 12-25 kW.

Table 3.9: Statistical analysis transient 20-25 kW

Time	Work delivered by the expander (J)	Standard Deviation (J)	Max	Min
6 s	11.101	0.711	12.708	9.829
12 s	12.309	0.781	14.074	9.829
24 s	12.832	0.552	13.873	11.718

NEDC cycle. In order to apply the control of the installation to realistic driving conditions, the engine is tested following the New European Driving Cycle (NEDC). The purpose of this test is to estimate the amount of power released by the exhaust gases during this cycle and estimate the points in which the expander could be started. Figure 3.38 shows the result of this test. During the urban part of the cycle, there is not enough power in the cycle to evaporate and produce power in the expander, because the engine is in warm up conditions and temperatures are too low. The vapour conditions in the boiler outlet begins approximately at second 900.

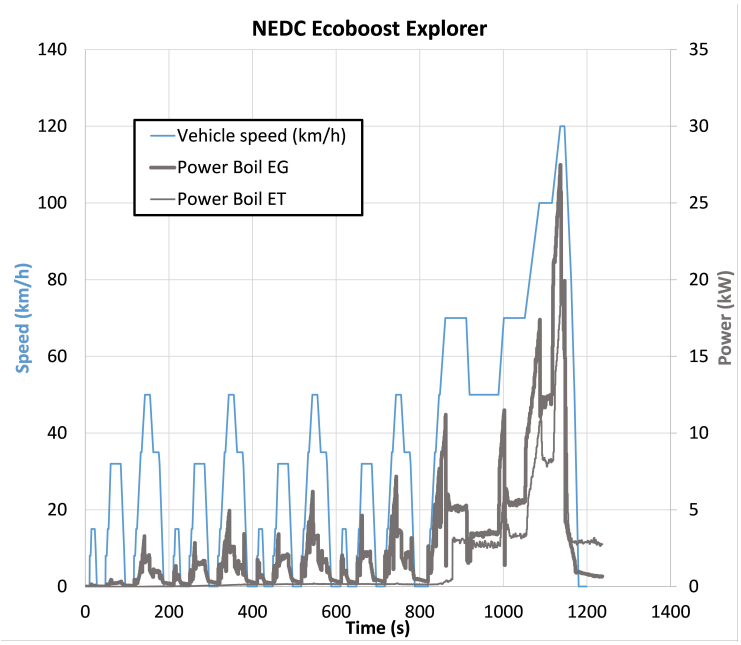

Figure 3.38: NEDC without expander

Although the exhaust gas mass flow changes very fast, the response in the exhaust line temperature is slower. The time response in temperatures is approximately 40 s, whereas in mass flows is 5 s, as it can be seen in Figure 3.35 and Figure 3.31. Moreover, the installation response to the NEDC is well controlled with the control layout performed. The urban cycle starts from idle and cold conditions and reaches the high power in few minutes, thus, there is no enough time to deliver enough power to the expander. It can be concluded that the engine testing conditions in NEDC cycle are not the most favourable ones taking into account the dynamic ORC behaviour. High loads and hot conditions should be the starting ideal operating points to test and validate the control of the ORC. Considering the results obtained in the previous section, the last part of the NEDC (starting at hot conditions) is tested. It corresponds to extra-urban cycle (the last acceleration from 70 km/h to 120 km/h of NEDC) after stabilizing during some minutes at the point of 70 km/h. Figure 3.39 shows the result of this test with the expander. In this case, there is enough power in the cycle to evaporate the ethanol and start the expander.

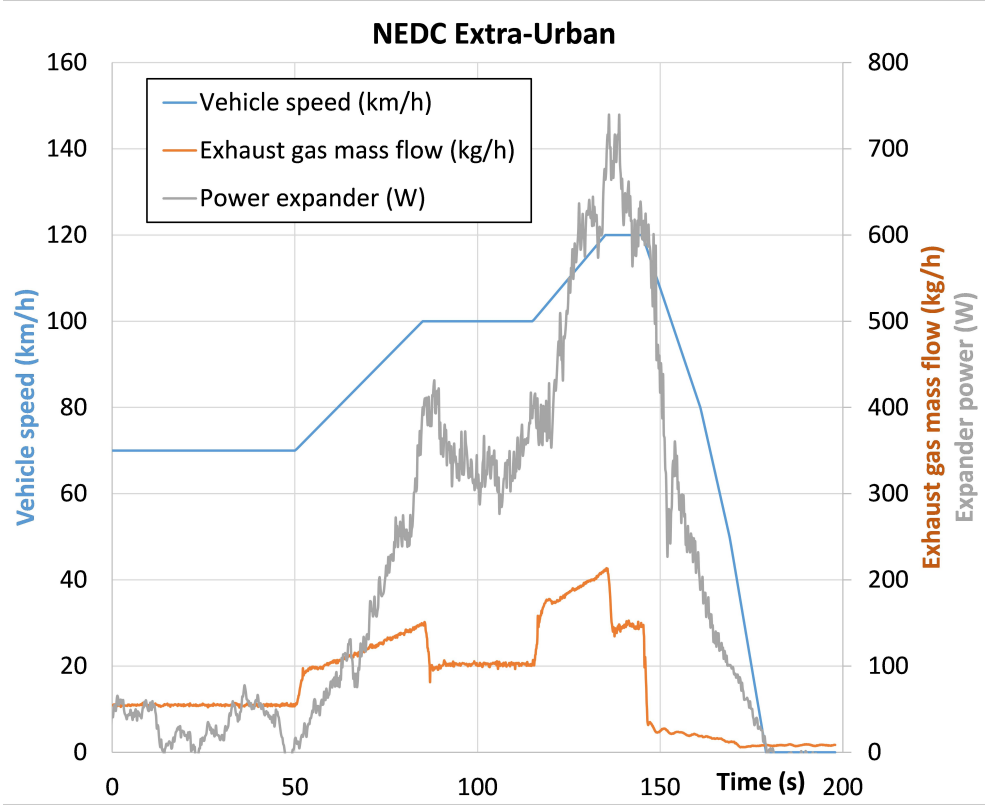

Figure 3.39: NEDC without expander

3.6 Summary

In this chapter, the experimental methods and results used to characterise an experimental ORC mock-up installed in a turbocharged 2.0 liter gasoline engine to recover waste heat in exhaust gases are described and presented. Energy balances for different boiler powers between 5 kW and 30 kW are presented, showing substantial differences in terms of mechanical power delivered by the expander. The expander power output value of these points varies from 0.21 kW to 1.83 kW respectively. The evolution in terms of several efficiency parameters have been reviewed by means of changing the main parameters affecting the ORC cycle, which are the expansion ratio, the expander speed and the outlet pressure of the expander. The following results have been obtained with available components based on non-commercial prototypes:

1. A potential of increasing ICE mechanical efficiency up to 3.7% could be reached at points of high load (25 kW) installing an ORC in a conventional turbocharged gasoline engine.

2. A maximum Carnot efficiency, Rankine ideal efficiency and Rankine real efficiency values of 79%, 19% and 6% could be obtained using a swash-plate expander to recover energy from exhaust gases. Similar values are achieved in the scientific literature.

3. Isentropic and volumetric efficiency are used to evaluate performance of the swash-plate expander. Maximum values of 38.5% and 38.2% were obtained respectively.

4. The installation response to dynamic transient tests (12-25 kW and 20-25 kW) is well controlled with the control layout performed with engine time steps up to 5s. NEDC extra urban transient cycle is performed using the same control obtaining a controllable system.

5. The control of the system considers both high inertia temperature effects (heating process in the heat exchangers) and low inertia pressure and mass flows effects (expansion-compression processes in the pump and the expander). The adaptive control lets the system adapt to these dynamic operating conditions of the engine.

6. Compression in the piston is more isothermal at lower expander speeds than at higher expander speeds. Lower expander speeds involve higher residence time of ethanol inside the cylinders. Consequently, heat transfer rates increases with lower expander speeds. Therefore, lower expander speeds involve more isothermal compression processes. The more power is

released by the boiler, the higher amount of indicated power is produced by means of higher pressure at the inlet of the expander machine.

7. NEDC cycle produce not enough power to run the expander in normal operating conditions starting from engine cold conditions. High loads and hot conditions should be the starting ideal operating points to test and validate the control of the ORC.

8. The slightly simple and robust control, based on adaptive PIDs, allows the control of the ORC in realistic driving profiles.

3.7 References

[34] A. Duparchy, P. Leduc, G. Bourhis, and C. Ternel. “Heat Recovery for next Generation of Hybrid Vehicles : Simulation and Design of a Rankine Cycle System”. In: *World Electric Vehicle Journal Vol.3* 3 (2009), pp. 1–17 (cit. on pp. 15, 46).

[82] S. Declaye, S. Quoilin, L. Guillaume, and V. Lemort. “Experimental study on an open-drive scroll expander integrated into an ORC (Organic Rankine Cycle) system with R245fa as working fluid”. In: *Energy* 55 (2013), pp. 173–183. ISSN: 03605442. DOI: 10.1016/j.energy.2013.04.003. URL: http://linkinghub.elsevier.com/retrieve/pii/S0360544213003034 (cit. on pp. 24, 81).

[99] T. Endo, S. Kawajiri, Y. Kojima, K. Takahashi, T. Baba, S. Ibaraki, T. Takahashi, and M. Shinohara. “Study on Maximizing Exergy in Automotive Engines”. In: *SAE International* 1 (2007), pp. 1–12 (cit. on pp. 28, 78).

[106] H. Neukirchner, T. Semper, D. Lüderitz, and O. Dingel. “Symbiosis of Energy Recovery and Downsizing”. In: *MTZ* 75.Innovative Engine Systems (2014), pp. 4–9 (cit. on p. 46).

[107] M. J. Moran, H. N. Shapiro, D. D. Boettner, and M. Bailey. *Fundamentals of Engineering Thermodynamics*. John Wiley & Sons, 2010, p. 944. ISBN: 0470495901. URL: http://books.google.com/books?id=oyt8iW6B4aUC{\&}pgis=1 (cit. on p. 65).

[108] M Lapuerta, O Armas, and J. J. Herna. “Diagnosis of DI Diesel combustion from in-cylinder pressure signal by estimation of mean thermodynamic properties of the gas”. In: *Applied Thermal Engineering* 19 (1999), pp. 513–529 (cit. on p. 65).

[109] B. N. Taylor and C. E. K. Kuyatt. “Guidelines for Evaluating and Expressing the Uncertainty of NIST Measurement Results”. In: *NIST Technical Note 1297* 1 (1994), p. 20 (cit. on p. 77).

CHAPTER 4

Organic Rankine Cycle model

Contents

Figures

Tables

4.1 Introduction

In the previous chapter, the experimental setup was presented. The main objective of this chapter consists of the description and validation of a global ORC simulation model and a specific submodel of the main limiting cycle factor, the swash-plate expander. The proposed models have been developed in this chapter using LMS Imagine.Lab Amesim platform. Models are consistent due to the slight deviation between experimental tests and modelled results. The purpose of these models are: firstly to help the understanding of those physical phenomena difficult to observe by means of experimentation and secondly to estimate the behaviour of the cycle without the need for experimental tests under operating conditions that might cause damages to the installation and / or people. The present chapter contains three parts:

- section 4.2 corresponds to the description of the global Organic Rankine model and the swash-plate model. The main assumptions and considerations of these models are presented in this section.
- section 4.3 focuses on the experimental validation of both the Global Organic Rankine Cycle model and the swash-plate model. Several points have been validated in order to assess the robustness of the model.
- section 4.4 presents a case study of a gasoline engine coupled to the global Organic Rankine model. The extra-urban part of the NEDC is simulated and ORC performance results are presented.

4.2 Description of the model

A comprehensive model of the Organic Rankine Cycle using Amesim is described in this paragraph. Considering the swash-plate expander as the most critical element, one additional specific submodel is implemented to model the physical phenomena inside the piston of the Swash-plate expander. The software package provides a 1D model suite to simulate and analyze multi-domain intelligent systems, and to predict their multi-disciplinary performances. This software consists of available object-oriented libraries, where the user should connect them properly and fix the parameters.

4.2.1 Global Organic Rankine Cycle model

A simple layout of the ORC consisting of a boiler, a positive displacement pump, a volumetric expander, a fluid receiver, a condenser and an expansion vessel is considered in this model. Figure 4.1 shows the AMESim model of the cycle based on the ORC installation. A detailed description for the main assumptions in this model are presented in the following subsections.

Working fluid. In the modelling of a particular working fluid it is crucial to be able to reproduce both the thermodynamic and transport properties of the working fluid. AMESim provides built-in physical-thermo property data of different fluids. In this case the working fluid is ethanol. Table 4.1 summarizes the main characteristics of the working fluid.

Table 4.1: Properties of ethanol

Property	**Ethanol**		
Chemical structure		C_2H_6O	
Critical Temperature	Tc	240.9	°C
Critical pressure	Pc	61.4	bar
Atmospheric boiling point	Tb	78.3	°C
Ozone depletion potential	ODP	0	-
Global Warming Potential	GWP	n/a	-
NFPA health hazard	H	2	-
NFPA flammability hazard	F	3	-
Auto ignition temperature	Tign	363	°C

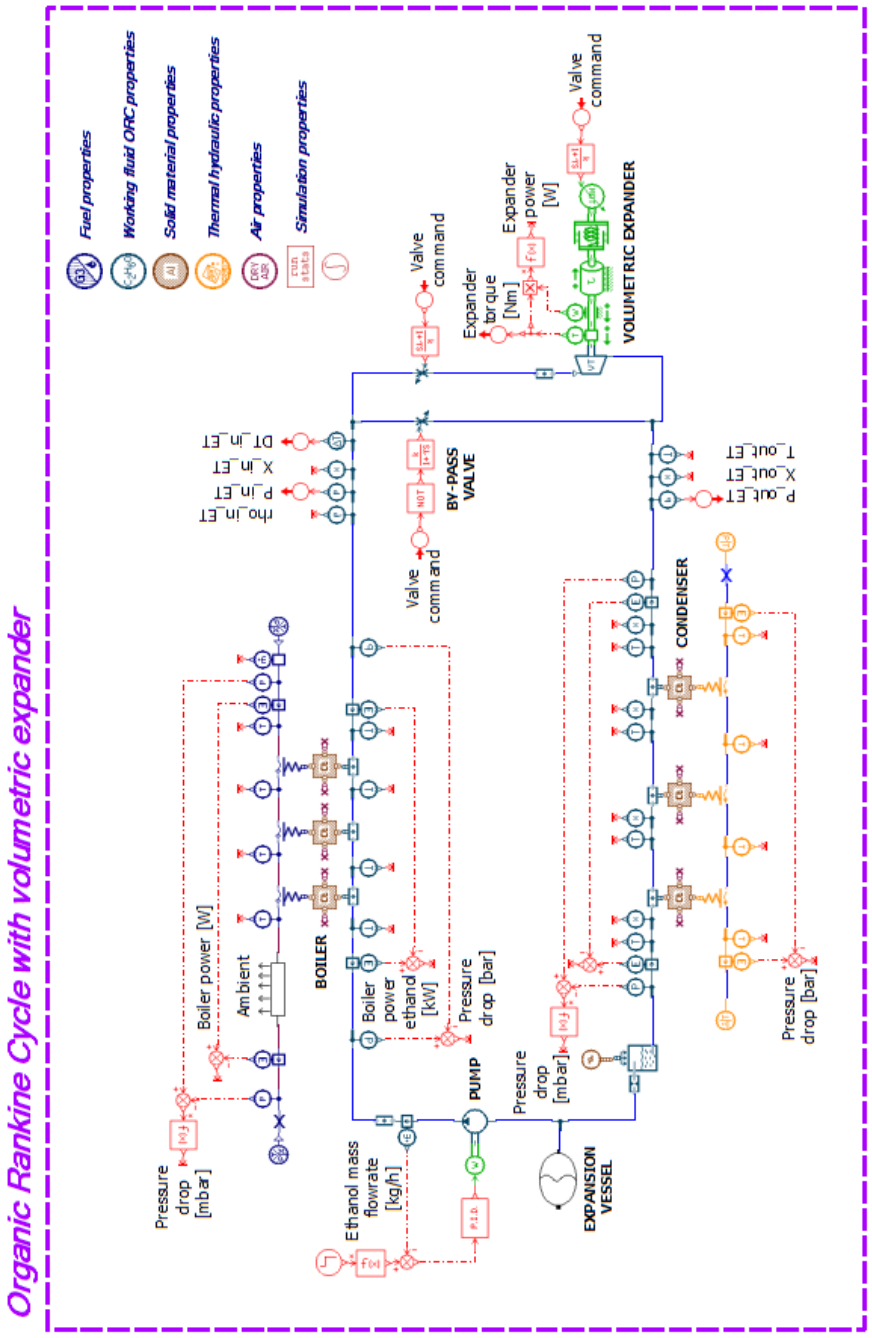

Figure 4.1: Organic Rankine cycle model

Heat exchangers. The boiler allows the heat transfer from exhaust gases to working fluid, based on plate and fin technology. On the other hand, condenser allows the heat transfer from working fluid to the coolant with the same heat transfer technology. A 1D discretization model with small volumes is presented by two counter-flow streams. In the case of the boiler, the exhaust gases and the ethanol represents the hot and cold stream respectively. In the case of the condenser, the ethanol and the cooling medium (water) represent the hot and cold stream respectively. In each element, the volume has been divided in 3 small volumes, which exchanges the net thermal power of the global element. The heat exchange process takes into account both convective and conducting (just in longitudinal direction) process. Depending on the process, (boiling or condensation) different implemented AMESim correlations have been taken into account. Shah correlation [110] and VDI for horizontal tubes correlation [111] are used for condensation and boiling process respectively. In order to improve the boiler model, thermal capacities are adjusted using a transient experimental test. This is performed varying the engine exhaust gases power from 20 kW to 25 kW. Hence, the experimental values of exhaust gases mass flow, inlet temperature in the exhaust gases side, ethanol mass flow, and temperature and pressure at the inlet of the boiler in the ethanol side are used to validate this model. The objective of this validation is to obtain a similar temperature profile at the outlet of the boiler in the ethanol side, considering thermal inertias.

Volumetric expander and by-pass valve. In the expander loop there are two elements, the by-pass valve and the volumetric expander. The Swash-plate expander is the main ORC element because it has a great impact in the overall system efficiency. The expander model uses three parameters to characterize the expander performance, i.e. indicated efficiency in Equation 4.1, mechanical efficiency in Equation 4.2 and volumetric efficiency in Equation 3.23. Isentropic efficiency can be also defined as the product of indicated and mechanical efficiency (Equation 4.3).

$$\eta_{exp,ind} = \frac{P_{exp,ind}}{P_{exp,is}} \tag{4.1}$$

$$\eta_{exp,mec} = \frac{P_{exp,sh}}{P_{exp,ind}} \tag{4.2}$$

$$\eta_{exp,is} = \eta_{exp,ind} \cdot \eta_{exp,mec} \tag{4.3}$$

$$P_{ind} = W_{ind} \cdot n_{cyl} \cdot \frac{N_{exp}}{60} \tag{4.4}$$

Where $P_{exp,sh}$ and $P_{exp,is}$ have been previously defined in Equation 3.10 and Equation 3.8 respectively. The indicated power is computed using Equation 4.4, where W_{ind} is the indicated work in J, N_{exp} is the expander speed in rpm and n_{cyl} is the number of expander cylinders. No leakages and internal pressure drops have been considered in this expander model. Instead of that, a correlation for the expander efficiencies have been introduced in the model. The by-pass valve is opened while the upstream conditions in the expander are not the optimal ones. In order to control the by-pass valve, a control loop has been developed. Figure 4.2 shows an scheme of this control loop. In the case of steady-state operating points, the by-pass valve remained closed and the expander valve remained open.

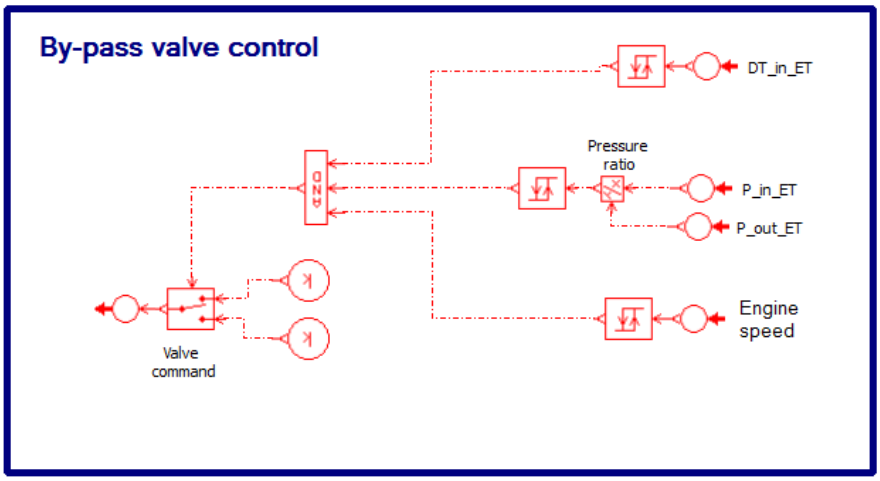

Figure 4.2: Control loop in the by-pass valve and expander

In this control three inputs are considered:

- Superheating at the inlet of the expander: It should be above 20 °C in order to avoid condensation drops during the expansion process.
- Pressure ratio: It should be between 5 and 12, which is considered the working range taking into account the pressure ratio range measured in the swash-plate expander (subsection 3.4.7).
- Engine speed (directly related to the expander speed): It should be between 1000 (to avoid problems related with lubrication issues of the swash-plate) and 5000 rpm (to avoid high mechanical losses).

A first order lag has been used in the valve command in order to avoid discontinuities of the system.

Pump. A fixed displacement pump is used in this model. The mass flow rate is obtained from volumetric efficiency. Mechanical, isentropic efficiencies and swept volume define the enthalpy drop through the pump. No correlations have been considered for efficiencies. Instead, some fixed values are specified for the points modelled, i.e. an isentropic efficiency of 80% [112] and a displacement of 5 cm^3.

Pipes and pressure drops. Internal piping losses in the system have been taken into account using hydraulic resistances. The transformation process is assumed isenthalpic. Using these elements both enthalpy and mass flow rates are computed. Pressure drops in the system have been calculated using correlations available in AMESim. The hydraulic diameter and the cross-sectional area are used to model different cross-sectional geometries. The pressure drops are regular and the friction factor depends on the flow regime and the relative roughness of the duct. Depending on the state of the fluid different correlations are applied: In a single phase flow (liquid or vapour) the Churchill [113] correlation is used, while in a two phase flow correlation the Mac Adams [114] correlation is implemented. This correlation is used for computing pressure drop inside tubes in vaporization process.

Expansion vessel. The expansion vessel has been simulated using a pneumatic piston, a mass and a two phase flow piston. It is presented in Figure 4.3. A pneumatic pressure and temperature source is used to fix the conditions inside the air tank. Values of 2 bar and 20 °C respectively are fixed in the pneumatic source. These values are consistent with the experimental values (Table 3.4). The mass simulates the expansion vessel membrane, therefore its value has been fixed to 500 g.

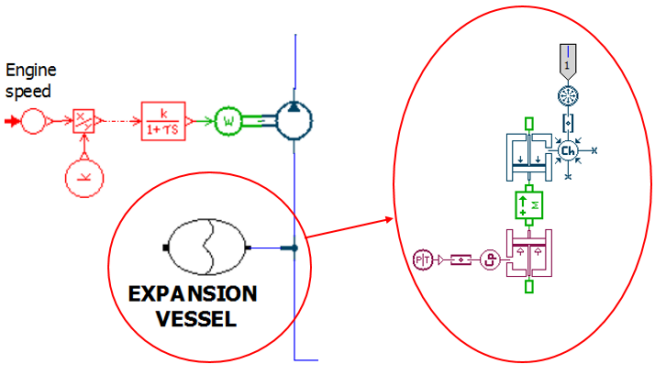

Figure 4.3: Expansion vessel model

4.2.2 Swash-plate specific model

As shown previously, the Swash-plate expander has been tested in this installation. Although in the global ORC model an AMESim submodel of the TPF library is used for modelling the expander using volumetric, isentropic and mechanical efficiencies, the need for a physical model of the expander has led to the development of a specific model for just the Swash-plate expander. Figure 4.4 shows the Swash-plate expander model. Bearing in mind the number of pistons in the swash-plate expander, the heat transfer in the compression and expansion process, the swash-plate mechanism and mechanical losses, a swash-plate expander model is developed to simulate the expander performance. It is modelled using AMESim and validated with the experimental tests performed with the expander. The comparison between P-V diagrams (experimental and modelled) is used to estimate the accuracy of the model.

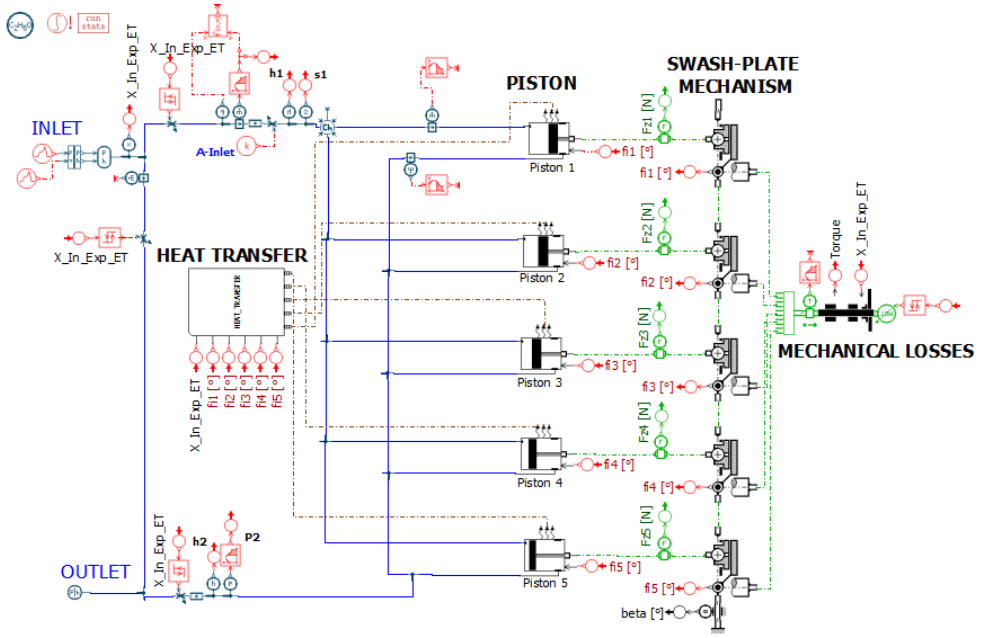

Figure 4.4: Swash-plate expander model

Figure 4.5 shows a zoom of the piston expander model in AMESim. The main part of the model consists of a two phase flow chamber with variable volume and pressure and temperature dynamics. This submodel has been modified from the AMESim original library model to take into account heat transfer during compression and expansion.

The filling (Intake valve) and emptying (Exhaust valve) processes provide the mass and pressure exchanges during these processes. The angle signal (obtained from the expander speed) is used in three parts of the model:

- In the heat transfer element: Although the expander is insulated, the expansion and compression do not follow an adiabatic process. The transformation is rather polytropic with a heat exchange between the working fluid and the expander walls due to friction, temperature differences and possible condensation effects in the piston chamber. Therefore, the angle signal is used to consider the compression and expansion angles and to apply for each process a heat transfer coefficient to model these phenomena.
- In the valves: The angle is considered to specify the intake and exhaust discharge coefficient at each particular angle.
- In the rotary-linear transformer: It is considered to calculate the absolute displacement in Equation 3.27. Therefore, the volume variation in Equation 3.28 of the piston as a function of the Swash-plate angle.

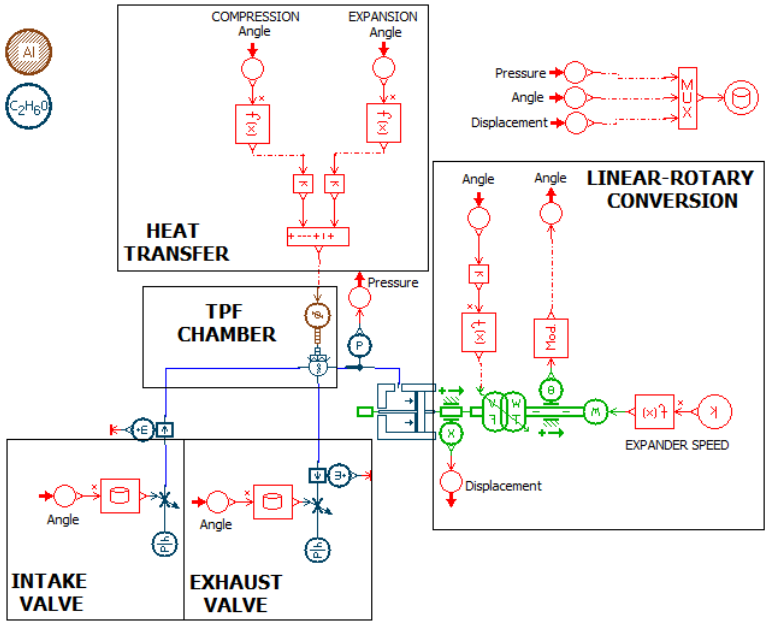

Figure 4.5: Zoom Swash-plate piston expander model

Regarding mechanical losses, they are estimated using experimental values [1]. The following correlation is obtained from experimental tests. It is a function of the expansion ratio and the expander speed.

$$M_l = 4528 - 0.1126 \cdot N_{exp} - 285.788 \cdot \frac{P_{in,exp,ET}}{P_{out,exp,ET}} \tag{4.5}$$

Where N_{exp} is the expander speed in rpm and $\frac{P_{in,exp,ET}}{P_{out,exp,ET}}$ is the expansion ratio through the expander. Figure 4.6 shows the Equation 4.5 validation between estimation and experimental values with a correlation coefficient of 96%.

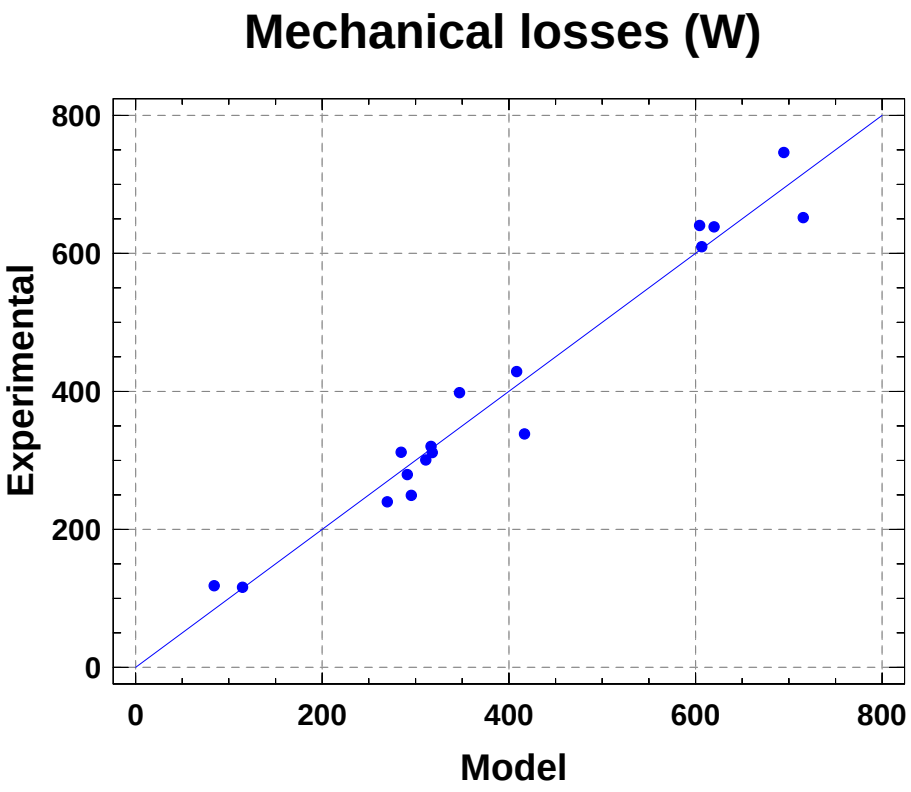

Figure 4.6: Validation of mechanical losses

4.3 Model validation

4.3.1 Global Organic Rankine Cycle model

In order to characterize the ORC system three points have been tested at different steady working conditions of the ORC system, varying the expander speed (P1: 2000 rpm, P2: 2500 rpm and P3: 3000 rpm). The engine steady-state operating point has remained constant with a value of 25 kW. The points presented in this study aims to show the recovery features at different expander operating points [1]. In these tests, the system has been controlled commanding three parameters: the pump speed, so as to control the ethanol mass flow through the installation, the expansion vessel balloon pressure, so as to control the outlet expander pressure and the expander speed, so as to control the high pressure at the expander inlet. Table 4.2 shows the ORC model inputs. For each operating point (P1, P2 and P3), the expander mass flow rate, the inlet pressure in the pump, the expander speed, the inlet EG temperature in the boiler, the EG pressure in the boiler, the EG mass flow rate and the inlet water temperature in the condenser are fixed.

Table 4.2: Inputs of the ORC model

Variable	P1	P2	P3	Units
$\dot{m}_{ET}$	73.85	75.99	74.79	kg/h
$P_{in,pump,ET}$	1.571	1.899	1.589	bar
N_{exp}	2001	2502	3003	rpm
$T_{in,b,EG}$	749.5	740	749	°C
$P_{out,b,EG}$	1.018	1.024	1.018	bar
$\dot{m}_{EG}$	154.98	159.47	155.25	kg/h
$T_{in,cond,W}$	48.5	49	48	°C

Table 4.3 shows the volumetric, the indicated, the mechanical (calculated using Equation 3.23, Equation 4.1 and Equation 4.2 respectively) and the isentropic expander efficiency (defined as the indicated efficiency times the mechanical efficiency in Equation 4.3). They have been fixed in the model.

Table 4.3: Experimental efficiencies of the Swash-plate expander

Variable	P1	P2	P3	Units
$P_{exp,is}$	3431	3413	3338	W
$P_{exp,ind}$	1739	2007	1874	W
$P_{exp,sh}$	1649	1543	1531	W
$\eta_{exp,vol}$	19.37%	17.21%	14.54%	-
$\eta_{exp,ind}$	50.68%	58.81%	56.14%	-
$\eta_{exp,mec}$	94.81%	76.90%	81.72%	-
$\eta_{exp,is}$	48.05%	45.22%	45.88%	-

Table 4.4 presents the model outputs for the three points tested. In each point three columns are presented, the first one, called "Pi E", corresponds to the experimental values, the second one, called "Pi M", corresponds to the modelled values and the last one, called "Dif.", corresponds to the absolute difference experimental-modelled. Temperatures are given in °C, pressures in bar, and torque in Nm. Figure 4.7, Figure 4.8, Figure 4.9 and Figure 4.10 show the model validation in each particular point. As regards temperatures, the maximum deviation corresponds to the inlet temperature in the expander at 2500 rpm expander speed, with a value of 3.28% (Figure 4.8). The remainder cycle temperatures are obtained with a difference lower than 3%. Regarding pressures, the maximum deviation corresponds to the inlet pressure in the condenser at 2500 rpm expander speed, with a value of 4.48% (Figure 4.8). The remainder pressures in the system are calculated with a difference of 3%. The last model parameter is the torque delivered by the expander (Figure 4.10), in which the maximum deviation is approximately 4%, which are in order of magnitude of the measurement errors.

Table 4.4: Outputs of the ORC model

Variable	P1 E	P1 M	Dif.	P2 E	P2 M	Dif.	P3 E	P3 M	Dif.	Units
$T_{out,pump,ET}$	47.5	46.5	0.31%	47	46	0.25%	48.5	46	0.70%	°C
$T_{out,b,ET}$	210	209	0.33%	215	199	3.28%	208	201	1.44%	°C
$T_{out,exp,ET}$	105	116	3.04%	109	107	0.50%	111	110	0.30%	°C
$T_{in,cond,ET}$	104	102.5	0.33%	103	99	1.16%	102	97	1.37%	°C
$T_{out,cond,ET}$	48	48.5	0.10%	48	48.5	0.17%	48	48.5	0.22%	°C
$T_{in,pump,ET}$	46.5	46	0.28%	46.5	46	0.23%	47.5	46	0.53%	°C
$T_{out,cond,W}$	74	71	0.71%	67	69	0.52%	73	71.5	0.38%	°C
$P_{out,pump,ET}$	34.26	34.26	0.01%	31.01	31.48	1.51%	31.77	31.16	1.92%	bar
$P_{in,exp,ET}$	28.65	29.57	3.20%	27	26.53	1.74%	26.01	26.36	1.33%	bar
$P_{in,cond,ET}$	1.89	1.89	0.20%	2.01	2.1	4.48%	1.9	1.88	0.95%	bar
τ_{exp}	7.81	7.98	2.18%	5.86	5.59	4.47%	4.87	4.96	1.85%	Nm

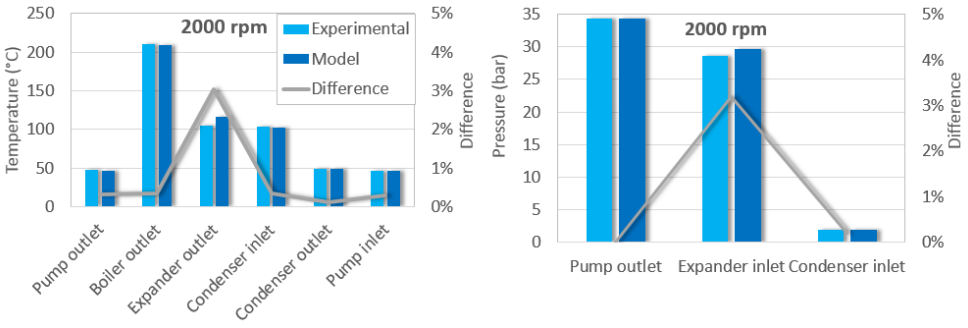

Figure 4.7: Validation of 2000 rpm

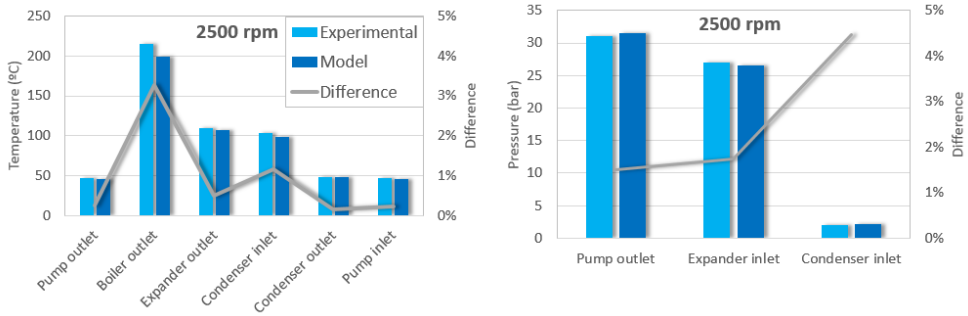

Figure 4.8: Validation of 2500 rpm

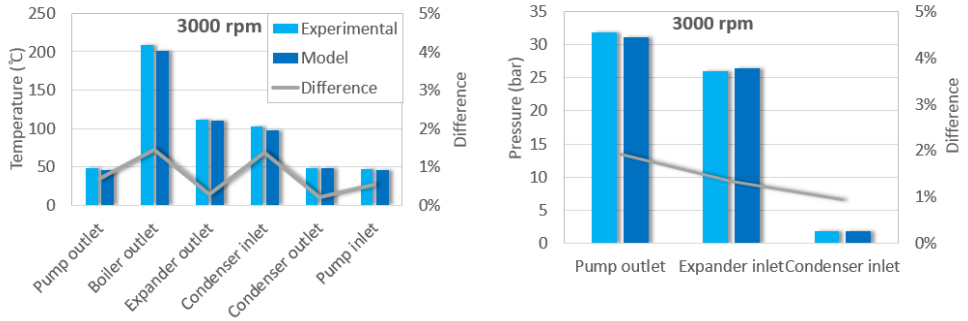

Figure 4.9: Validation of 3000 rpm

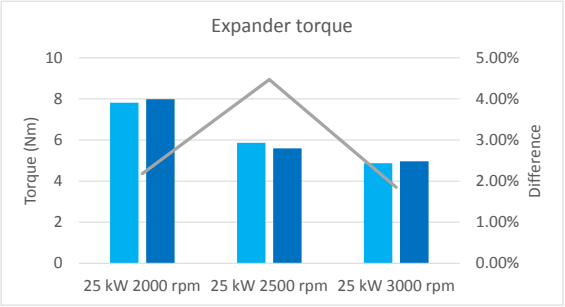

Figure 4.10: Validation of torque

Regarding the thermal inertias of the boiler, the modelled and experimental temperature curves at the ethanol boiler outlet are compared as a function of time. As shown in Figure 4.11, the outlet boiler temperature in the ethanol side considering a mass of 3 kg (1 kg in each node) fits well with the experimental value. In this figure, the real estimation of the boiler mass is also plotted. Temperature differences lower than 4% are found comparing modelled and experimental values.

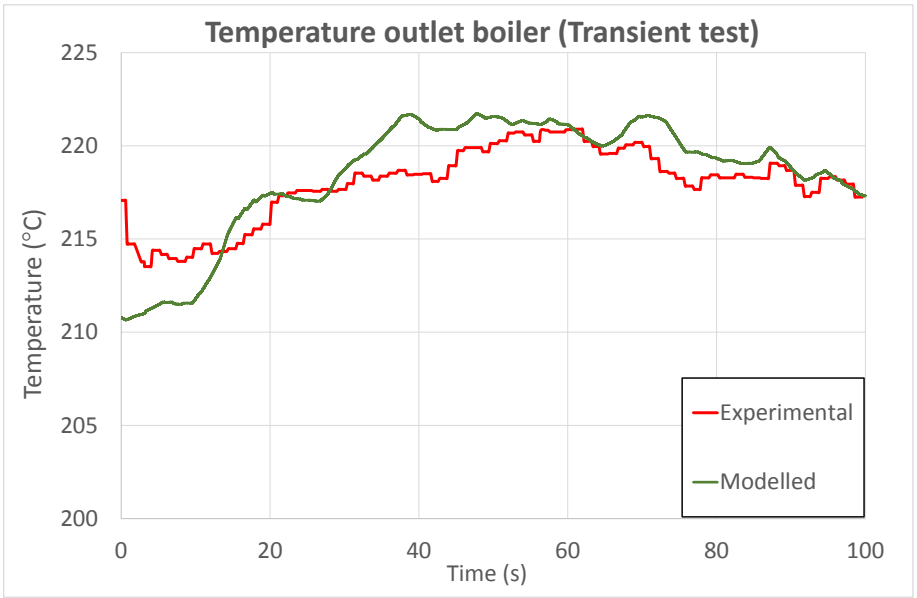

Figure 4.11: Validation of temperature in the boiler

Using the same methodology previously explained, the isentropic, indicated, mechanical and volumetric efficiency have been calculated in the case of 12 kW and 20 kW. They are correlated as a function of expansion ratio, expander speed and inlet density [115].

The indicated, isentropic, mechanical and volumetric efficiency are presented in Equation 4.6, Equation 4.7, Equation 4.8 and Equation 4.9 with a correlation coefficient of 97.68%, 97.88%, 97.71% and 99.18% respectively.

$$\begin{aligned}\eta_{exp,ind} &= 14.0343 - 0.0142681\cdot\gamma - 2.21228\cdot\delta - 2.19028\cdot\alpha \\ &+ 0.0000690197\cdot\gamma\cdot\delta + 1.19751\cdot\delta\cdot\alpha + 0.0128971\cdot\alpha\cdot\gamma \\ &- 0.165978\cdot\alpha^2\cdot\delta - 0.003142\cdot\alpha^2\cdot\gamma - 5.42654E-8\cdot\gamma^2\cdot\alpha\end{aligned} \tag{4.6}$$

$$\begin{aligned}\eta_{exp,is} &= 4.29509 - 0.00389453\cdot\gamma - 0.224077\cdot\delta - 1.51189\cdot\alpha \\ &- 0.00000702944\cdot\gamma\cdot\delta + 0.138259\cdot\delta\cdot\alpha + 0.00300458\cdot\alpha\cdot\gamma \\ &- 0.019192\cdot\alpha^2\cdot\delta - 0.000548418\cdot\alpha^2\cdot\gamma + 4.01272E-9\cdot\gamma^2\cdot\alpha\end{aligned} \tag{4.7}$$

$$\begin{aligned}\eta_{exp,mec} &= -1.53033 + 0.00422232\cdot\gamma + 1.51436\cdot\delta - 1.87031\cdot\alpha \\ &- 0.0000698883\cdot\gamma\cdot\delta - 0.816831\cdot\delta\cdot\alpha - 0.00488144\cdot\alpha\cdot\gamma \\ &+ 0.120578\cdot\alpha^2\cdot\delta + 0.00155725\cdot\alpha^2\cdot\gamma + 5.04689E-8\cdot\gamma^2\cdot\alpha\end{aligned} \tag{4.8}$$

$$\begin{aligned}\eta_{exp,vol} &= -2.42477 + 0.727519\cdot\beta - 0.0539788\cdot\beta^2 + 0.00901362\cdot\delta \\ &- 0.0000962218\cdot\delta^2\end{aligned} \tag{4.9}$$

Where α, β, γ and δ are defined in Equation 4.10, Equation 4.11, Equation 4.12 and Equation 4.13.

$$\alpha = \ln\frac{P_{in,exp,ET}}{P_{out,exp,ET}} \tag{4.10}$$

$$\beta = \ln N_{exp} \tag{4.11}$$

$$\gamma = N_{exp} \tag{4.12}$$

$$\delta = \rho_{in,exp,ET} \tag{4.13}$$

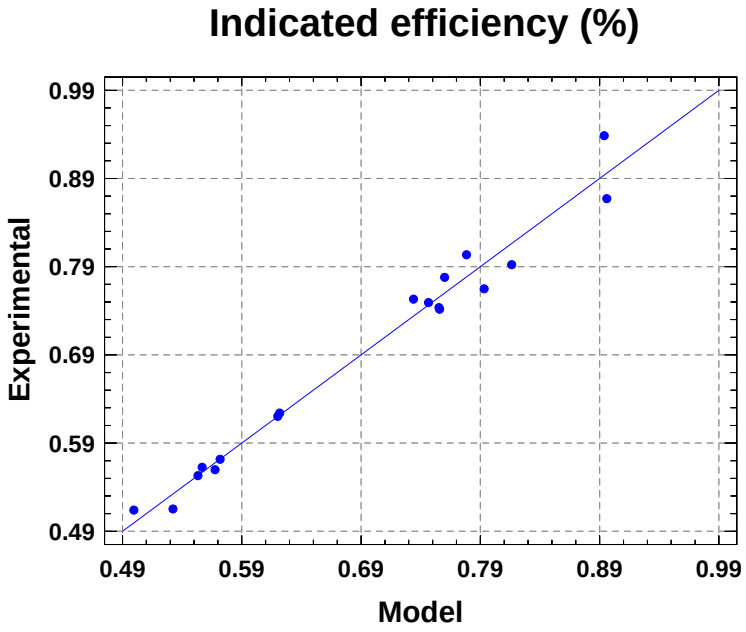

Figure 4.12: Validation of indicated efficiency correlation

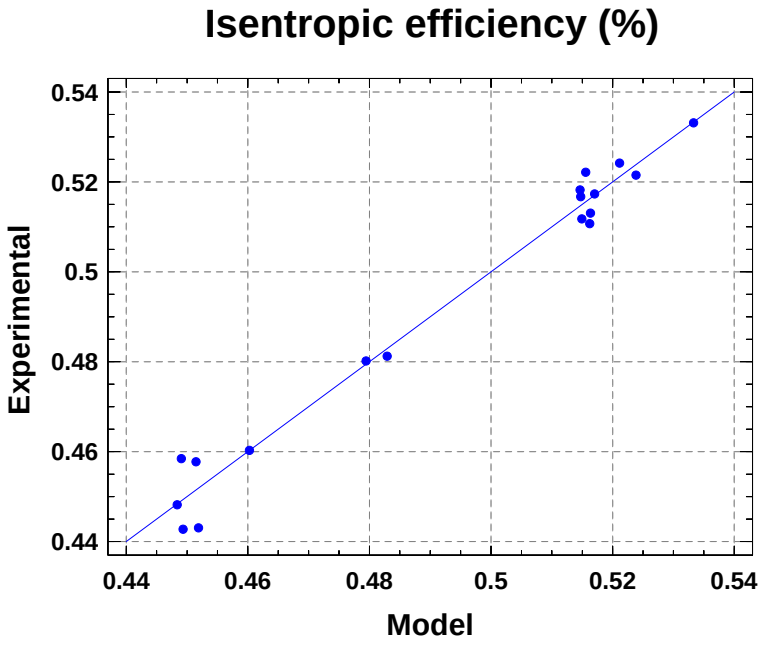

Figure 4.13: Validation of isentropic efficiency correlation

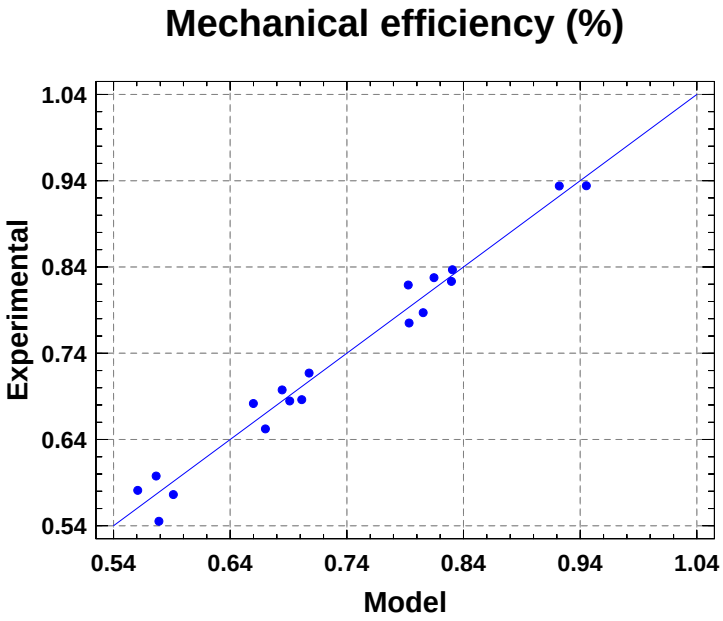

Figure 4.14: Validation of mechanical efficiency correlation

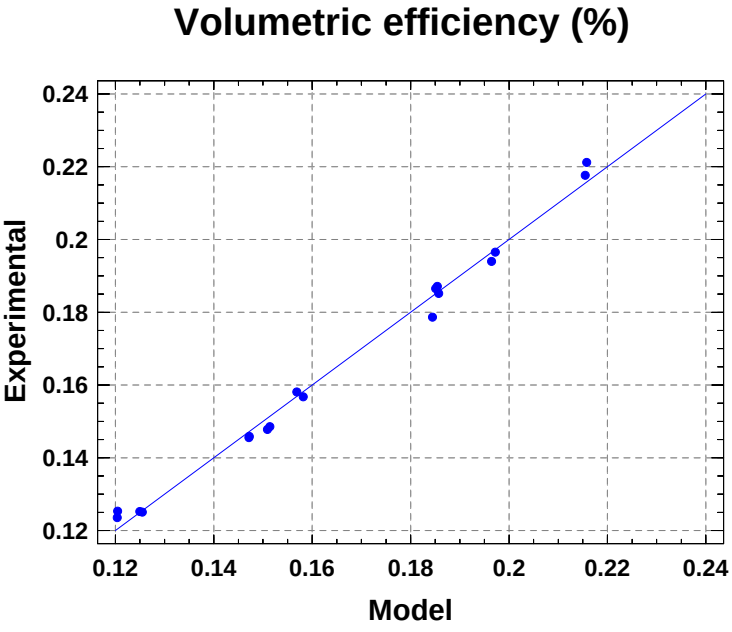

Figure 4.15: Validation of volumetric efficiency correlation

4.3.2 Swash-plate specific model

The modelled and experimental pressure variation curves inside the expander chamber are compared for the three points tested in previous sections (3000 rpm, 2500 rpm and 2000 rpm) in Figure 4.16, Figure 4.17 and Figure 4.18. It is found quite good agreement between experimental (light blue) and modelled (dark blue) results in terms of indicated work delivered by the expander. In the right corner of these diagrams both the indicated work and the expander speed are shown. Differences up to 10.5% could be found in these models due to pressure drop in the valves and effects of pulsating flow, which is not modelled in AMESim with the Two-Phase flow library.

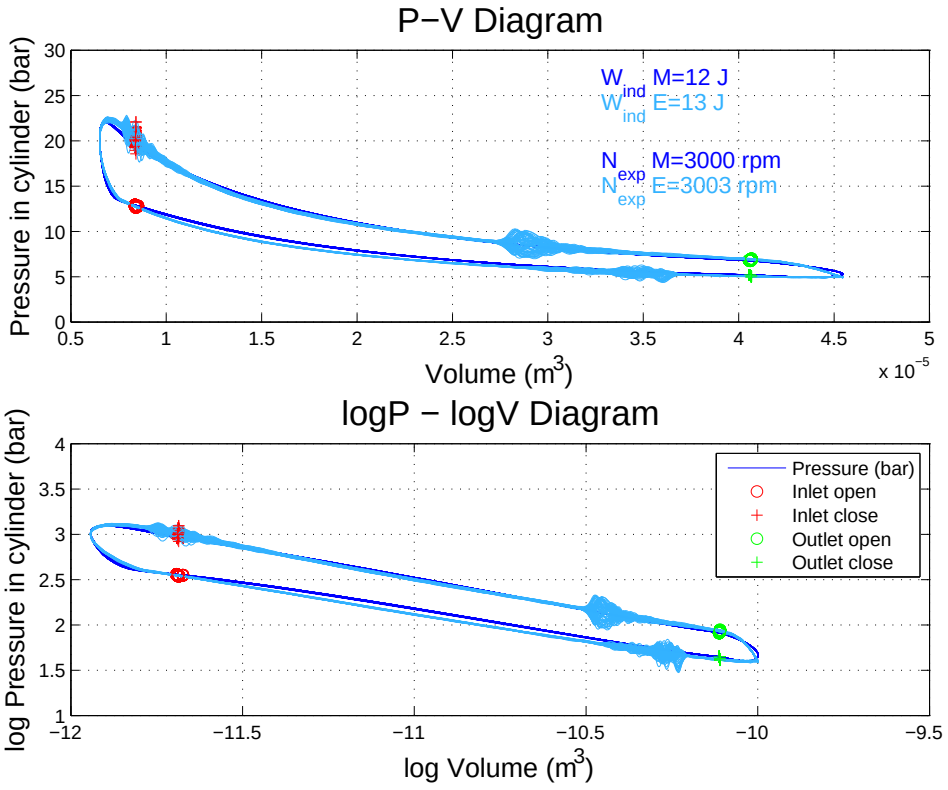

Figure 4.16: Validation P-V Diagram 3000 rpm

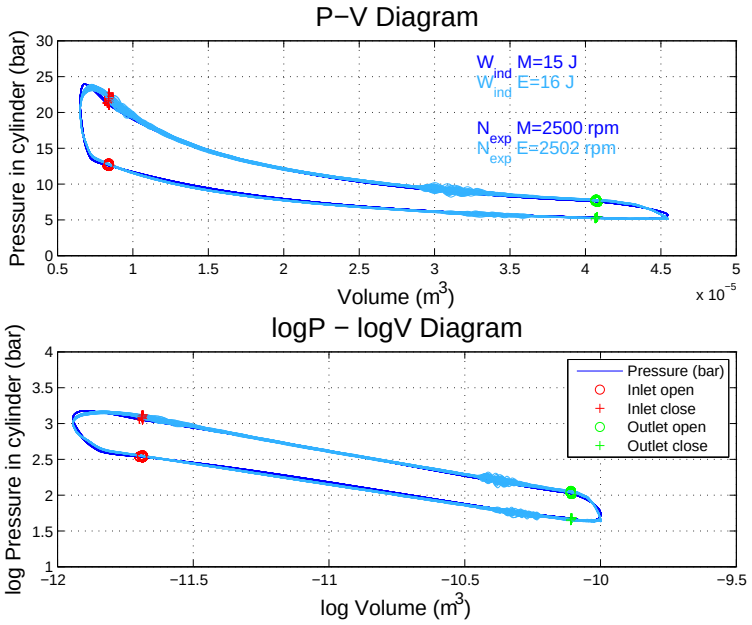

Figure 4.17: Validation P-V Diagram 2500 rpm

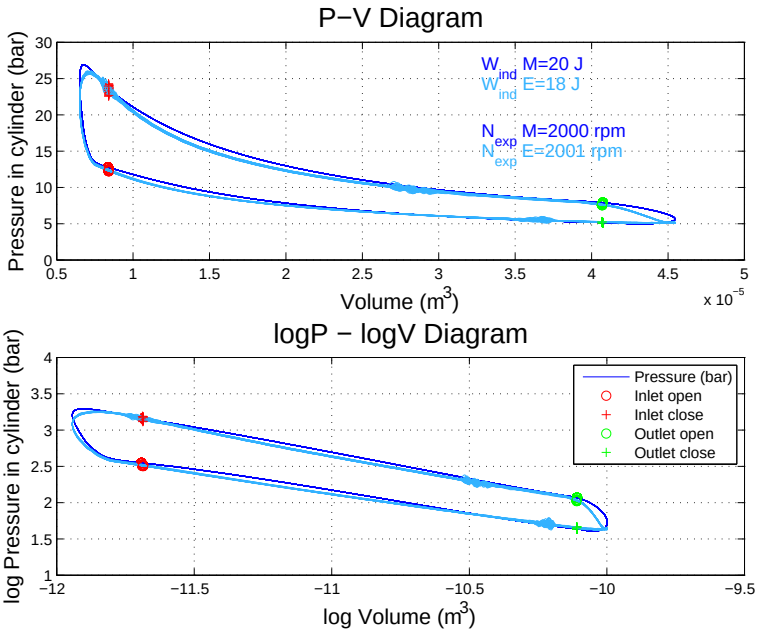

Figure 4.18: Validation P-V Diagram 2000 rpm

Table 4.5 summarizes the Swash-plate model result. The model inputs are obtained from measurements of inlet pressure and expander speed. In order to take into account differences between heat transferred in the three points, the compression and expansion coefficients are modified. In this model the higher the expander speed is, the higher heat transfer rate should be imposed to the model. Table 4.5 also shows the indicated power results in watts. The maximum power deviation in the model corresponds to 10% in the 3000 rpm expander operating point, which is considered acceptable to predict flow behaviour. Although the P-V diagram of point P3 fits better than the others, this effect is not noticeable comparing the powers in watts due to the expander speed (Equation 4.4). Besides, the model predicts properly the filling and emptying processes as it can be seen in Figure 4.16, Figure 4.17 and Figure 4.18.

Table 4.5: Results of the Swash-plate model

Variable	**P1**	**P2**	**P3**	**Units**	**I/O**	**Exp./Model**
$P_{in,exp,ET}$	28.65	27	26.01	bar	Input	E
N_{exp}	2001	2502	3003	rpm	Input	E
W_{ind}	18	16	13	J	-	E
W_{ind}	20	15	12	J	Output	M
P_{ind}	1739	2007	1874	W	-	E
P_{ind}	1857	1877	1678	W	Output	M
Dif. Power (%)	6.79%	6.48%	10.46%	-	-	-

4.4 Case study: ORC coupled to a MVEM

In order to evaluate the potential of the Organic Rankine Cycle, a Mean Value Engine Model (naturally aspirated 2 l gasoline engine) with a clutch, a gearbox and a basic control on a driving cycle is used as heat ORC source. MVEM are mainly used for low frequency control loop design and validation, but also vehicle integration studies. This kind of model needs to be provided with maps or correlations as inputs for volumetric efficiency, indicated efficiency and exhaust efficiency or exhaust temperature. As stated in chapter 3, NEDC cycle produce not enough power to run the expander in normal operating conditions starting from engine cold conditions. Therefore, the NEDC extra-urban part has been simulated in this case study. The driving profile simulated in this model is similar to the one presented in the transient experimental section (Figure 3.39). It corresponds to the higher exhaust energy recovery potential. The expander and by-pass control has been made according to Figure 4.2. Regarding the pump speed, it has been controlled according to the engine speed (with a ratio of 10), in agreement with the order of magnitude of the experimental tests presented in chapter 3.

The main characteristics of the model are:

- 2.0 L gasoline engine (MVEM)
- Naturally aspirated
- Roller test bench configuration
- Personal driving cycle (last part of the NEDC)
- Organic Rankine Cycle coupled to the MVEM
- Ethanol as working fluid
- Volumetric expander and pump
- Expansion vessel model to control the low pressure in the ORC

Figure 4.19 shows the Mean Value Engine Model coupled to the ORC. In the following subsections the pressure drop, the expander power and the improvement in torque, bsfc and fuel conversion efficiency [10] of the system engine + ORC compared to the original engine are presented.

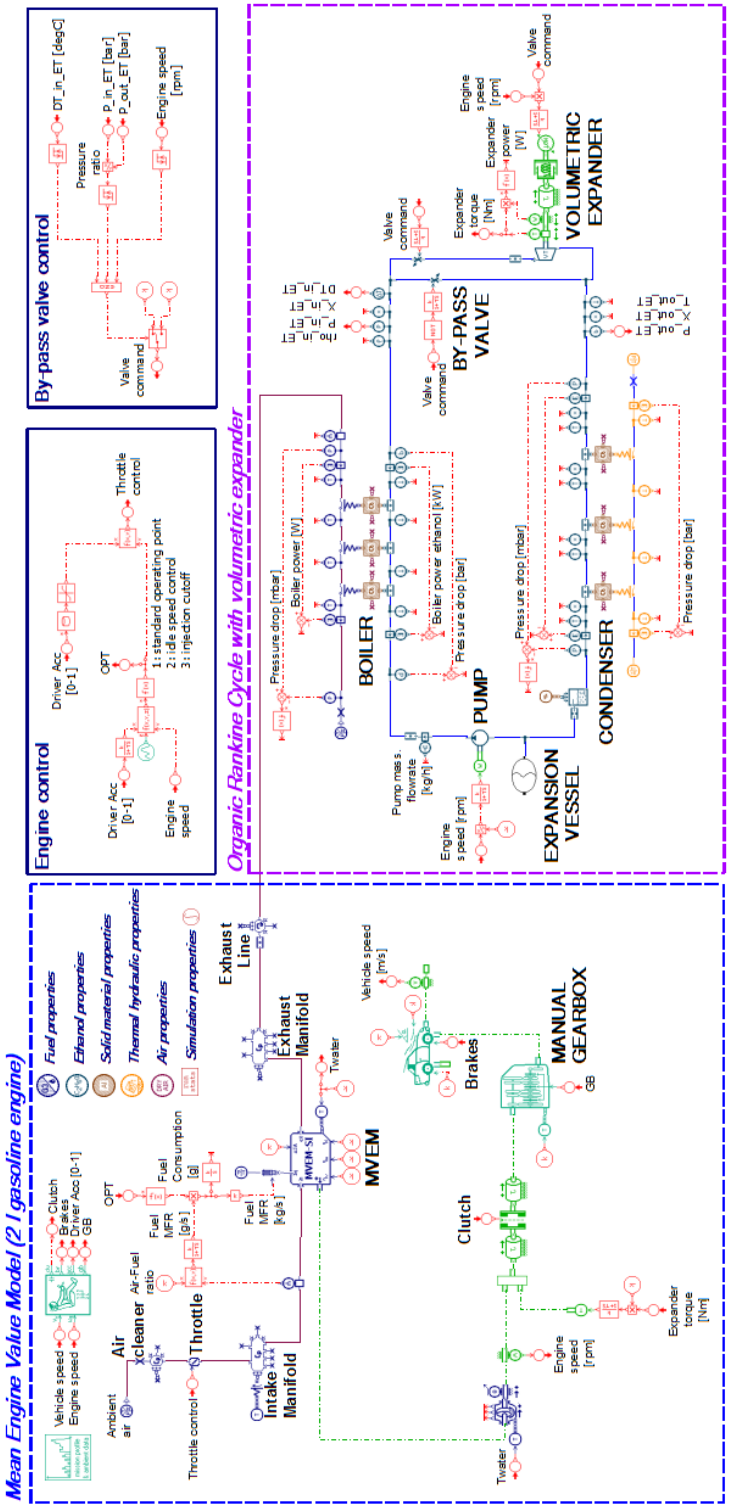

Figure 4.19: Mean Value Engine Model with ORC

4.4.1 Pressure drop in the boiler

Figure 4.20 shows the pressure drop in the boiler. The exhaust gases pressure drop (in mbar) is plotted in red in the left axis and the ethanol pressure drop (in bars) is plotted in blue in the right axis. The vehicle velocity (in m/s) is plotted in black in the left axis. The pressure drop in the boiler varies between 5-20 mbar, depending on the engine operating point. Ethanol pressure drop in the boiler varies between 2-6 bar. Therefore, they are in the order of magnitude of the ones presented in the experimental tests (chapter 3).

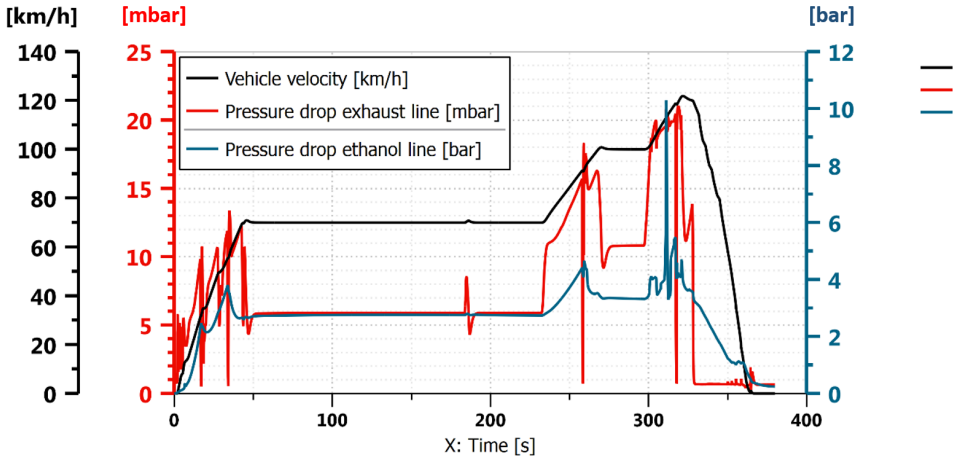

Figure 4.20: Exhaust gas pressure drop in the boiler in mbar (left axis) and ethanol pressure drop in the boiler in bar (right axis)

4.4.2 Power delivered in the expander

Figure 4.21 shows the power delivered by the expander during the extra-urban part of the NEDC. On the left axis the vehicle velocity (in km/h) and on the right axis the expander power (in watts) is plotted in blue. The expander operation response is obtained from the control presented in Figure 4.2. The maximum power delivered by the expander in the experimental test is approximately 800 W (Figure 3.39), which is the same value as in the simulation. The shape of the power delivered by the expander is also similar to the tested one.

4.4.3 Impact on vehicle torque

In order to evaluate the ORC impact on the engine, the torque delivered by the expander has been added to the torque delivered by the engine (yellow line). It is compared to the initial engine torque (blue line). It is presented in Figure 4.22. As it can be seen in this figure, an additional torque is added when the expander is running (at 310 s approximately). It can increase the boost up to 17 Nm. Therefore, this implies an additional torque of 18% compared to the original engine configuration.

4.4.4 Impact on bsfc and fuel conversion efficiency

As shown in Figure 4.22, the WHRS is a suitable technology to recover energy in the high load NEDC operating points (at 120 km/h). Therefore, in order to estimate the potential of this technology, both fuel conversion efficiency and brake specific fuel consumption (bsfc) are computed and presented in Figure 4.23 during the expander running period. As it is shown in this figure, a 2.5% improvement in fuel conversion efficiency can be obtained as a direct consequence of the 23.5 g/kWh reduction in bsfc comparing the system engine + ORC to the original engine configuration. In this figure, a discontinuity appears in the second 317 due to the simulation of the driver gear change in the vehicle.

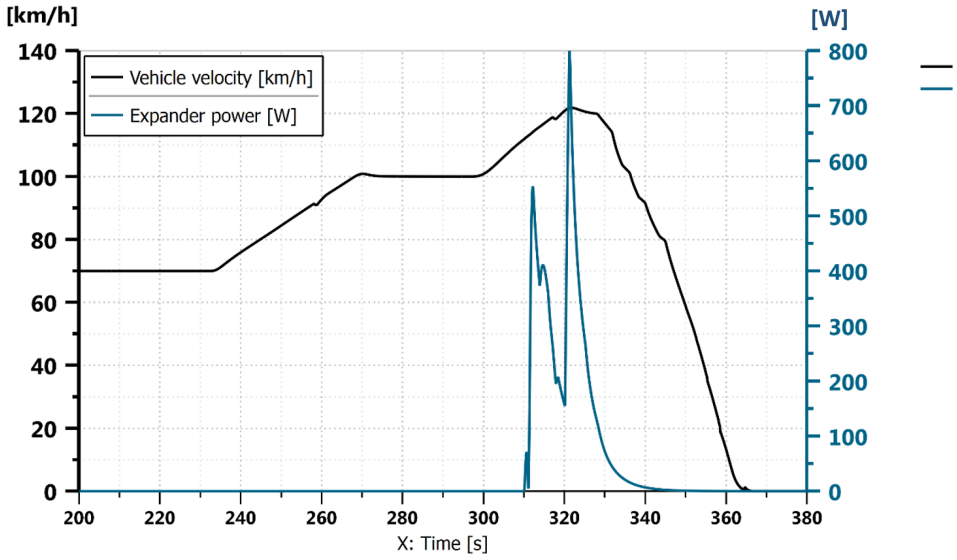

Figure 4.21: Vehicle velocity in km/h (left axis) and expander power in watts (right axis)

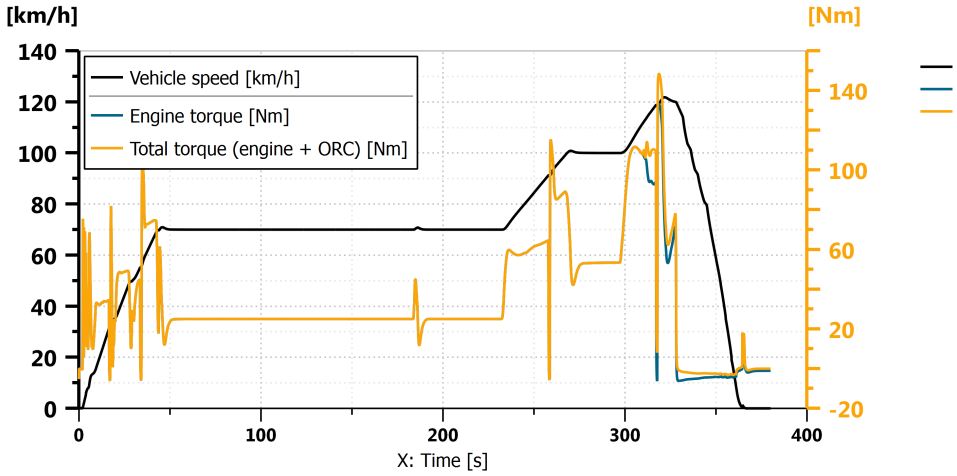

Figure 4.22: Engine torque in Nm (blue line) and Engine + ORC torque in Nm (yellow line)

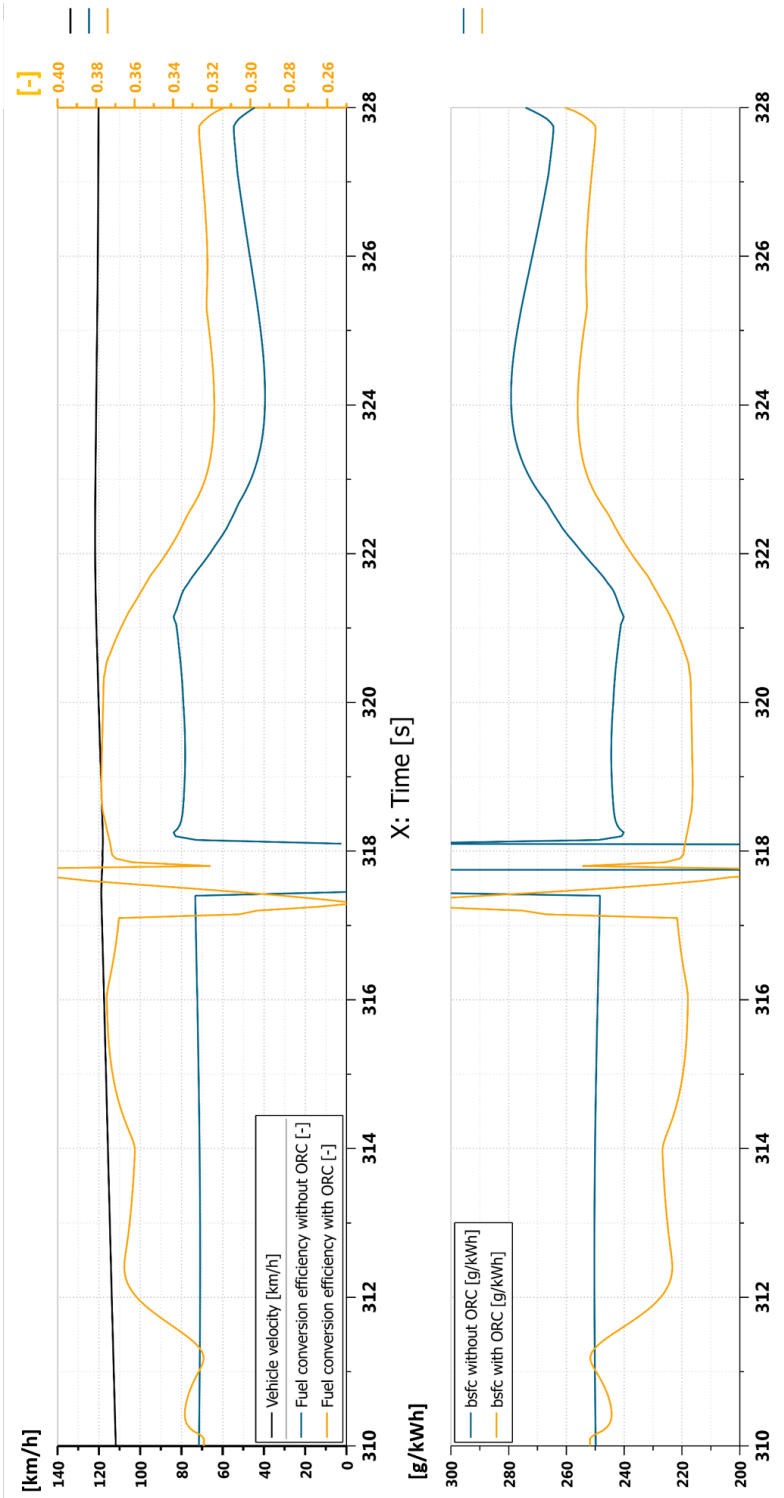

Figure 4.23: Comparison between engine efficiency and bsfc in g/kWh with and without the ORC

4.5 Summary

The presented chapter describes and analyzes some models based on an experimental ORC installation installed in a turbocharged 2.0 l gasoline engine to recover waste heat in exhaust gases. These models correspond on one side to the global ORC cycle and on the other side to a specific submodel of the Swash-plate expander. The performance parameters comparison have been made in three points by means of changing the inputs and obtaining the outputs of the model. The results are summarized in the following points:

- An ORC model is developed using LMS Imagine.Lab Amesim platform. This model allows to simulate the main parameters measured in the cycle. Comparing the three steady-state operating points, a maximum pressures and temperatures deviation of 4% and 5% regarding torque is attained.
- A Swash-plate expander model is presented using the LMS Imagine.Lab Amesim platform. This model represents the fluid dynamic Swash-plate behaviour using discharge coefficients, displacement laws, heat transfer coefficients and mechanical losses. The P-V diagram is measured by a piezoelectric pressure sensor and is compared to the expander model. Maximum indicated power deviation of 10% is achieved at point of 3000 rpm.
- A case study with a Mean Value Engine Model (naturally aspirated 2 l gasoline engine) with a clutch, a gearbox and a basic control on a driving cycle is used as the Organic Rankine Cycle heat source. The maximum power delivered by the expander in the extra-urban part of the NEDC is approximately 800 W (Figure 3.38), which is the same value as in the simulation. A potential fuel conversion efficiency improvement of 2.5% is obtained in the high operating points of the NEDC (120 km/h) as a direct consequence of the 23.5 g/kWh bsfc reduction comparing the system engine + ORC to the original engine configuration.

4.6 References

[1] J. Galindo, S. Ruiz, V. Dolz, L. Royo-Pascual, R. Haller, B. Nicolas, and Y. Glavatskaya. "Experimental and thermodynamic analysis of a bottoming Organic Rankine Cycle (ORC) of gasoline engine using swash-plate expander". In: *Energy Conversion and Management* 103 (2015), pp. 519–532. ISSN: 01968904. DOI: 10.1016/j.enconman.2015.06.085. URL: http://linkinghub.elsevier.com/retrieve/pii/S0196890415006470 (cit. on pp. vii, 13, 23, 28, 115, 116, 181).

[10] J. B. Heywood. *Internal combustion engine fundamentals*. 1988, pp. 1–930. ISBN: 007028637X. URL: http://books.google.es/books/about/Internal{_}combustion{_}engine{_}fundamentals.html?id=u9FSAAAAMAAJ{\&}pgis=1 (cit. on pp. 2, 15, 126).

[110] M. Shah. "A General Correlation for Heat Transfer During Film Condensation inside Pipes". In: *International Journal of Heat and Mass Transfer* 22 (1979), pp. 547–556. ISSN: 00179310. DOI: 10.1016/0017-9310(79)90058-9 (cit. on p. 110).

[111] D. Steiner and J. Taborek. "Flow Boiling Heat Transfer in Vertical Tubes Correlated by an Asymptotic Model". In: *Heat transfer engineering* 13 (2010), pp. 322–329. URL: http://65.54.113.26/Publication/3107655/flow-boiling-heat-transfer-in-vertical-tubes-correlated-by-an-asymptotic-model (cit. on p. 110).

[112] E. S. Richardson. "Thermodynamic performance of new thermofluidic feed pumps for Organic Rankine Cycle applications". In: *Applied Energy* 161 (2016), pp. 75–84. ISSN: 03062619. DOI: 10.1016/j.apenergy.2015.10.004. URL: http://dx.doi.org/10.1016/j.apenergy.2015.10.004 (cit. on pp. 112, 178).

[113] S. Churchill. "Friction-factor equation spans all fluid flow regimes". In: *Chem. Eng.* (1977), pp. 91–92 (cit. on p. 112).

[114] R. McAdams, W.H., Woods, W.K., and Bryan. "Vaporization inside horizontal tubes -II- Benzene-oil mixtures". In: *Trans. ASME* 64 (1942), p. 193 (cit. on p. 112).

[115] S. Quoilin. "Sustainable energy conversion through the use of Organic Rankine Cycles for waste heat recovery and solar applications". PhD thesis. 2011, pp. 1–183. ISBN: 0-7803-3213-X. arXiv: 9605103 [cs]. URL: http://orbi.ulg.ac.be/handle/2268/96436 (cit. on p. 120).

CHAPTER 5

Thermodynamic evaluation of the cycle

Contents

Figures

5.1 Introduction

In the previous chapter a model of the ORC has been presented. In order to understand the operating conditions and limitations of the cycle, a thermodynamic evaluation of the working fluid and an exergetic analysis of the cycle are presented in this chapter.

The present chapter contains two parts:

- section 5.2 corresponds to the description and comparison of six different working fluids (water, ethanol, MM, R245fa, n-pentane and R1234ze). The engine operating conditions (inlet exhaust temperature) and the cycle operating conditions (superheating and evaporation pressure) have been varied to understand the behaviour of the cycle in term of pinch point, the expander power and the output volume flow rate at the outlet of the expander.

- section 5.3 focuses on the advanced and conventional exergy analysis [116] of the Organic Rankine Cycle. Exergy analysis can identify the sources, magnitude and location of thermodynamic inefficiencies of a system, which can give the appropriate information for improving the overall efficiency of the system focusing on the worse exergy balance elements. The conventional exergy analysis has traditionally been studied and applied to some applications in ICE [117, 118]. However, this analysis is used to evaluate the performance of an individual component, without taking into account interactions among components. Therefore, the advanced exergy analysis was proposed to evaluate energy conversion systems by splitting the exergy in endogenous/exogenous and avoidable/unavoidable. Splitting the exergy into unavoidable and avoidable provides a measure of the potential of improving the efficiency of this component. On the other hand, splitting the exergy into endogenous and exogenous provides information between interactions among system components. The objective of this section is to quantify, on the basis of reasonable assumptions, the impact of improvements in each component of the system to the global performance of the system using an advanced exergy analysis method.

5.2 Working fluids

5.2.1 Selection of working fluids

Characteristics of the working fluids have been extensively explained in subsection 2.3.1. Considering these characteristics, a pre-selection of 6 working fluids has been made for the ORC application. Figure 5.1 shows the T-s diagram of the considered working fluids (Water in blue, ethanol in black, MM in orange, R245fa in red, n-pentane in green and R1234ze in purple).

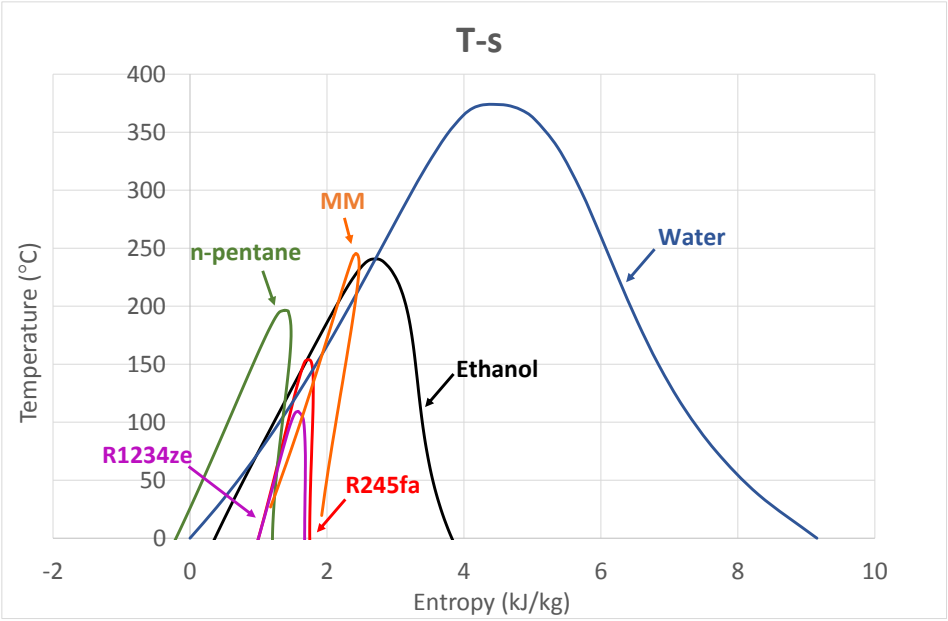

Figure 5.1: T-s diagram

The characteristics of the fluids are summarized in Table 5.1. Ethanol is an alcohol, MM is a siloxane, n-pentane is an hydrocarbon, HFC-245fa and HFO-1234ze are refrigerant fluids. HFC-245fa has been used for a long time in ORC applications. However, due to its high level of GWP, its use will be phased down in the forecoming years. Therefore, new refrigerant working fluids are considered, i.e. the HFO-1234ze. By contrast, n-pentane, MM and ethanol have low GWP and ODP levels. However, their flamability is higher than for the refrigerant fluids. Table 5.1 shows the properties of the working fluids. As previously explained, no existing working fluid has the best characteristics in all the aspects. Therefore, these 6 working fluids have been compared by means of sensitivity studies.

Table 5.1: Properties of working fluids

Parameters	**HFC-245fa**	**HFO-1234ze**	**Ethanol**	**Water**	**n-pentane**	**MM**
Chemical formula	$CF_3CH_2CHF_2$	$CF_3CH{=}CHF$	CH_3CH_2OH	H_2O	$CH_3CH_2CH_2CH_2CH_3$	$C_6H_{18}OSi_2$
Tc (°C)	154.16	109.51	240.9	373.94	197	245.5
Pc (bar)	36.5	36.36	61.4	220.6	33.6	19.39
Molar weight (kg/kmol)	134	114	46.06	18	72.15	162.4
Slope	Dry	Dry	Wet	Wet	Dry	Dry
Flammability class	Non flammable	Non flammable	Severe Flammability	-	Serious Flammability	Low Flammability
ASHRAE Std 34 safety class	B1	A2L	A3	-	A3	B1
Atmospheric Life (yr)	7.6	0.0388	0.01	-	<0.01	<0.01
ODP	0	0	0	-	0	0
GWP	1030	4	1	-	11	-
Boiling point (°C)	14.96	-19	78.37	100	36.1	100.52
Melting point (°C)	-103	ND	-114	0	-129.8	-68.22
Ignition temperature (°C)	412	368	363	-	260	340
Latent heat at boiling point (kJ/kg)	196.23	184.28	920.66	2264.76	167.19	230.4
Vapour density at 300 K (kg/m^3)	9.13	11.65	0.163	0.02579	2.223	0.4018
Liquid density at 300 K (kg/m^3)	1333.5	1240.56	783.7	996.5	618.8	756.8
Vapour specific heat at 300 K (kJ/kgK)	0.96	0.88	1.53	1.889	1.716	1.478
Liquid specific heat at 300 K (kJ/kgK)	1.33	1.32	2.44	4.18	2.325	1.91

In the first study, the exhaust gas temperature and the evaporating pressure have been varied between 250 °C - 673 °C and 5 bar - 40 bar respectively in order to understand the behaviour of such fluids under different engine operating conditions. The exhaust gas mass flow is constant with a value of 48 g/s (Table 3.1). The results are presented in subsection 5.2.2. The superheating remained constant with a value of 20 °C to be able to compare all the fluids with the same operating conditions. Three output parameters have been compared: the pinch point (Figure 5.2), the expander power (Figure 5.3) and the output volume flow rate at the outlet of the expander (Figure 5.4). In these figures, there are three types of thermodynamic limits:

- PP (Pinch point): The pinch point can not be lower than 10 °C to ensure the proper heat transfer in the boiler [119].
- TP (Two Phase): This limit is related to the working fluid phase at the outlet of the expander, it should be in vapor phase to avoid drop formation and expander damage.
- DT (Degradation Temperature): There are some fluids that can not be superheated above a temperature to avoid degradation.

As it can be seen in Figure 5.2, ethanol has the higher pinch point operating range and can be used almost in all the range without any limit. The pinch point varies between 10 °C and 170 °C. Compared to water, it has a wider operating range because water can only operate under higher inlet operating temperatures. In order to increase the operating range, a higher degree of superheating should be considered, but in this case the power released in the condenser increases substantially. R-245fa and n-pentane can operate in almost all range of inlet temperatures, taking into account that there is a limit in the lower evaporating pressure due to Two Phase conditions and in the higher evaporating pressure due to Degradation temperature. The last two fluids (R-1234ze and MM) have higher operating restrictions and can only be operated between 30 - 35 bar and 5 - 20 bar respectively. Considering these limitations, the power delivered by the expander and the output volume flow rate have been computed. As shown in Figure 5.3, the power delivered by the expander for the R-245fa, R-1234ze and n-pentane are very low (lower than 2 kW) compared to the rest of the fluids. The ethanol expander power output range goes from 1 kW to 4.5 kW and the water from 2 kW to 6 kW. However, the latter can only operate under high engine exhaust temperatures. Figure 5.4 shows the outlet volume flow rate in the expander. R245fa, n-pentane, R1234ze and ethanol have the same order of magnitude, with a maximum value of $0.009\,m^3\,s^{-1}$ for the ethanol. For MM and water the maximum volume flow rate is $0.014\,m^3\,s^{-1}$ and $0.025\,m^3\,s^{-1}$ respectively. In the case of water, it could be a problem because

of the volumetric expansion ratio needed. This will imply bigger expansion machines and problems with the packaging for the vehicle applications.

In the second study, the superheating temperature and the evaporating pressure has been varied between 20 °C - 40 °C (except the water that have been varied between 200 °C - 300 °C) and 5 bar - 40 bar respectively in order to understand the behaviour of such fluids under different cycle operating conditions. The results are presented in subsection 5.2.3. The inlet exhaust gases temperature has remained constant with a value of 673 °C to be able to compare all the fluids with the same engine operating conditions. Three output parameters have been compared: the pinch point (Figure 5.5), the expander power (Figure 5.6) and the output volume flow rate at the outlet of the expander (Figure 5.7). As it can be seen in Figure 5.5, there is no limitation in this case regarding the pinch point, because in this case the higher exhaust temperature has been used. Moreover, the superheating temperature in the water has been increased to avoid this limitation. The higher level of pinch point is found for the n-pentane (value of 480 °C) and the lower level is found for the water (value of 10 °C). Considering these limitations, the power delivered by the expander and the output volume flow rate have been computed. As it can be seen in Figure 5.6, the water delivers the highest expander power (greater than 6.6 kW) compared to the rest of the fluids. The ethanol expander power output range goes from 1 kW to 4.5 kW. The rest of the fluids achieve lower expander power. Differences between level of superheating in the water and ethanol can be seen. Figure 5.7 shows the outlet volume flow rate in the expander. R245fa, n-pentane and R1234ze have the same order of magnitude, with the maximum value of $0.005\,m^3\,s^{-1}$ for the n-pentane. The water has double volume flow rate compared to ethanol, which will have an effect on the size of the expander machine.

To sum up, R-245fa and R-1234ze have smaller Mollier diagram, lower critical temperature values and lower enthalpy drop in the boiling process. Therefore, considering a fixed exhaust power source, the fluid mass flow increases as enthalpy drop decreases. Moreover, vapor isobars are closer than for other fluids such as ethanol and water. This implies lower enthalpy drop in the expansion process and thus lower power delivered by the expander in these fluids. The volume flow rate is lower than for the ethanol or water, due to the high density of these fluids in vapor conditions. Water has been widely used in the Rankine cycle, however it is not the ideal working fluid due to its thermal characteristics. The size of the expander and the condenser will be bigger because of the volumetric flow rate and the degree of superheating. It will have an effect on the pinch point. MM and n-pentane are good candidates for the exhaust gases temperature range of vehicles, with a smaller operating range than ethanol. Ethanol has good thermal characteristics in the whole range of ICE temperatures (diesel and gasoline).

5.2.2 Variation of the heat source conditions

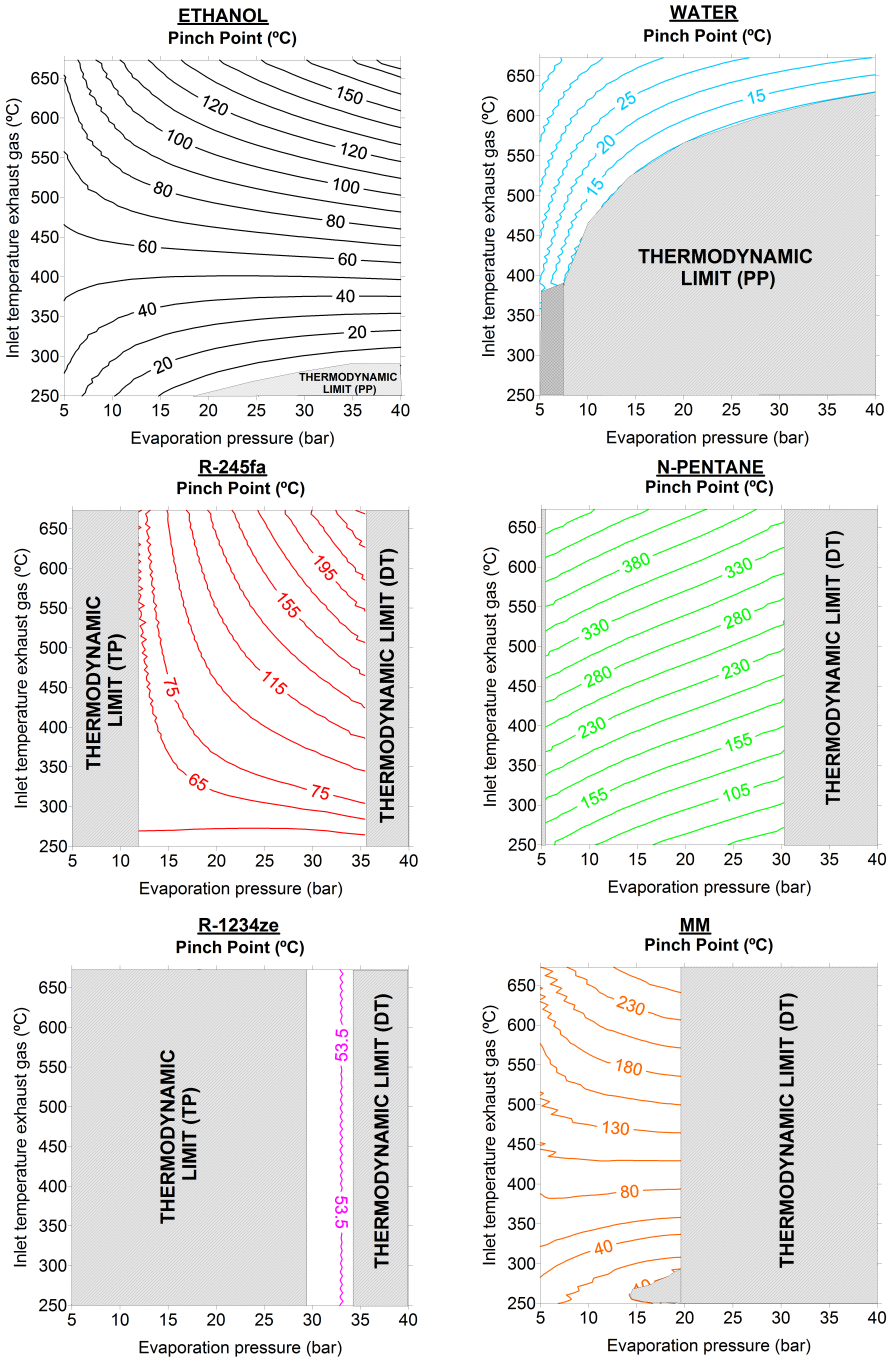

Figure 5.2: Pinch point working fluids

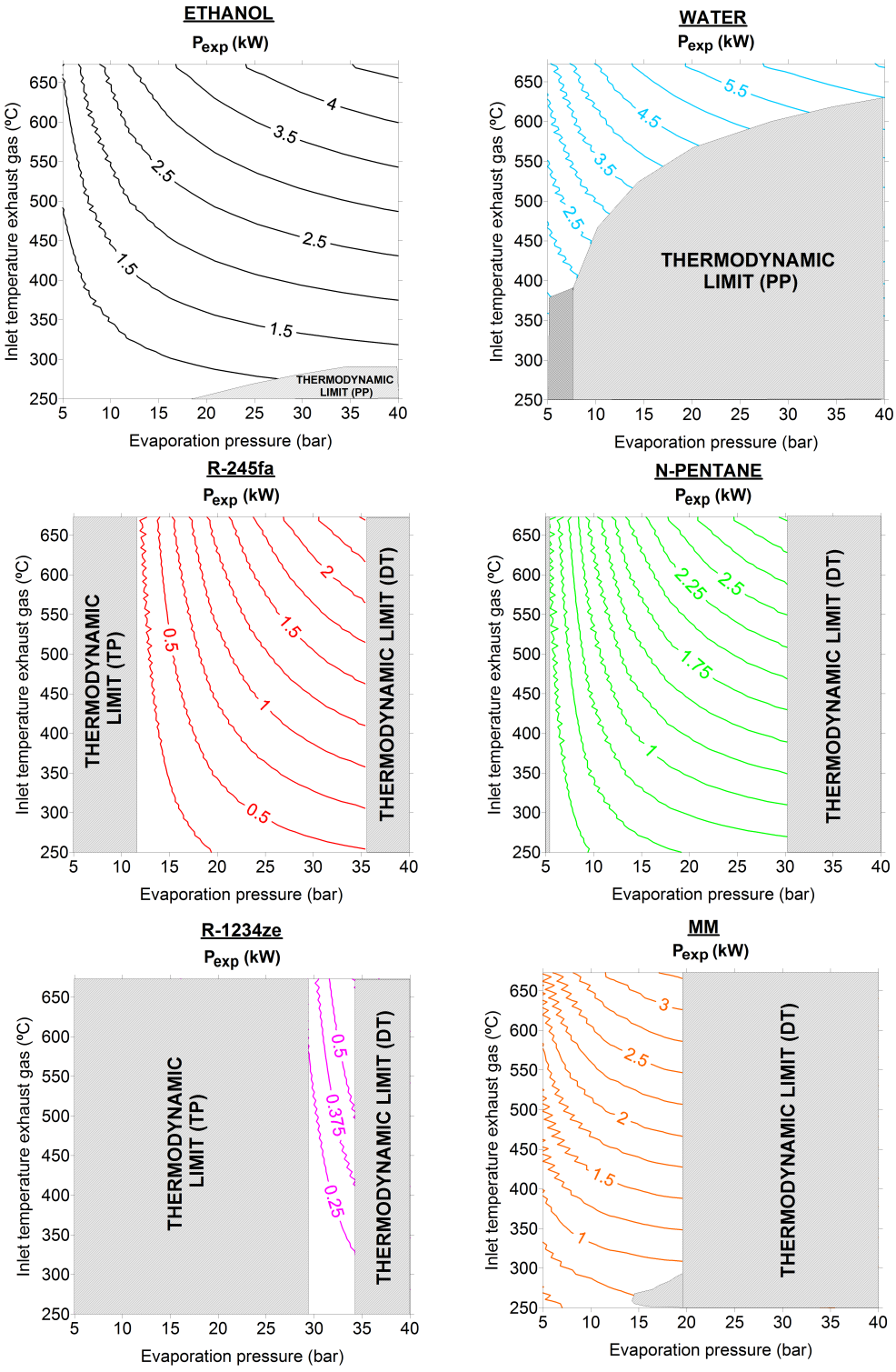

Figure 5.3: Expander power working fluids

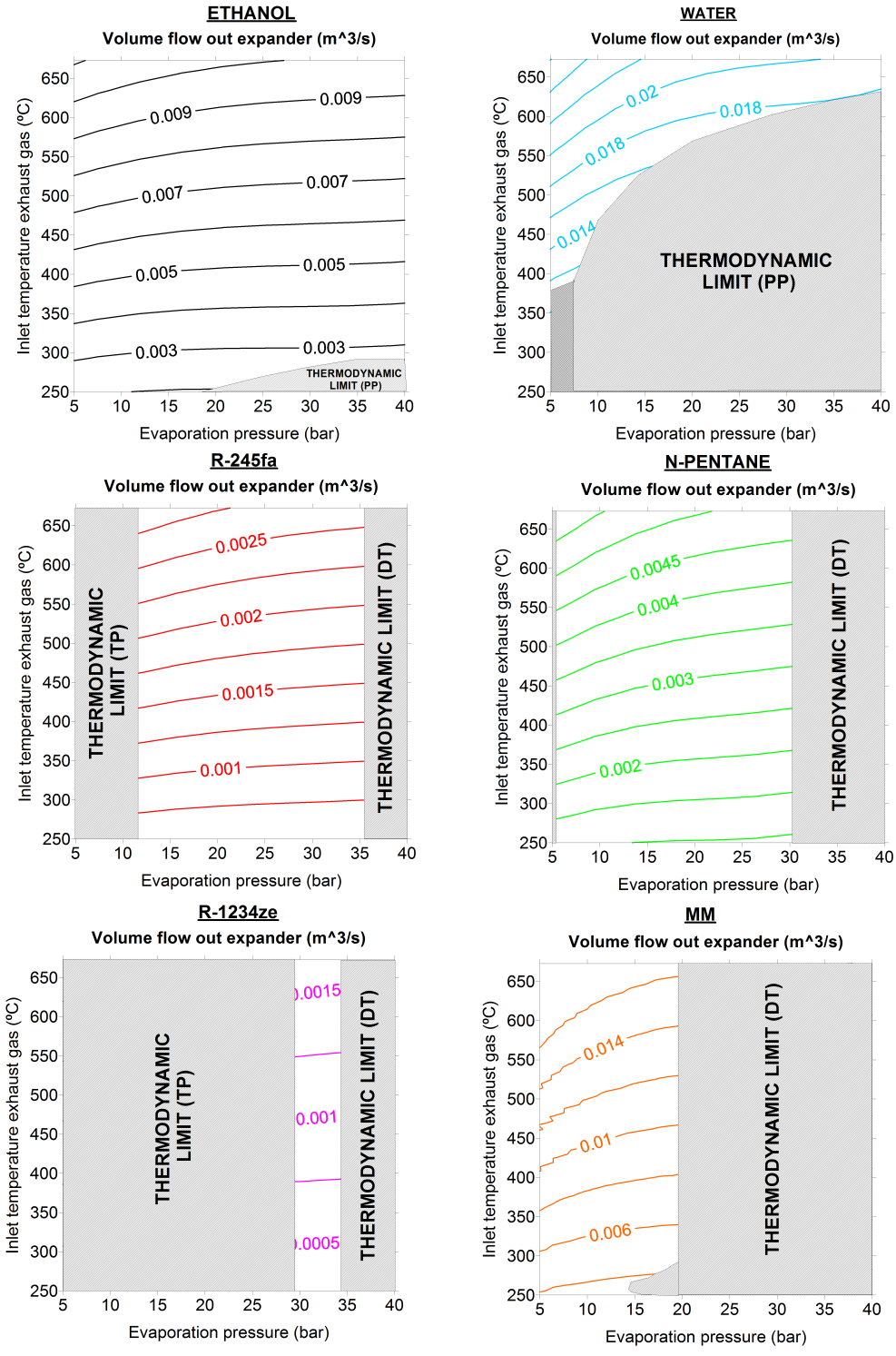

Figure 5.4: Volumetric flow rate working fluids

5.2.3 Variation of cycle conditions

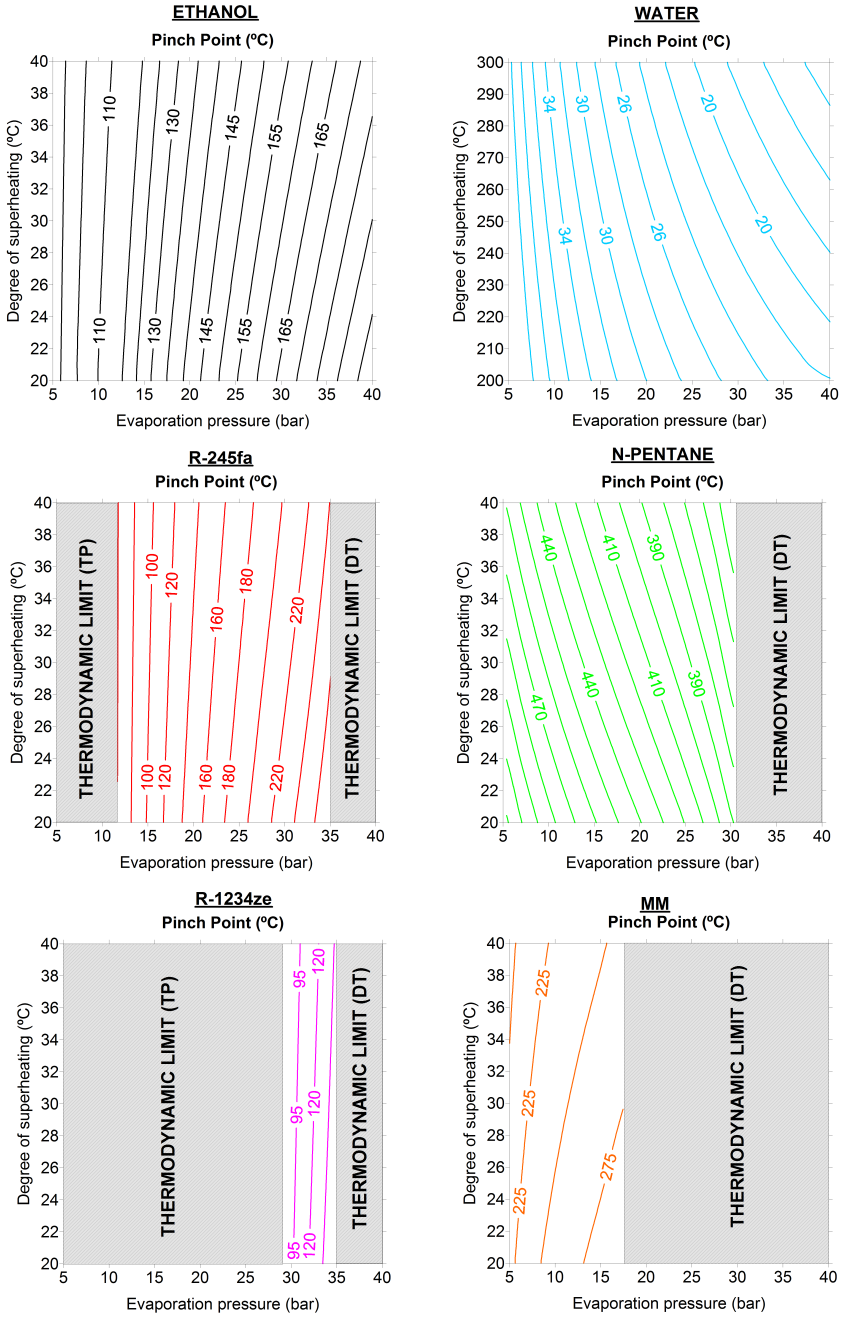

Figure 5.5: Pinch point working fluids

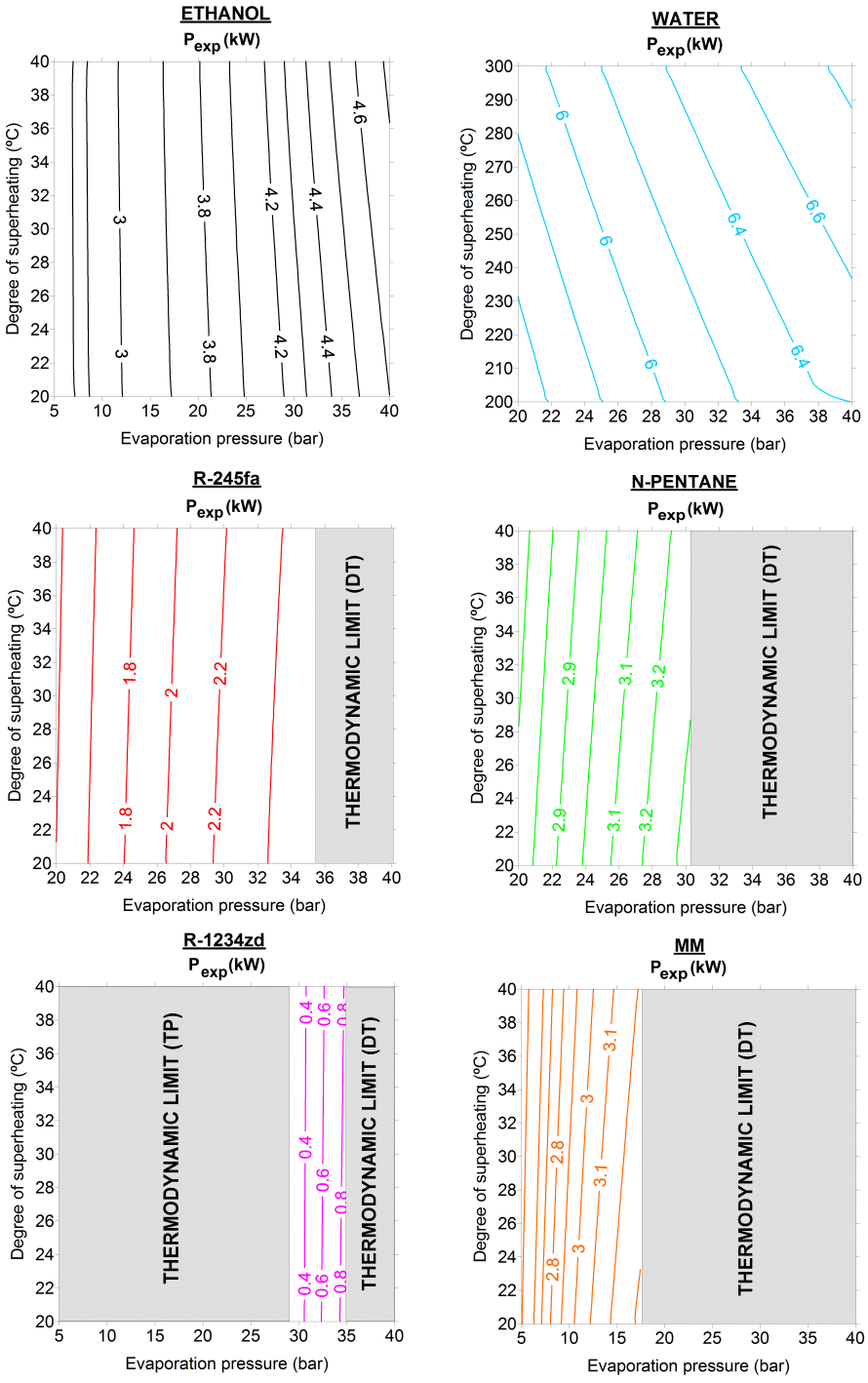

Figure 5.6: Expander power working fluids

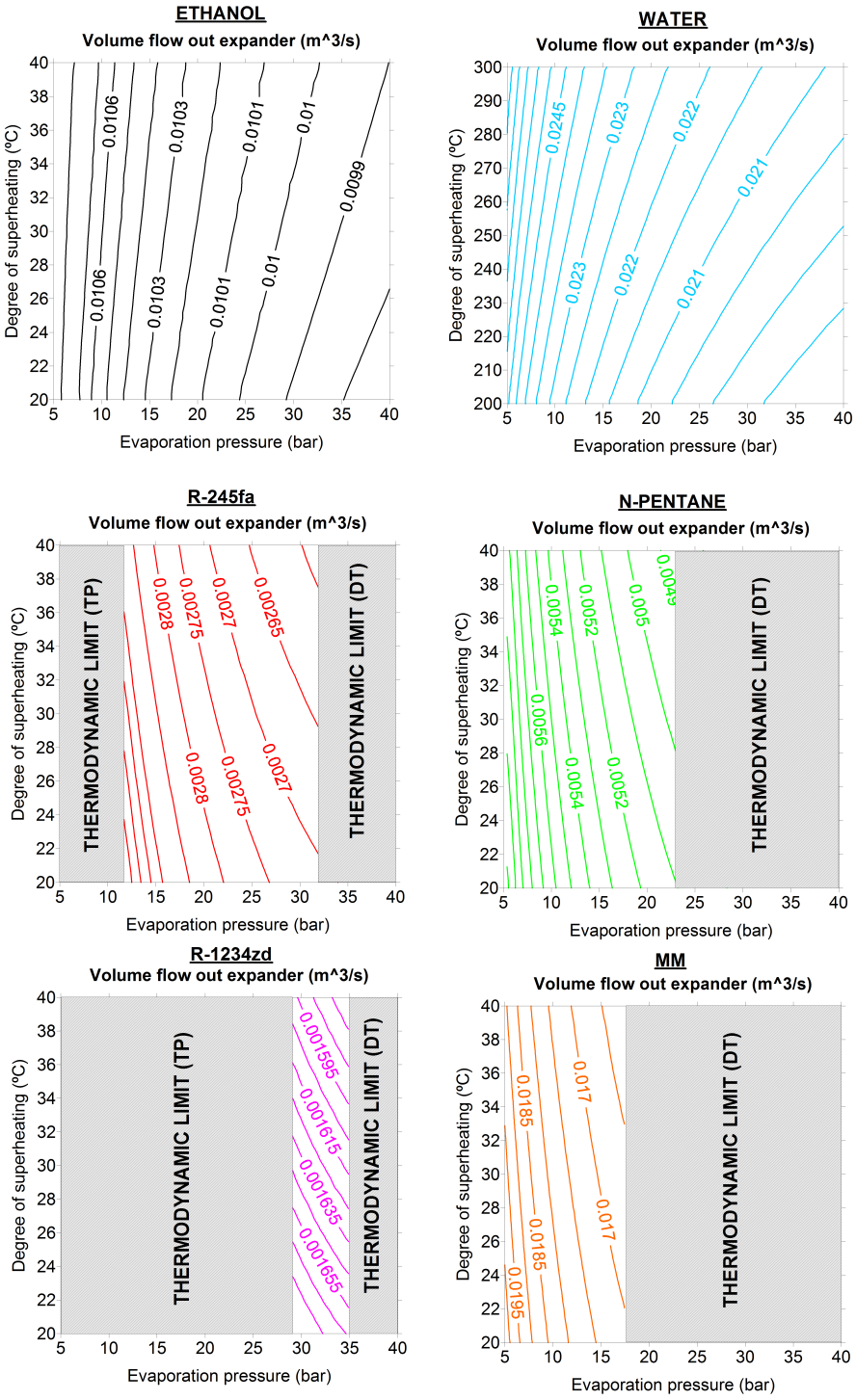

Figure 5.7: Volumetric flow rate working fluids

5.3 Advanced exergy analysis

Figure 5.8 shows a simplified diagram of the ORC. References to this diagram will be made during the whole section. In this figure, the main elements of the cycle are presented, i.e. boiler, expander, condenser and a pump. The working fluid used in this analysis is ethanol.

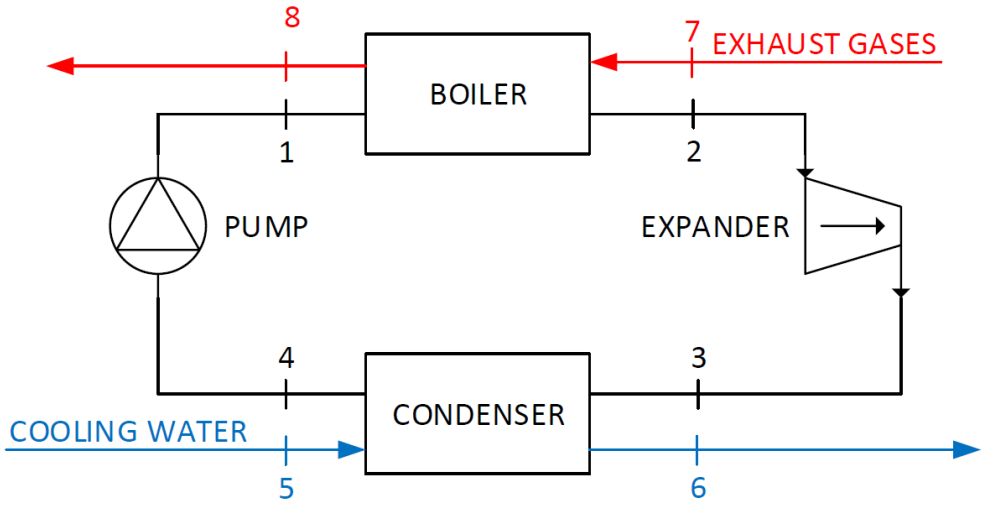

Figure 5.8: ORC diagram advanced exergy analysis

The main assumptions in analyzing the ORC are as follows:

- In order to perform the exergetic analysis of this system, thermodynamic cycle method [120] is chosen because it is the most convenient method and provides the best results for systems in which a thermodynamic cycle can be defined.
- The system works under steady state conditions.
- Energy losses and changes in kinetic and potential energies are neglected.

5.3.1 Conventional exergy analysis

The basic equations of the conventional exergy analysis for the K^{th} component of the system (boiler, expander, condenser or pump) are presented in Equation 5.1 and Equation 5.2. Using the thermodynamic terms for exergy of fuel and product, the exergy balances for the K^{th} component and for the overall system can be defined.

$$\dot{E}_{F,k} = \dot{E}_{P,k} + \dot{E}_{D,k} \tag{5.1}$$

$$\dot{E}_{F,tot} = \dot{E}_{P,tot} + \dot{E}_{D,tot} + \dot{E}_{L,tot} \tag{5.2}$$

$$\varepsilon_k = \frac{\dot{E}_{P,k}}{\dot{E}_{F,k}} = 1 - \frac{\dot{E}_{D,k}}{\dot{E}_{F,k}} \tag{5.3}$$

$$y_{D,k} = \frac{\dot{E}_{D,k}}{\dot{E}_{F,k}} \tag{5.4}$$

$$y^*_{D,k} = \frac{\dot{E}_{D,k}}{\dot{E}_{D,tot}} \tag{5.5}$$

Where $\dot{E}_{F,k}$, $\dot{E}_{P,k}$ and $\dot{E}_{D,k}$ are respectively the exergy rate of fuel, product and internal exergy loss in the K^{th} component. The subscript tot means the total amount of the overall system. $\dot{E}_{L,tot}$ corresponds to external exergy loss in the overall system. ε_k, $y_{D,k}$ and $y^*_{D,k}$ are the exergy efficiency, the exergy destruction ratio and the exergy rate of fuel with the total exergy destruction respectively. The exergy destruction (or internal exergy loss) is the exergy destroyed due to irreversibility within a system or a K^{th} component. At the component level, exergy flows are associated with fuel or product in each component. Therefore, the exergy loss in the K^{th} component is related with the transfer of thermal energy to the ambient (heat loss). The exergy loss (or external exergy loss) is the exergy transfer from the system to the surroundings. Considering the boundaries of the component analysis fixed at ambient temperature, the exergy loss is 0 and the thermodynamic inefficiencies consist only of exergy destruction. Therefore, the exergy loss is related only with the overall system and not with the K^{th} component. The energy and exergy balances for the system components as control volumes are presented in Table 5.2 and Table 5.3.

Table 5.2: Energy balance equations

Cycle component	**Energy balance equations**
Expander	$\eta_{exp} = \frac{P_{exp}}{P_{exp,is}}$, $P_{exp,is} = \dot{m}_{et} \cdot (h_2 - h_{3,is})$, $P_{exp} = \dot{m}_{et} \cdot (h_2 - h_3)$
Pump	$\eta_{pump} = \frac{P_{pump,is}}{P_{pump}}$, $P_{pump,is} = \dot{m}_{et} \cdot (h_{1,is} - h_4)$, $P_{pump} = \dot{m}_{et} \cdot (h_1 - h_4)$
Condenser	$P_{cond} = \dot{m}_{et} \cdot (h_3 - h_4)$
Boiler	$P_b = \dot{m}_{et} \cdot (h_2 - h_1)$

Table 5.3: Exergy balance equations

Cycle component	Energy balance equations
Expander	$\dot{E}_2 = \dot{E}_3 + P_{exp} + \dot{E}_{D,exp}$
Pump	$\dot{E}_4 + P_{pump} = \dot{E}_1 + \dot{E}_{D,pump}$
Condenser	$\dot{E}_3 + \dot{E}_5 = \dot{E}_4 + \dot{E}_6 + \dot{E}_{D,cond}$
Boiler	$\dot{E}_7 + \dot{E}_1 = \dot{E}_2 + \dot{E}_8 + \dot{E}_{D,b}$

5.3.2 Advanced exergy analysis [116]

In the advanced exergy analysis, the rate of exergy destruction in the Kth component of the system is split into endogenous / exogenous and avoidable / unavoidable.

Endogenous/Exogenous. Endogenous exergy destruction in Kth component is related to the irreversibility occurring inside this component, whereas the exogenous part is associated with the irreversibilites taking place in the rest of the components of the system. Therefore, the endogenous exergy destruction in Kth component ($\dot{E}^{EN}_{D,k}$) is the part of the total exergy destruction in the Kth component ($\dot{E}_{D,k}$) obtained considering that all the components operate ideally and that the component being examined operates with real efficiency (Hybrid Cycle). In a Hybrid Cycle only one component is real, i.e., operates with its real efficiency, while all other components operate in a theoretical way. In this case, the exergy destruction within the component being considered represents the endogenous exergy destruction. Thus, step-by-step introducing irreversibilities successively in each system component the endogenous exergy destruction within each component is calculated. Therefore, in order to compute the endogenous exergy destruction in the Kth component ($\dot{E}^{EN}_{D,k}$), a Hybrid Cycle for each component has to be simulated. Exogenous exergy destruction ($\dot{E}^{EX}_{D,k}$) is the difference between the exergy destruction value of the variable within the component in the real system ($\dot{E}_{D,k}$) and the endogenous part ($\dot{E}^{EN}_{D,k}$). Equation 5.6 shows the splitting between both parts, where EN and EX indicate the endogenous and exogenous parts, respectively.

$$\dot{E}_{D,k} = \dot{E}^{EN}_{D,k} + \dot{E}^{EX}_{D,k} \tag{5.6}$$

Moreover, the exogenous exergy destruction can be further split (Equation 5.7) to the effect of exergy destruction within the rth component caused by the exergy destruction of the Kth component and a term called mexogenous exergy destruction $\dot{E}_{D,k}^{MX}$ [121], which considers the simultaneous interactions of all other n-1 elements.

$$\dot{E}_{D,k}^{EX} = \dot{E}_{D,k}^{MX} + \sum_{\substack{r=1 \\ r \neq k}}^{n} \dot{E}_{D,k}^{EX,r} \tag{5.7}$$

Avoidable/Unavoidable. Unavoidable exergy destruction in Kth component cannot be reduced due to technological limitations (material characteristics, production costs and manufacturing methods). The avoidable part, which is the remaining part, can be reduced by improving the design of this component. Therefore, the unavoidable exergy destruction ($\dot{E}_{D,k}^{UN}$) is the part of total exergy destruction within the Kth component ($\dot{E}_{D,k}$) considering that all the components operate in unavoidable conditions. Avoidable exergy destruction ($\dot{E}_{D,k}^{AV}$) of the Kth component is the difference between the exergy destruction value of the variable within the Kth component in the real system ($\dot{E}_{D,k}$) and the unavoidable part ($\dot{E}_{D,k}^{UN}$). Equation 5.8 shows the splitting between both parts, where UN and AV indicate the unavoidable and avoidable parts, respectively.

$$\dot{E}_{D,k} = \dot{E}_{D,k}^{UN} + \dot{E}_{D,k}^{AV} \tag{5.8}$$

In order to obtain the unavoidable exergy destruction Equation 5.9 was proposed by Tsatsaronis et. al [122]. In order to obtain the ratio $\left(\frac{\dot{E}_D}{\dot{E}_P}\right)_k^{UN}$ for the Kth component, the system is solved considering that each component operates under the best possible conditions considering technological limitations. This ratio is the main parameter to calculate the unavoidable part of the exergy destruction rate of each individual component in a real process.

$$\dot{E}_{D,k}^{UN} = \dot{E}_{P,k} \cdot \left(\frac{\dot{E}_D}{\dot{E}_P}\right)_k^{UN} \tag{5.9}$$

Combination of the splitting. By combining the two splitting approaches, the unavoidable-exogenous ($\dot{E}_{D,k}^{UN,EX}$), the unavoidable-endogenous ($\dot{E}_{D,k}^{UN,EN}$), the avoidable-exogenous ($\dot{E}_{D,k}^{AV,EX}$) and the avoidable-endogenous ($\dot{E}_{D,k}^{AV,EN}$) values can be obtained using Equation 5.10, Equation 5.11, Equation 5.12 and Equation 5.13.

$$\dot{E}_{D,k}^{UN,EN} = \dot{E}_{P,k}^{EN} \cdot \left(\frac{\dot{E}_D}{\dot{E}_P} \right)_k^{UN} \tag{5.10}$$

$$\dot{E}_{D,k}^{UN,EX} = \dot{E}_{D,k}^{UN} - \dot{E}_{D,k}^{UN,EN} \tag{5.11}$$

$$\dot{E}_{D,k}^{AV,EN} = \dot{E}_{D,k}^{EN} - \dot{E}_{D,k}^{UN,EN} \tag{5.12}$$

$$\dot{E}_{D,k}^{AV,EX} = \dot{E}_{D,k}^{EX} - \dot{E}_{D,k}^{UN,EX} \tag{5.13}$$

Assumptions In this analysis, three thermodynamic cycles are proposed, i.e. real, ideal and unavoidable. The following assumptions are adopted:

- For the real cycle - the isentropic efficiency of the expander machine and the pump, pinch point and pressure drops in heat exchangers are obtained by experimental values presented in subsection 3.4.1. This analysis is applied to the point of 30 kW because of its higher recovery potential.
- For the ideal cycle - isentropic efficiencies of expander and pump and efficiencies of condenser and boiler are considered 100%. Pressure drops are assumed to be zero on condenser and boiler processes.
- For the unavoidable cycle - efficiencies of the expander and the pump are considered respectively 80% [91] and 95% [123], assuming this is the maximum that could be achieved due to technological limitations [119]. Pinch points and pressure drops in this cycle are lower than the real cycle but also considering technological limitations.

Table 5.4 shows a summary of these variables used to define the different cycles.

Table 5.4: Assumptions for real, ideal and unavoidable

Component	Real		Ideal		Unavoidable	
Expander	η_{exp}	43%	η_{exp}	100%	η_{exp}	80%
Condenser	ΔT_{pp} (°C)	5	ΔT_{pp} (°C)	0	ΔT_{pp} (°C)	2
	ΔP	1.60%	ΔP	0%	ΔP	1%
	ε_{cond}	83%	ε_{cond}	100%	ε_{cond}	90%
Pump	η_p	89%	η_p	100%	η_p	95%
Boiler	ΔT_{pp}(°C)	50	ΔT_{pp}(°C)	0	ΔT_{pp}(°C)	10
	ΔP	0.79%	ΔP	0%	ΔP	0.50%
	ε_b	98%	ε_b	100%	ε_b	99%

5.3.3 Simulation results and discussion

For the exergy analysis, steady-state simulations are performed by modeling the cycle described in Figure 5.8. As shown in Figure 5.9, the evaporation process corresponds to 1-2, the expansion process to 2-3, the condensation process to 3-4 and the pumping process to 4-1. The major difference between these cycles correspond to the expansion process (2-3). In order to optimize the cycle (get the maximum power in the expander) and avoid entering the two-phase zone during expansion, the high pressure has been set to $0.65{*}P_{critical}$ and the low pressure to 1 bar to avoid air intakes in the ducts. Depending on the cycle, different pressure drops have been taken into account.

Figure 5.10 shows the evaporation process in the three cycles: ideal, real and unavoidable. In all these cycles, the inlet temperature and the mass flow of exhaust gases have remained constant. Depending on the cycle, the pinch point changed from 50 °C in the real case, 10 °C in the unavoidable case and 0 °C in the ideal one. A change of temperature at the outlet of exhaust gases implies a change in the power released by the boiler and thus the ethanol mass flow. Therefore, in order to visualize the evaporation process for the three cycles, the power percentage has been plotted in the X axis. The exergy destruction in the boiler is proportional to the area of the heat exchange between exhaust gases and ethanol. As it can be seen in Figure 5.10, the exergy destruction in the ideal case is lower than the real one.

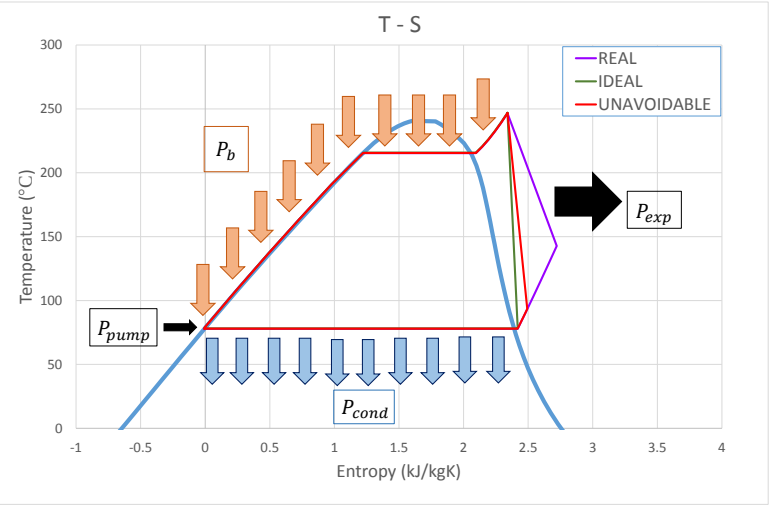

Figure 5.9: Ideal, real and unavoidable cycles in the T-S Diagram

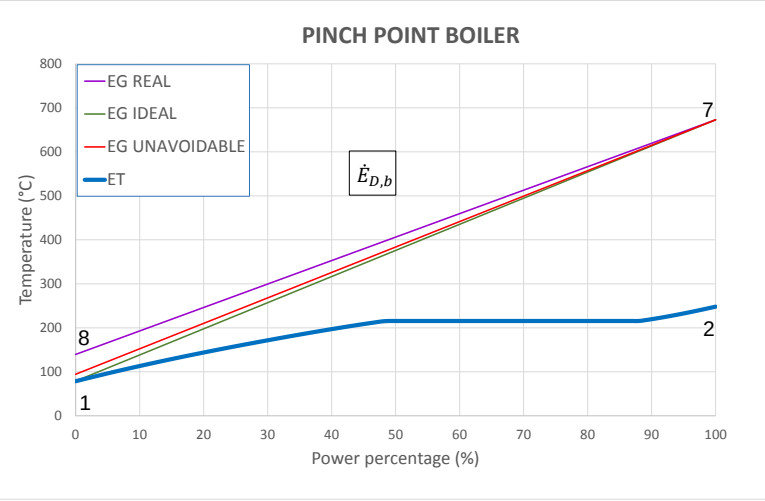

Figure 5.10: Ideal, real and unavoidable cycles in the evaporation process

Table 5.5, Table 5.6 and Table 5.7 indicate the thermodynamic properties and the mass flow rates at different state points of the ORC (Figure 5.8) under real, ideal and unavoidable conditions respectively. As previously mentioned, the ethanol mass flow in the cycle is higher in the ideal case than in the real one due to thermodynamic restrictions. Pressure drop in the boiler and the condenser have been considered both in the real and unavoidable case. The last two columns are related with the calculation of exergy in each state point.

Table 5.5: Thermodynamic properties and mass flow rates of the ORC in real conditions

Point	$T(°C)$	$P(bar)$	$h(kJ/kg)$	$\dot{m}(kg/s)$	$s(kJ/kgK)$	$e(kJ/kg)$	$\dot{E}(kW)$
1	78.54	39.65	262.8	0.02623	1.028	17.49	0.459
2	246.6	39.65	1336	0.02623	3.39	386.8	10.146
3	142.7	0.984	1229	0.02623	3.768	166.7	4.373
4	77.53	0.984	256.9	0.02623	1.026	12.16	0.319
5	50	1.5	209.4	0.2083	0.7037	4.252	0.886
6	74.88	1.5	313.5	0.2083	1.014	15.87	3.306
7	672.8	1.071	985	0.04799	6.888	331	15.885
8	128.5	1.013	403	0.04799	5.996	14.86	0.713

Table 5.6: Thermodynamic properties and mass flow rates of the ORC in ideal conditions

Point	$T(°C)$	$P(bar)$	$h(kJ/kg)$	$\dot{m}(kg/s)$	$s(kJ/kgK)$	$e(kJ/kg)$	$\dot{E}(kW)$
1	78.74	39.96	263.5	0.02923	1.029	17.63	0.515
2	247	39.96	1336	0.02923	3.39	387.2	11.318
3	78.5	1	1087	0.02923	3.39	137.6	4.022
4	77.94	1	258.2	0.02923	1.029	12.35	0.361
5	50	1.5	209.4	0.2083	0.7037	4.252	0.886
6	77.81	1.5	325.8	0.2083	1.049	17.68	3.683
7	672.8	1.071	985	0.04799	6.888	331	15.885
8	78.74	1.013	352.7	0.04799	5.862	4.346	0.209

Table 5.7: Thermodynamic properties and mass flow rates of the ORC in unavoidable conditions

Point	$T(°C)$	$P(bar)$	$h(kJ/kg)$	$\dot{m}(kg/s)$	$s(kJ/kgK)$	$e(kJ/kg)$	$\dot{E}(kW)$
1	78.58	39.76	262.9	0.02845	1.028	17.52	0.498
2	246.7	39.76	1336	0.02845	3.39	386.9	11.007
3	93.45	0.99	1136	0.02845	3.531	145	4.125
4	77.68	0.99	257.4	0.02845	1.027	12.23	0.348
5	50	1.5	209.4	0.2083	0.7037	4.252	0.886
6	75.84	1.5	317.6	0.2083	1.026	16.45	3.427
7	672.8	1.071	985	0.04799	6.888	331	15.885
8	88.58	1.013	362.6	0.04799	5.89	5.984	0.287

Table 5.8 shows the net power and the cycle energy efficiency and cycle exergy efficiency for ideal, unavoidable and real cases. As it can be seen, net power is reduced in the real cycle because of two effects: lower ethanol mass flow due to higher pinch point in the boiler and lower isentropic efficiency in the expander. As a global consequence, both the cycle energy efficiency (defined as the net power divided by the power of the boiler) and cycle exergy efficiency (defined as the net power divided by the exergy rate of fuel in the boiler) are reduced comparing to the ideal cycle. Therefore, cycle efficiency corresponds to 22.72% in the ideal case and technical limitations give a value of 18.13% in the case of unavoidable cycle. The real cycle gives a value of 9.42%. These values correspond to the ones found in literature [124].

Table 5.8: Power and efficiency of ideal, unavoidable and real cycles

	Ideal	**Unavoidable**	**Real**
$P_{exp}(kW)$	7.28	5.69	2.81
$P_{pump}(kW)$	0.15	0.16	0.15
$P_{net}(kW)$	7.12	5.53	2.65
$P_b(kW)$	31.35	30.53	28.15
$P_{cond}(kW)$	24.23	25	25.5
$\dot{E}_b(kW)$	15.67	15.59	15.17
η_{cycle}	22.72%	18.13%	9.42%
ε_{cycle}	45.44%	35.48%	17.48%

Considering conventional exergy equations applied to this particular application and presented in Table 5.3, the following results are obtained. The total exergy fuel rate is the difference between exergy rates of exhaust gases entering and ethanol leaving the boiler. The expander power output considered the rate of total products exergy. Table 5.9, Table 5.10 and Table 5.11 show the results of conventional exergy analysis for ORC under real, ideal and unavoidable conditions respectively.

Table 5.9: Results of conventional exergy analysis under real conditions

Component	$\dot{E}_F(kW)$	$\dot{E}_P(kW)$	$\dot{E}_D(kW)$	ε_k	$y_{D,k}$	$y^*_{D,k}$
Expander	5.77	2.81	2.97	49%	51%	29%
Pump	0.33	0.14	0.19	42%	58%	2%
Condenser	4.05	2.42	1.63	60%	40%	16%
Boiler	15.17	9.69	5.48	64%	36%	53%
Overall System	15.17	2.81	10.84	18%	71%	100%

Table 5.10: Results of conventional exergy analysis under ideal conditions

Component	$\dot{E}_F(kW)$	$\dot{E}_P(kW)$	$\dot{E}_D(kW)$	ε_k	$y_{D,k}$	$y^*_{D,k}$
Expander	7.3	7.28	0.02	99.8%	0.2%	0.3%
Pump	0.15	0.15	0	99.6%	0.4%	0%
Condenser	3.66	2.8	0.86	76.4%	23.6%	15%
Boiler	15.68	10.8	4.87	68.9%	31.1%	84.7%
Overall System	15.68	7.28	5.8	46.4%	36.7%	100%

Table 5.11: Results of conventional exergy analysis under unavoidable conditions

Component	$\dot{E}_F(kW)$	$\dot{E}_P(kW)$	$\dot{E}_D(kW)$	ε_k	$y_{D,k}$	$y^*_{D,k}$
Expander	6.88	5.69	1.19	83%	17%	16%
Pump	0.22	0.15	0.07	67%	33%	1%
Condenser	3.78	2.54	1.24	67%	33%	16%
Boiler	15.6	10.51	5.09	67%	33%	67%
Overall System	15.6	5.69	7.59	36%	49%	100%

Based on the results obtained from conventional analysis (Table 5.9), the overall system should be improved following priorities for the components with higher exergy destruction: boiler (5.48 kW), expander (2.97 kW), condenser (1.63 kW) and pump (0.19 kW). In order to increase the ORC efficiency reductions in exergy destruction rates are needed. From a conventional exergy analysis, it is not possible to distinguish between irreversibilities occurring in other components and the component itself.

The advanced exergy analysis [125] evaluates the detailed interactions between components of the overall system, and the real improvement potential of a component within a system. In the advanced exergy analysis the endogenous exergy destruction rate for the K^{th} component is obtained by calculating several cycles (the same as number of components) considering the component under study operates with real values of the parameter and the rest with ideal conditions. The exogenous exergy destruction rate is calculated as a difference to the total exergy destruction (Equation 5.6). The unavoidable exergy destruction rate is obtained when all the components work under unavoidable conditions. Once the unavoidable conditions are calculated, the ratio of exergy destruction to the product exergy rate is computed (Equation 5.9). The avoidable exergy destruction rate is computed as a difference (Equation 5.8). To split the exergy between unavoidable-exogenous, unavoidable-endogenous, avoidable-exogenous and avoidable-endogenous Equation 5.10, Equation 5.11, Equation 5.12 and Equation 5.13 are applied.

Results from the advanced exergy analysis are presented in Table 5.12. Figure 5.11 shows a flow chart of exergy destruction rate in the K^{th} component. It summarizes and clarifies the exergy splitting process.

Table 5.12: Results of advanced exergy analysis (kW)

Component	$\dot{E}_D$	$\dot{E}_D^{EN}$	$\dot{E}_D^{EX}$	$\dot{E}_D^{AV}$	$\dot{E}_D^{UN}$	$\dot{E}_D^{AV,EN}$	$\dot{E}_D^{UN,EN}$	$\dot{E}_D^{AV,EX}$	$\dot{E}_D^{UN,EX}$
Boiler	5.48	5.48	0	0.79	4.69	0.79	4.69	0	0
Expander	2.97	3.29	-0.32	2.38	0.59	2.63	0.66	-0.25	-0.07
Condenser	1.63	1.37	0.26	0.46	1.18	0.27	1.1	0.19	0.08
Pump	0.19	0.21	-0.02	0.12	0.07	0.13	0.08	-0.01	-0.01
Overall System	10.27	10.35	-0.07	3.75	6.52	3.82	6.53	-0.07	0

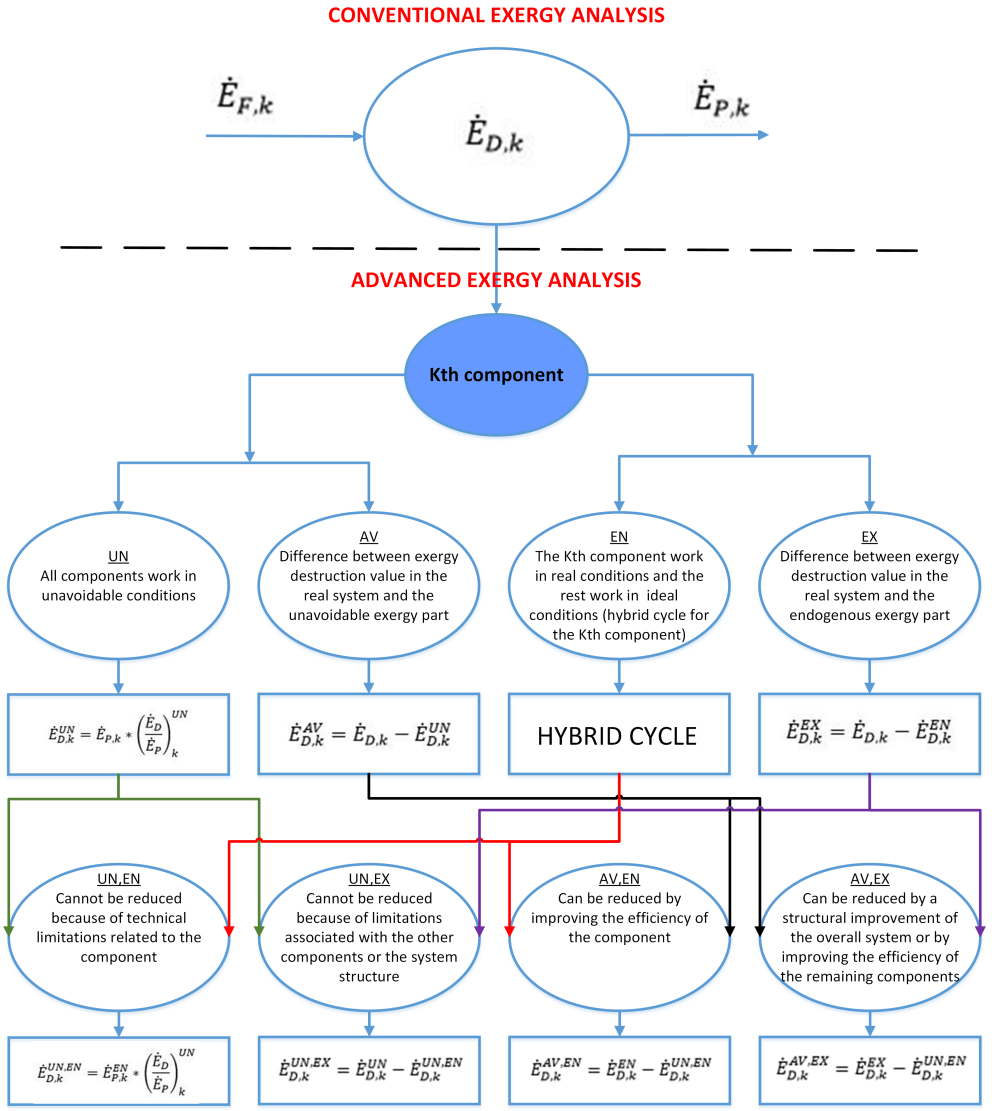

Figure 5.11: Flow chart of exergy destruction rate (Conventional and Advanced) in the Kth component

As shown in Table 5.12, the value of endogenous exergy is greater than the value of exogenous exergy in all the system components. Therefore, the greatest contribution to the exergy destruction rate in each of the components comes from the internal irreversibility of the component itself. Regarding the exogenous exergy, the condenser have the highest value (0.26 kW). Therefore, a modification in the other component efficiencies can lead to a reduction in the exergy destruction rate of this element and an improvement in overall cycle efficiency. Interactions between different components can be positive or negative. These two impacts could be the result of mass flow changes or thermodynamic property variation of material flows through the K^{th} component due to the introduction of additional irreversibilities in the system. In this system, some components have values of endogenous exergy greater than the exergy destruction rate itself. This can be analysed by the results of the specific advanced exergy analysis presented in Table 5.13. Table 5.13 shows that the system is more efficient (less exergy destroyed in kJ/kg for all the components) in the endogenous case than in the real case. However, changing the conditions from the ideal case to the endogenous case (the K^{th} component is real and the rest are ideal), the ethanol mass flow changes between both cases due to changes in the pinch point. Hence, the result is that the endogenous exergy destruction rate in kW is higher than the real exergy destruction rate in the expander and pump (Table 5.12).

Table 5.13: Results of advanced exergy analysis (kJ/kg)

Component	$\dot{E}_D$	$\dot{E}_D^{EN}$	$\dot{E}_D^{EX}$	$\dot{E}_D^{AV}$	$\dot{E}_D^{UN}$	$\dot{E}_D^{AV,EN}$	$\dot{E}_D^{UN,EN}$	$\dot{E}_D^{AV,EX}$	$\dot{E}_D^{UN,EX}$
Expander	113.1	112.5	0.6	90.68	22.42	90.08	22.42	0.6	0
Pump	7.22	7.17	0.05	4.64	2.59	4.56	2.61	0.07	-0.02
Condenser	62.28	46.84	15.44	17.38	44.9	9.11	37.72	8.27	7.17
Evaporator	209.09	187.51	21.59	30.27	178.83	27.01	160.5	3.26	18.33
Overall System	391.7	354.02	37.68	142.97	248.73	130.77	223.25	12.2	25.48

Another important point observed from Table 5.12 is that a total amount of 3.75 kW could be lowered taking into account that only the avoidable part of the exergy destruction rate can be reduced. This part of the exergy is higher than the unavoidable part in the expander (2.38 kW vs 0.59 kW) and the pump (0.12 vs 0.07 kW). These components will have the highest improvement potential by technical modifications of the components. As the avoidable-endogenous part corresponds to the part of the exergy destruction rate, which can be reduced by increasing the efficient of the component, it will be the main focus. The avoidable-endogenous rate is higher than the unavoidable-endogenous rate in the expander and the pump. As stated before, technical modifications of these components will improve efficiency of the ORC system. Regarding the avoidable-exogenous rate, it is higher than the exogenous-unavoidable rate in

the condenser. Therefore, efficiency improvements of other components play an important role in enhancing the condenser efficiency. The avoidable-endogenous part of the exergy destruction is higher than the avoidable-exogenous part in all the components. This difference is much higher in the expander, thus an optimization of this component will be essential to improve the global ORC performance. Results of splitting exergy destruction rate of the components are shown in Figure 5.12, Figure 5.13, Figure 5.14 and Figure 5.15. As a global consequence, under the working conditions for the present work, there is a high improvement potential for the ORC system by focusing in the expander. From the total exergy destruction rate in the expander (2.97 kW), the greatest part of the exergy (88%) can be reduced by technological improvement of the component itself (avoidable-endogenous). In the pump, condenser and boiler this potential is reduced to 70%, 16% and 14% respectively.

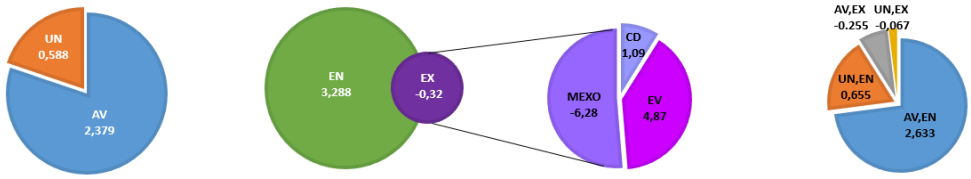

Figure 5.12: Results of splitting the exergy destruction rate for the expander

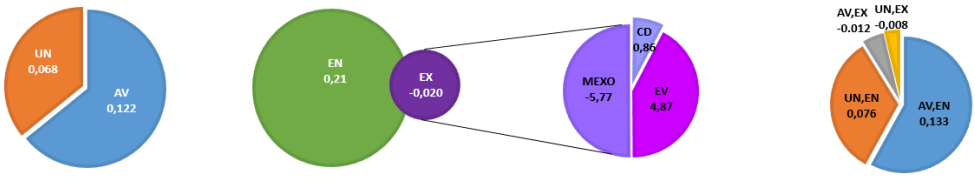

Figure 5.13: Results of splitting the exergy destruction rate for the pump

Figure 5.14: Results of splitting the exergy destruction rate for the condenser

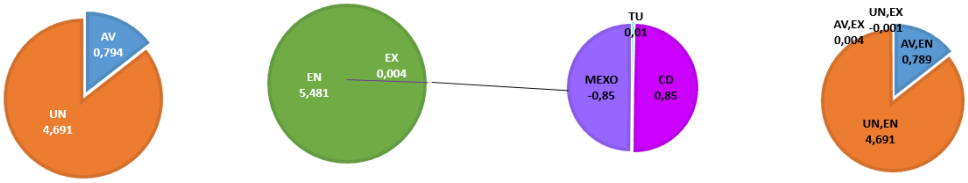

Figure 5.15: Results of splitting the exergy destruction rate for the boiler

5.3.4 Sensitivity exergetic analysis

The expander isentropic efficiency and pinch point are the critical parameters of this cycle, therefore, a sensibility analysis varying both parameters is presented. Cycle efficiency as a function of both parameters is plotted in Figure 5.16. Blue lines correspond to boiler power and red ones to expander power in kW. The green point corresponds to the unavoidable conditions.

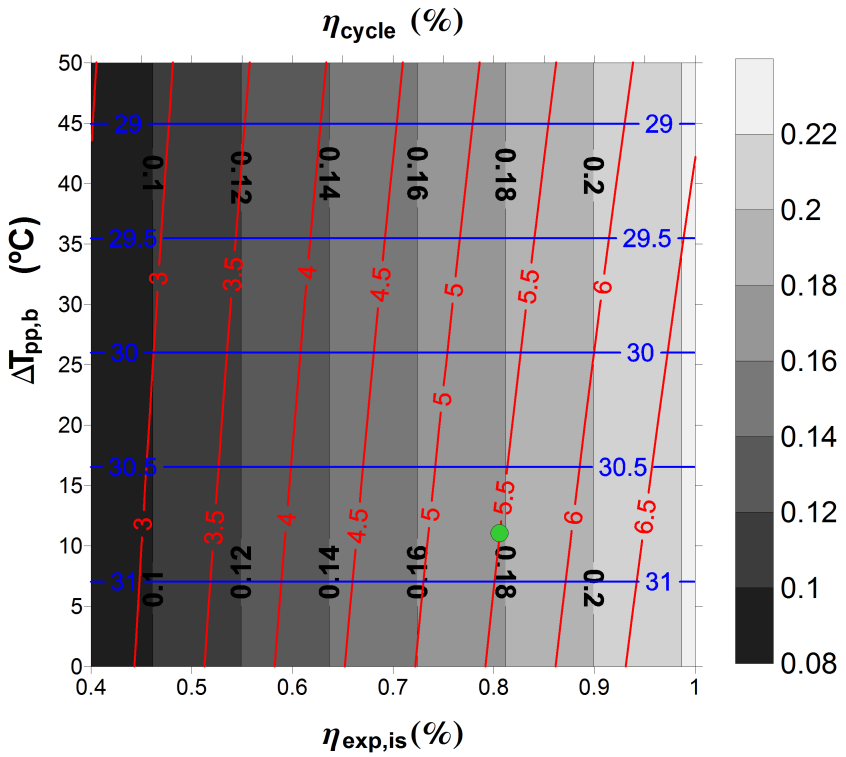

Figure 5.16: Cycle efficiency, boiler exchanged power (blue lines, kW) and expander power (red lines, kW) as a function of the pinch point and expander isentropic efficiency

As shown in Figure 5.16, the pinch point has a direct influence in the boiler power. The boiler power decreases as the pinch point increases as a consequence of the temperature difference in the boiler. Regarding the expander power, it increases with higher expander insentropic efficiency and lower pinch point. The former has an influence on the enthalpy drop in the expansion process and the latter on the ethanol mass flow in the cycle. The relation between both values gives the cycle energy efficiency. A maximum value of 21% can be obtained in the best conditions of the cycle. Figure 5.17 is presented in order to discriminate the contributions of each component to the global exergy destruction rate. Blue lines correspond to the boiler, red ones to the expander, green ones to the condenser and purple ones to the pump exergy destruction rate in kW. The sum of exergy destruction rates for all the components is plotted as a contour map behind them.

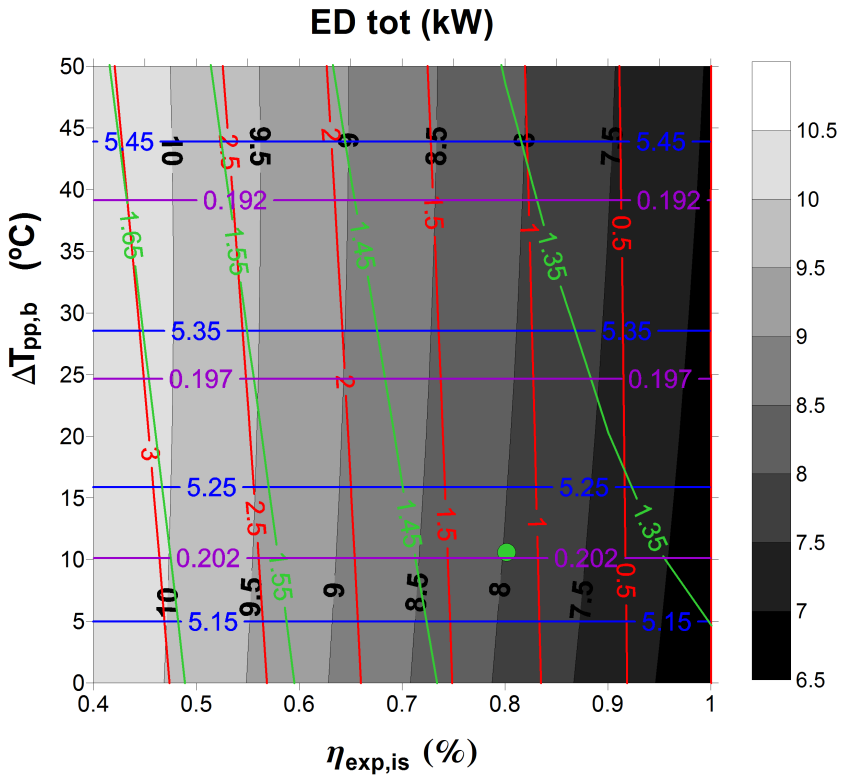

Figure 5.17: Contribution of boiler (blue lines, kW), expander (red lines, kW), condenser (green lines, kW) and pump (purple lines, kW) to the global exergy destruction rate (kW) as a function of the pinch point and expander isentropic efficiency

As it can be seen in Figure 5.17, exergy destruction rate in the boiler and the pump depends on the pinch point. The former increases with pinch point and the latter decreases with it. Boiler exergy destruction rate increases because the area between ethanol evaporation process and the exhaust gases process increases too (Figure 5.10). As the temperature difference decreases with higher pinch points, the boiler power released to the cycle is lower and thus, the ethanol mass flow too. This is the reason why the exergy destruction in the pump decreases with the pinch point and remains approximately constant with expander isentropic efficiency. As stated before, increasing the expander isentropic efficiency will reduce the exergy destruction rate in the expander. The relation with the condenser depends on both parameters, the pinch point (and thus, the ethanol mass flow) and the expander isentropic efficiency. To sum up, reducing the pinch point in the boiler and increasing the expander isentropic efficiency will reduce the exergy destruction rate from 10.5 kW to 6.5 kW.

5.4 Summary

This chapter presents the thermodynamic evaluation of the cycle, considering both the working fluid and an exergetic analysis. The following main results have been obtained:

- Refrigerant fluids (R-245fa and R-1234ze) have smaller Mollier diagram, lower critical temperature values and lower enthalpy drop in the boiling process. Therefore, considering a fixed exhaust power source, the fluid mass flow increases as enthalpy drop decreases. Moreover, vapor isobars are closer than for other fluids such as ethanol and water. This implies lower enthalpy drop in the expansion process and thus lower power delivered by the expander for these fluids. The volume flow rate is lower than for the ethanol or water, due to the high density of these fluids in vapor conditions. Water has been widely used in the Rankine cycle, however it is not the ideal working fluid due to its thermal characteristics. The size of the expander and the condenser would be bigger because of the volumetric flow rate and the degree of superheating. It would have an effect on the pinch point. MM and n-pentane are good candidates for the exhaust gases temperature range of vehicles, with a smaller operating range than ethanol. Ethanol has good thermal characteristics in the whole range of ICE temperatures (diesel and gasoline).

- Conventional analysis shows that the overall system should be improved following priorities for the components in this order: boiler (5.48 kW), expander (2.97 kW), condenser (1.63 kW) and pump (0.19 kW). From a conventional exergy analysis, it is not possible to distinguish between irreversibilities occurring in other components and the component itself. The advanced exergy analysis evaluates the detailed interactions between components of the overall system and the real potential of improvement for a component within a system. Therefore, the advanced exergy analysis suggests that the first priority should be given to the expander (88% reduction by the technological improvement of the component itself), followed by the pump (70%), condenser (16%) and boiler (14%).

- The value of endogenous exergy (internal irreversibilities) is greater than the value of exogenous exergy (external irreversibilities) for all the system components. Therefore, the greatest contribution to the exergy destruction rate for each of the components comes from the internal irreversibility of the component itself and a minimum exergy destruction comes from other components as external irreversibility. Regarding to exogenous (external irreversibilities) exergy destruction, the condenser has the highest value

(0.26 kW, 16% of the total exergy destruction rate). Therefore, modifications of the other components efficiencies can lead to a reduction in the exergy destruction rate of this component and an improvement in cycle efficiency.

- A total amount of 3.75 kW (36.5% of exergy destruction rate) could be lowered taking account that only the avoidable part (maximum efficiencies considering the technical restrictions of the cycle components) of the exergy destruction rate can be reduced. This part of the exergy is higher than the unavoidable part for the expander (2.38 kW vs 0.59 kW) and the pump (0.12 vs 0.07 kW). These two components will have the highest improvement potential by technical modifications of the components.

- Considering the sensibility analysis, varying the pinch point from 0 °C to 50 °C in the boiler and the expander isentropic efficiency from 0.4 to 1 under the working conditions of the study, a maximum cycle efficiency of 21% can be obtained in comparison with 10% in the real conditions. Regarding the overall exergy destruction rate of the cycle, it could be lowered from 10.5 kW to 6.5 kW.

5.5 References

[91] H. Kunte and J. Seume. “Partial Admission Impulse Turbine for Automotive ORC Application”. In: *SAE Technical Papers* 6 (2013). DOI: 10.4271/2013-24-0092. URL: http://www.scopus.com/inward/record.url?eid=2-s2.0-84890407668{\&}partnerID=tZOtx3y1 (cit. on pp. 25, 152).

[116] G. Tsatsaronis and T. Morosuk. “A general exergy-based method for combining a cost analysis with an environmental impact analysis. Part I – Theoretical Development”. In: *Asme Imece2008-67218* (2008), p. 10 (cit. on pp. 137, 150).

[117] M. Ehyaei, P. Ahmadi, F. Atabi, M. Heibati, and M. Khorshidvand. “Feasibility study of applying internal combustion engines in residential buildings by exergy, economic and environmental analysis”. In: *Energy and Buildings* 55 (2012), pp. 405–413. ISSN: 03787788. DOI: 10.1016/j.enbuild.2012.09.002. URL: http://linkinghub.elsevier.com/retrieve/pii/S0378778812004501 (cit. on p. 137).

[118] M. Özkan, D. B. Özkan, O. Özener, and H. Yılmaz. “Experimental study on energy and exergy analyses of a diesel engine performed with multiple injection strategies: Effect of pre-injection timing”. In: *Applied Thermal Engineering* 53.1 (2013), pp. 21–30. ISSN: 13594311. DOI: 10.1016/j.applthermaleng.2012.12.034. URL: http://www.sciencedirect.com/science/article/pii/S1359431113000082 (cit. on p. 137).

[119] Y.-R. Li, J.-N. Wang, and M.-T. Du. “Influence of coupled pinch point temperature difference and evaporation temperature on performance of organic Rankine cycle”. In: *Energy* 42.1 (2012), pp. 503–509. ISSN: 03605442. DOI: 10.1016/j.energy.2012.03.018. URL: http://linkinghub.elsevier.com/retrieve/pii/S0360544212002095 (cit. on pp. 140, 152).

[120] S. Kelly, G. Tsatsaronis, and T. Morosuk. “Advanced exergetic analysis: Approaches for splitting the exergy destruction into endogenous and exogenous parts”. In: *Energy* 34.3 (2009), pp. 384–391. ISSN: 03605442. DOI: 10.1016/j.energy.2008.12.007. URL: http://linkinghub.elsevier.com/retrieve/pii/S036054420800323X (cit. on p. 148).

[121] L. Wang, Y. Yang, T. Morosuk, and G. Tsatsaronis. “Advanced thermodynamic analysis and evaluation of a supercritical power plant”. In: *Energies* 5.6 (2012), pp. 1850–1863. ISSN: 19961073. DOI: 10.3390/en5061850 (cit. on p. 151).

[122] G. Tsatsaronis and M. Park. “On avoidable and unavoidable exergy destructions and investment costs in thermal systems”. In: *Energy Conversion and Management* 43.9-12 (2002), pp. 1259–1270. ISSN: 01968904. DOI: 10.1016/S0196-8904(02)00012-2 (cit. on p. 151).

[123] A. Keçebaş and H. Gökgedik. “Thermodynamic evaluation of a geothermal power plant for advanced exergy analysis”. In: *Energy* 88 (2015), pp. 746–755. ISSN: 03605442. DOI: 10.1016/j.energy.2015.05.094 (cit. on p. 152).

[124] A. S. Panesar, R. E. Morgan, N. D. D. Miché, and M. R. Heikal. “Working fluid selection for a subcritical bottoming cycle applied to a high exhaust gas recirculation engine”. In: *Energy* 60 (2013), pp. 388–400. ISSN: 03605442. DOI: 10.1016/j.energy.2013.08.015. URL: http://dx.doi.org/10.1016/j.energy.2013.08.015 (cit. on p. 156).

[125] T. Morosuk and G. Tsatsaronis. “Strengths and Limitations of Advanced Exergetic Analyses”. In: *Volume 6B: Energy* November (2013), V06BT07A026. DOI: 10.1115/IMECE2013-64320. URL: http://proceedings.asmedigitalcollection.asme.org/proceeding.aspx?doi=10.1115/IMECE2013-64320 (cit. on p. 158).

CHAPTER 6

Economic evaluation of the Organic Rankine Cycle

Contents

Figures

Tables

6.1 Introduction

THE thermo-economic evaluation of an ORC is presented in this chapter. The final implementation of this technology by manufacturers will depend on economical parameters (Payback, Net Present Value and Specific Investment Cost). Therefore in this chapter a mathematical model of the Organic Rankine Cycle is presented to optimize the cycle from a thermo-economic and sizing point of view. These criteria are optimized with different cycle values. The present chapter contains three parts:

- section 6.2 corresponds to the description of the mathematical model. Moreover, sensitivity studies are also presented in order to understand how to minimize the costs of the ORC. The final part of this section is dedicated to obtaining an optimal solution by using a multi-objective algorithm. Multi-objective optimization results show that the optimum solution depends on the importance of each objective to the final solution. Considering thermo-economic criteria as the main objective, greater sizes will be required. Considering sizing criteria as the main objective, higher thermo-economic parameters will be obtained. Therefore, in order to select a single-solution from the Pareto frontier, a multiple attribute decision-making method (TOPSIS) is implemented in order to take into account the preferences of the Decision Maker.

- section 6.3 presents the impact that ORC has on the engine performance (increase of cooling loads, total weight, pumping losses and net engine power in the vehicle). Moreover, the potential of the ORC in real driving conditions is presented in the last part of this section taking as a reference a test campaign of three weeks. The efficiency improvement of each operating point will be computed.

6.2 Economic model

Figure 6.1 shows a diagram of the ORC designed for a waste heat recovery application. This diagram has been derived from Figure 5.8. Boiler and condenser are divided in three areas, corresponding to single-phase liquid, two phase and single-phase vapor. Figure 6.2 shows the ethanol T-S diagram. Points from 1 to 4 indicate the ethanol cycle, points 7 and 8 indicate the exhaust gas heat transfer process and points 5 and 6 indicate the cooling water process. Additionally, 8 more states have been added to the original ORC diagram in order to take into account the division between single phase and two phase in the evaporator and condenser.

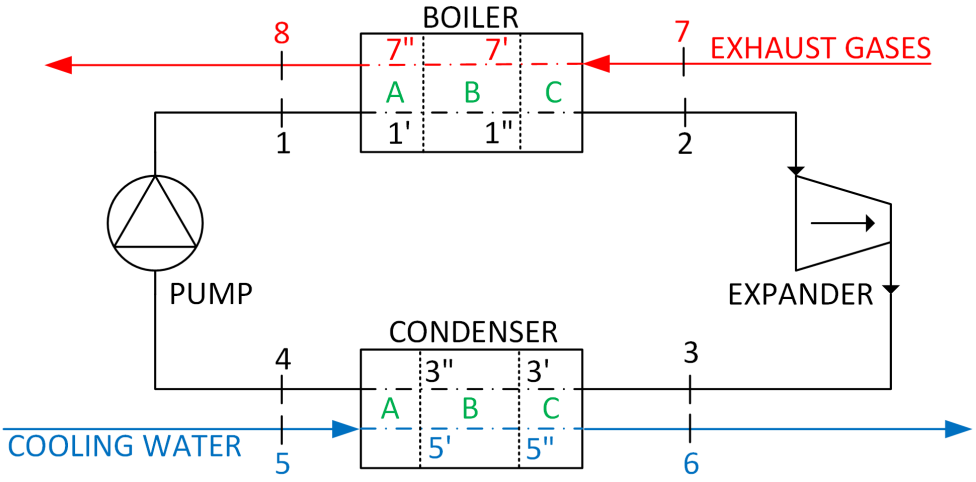

Figure 6.1: ORC diagram economic analysis

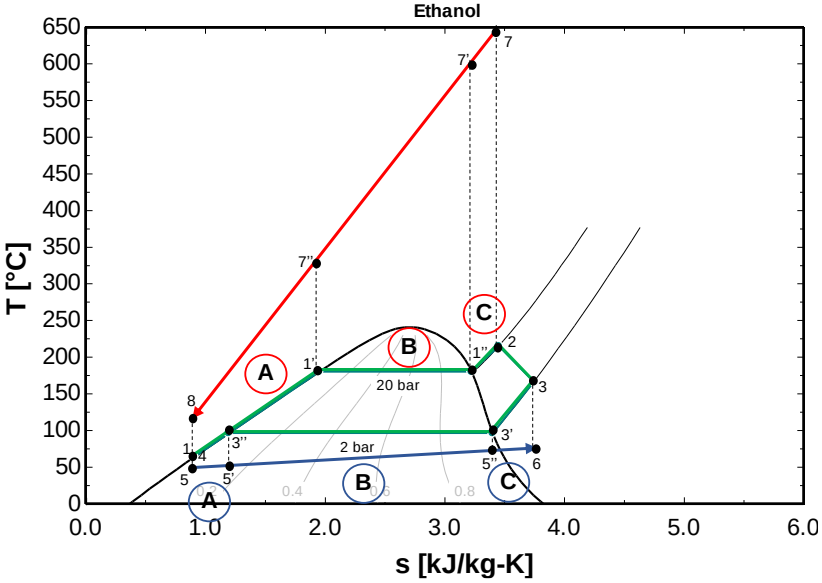

Figure 6.2: T-S ethanol diagram with state points

6.2.1 Mathematical model

A thermodynamic model of a bottoming ORC is used to evaluate the performance of the system. This model can be divided in the following elements:

Boiler and condenser model. Plate heat exchangers are modeled by means of the Logarithmic Mean Temperature Difference (LMTD), considering a three-zone approach. Each of them is characterized by a heat transfer coefficient (U) and area (A). The evaporator geometric parameters are presented in Table 6.1. Geometric parameters of the condenser are the same as the evaporator, except for the width, which is 0.4 m.

Table 6.1: Boiler geometric parameters

Parameter	Description	Value
$Dh = 2a$	Hydraulic diameter	0.008 m
Wi	Width	0.1 m
L	Length	0.4 m
d_{pl}	Thickness plate	0.002 m
β	Chevron angle	0.008°
k_{pl}	Thermal conductivity	14.9 W/mK

The heat transfer coefficient of a plate heat exchanger is computed as:

$$\frac{1}{U} = \frac{1}{\alpha_{ET}} + \frac{1}{\alpha_{EG}} + \frac{d_{pl}}{k_{pl}} \tag{6.1}$$

Where α_{ET} and α_{EG} are the convective heat transfer in the ethanol and the exhaust gas side respectively, d_{pl} is the thickness of the plate and k_{pl} is the thermal conductivity of the plate. Fouling resistances are neglected because it is assumed that plate heat exchangers are new. The total heat exchanger area in each heat exchanger (Boiler and Condenser) is the sum of each zone (A, B and C in Figure 6.2):

$$A_{tot} = A_A + A_B + A_C = (N_{pl} - 2) \cdot L \cdot Wi \tag{6.2}$$

Where A_{tot} is the total heat transfer area, N_{pl} is the number of plates, L and Wi are the length and width of the plate exchanger respectively.

Single phase (Zone A and C). For the convective heat transfer (Equation 6.3) and pressure drop (Equation 6.4) in the single phase the Thonon correlation [126] is used. This correlation is the same as the correlation used in the work of Quoilin et al. [127] and Lecompte et al. [128] for a plate heat exchanger.

$$Nu = 0.299 \cdot Re^{0.645} \cdot Pr^{\frac{1}{3}} \tag{6.3}$$

$$f = 0.685 \cdot Re^{-0.172} \tag{6.4}$$

$$\Delta P = \frac{2 \cdot f \cdot G^2}{\rho \cdot D_h} \cdot L \tag{6.5}$$

Where f is the friction factor, G is the mass flow velocity, ρ is the mean fluid density, D_h is the hydraulic diameter and L is the length of the plate exchanger.

Boiling heat transfer coefficient (Zone B in the boiler). The boiling heat transfer coefficient is estimated by Chen [129] correlation. This correlation was tested with available data of water and organic fluids, including alcohols. This heat exchange coefficient takes into account two mechanisms: an effective Reynolds number factor (F) and a bubble-growth suppression factor (S). The first factor (F) is the ratio of the two-phase Reynolds number to the liquid Reynolds number and it is assumed as a function of the Martinelli parameter X_{tt} [130]. The second one (S) is defined as the ratio of the effective superheat to the total superheat of the wall. These two functions were determined empirically from experimental data.

$$\alpha_{tp} = S \cdot \alpha_{NcB} + F \cdot \alpha_{cv} \tag{6.6}$$

$$\alpha_{NcB} = 0.00122 \cdot \frac{k_l^{0.79} \cdot Cp_l^{0.45} \cdot \rho_l^{0.49} \cdot g^{0.25}}{\sigma^{0.5} \cdot \mu_l^{0.29} \cdot h_{fg}^{0.24} \cdot \rho_v^{0.24}} \cdot \Delta T^{0.24} \cdot \Delta P^{0.75} \tag{6.7}$$

$$\alpha_{cv} = 0.023 \cdot Re_l^{0.8} \cdot Pr_l^{0.4} \cdot \frac{k_l}{D_h} \tag{6.8}$$

$$F = \left(\frac{Re}{Re_l}\right)^{0.8} \tag{6.9}$$

$$S = \left(\frac{\Delta T_e}{\Delta T}\right)^{0.99} \tag{6.10}$$

Where k is the thermal conductivity, Cp is the specific heat, ρ is the density, σ is the surface tension, μ is the dynamic viscosity, h_{fg} is the latent heat of vaporization, ΔT_e is the effective superheat with flow, ΔT is the superheat and ΔP is the difference in vapor pressure corresponding to ΔT.

Pressure drop is computed with the same equation as the single phase (Equation 6.5), using Hsieh correlation [131] to obtain the friction factor in the boiling phase.

$$f = 61000 \cdot Re_{eq}^{-1.25} \tag{6.11}$$

Where Re_{eq} is the equivalent Reynolds number considering liquid flow conditions.

Condensation heat transfer coefficient (Zone B in the condenser). The condensation heat transfer coefficient and friction factor (pressure drop) are estimated by Kuo [132] correlation. This correlation has been developed for vertical plate heat exchangers using R410A. Results are similar to Shah correlation developed for ethanol inside pipes [133].

$$\alpha_{tp} = \alpha_l \cdot (0.25 \cdot Co^{-0.45} \cdot Fr_l^{0.25} + 75 \cdot Bo^{0.75}) \tag{6.12}$$

$$\alpha_l = 0.2092 \cdot \left(\frac{k_l}{D_h}\right) \cdot Re_l^{0.78} \cdot Pr_l^{\frac{1}{3}} \cdot \left(\frac{\mu_{av}}{\mu_{wall}}\right)^{0.14} \tag{6.13}$$

$$f = 21500 \cdot Re_{eq}^{-1.14} \cdot Bo^{-0.085} \tag{6.14}$$

Where Co, Fr, Bo, Pr and Re are respectively the Convection, Froude, Boiling, Prandtl and Reynolds numbers defined in Equation 6.15, Equation 6.16, Equation 6.18 and Equation 6.19 respectively.

$$Co = \left(\frac{\rho_g}{\rho_l}\right) \cdot \left(\frac{(1 - X_m)}{X_m}\right)^{0.8} \tag{6.15}$$

$$Fr = \frac{G^2}{\rho_l^2 \cdot g \cdot D_h} \tag{6.16}$$

$$Bo = \frac{q}{G \cdot i_{fg}} \tag{6.17}$$

$$Pr = \frac{\mu_l \cdot C_{p,l}}{k_l} \tag{6.18}$$

$$Re = \frac{D_h \cdot V_{TP} \cdot \rho_l}{\mu_l} \tag{6.19}$$

Where V_{TP} is the effective two-phase velocity, g is the gravity, i_{fg} is the enthalpy of vaporization and X_m is the average vapor quality value for the two phase mixture or between inlet and outlet.

Expander model. The expander has been characterized by the isentropic efficiency. The maximum value of the isentropic efficiency is fixed by the built-in volumetric expansion ratio. As previously stated in chapter 3, expander speeds below 3500 rpm (and therefore higher pressure ratios than optimal one) lead to an expander performance drop mainly due to the effect of leakages, whereas higher expander speed and lower pressure ratios lead to a sharp reduction in the expander isentropic efficiency mainly due to the effects of mechanical losses and intake pressure drop. For a given rotational speed and mass flow rate, the isentropic efficiency is mainly function of the pressure ratio (Equation 6.20). This hypothesis is applied in order to simplify the model. Therefore, a correlation derived from experimental results (30 kW) has been used to model the expander performance for the pressure levels from 20 to 40 bar. The isentropic efficiency has been correlated as a function of the pressure ratio using experimental data with a correlation coefficient of 92.35%.

$$\eta_{exp,is} = f\left(\frac{P_{in,exp,ET}}{P_{out,exp,ET}}\right) \tag{6.20}$$

The characterization of the expander size has been made using the "Volume Coefficient" (VC) [134] in m^3/MJ. This expression (Equation 6.21) takes into account the volumetric expansion ratio and constitutes a representative factor of the actual size of the volumetric machine.

$$VC = \frac{\dot{V}_{out}}{P_{exp}} \tag{6.21}$$

Where $\dot{V}_{out}$ is the volumetric flow at the outlet of the expander and P_{exp} is the power delivered by the expander in the expansion process.

Pump. The pump has been characterized by its isentropic efficiency, which is assumed to be constant with a value of 80% as a representative efficiency of these machines [112].

Cycle model. The global cycle model is obtained by computing the energy balance equations for each component, similar to Table 5.2. The boundary conditions of the experimental tests have been imposed to the mathematical model (temperatures and mass flows). Moreover, the efficiency of the expander as a function from the pressure ratio of the real experimental tests is also the input of the model. In order to obtain the optimal point, sensitivity studies are conducted using the evaporation pressure and the superheating. Therefore, using the thermodynamic properties of the state points, the net power (Equation 6.22) and the cycle efficiency (Equation 6.23) can be defined.

$$P_{net} = P_{exp} - P_{pump} \tag{6.22}$$

$$\eta_{ORC} = \frac{P_{net}}{P_b} \tag{6.23}$$

Where P_{net} is the net power and η_{ORC} is the cycle efficiency.

Economic model. The thermodynamic mathematical model of the cycle, described in the previous paragraph, is expanded by considering costs of the main elements in the cycle. These costs are estimated from the work of Quoilin et al. [127] and they are presented in Table 6.2.

Table 6.2: Component costs

Component	Dependent variable	Cost [€]
Expander	Volume flow rate (m^3/s)	$1.5 \cdot (225 + 170 \cdot \dot{V}_{in})$
Boiler	Heat exchange area (m^2)	$1.5 \cdot (190 + 310 \cdot A_{tot,b})$
Condenser	Heat exchange area (m^2)	$190 + 310 \cdot A_{tot,c}$
Pump	Pump power (W)	$900 \cdot \left(\frac{P_{pump}}{300}\right)^{0.25}$
Liquid receiver	Volume (l)	$31.5 + 16 \cdot Vol$
Piping	Pipe diameter (mm) Pipe length (m)	$(0.897 + 0.21 \cdot d_{pipe}) \cdot L_{pipe}$
Working fluid	Mass (kg)	$20 \cdot M$
Hardware	-	300
Control system	-	500
Labor	Total component costs (€)	$0.5 \cdot TCC$

As Quoilin et al. [127] consider in their work, the estimated cost of commercial volumetric compressors is multiplied by a factor of 1.5 to obtain the estimated cost of the volumetric expander, in order to consider the low maturity level of the volumetric expander for these type of applications. In the case of the evaporator, which should withstand high temperatures in the exhaust gases side and high pressures and thermal stress in the ethanol side, the multiplying factor is also assumed to be 1.5. Diameters and lengths of pipes are measured in the experimental facility in order to obtain the representative values for these tubes. The total ethanol mass of the system is calculated from the real volume of ethanol in the installation and the density, assuming that half of heat exchangers and liquid receiver are filled with liquid and half with vapor.

One of the thermo-economic objective functions most used in the literature is the Specific Investment Cost (SIC) parameter in €/kW [135], which is defined in Equation 6.24.

$$SIC = \frac{C_{lab} + C_{cp}}{P_{net}} \tag{6.24}$$

Where C_{lab} and C_{cp} are the costs of the components. Moreover, the Net Present Value and Payback analysis are defined in Equation 6.25 and Equa-

tion 6.26.

$$NPV = -C_o + \sum_{t=1}^{T} \frac{C_t}{(1+r)^t} \tag{6.25}$$

$$PB = \frac{C_o}{C_t} \tag{6.26}$$

Where C_t is the net cash inflow during the period t, C_o is the total investment cost, r is the discount rate and t is the number of periods. The net cash inflow is computed using the specific fuel consumption for this engine operating point and estimated the number of vehicle operating hours in a year. The higher engine operating point (30 kW of thermal power) is used because it involves greater recovery potential from the exhaust.

$$SFC = \frac{f_{cs}}{P_{eng}} \tag{6.27}$$

$$S_{ORC} = SFC \cdot P_{net} \tag{6.28}$$

$$C_t = \left(\frac{S_{ORC} \cdot hr_{year}}{\rho_f} \right) \cdot C_f \tag{6.29}$$

Where f_{cs} is the fuel consumption in kg/h, P_{eng} is the engine power, SFC is the specific fuel consumption, hr_{year} is the number of operating hours of a vehicle in a year, ρ_f is the density of the fuel and C_f is the cost per litre of the fuel.

Although several thermodynamic and economic parameters have been presented in the previous section, three objective functions have been considered in order to simplify the optimization of the system: SIC in €/kW, boiler area ($A_{tot,b}$) in m^2 and expander size (VC) in m^3/MJ. The Specific Investment Cost has been chosen as a global parameter of the thermo-economic behavior of the system. The remainder economic parameters (NPV and PB) are characterized by high degree of uncertainty due to the estimation of the fuel price (C_f) and the number of ORC operating hours during a year (hr_{year}). Therefore, to study the influence of these parameters, two parametric studies are conducted after the optimization of the system.

Assumptions The main assumptions in analyzing the ORC are as follows:

- Pressure drop at the ethanol side is low comparing to the level of pressure in the system. Therefore, for this first approach it is neglected.
- The system works under steady state conditions.
- The heat source is exhaust gas at 673 °C, with mass flow rate of 48 g/s. It corresponds to 30 kW thermal power in the boiler (defined in Table 3.1).
- The condenser is cooled with water at 50 °C, and a flow rate of 990 l/h.
- The degree of superheating at the expander inlet is 35 °C.
- The degree of subcooling after the condenser is 30 °C.
- Boiler is vertical heat exchanger type and the condenser is a vertical plate heat exchanger.
- A discount rate of 4% and 10 years are fixed in the calculation of NPV and PB [136]. The cost of fuel is estimated to 1€/l.
- The total number of hours of the ORC is estimated to 1100h a year (3 hour each day as average value).

The model has been validated with experimental results in our ORC facility [1], and differences between model and experimental variables are lower than 5%.

6.2.2 Thermo-economic results

The goal of this study is to optimize the cycle using both thermo-economic criterion (SIC) and sizing criteria (Boiler-Condenser area and VC). In order to analyze the behavior of these criteria in different conditions of the cycle, a sensibility analysis is presented varying the main parameters of the cycle, which are the evaporating pressure and superheating temperature.

Figure 6.3 shows the net power, defined as the difference between expander and pump power in kW (Equation 6.22) in grey scale. Blue lines correspond to SIC in €/kW (Equation 6.24) and red lines correspond to Total costs (Sum of costs in Table 6.2).

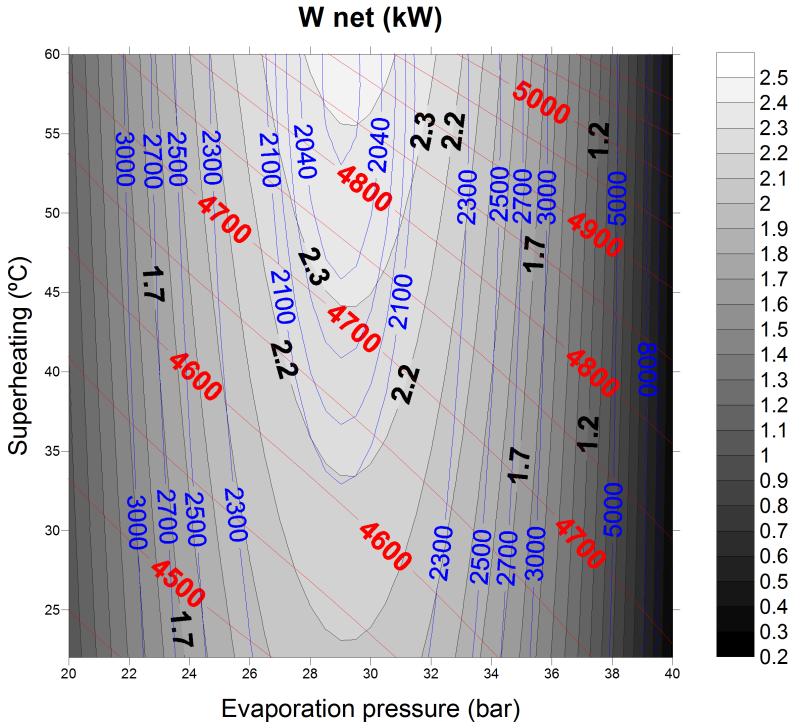

Figure 6.3: Net power in kW (grey scale), SIC in €/kW (blue lines) and total cost in € (red lines)

The isentropic efficiency of expander (Equation 6.20) has an important effect on the pressure level. When evaporation pressure is approximately 29 bar the expander works with an optimal expansion ratio and expander isentropic efficiency is maximum, consequently, maximum power is obtained from the cycle. Regarding superheating temperature, increasing its value produces higher enthalpy drop through the expander. Consequently, net power has a peak for evaporation pressure of approx. 29 bar and close to the superheating temperature of 60 °C. Maximum net power corresponds to 2.41 kW (in the same zone). Regarding total costs, they increase with higher pressure level and superheating temperature.

Figure 6.4 shows the Total Cost, defined as the sum of costs from Table 6.2 in grey scale. Purple lines correspond to the cost of the pump in €, blue ones to the cost of the evaporator in € and green ones to the cost of the condenser in €. The expander cost does not vary substantially under the hypothesis from Table 6.2 with these input parameters. Therefore, it is not plotted in Figure 6.4.

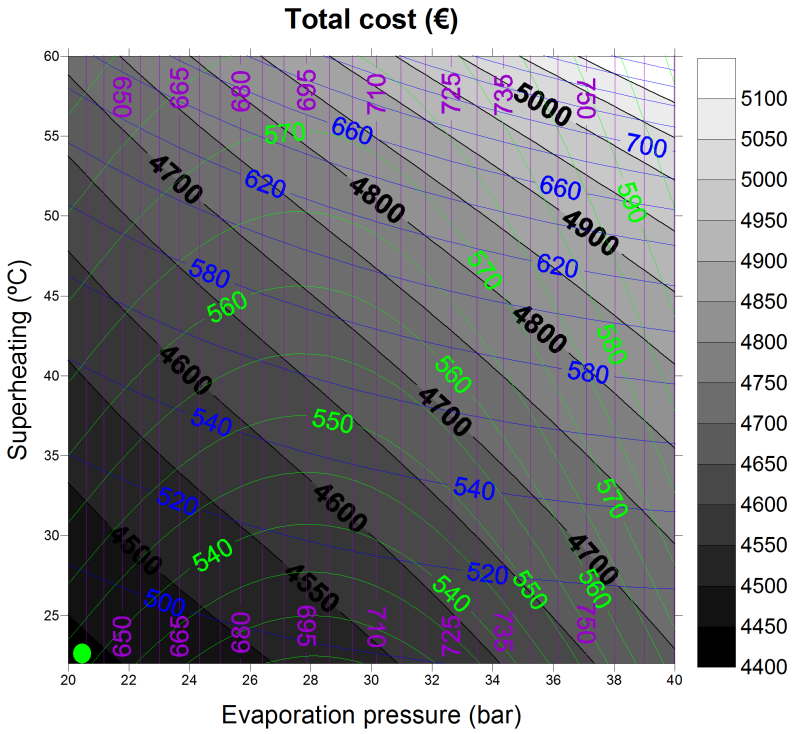

Figure 6.4: Total cost in € (grey scale) of ORC elements, cost of the pump in € (purple lines), cost of the boiler in € (blue lines) and cost of the condenser in € (green lines)

The cost of the pump is a function of the required power, therefore, considering constant mass flow values, it increases with higher levels of pressure. The cost of the boiler increases with higher pressure level and superheating temperature. However, the latter has higher effect than the former as it can be seen in the direction of the lines with the same cost. The reason is that as pressure and superheating temperature increase the pinch point temperature difference tends to decrease and therefore, to maintain this temperature difference, the heat transfer area in the boiler should increase. Regarding the condenser, it is similar to the boiler. However, in this particular case, the expander isentropic efficiency has an effect on temperature at the inlet of the condenser. As a final consequence, SIC parameter is optimized in this particular case at 28 bar and 60 °C of superheating temperature, with a cost of 2030 €/kW.

Regarding sizing criterion, three parameters are presented in Figure 6.5, which are Boiler area in m^2 (blue lines), the Volume Coefficient of the expander in m^3/MJ (purple lines) and the condenser area in m^2 (green lines). The change in pump size is negligible and it is not shown in Figure 6.5.

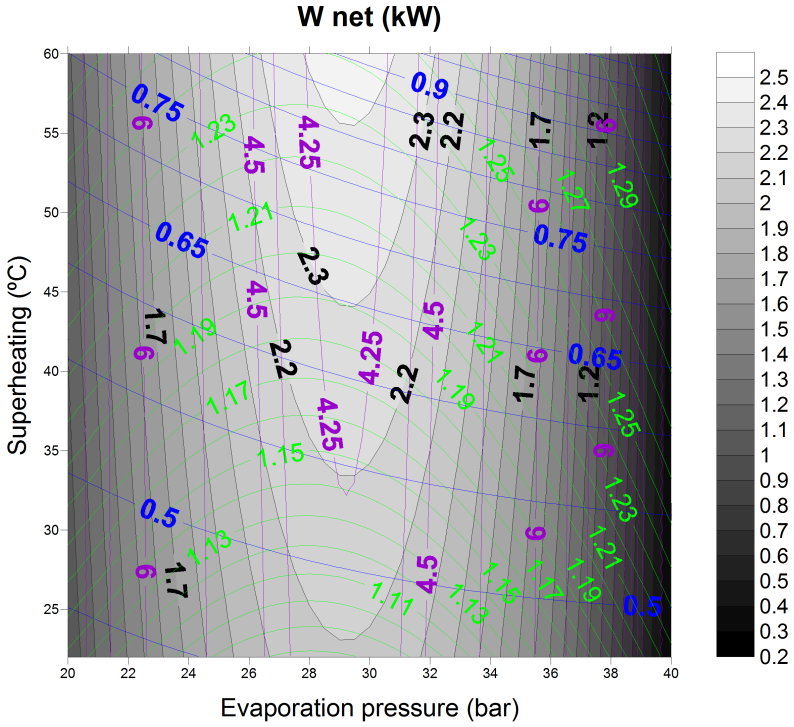

Figure 6.5: Net power in kW (grey scale), area of boiler in m^2 (blue lines), expander size (VC) in m^3/MJ (purple lines) and condenser in m^2 (green lines)

As previously stated, higher pressure levels and temperature of the working fluid reduce the pinch point in the evaporator and increase the heat exchange area in the boiler. The expander size (VC) increases slightly with superheating temperature with a similar trend to SIC. This parameter depends on the specific volume at the outlet of the expander and the work delivered by the expander. As the work delivered by the expander is strongly influenced by the expander isentropic efficiency, the optimal values for this parameter are close to the zone with maximum isentropic efficiencies. Higher superheating values implies higher volume flow rates at the outlet of the expander. Therefore, the result is a global increase of the volume coefficient (VC) in the areas where the expander isentropic efficiency is minimal. Regarding the condenser, the area depends on the temperature at the outlet of the expander, which is a function of the expander isentropic efficiency. The tendency is similar to the boiler area behavior. Consequently, optimum volume coefficient is achieved at lower levels of superheating and pressures between 28 bar and 32 bar.

6.2.3 Optimization of the ORC using a Genetic Algorithm

The main parameters of the ORC have been varied using a multi-objective optimization algorithm in order to optimize the system from a thermo-economic and sizing point of view. Hence, a genetic algorithm (GA) is used. GA was invented by Holland [137] and it is a heuristic method based on the application of the nature selection and genetics into computer science. Three main operators are considered in GA: Selection, cross-over and mutation operator. Selection operator is used to select the fitter individuals from the current generation, hence, intends to reduce diversity of population. Crossover operator is conducted to obtain new individuals. Mutation operator modifies the value of individuals to avoid local optimum. Therefore, these two last parameters try to increase the diversity of the population. In this study the Volume Coefficient (VC), the boiler area ($A_{tot,b}$) and Specific Investment Cost (SIC) are evaluated as objective functions of the decision variables (Equation 6.30, Equation 6.31 and Equation 6.32).

$$A_{tot,b} = f(P_1, P_3, SH, \dot{m}_{et}, T_8) \tag{6.30}$$

$$VC = f(P_1, P_3, SH, \dot{m}_{et}, T_8) \tag{6.31}$$

$$SIC = f(P_1, P_3, SH, \dot{m}_{et}, T_8) \tag{6.32}$$

Where P_1 is the evaporation pressure, P_3 is the condensation pressure, SH is the degree of superheating, $\dot{m}_{et}$ is the ethanol mass flow and T_8 is the temperature at the outlet of exhaust gases (Figure 6.1). The multi-objective optimization problem of the ORC system is performed by using a GA in ModeFRONTIER. The parameters setting in the GA are shown in Table 6.3.

Table 6.3: Parameters of GA

Parameter	Value
Type of algorithm	MOGA-II [138]
Number of Generations	100
Probability of Directional Cross-Over	0.5
Probability of Selection	0.05
Probability of Mutation	0.1

Table 6.4 shows the upper and lower limits of the decision variables. These values correspond with technological limits of the ORC mock-up. Condensing pressure upper bound limit corresponds to safety valves value, evaporating

pressure upper bound limit corresponds to the critical pressure of ethanol, superheating and ethanol mass flow are limited by the degradation and condensing temperature of ethanol and temperature at the outlet of the boiler in the EG side is limited to avoid condensation of water in the exhaust. Moreover, optimum values for the decision variables are far from these lower and upper bounds.

Table 6.4: Limits of decision variables

Decision variables	Lower bound	Upper bound
Evaporation pressure (bar)	10	60
Condensing pressure (bar)	2	4
Superheating (°C)	0	50
Ethanol mass flow (kg/s)	0.01	0.06
Outlet temperature EG (°C)	100	200

Moreover, some restrictions are imposed to the GA:

- Pinch point in the boiler and the condenser should be greater than 10 °C and 5 °C respectively.
- Temperature at the outlet of the boiler (T_4 in Figure 6.2) should be lower than the ethanol degradation temperature. From our experience working with this fluid, it is approximately 250 °C.

The aim of a multi-objective optimization problem using this Genetic Algorithm is to find the Pareto frontier optimal solution. Each point of the frontier represents one potential solution in the multi-objective optimization problem. Therefore, any point is better than another in the frontier, just the improvement of one of them involves worsening the others. The selection of the final optimum depends on the importance of each objective. Figure 6.6, Figure 6.7 and Figure 6.8 show the different views of the optimization. Figure 6.6 shows $A_{tot,b}$ vs SIC (VC in colored bubbles), Figure 6.7 shows $A_{tot,b}$ vs VC (SIC in colored bubbles) and Figure 6.8 shows VC vs SIC ($A_{tot,b}$ in colored bubbles). The optimum solution depend on the importance of each objective:

- Considering SIC as the main objective, greater boiler area will be required. Therefore, with the optimal SIC value of 2264 €/kW, the $A_{tot,b}$ area will be 0.67 m^2 and the VC 3.26 m^3/MJ. This value has been plotted in Figure 6.6, Figure 6.7 and Figure 6.8 using a green circle (point C).

- Considering sizing of the boiler as the main objective, higher SIC will be obtained. Therefore, with the optimal $A_{tot,b}$ value of 0.076 m^2, the SIC will be 5475 €/kW and the VC 4.16 m^3/MJ. This value has been plotted in Figure 6.6, Figure 6.7 and Figure 6.8 using an orange circle (point A).
- Considering sizing of the expander as the main objective, higher SIC and boiler area will be obtained. Therefore, with the optimal VC value of 2.22 m^3/MJ, the final values will be 0.17 m^2 and 3581 €/kW. This value has been plotted in Figure 6.6, Figure 6.7 and Figure 6.8 using a purple circle (point B).

Therefore, in order to select a single-solution from the Pareto frontier, a methodology [139] is implemented to consider the preferences of the Decision Maker. The Technical for Order Preference by Similarity to an Ideal Solution (TOPSIS) [140] is applied to select the final solution on the Pareto Frontier. This method considers the distances to both positive ideal solution and negative ideal solution. In this method, the weight factor is defined for each optimization parameter. Considering the weight factors as 0.5 for SIC, 0.3 for $A_{tot,b}$ and 0.2 for VC and the boundaries of this particular application (ORC coupled to a turbocharged engine), the result is optimized with values of 0.48 m^2 ($A_{tot,b}$), 2515 €/kW (SIC) and 2.62 m^3/MJ (VC). The condenser area ($A_{tot,c}$) in this case is 0.90 m^2.

The boiler and condenser heat transfer area are in the order of magnitude of the one tested in the mock-up, with a slight improvement due to the optimization process. Taking into account the volume of the heat exchangers tested in the installation and the improvement in size due to the optimization, the approximate boiler and condenser volumes are around 800 cm^3 and 200 cm^3 respectively. Regarding the expander, the Volume Coefficient optimal value is 2.62 cm^3/J (VC), this means that with this optimal solution it is needed a displacement of at least 55 cm^3 to produce 20 J in the expander.

The decision variables of this optimum are: 47 bar (evaporation pressure), 3.3 bar (condensing pressure), 9 °C (superheating temperature), 0.028 kg/s (ethanol mass flow) and 100 °C (outlet temperature). This value has been plotted in Figure 6.6, Figure 6.7 and Figure 6.8 using a red circle (point D).

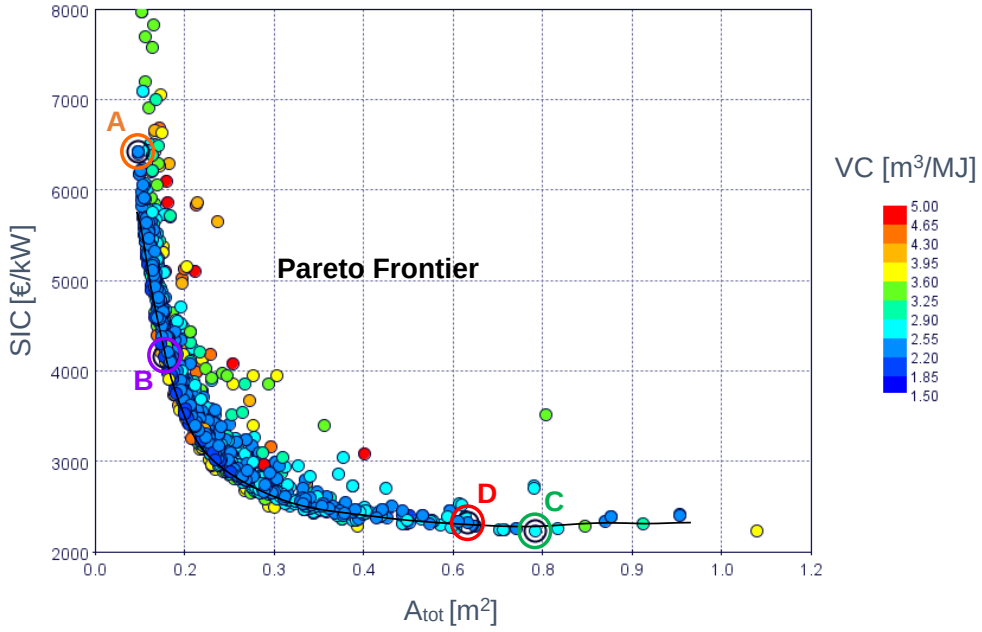

Figure 6.6: Optimization of $A_{tot,b}$ vs SIC

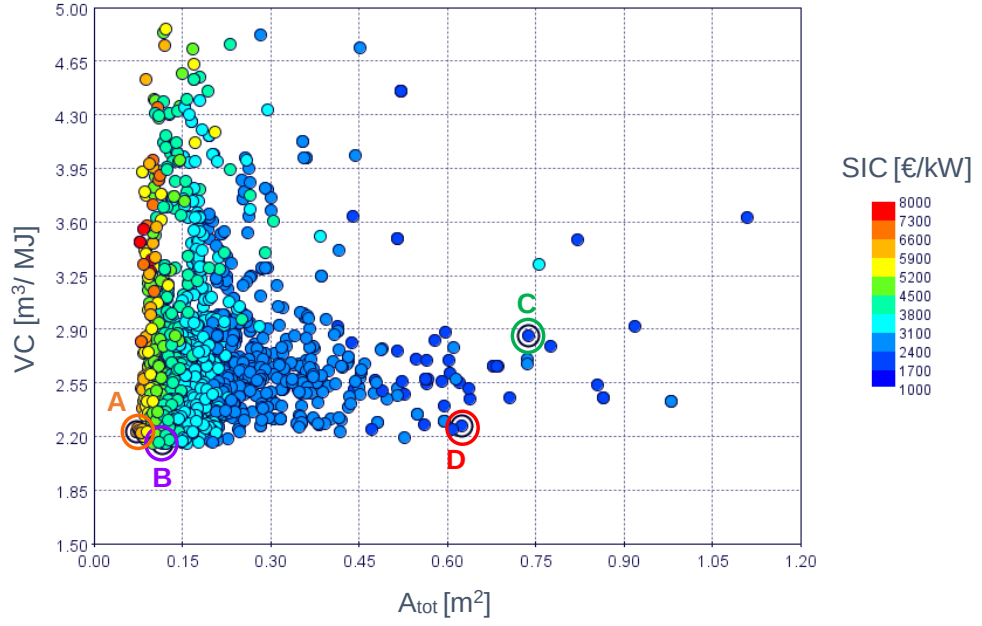

Figure 6.7: Optimization of $A_{tot,b}$ vs VC

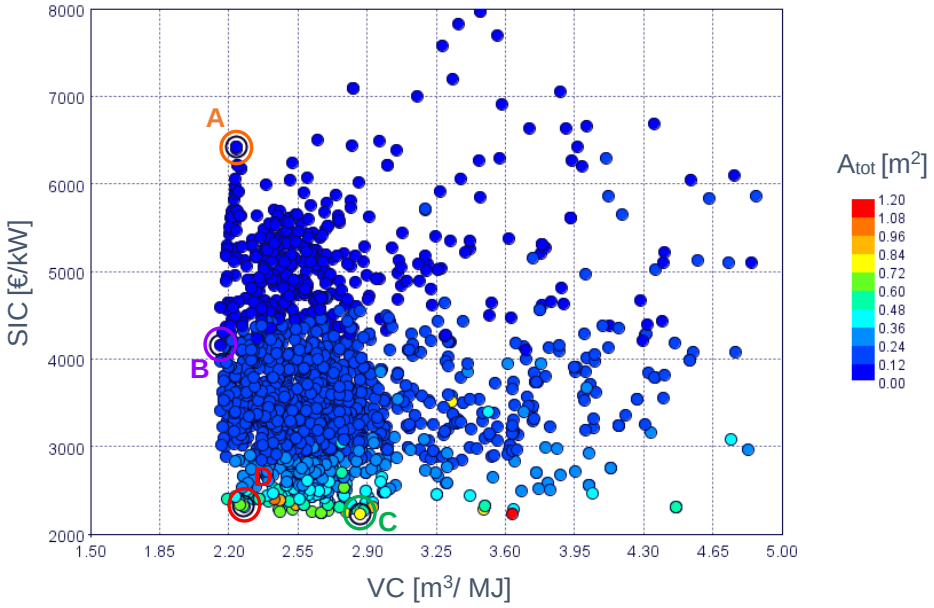

Figure 6.8: Optimization of VC vs SIC

Additionally, two parametric studies are conducted in order to compute the project profitability by means of NPV and PB. In order to compute the cash flows during the project, an estimation regarding the fuel price and the number of hours is performed. As these factors present high level of uncertainty a parametric study is presented to take into account the variability of these parameters.

The cost of fuel has been initially estimated to 1 €/l. However, due to ongoing fuel price changes, this parameter fluctuates over time. Figure 6.9 shows the evolution of PB and NPV with fuel price. PB indicates the period of years before the ORC system can produce a net profit [141]. NPV is a long-term financial tool which helps an individual or a firm to decide whether to make an investment. The pressure and superheating temperature are fixed to optimum ones obtained from the previous analysis. Rising fuel prices from 0.6 to 2.4 €/l involve a reduction in the PB parameter from 8 to 2 years and an increase of NPV from -300 € to 11000 €.

The number of hours of an ORC operating in a year is estimated to 1100 h, which is approximately 3 hour/day. However, due to differences between countries and vehicle users regarding the average time spent in a vehicle, a parametric study is presented in Figure 6.10. Rising the number of hours per day from 0.5 h (182.5 h/year) to 7.5 h (2737.5 h/year) involves a reduction of PB from 18 to 2 years and NPV increases from -2500 € to 12500 €.

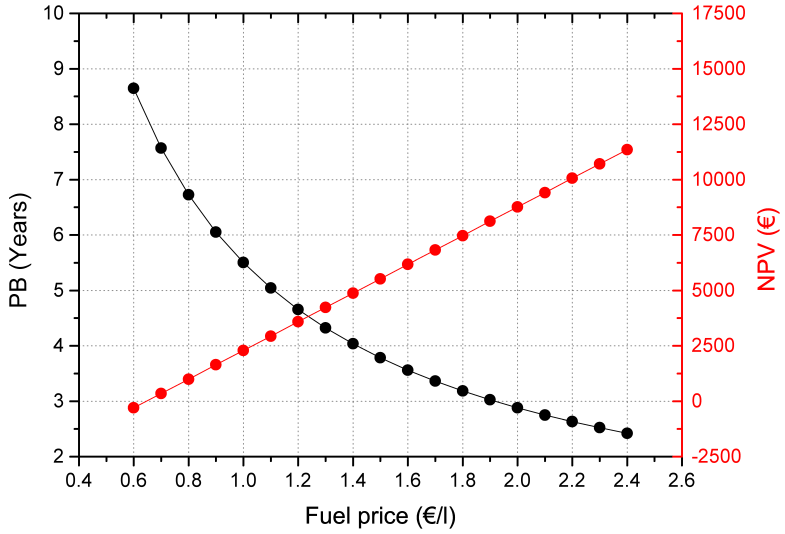

Figure 6.9: PB and NPV evolution vs Fuel Price

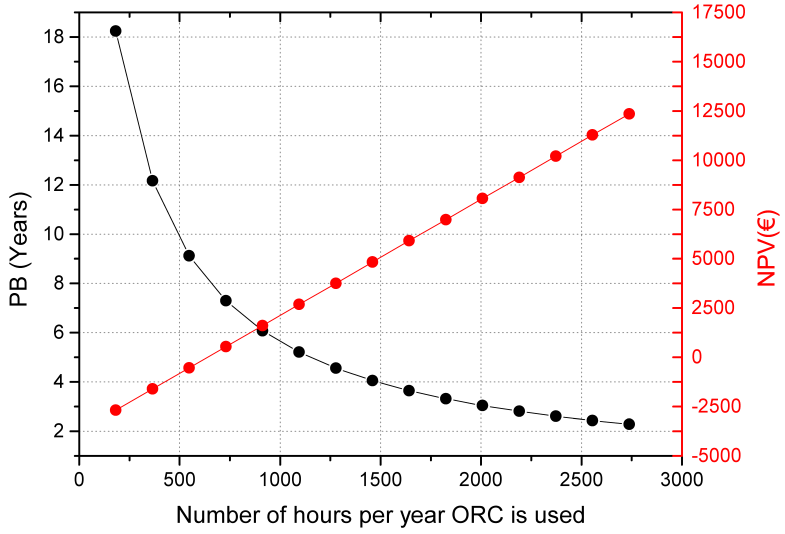

Figure 6.10: Payback and NPV evolution vs the number of hours the ORC is used

As a consequence, both the fuel price and the number of hours running the ORC are critical parameters to consider in the payback estimation. These results in savings have a reasonable payback period [142] and lower risks comparing to other technologies [27].

6.3 Global evaluation of an ORC

The objective of this part is to evaluate the impact of ORC on the engine performance. Points of the experimental chapter (section 3.4) will be used in this subsection.

6.3.1 Effects of ORC integration on the engine

The main effects produced by an ORC based energy recovery are as follows:

- Increase of net engine power ($P_{exp,sh} - P_{pump,el}$) due to the WHRS
- Increase of cooling loads comparing to the original engine
- Increase of total engine weight
- Increase of pumping losses in the engine due to additional pressure drop through the exhaust line
- Increase of global engine power in the vehicle

6.3.1.1 Increase of net engine power due to WHRS

Figure 6.11 shows the increase of $\eta_{ORC,eng,mec}$ (defined in Equation 3.17) and the net power in kW as a function of the expansion ratio for the five experimental boiler powers presented in section 3.4.

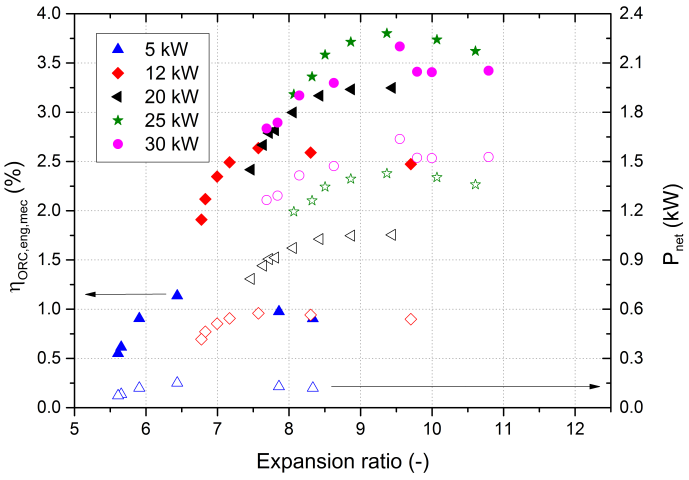

Figure 6.11: Increase of $\eta_{ORC,eng,mec}$ and net power (P_{net}) as a function of expansion ratio

The highest net power obtained from the ORC system corresponds to approximately 1.8 kW, delivered at the IC engine operating point with 30 kW of heat energy in the exhaust gases (boiler power). The highest increase in engine power is obtained for the 25 kW of boiler power, with an improvement in $\eta_{ORC,eng,mec}$ of 3.9 % (defined in Equation 3.17). The shape of each boiler power is similar to the one presented in Figure 3.21.

6.3.1.2 Increase of cooling loads comparing to the original engine

Figure 6.12 shows the cooling power released in the condenser in the experimental points tested in the ORC mock-up. The range goes from 4.5 kW for the low engine operating point up to 25 kW for the highest engine operating point.

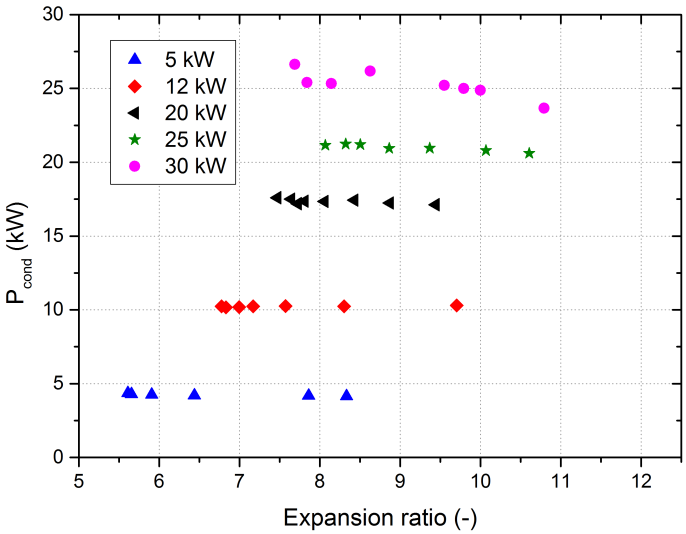

Figure 6.12: Condenser power (P_{cond}) as a function of expansion ratio

Figure 6.13 shows the ratio between the ORC and the engine cooling power demand. Adding a WHR system increases between 20 % and 40% the need for heat rejection on the vehicle because Rankine cycle condenser needs to be cooled down using the engine cooling water (at 90 °C).

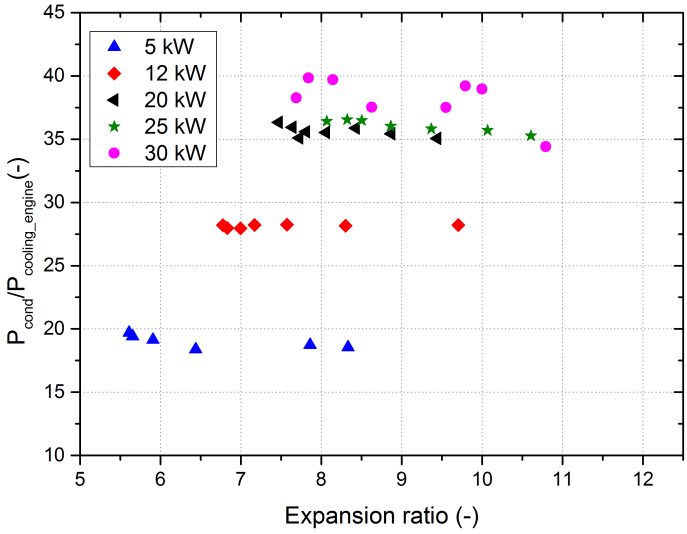

Figure 6.13: Increase of vehicle cooling load as a function of expansion ratio

6.3.1.3 Increase of total engine weight

The extra-weight of the ORC unit should be considered to compute the final improvement of the engine power. This weight produces a propulsion energy increase which can reduce the efficiency of the energy recovery using this WHR system. The increase of weight has an effect on the needed vehicle power to maintain a constant vehicle speed. Therefore, taking into account a displacement without a road slope, the extra-power can be computed using Equation 6.33.

$$P_{weight} = m_{WHRS} \cdot g \cdot s_{ve} \cdot F_{rr} \tag{6.33}$$

Where m_{WHRS} is the weight (kg) of the Waste Heat Recovery System, g is the gravitational acceleration, s_{ve} is the speed of the vehicle (m/s) and F_{rr} is the rolling resistance factor. Considering as an example, the total ORC mass as 30 kg and the implementation in the Ford Explorer (points of Table 3.1, with $F_{rr} = 0.02$ [143] and approximately null slope), the extra-power can be obtained from original configuration of the vehicle.

Figure 6.14 shows the result of this computation for the five engine operating points considered through all the document. A maximum mechanical power increase of 0.2 kW is needed in working conditions when the vehicle is 126 km/h to compensate the increment of vehicle weight due to the ORC system.

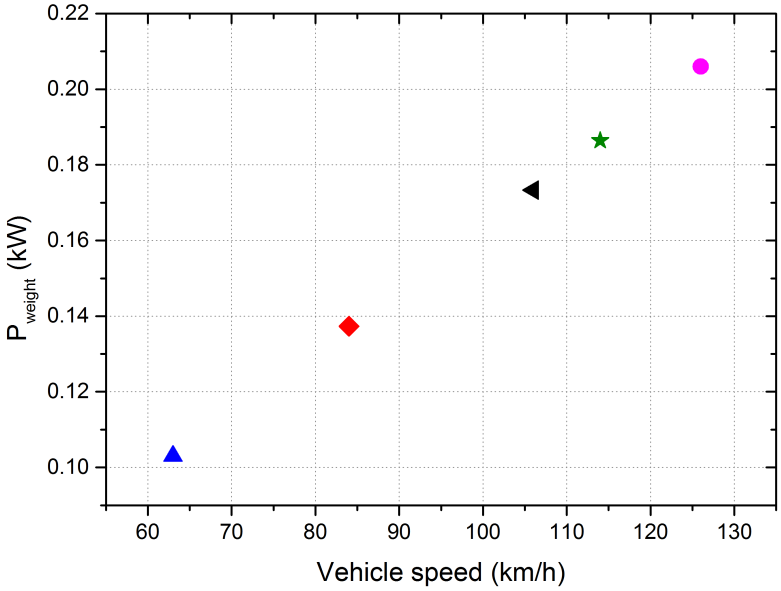

Figure 6.14: Increase of engine power requirements in each vehicle speed

6.3.1.4 Increase of engine pumping losses

As a first approximation, it has been considered that the engine provides the extra-power needed to overcome the pressure losses produced by the ORC. This power can be computed by the following equation:

$$P_{ploss} = \int_{b,i}^{b,o} \dot{V}_b \cdot dP \tag{6.34}$$

Where $\dot{V}_b$ is the volumetric flow rate in $m^3\,s^{-1}$. Pressure loss in the exhaust gas side has been computed using two pressure sensors installed upstream and downstream of the boiler (Figure 3.6). It has been considered a constant pressure loss through the boiler. Therefore, Equation 6.34 can be simplify to Equation 6.35.

$$P_{ploss} = \frac{\dot{V}_{b,i} + \dot{V}_{b,o}}{2} \cdot \Delta P_b \tag{6.35}$$

Figure 6.15 shows the pressure loss through the boiler for the five engine operating points. Maximum value of 60 mbar is obtained for the engine operating point when boiler power is 30 kW. Regarding the pressure loss maximum power, around 0.55 kW of mechanical power is needed to compensate the increment

of pumping losses due to the boiler installed in the exhaust line. As it can be seen in this figure, the power increases approximately as a cubic function of the exhaust gass mass flow. Therefore, the increase of back pressure in the engine is one of the main challenges in the high engine operating points (high volumetric flow rate).

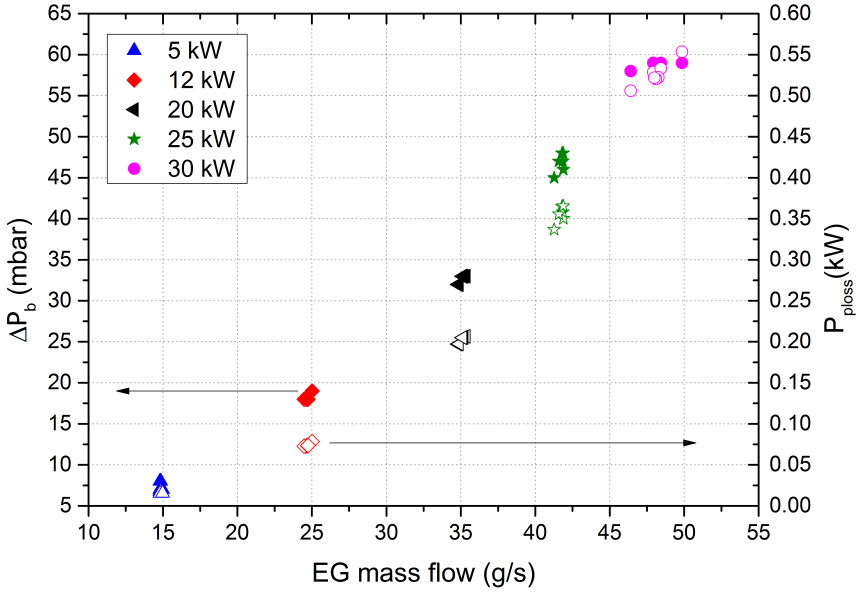

Figure 6.15: Increase of engine pumping losses as a function of exhaust gases mass flow

6.3.1.5 Increase of global engine power in the vehicle

Considering all the drawbacks of the ORC technology, the global improvement of engine performance could be evaluated using Equation 6.36.

$$\Delta P_{WHRS,net} = \frac{P_{net} - P_{ploss} - P_{weight}}{P_{eng}} \tag{6.36}$$

Pressure and weight losses should be considered in the evaluation of the WHR performance because of the similar order of magnitude for the power level. Figure 6.16 shows the power increase for the five engine operating points. For the low engine operating point (63 km/h) the ORC has no benefit because the power delivered by the expander is not high enough to compensate the loss of power due to the higher back pressure and weight. Above 105 km/h the WHR

system provides a net output power increase up to 2% compared to the original system. Therefore, this result confirms that this type of technology is feasible only at high vehicle speed or load, with a high recovery potential.

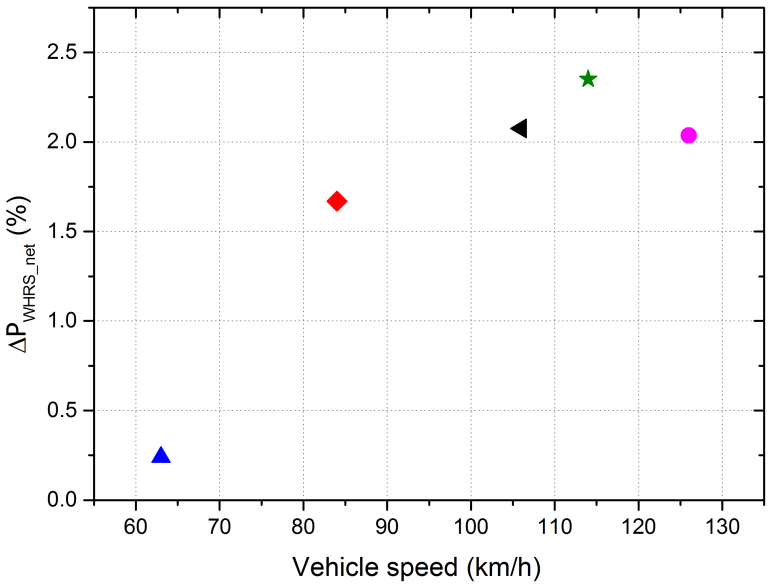

Figure 6.16: Increase of net engine power as a function of vehicle speed

6.3.2 Overall evaluation of the dual system ORC-ICE

Figure 6.17 shows for each engine operating point the contribution of back-pressure losses, weight and net improvement to the total WHRS improvement. The increase of total weight and engine back-pressure has a considerable impact on the potential of the ORC. Although the WHRS potential is greater, only the blue part of the bar chart could be effectively exploited. As vehicle velocity increases, the contribution of weight to the total percentage decreases and the engine-back pressure increases. In the 63 km/h engine operating point, the effect of weight (0.78 %) is worse than the improvement of ORC (0.24 %). Between 84 km/h and 114 km/h, the sum of weight and back-pressure percentage is approximately 50% of the $\Delta P_{WHRS,net}$ percentage. For the 126 km/h engine operating point, this percentage increases up to 80%.

The iteraction between the dual system ICE-ORC will also have an effect on the economical parameters presented in section 6.2, increasing the Payback parameter (for 1100 h and 1 €/l) from 5.5 years to 9.

Consequently, the design of the boiler (increment in the exhaust line back pressure), the weight, system compactness and the control of the optimal operating conditions are critical aspects for the implementation and feasibility of these cycles for the ICE waste heat recovery.

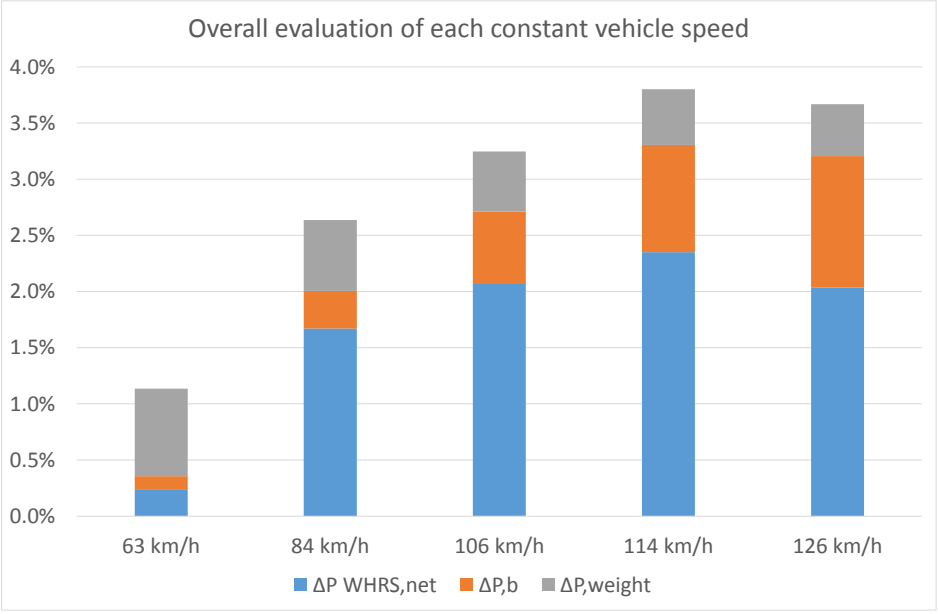

Figure 6.17: Overall evaluation of an ORC

6.3.3 Application to a real driving cycle profile

In order to assess the potential of the ORC at real driving conditions, experimental data was collected during a test campaign of 3 weeks in which every car trip of a non professional driver was recorded by Payri el al. [144].

The results of these tests are presented for the urban (Figure 6.18), interurban (Figure 6.19) and extra-urban (Figure 6.20) driving cycles using a histogram. In each of these figures the number of times that the driver is in each range of velocity and the percentage of the total time is plotted versus the vehicle speed in km/h. The same vehicle speeds have been considered as in Table 3.1. Therefore, in Figure 6.18, the driver is almost 99.8 % of the total time with a vehicle speed lower than 63 km/h.

In the case of the inter-urban driving profile, the speed is 56 % of time below 63 km/h, 23 % of time between 63 km/h and 84 km/h, and 20 % of time between 84 km/h and 106 km/h. In the case of the extra-urban driving profile, the speed is 11 % of time below 63 km/h, 13 % of time between 63 km/h and 84 km/h, and 18 % of time between 84 km/h and 106 km/h, 12 % of time between 106 km/h and 112 km/h and 46 % between 112 km/h and 126 km/h.

Considering the percentage of time for each driving profile and the increment of each operating point (presented in Figure 6.16), the final increase in power output for the urban driving profile is 0.3 %, for the inter-urban driving profile is 1 % and for the extra-urban driving profile is about 2 %. Therefore, the implementation of this system will be focused on extra-urban conditions (high load or high engine speed operating point) in order to obtain a higher WHRS performance rate.

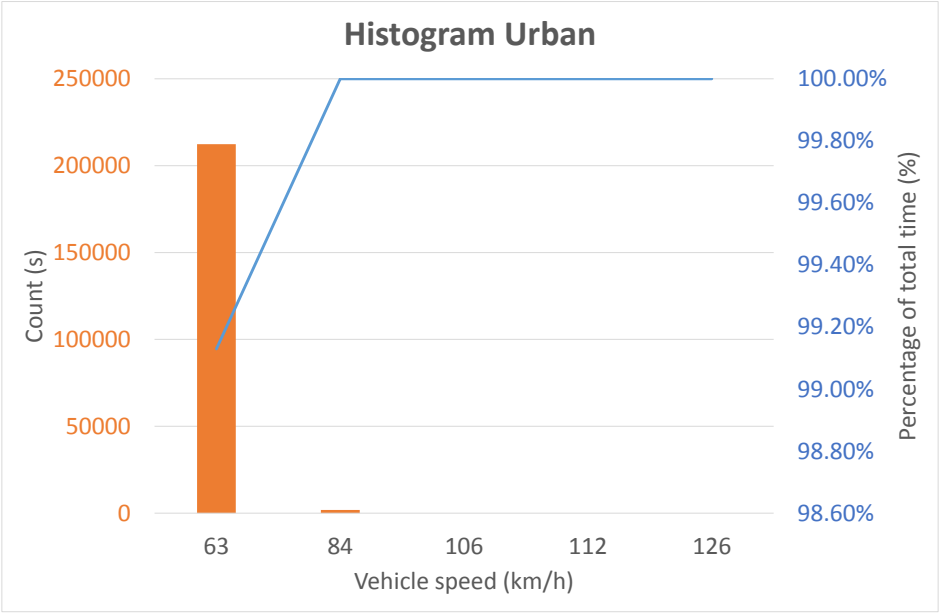

Figure 6.18: Histogram Urban Driving Profile

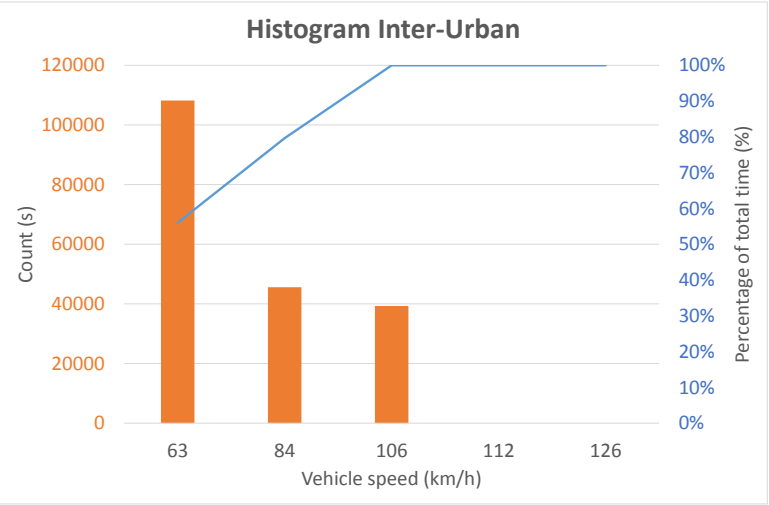

Figure 6.19: Histogram Inter-Urban Driving Profile

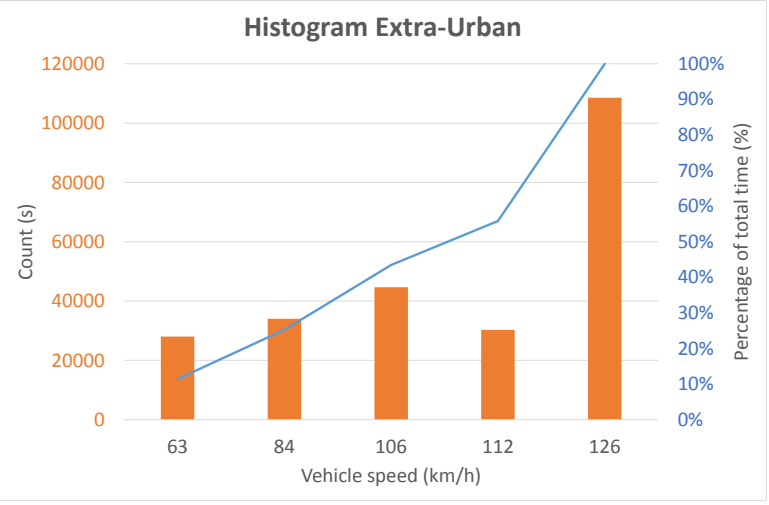

Figure 6.20: Histogram Extra-Urban Driving Profile

6.4 Summary

The presented chapter analyzes and evaluates three thermodynamic optimization criteria using a mathematical model of a bottoming ORC coupled to a 2l turbocharged gasoline engine. Different selection criteria are presented: Thermodynamic parameters (net power), sizing parameters (Boiler area, VC and condenser area) and economic parameters (SIC, PB and NPV). The following results have been obtained:

- SIC parameter is optimized for the pressure level in which the isentropic efficiency is maximum and for higher level of superheating. The maximum value of the isentropic efficiency is fixed by the built-in volumetric expansion ratio. Consequently, net power has a peak for the pressure level between 28-30 bar and a degree of superheating of 60 °C. Minimum value of SIC is approximately 2030 €/kW.

- VC and $A_{tot,b}$ are optimized at lower levels of superheating and pressures between 28-32 bar. Higher pressure and temperature levels of the working fluid reduce the pinch point in the evaporator, increasing the boler heat exchange area. Regarding the expander, as the superheating increases, the size parameter increases too. This parameter depends on the volumetric flow rate and the isentropic specific enthalpy drop through the expander. Higher superheating values imply higher levels of isentropic enthalpy drop and proportionally higher volume outlet flow rates across the expander.

- Multi-objective optimization results using the GA show that the optimum solution depends on the importance of each objective to the final solution. Considering SIC as the main objective, greater boiler areas and expander size will be required. Considering VC as the main objective, greater SIC will be required. Considering $A_{tot,b}$ as the main objective, medium expander size and SIC will be obtained.

- The final increase in power output for the urban driving profile is 0.3 %, for the inter-urban driving profile is 1 % and for the extra-urban driving profile is about 2 %. Therefore, the implementation of this system will be focused on extra-urban conditions (high load or high engine speed operating point) in order to obtain a higher performance rate in the WHRS.

6.5 References

[1] J. Galindo, S. Ruiz, V. Dolz, L. Royo-Pascual, R. Haller, B. Nicolas, and Y. Glavatskaya. "Experimental and thermodynamic analysis of a bottoming Organic Rankine Cycle (ORC) of gasoline engine using swash-plate expander". In: *Energy Conversion and Management* 103 (2015), pp. 519–532. ISSN: 01968904. DOI: 10.1016/j.enconman.2015.06.085. URL: http://linkinghub.elsevier.com/retrieve/pii/S0196890415006470 (cit. on pp. vii, 13, 23, 28, 115, 116, 181).

[27] M. Bailey. "Comparative Evaluation of Three Alternative Power Cycles for Waste Heat Recovery from the Exhaust of Adiabatic Diesel Engines". In: *DOE NASA, United Technologies Research Center* 86953 (1985). ISSN: 04999320 (cit. on pp. 13, 191).

[112] E. S. Richardson. "Thermodynamic performance of new thermofluidic feed pumps for Organic Rankine Cycle applications". In: *Applied Energy* 161 (2016), pp. 75–84. ISSN: 03062619. DOI: 10.1016/j.apenergy.2015.10.004. URL: http://dx.doi.org/10.1016/j.apenergy.2015.10.004 (cit. on pp. 112, 178).

[126] B. Thonon, R. Vidil, and C. Marvillet. "Recent Research and Developments in Plate Heat Exchangers". English. In: *Journal of Enhanced Heat Transfer* 2.1-2 (1995), pp. 149–155. ISSN: 1065-5131. DOI: 10.1615/JEnhHeatTransf.v2.i1-2.160. URL: http://www.dl.begellhouse.com/journals/4c8f5faa331b09ea,3ad0afe360a3d751,5fffa7650c786752.html (cit. on p. 175).

[127] S. Quoilin, S. Declaye, B. F. Tchanche, and V. Lemort. "Thermo-economic optimization of waste heat recovery Organic Rankine Cycles". In: *Applied Thermal Engineering* 31.14-15 (2011), pp. 2885–2893. ISSN: 13594311. DOI: 10.1016/j.applthermaleng.2011.05.014. URL: http://dx.doi.org/10.1016/j.applthermaleng.2011.05.014 (cit. on pp. 175, 178, 179).

[128] S. Lecompte, H. Huisseune, M. van den Broek, S. De Schampheleire, and M. De Paepe. "Part load based thermo-economic optimization of the Organic Rankine Cycle (ORC) applied to a combined heat and power (CHP) system". In: *Applied Energy* 111 (2013), pp. 871–881. ISSN: 03062619. DOI: 10.1016/j.apenergy.2013.06.043. URL: http://linkinghub.elsevier.com/retrieve/pii/S0306261913005503 (cit. on p. 175).

[129] J. C. Chen. "Correlation for boiling heat transfer to saturated fluids in convective flow". In: *Industrial & Engineering Chemistry Process Design and development* 5.3 (1966), pp. 322–329. ISSN: 01964305. DOI: 10.1021/i260019a023. URL: http://pubs.acs.org/doi/pdf/10.10

21/i260019a023$\backslash$npapers3://publication/uuid/1ABFD2F3-EA32-4B69-BE88-0A22F931A08C (cit. on p. 175).

[130] R. Lockhart, R.W., Martinelli. "Proposed Correlation of Data for Isothermal Two-Phase Two-Component Flow in Pipes". In: *Chemical Engineering Progress* 45 (1949), pp. 39–48 (cit. on p. 175).

[131] Y. Hsieh and T. Lin. "Saturated flow boiling heat transfer and pressure drop of refrigerant R-410A in a vertical plate heat exchanger". In: *International Journal of Heat and Mass Transfer* 45.5 (2002), pp. 1033–1044. ISSN: 00179310. DOI: 10.1016/S0017-9310(01)00219-8. URL: http://www.sciencedirect.com/science/article/pii/S0017931001002198 (cit. on p. 176).

[132] W. S. Kuo, Y. M. Lie, Y. Y. Hsieh, and T. F. Lin. "Condensation heat transfer and pressure drop of refrigerant R-410A flow in a vertical plate heat exchanger". In: *International Journal of Heat and Mass Transfer* 48.25-26 (2005), pp. 5205–5220. ISSN: 00179310. DOI: 10.1016/j.ijheatmasstransfer.2005.07.023 (cit. on p. 176).

[133] J. R. García-Cascales, F. Vera-García, J. M. Corberán-Salvador, and J. Gonzálvez-Maciá. "Assessment of boiling and condensation heat transfer correlations in the modelling of plate heat exchangers". In: *International Journal of Refrigeration* 30.6 (2007), pp. 1029–1041. ISSN: 01407007. DOI: 10.1016/j.ijrefrig.2007.01.004 (cit. on p. 176).

[134] D. Maraver, J. Royo, V. Lemort, and S. Quoilin. "Systematic optimization of subcritical and transcritical organic Rankine cycles (ORCs) constrained by technical parameters in multiple applications". In: *Applied Energy* 117 (2014), pp. 11–29. ISSN: 03062619. DOI: 10.1016/j.apenergy.2013.11.076. URL: http://dx.doi.org/10.1016/j.apenergy.2013.11.076 (cit. on p. 177).

[135] S. Lecompte, S. Lemmens, H. Huisseune, M. Van Den Broek, and M. De Paepe. "Multi-objective thermo-economic optimization strategy for ORCs applied to subcritical and transcritical cycles for waste heat recovery". In: *Energies* 8.4 (2015), pp. 2714–2741. ISSN: 19961073. DOI: 10.3390/en8042714 (cit. on p. 179).

[136] F. Heberle and D. Brüggemann. "Thermo-economic analysis of zeotropic mixtures and pure working fluids in organic rankine cycles for waste heat recovery". In: *3rd International Seminar on ORC Power Systems* 53 (2013), pp. 1689–1699. ISSN: 1098-6596. DOI: 10.1017/CBO9781107415324.004. arXiv: arXiv:1011.1669v3 (cit. on p. 181).

[137] J. H. Holland. *Adaptation in natural and artificial systems: An introductory analysis with applications to biology, control, and artificial intelligence.* Masachusetts: MIT Press, 1992 (cit. on p. 185).

[138] C. Poloni. "Hybrid GA for multi objective aerodynamic shape optimization". In: *Genetic algorithms in engineering and computer science* 33 (1995), pp. 397–415 (cit. on p. 185).

[139] J. C. Ferreira, C. M. Fonseca, and A Gaspar-Cunha. "Methodology to select solutions from the pareto-optimal set: A comparative study". In: *Proceedings of GECCO 2007: Genetic and Evolutionary Computation Conference* (2007), pp. 789–796. DOI: 10.1145/1276958.1277117. URL: http://www.scopus.com/inward/record.url?eid=2-s2.0-34548064369{\&}partnerID=40{\&}md5=54135b3d61ca8d41d13c67384fd5ff92 (cit. on p. 187).

[140] Z. Yue. "A method for group decision-making based on determining weights of decision makers using TOPSIS". In: *Applied Mathematical Modelling* 35.4 (2011), pp. 1926–1936. ISSN: 0307904X. DOI: 10.1016/j.apm.2010.11.001. URL: http://dx.doi.org/10.1016/j.apm.2010.11.001 (cit. on p. 187).

[141] X.-Q. Wang, X.-P. Li, Y.-R. Li, and C.-M. Wu. "Payback period estimation and parameter optimization of subcritical organic Rankine cycle system for waste heat recovery". In: *Energy* 88 (2015), pp. 734–745. ISSN: 03605442. DOI: 10.1016/j.energy.2015.05.095. URL: http://www.sciencedirect.com/science/article/pii/S0360544215006970 (cit. on p. 189).

[142] U. Energy. "Waste Heat Recovery: Technology Opportunities in the US Industry". In: *Waste Heat Recovery: Technology Opportunities in the US Industry* (2008), pp. 1–112. URL: http://www1.eere.energy.gov/manufacturing/intensiveprocesses/pdfs/waste{_}heat{_}recovery.pdf (cit. on p. 191).

[143] C. Koffler and K. Rohde-Brandenburger. "On the calculation of fuel savings through lightweight design in automotive life cycle assessments". In: *International Journal of Life Cycle Assessment* 15.1 (2010), pp. 128–135. ISSN: 09483349. DOI: 10.1007/s11367-009-0127-z (cit. on p. 194).

[144] F. Payri, C. Guardiola, B. Pla, and D. Blanco-Rodriguez. "A stochastic method for the energy management in hybrid electric vehicles". In: *Control Engineering Practice* 29 (2014), pp. 257–265. ISSN: 09670661. DOI: 10.1016/j.conengprac.2014.01.004. URL: http://dx.doi.org/10.1016/j.conengprac.2014.01.004 (cit. on p. 198).

CHAPTER 7

Conclusions and future works

Contents

7.1 Introduction

DURING the present work, a scientific contribution has been done for the use of Organic Rankine Cycles as a path to recover Waste Heat from the Internal Combustion Engines. The methodology employed throughout the document is based on:

- Experimental tests
- Simulation model
- Thermodynamic studies
- Thermo-economic studies

In the first part, the achievements made by the experimental tests are presented by means of steady-state and transient operating conditions. The second part presents the simulation model developed using LMS Imagine.Lab Amesim platform, both for the global Organic Rankine Cycle and the swash-plate expander. The third part is focused on the theoretical studies about working fluids, exergy analysis and thermo-economic variables. The last part explains the future working plan regarding the implementation of these cycles in ICE.

7.2 Main contributions

7.2.1 Experimental tests

In order to asses the potential of Organic Rankine Cycles as a way to improve engine efficiency using the exhaust gas as a heat source, an experimental installation is built and coupled to a 2 l turbocharged engine. The working fluid used in this installation is ethanol and the expander machine is a volumetric expander (Swash-plate type).

Steady-state tests A potential of increasing ICE mechanical efficiency up to 3.7% could be reached for the points of high load (25 kW) by installing an ORC to a conventional turbocharged gasoline engine. A maximum Carnot efficiency, Rankine ideal efficiency and Rankine real efficiency values of 79%, 19% and 6% could be obtained using a swash-plate expander to recover energy from exhaust gases. Regarding the expander, a maximum isentropic and volumetric efficiency value of 48.5% and 38.2% are obtained respectively.

Transient tests A slightly simple and robust control based on adaptive PIDs, allows the control of the ORC in realistic driving profiles. NEDC cycle does not produce enough power to run the expander in normal operating conditions starting from engine cold conditions. High loads and hot conditions should be the starting ideal conditions to test and validate the control of the ORC. Considering the implementation of this cycle in real driving conditions, the final increase in power output for the urban driving profile (99% of the time with a vehicle speed lower than 63 km/h) is 0.3 % taking into account the improvement and the percentage of total time in stationary conditions. For the extra-urban driving profile (almost 50% of the time with a vehicle speed around 120 km/h) the improvement is about 2 %. Therefore, the implementation of this system only makes sense in case of extra-urban conditions, where the vehicle has a constant speed at high load or/and engine speed in a motorway.

Regarding the expander, compression in the cylinder is more isothermal at lower expander speeds than at higher expander speeds. Lower expander speeds involve higher residence time of ethanol inside the cylinders. Consequently, heat transfer rates increases with lower expander speeds. Therefore, lower expander speeds involve more isothermal compression processes. The more power is released by the boiler, the higher amount of indicated power is produced by means of higher pressure at the inlet of the expander machine.

7.2.2 Simulation model

The proposed models developed in this chapter using AMESim are consistent due to slight deviation between tests and modelled results. The purpose of these models are: firstly to help the understanding of those physical phenomena difficult to observe by means of experimentation and secondly to estimate the behaviour of the cycle without the need for experimental tests under operating conditions that might cause damages to the installation and / or people.

Global Organic Rankine Cycle model validation The Amesim model allows to simulate the main parameters measured in the cycle. Comparing the three steady operating points, a maximum deviation of 4% is attained regarding the pressures and temperatures and a value of 5% is attained regarding the torque. Moreover, this model is coupled to a Mean Value Engine Model, to simulate NEDC conditions. Similar results are obtained by the simulation model regarding the power delivered by the expander.

Swash-plate model validation The model represents the fluid dynamic behavior of the Swash-plate using discharge coefficients, displacement laws, heat transfer coefficients and mechanical losses. The P-V diagram is measured by a piezoelectric pressure sensor and is compared to the expander model. Maximum deviation of 10% for the indicated power is achieved at the point of 3000 rpm.

Case study A Mean Value Engine Model is used as a heat source for the Organic Rankine Cycle. A potential improvement of 2.5% in fuel conversion efficiency is obtained for the high operating points of the NEDC (120 km/h) as a direct consequence of the 23.5 g/kWh reduction in bsfc comparing the system engine + ORC to the original engine configuration.

Differences between theoretical and experimental studies can be drawn due to the heat exchanger effectiveness and expander efficiency. The temperature at the outlet of the heat exchanger should be above 100 °C to avoid condensation effects that could damage the exhaust line. Moreover, expander efficiency is imposed as a correlation, which can have an effect on the global performance of the ORC.

7.2.3 Thermodynamic studies

In order to fulfil the theoretical methodology, a 1D code is developed to evaluate the performance of the Organic Rankine Cycles in a simple way. This code uses NIST database to compute the thermodynamic properties of the fluids. Using

this tool, several optimization and sensitivity studies have been developed in order to understand the viability of these cycles. Two main topics have been presented in this work: working fluids and exergetic analysis.

Working fluids A pre-selection of 6 working fluids has been made taking into account the ORC application. Refrigerant fluids (R-245fa and R-1234ze) have smaller Mollier diagram, lower critical temperature values and lower enthalpy drop across the boiler. Therefore, considering a fixed exhaust power source, the fluid mass flow increases as enthalpy drop decreases. Moreover, vapour isobars are closer than for the other fluids such as ethanol and water. This implies lower enthalpy drop in the expansion process and thus lower power delivered by the expander for these fluids. The volume flow rate is lower than for the ethanol or water, due to the high density of these fluids in vapour conditions. Water has been widely used in the Rankine cycle, however it is not the ideal working fluid due to its thermal characteristics. The size of the expander and the condenser will be bigger because of the volumetric flow rate and the degree of superheating. It will have an effect on the pinch point. MM and n-pentane are good candidates for the exhaust gases temperature range of vehicles, with a smaller operating range than ethanol. Ethanol has good thermal characteristics in the whole range of ICE temperatures (diesel and gasoline).

Exergetic analysis Conventional analysis shows that the overall system should be improved following priorities for the components in this order: boiler (5.48 kW), expander (2.97 kW), condenser (1.63 kW) and pump (0.19 kW). From a conventional exergy analysis, it is not possible to distinguish between irreversibilities occurring in other components and the component itself. The advanced exergy analysis evaluates the detailed interactions between components of the overall system, and the real potential of improvement for a component within a system. Therefore, the advanced exergy analysis suggests that the first priority should be given to the expander (88% reduction by the technological improvement of the component itself (avoidable-endogenous)), followed by the pump (70%), condenser (16%) and boiler (14%). A total amount of 3.75 kW, 36.5% of exergy destruction rate, could be lowered in the forthcoming years, taking account that only the avoidable part (maximum efficiencies considering technical restrictions of the cycle components) of the exergy destruction rate can be reduced. This part of the exergy is higher than the unavoidable part in the expander (2.38 kW vs 0.59 kW) and the pump (0.12 vs 0.07 kW). These two components will have the highest improvement potential by technical modifications of the components. This improvement will imply an increase of the WHRS benefit $\eta_{ORC,eng}$ (Equation 3.16) from 1.19 % to almost 2.5% for the 120 km/h operating point (30 kW of exhaust power).

7.2.4 Thermo-economic analysis

A methodology to optimize the ORC coupled to Internal Combustion Engines for vehicle application is presented using a multi-objective optimization algorithm. In this study, three objective functions are used in the optimization as a function of the decision variables: a parameter related to the expander size, the Volume Coefficient (VC) in m^3/MJ, the boiler area ($A_{tot,b}$) in m^2 and the Specific Investment Cost (SIC) in €/kW. Multi-objective optimization results show that the optimum solution depends on the importance of each objective to the final solution (Pareto Diagram). Considering SIC as the main objective, greater boiler area will be required. Therefore, with an optimal value of SIC of 2264 €/kW, the $A_{tot,b}$ area will be 0.67 m^2 and the VC 3.26 m^3/MJ. Considering sizing of the boiler as the main objective, higher SIC will be obtained. Therefore, with an optimal value of $A_{tot,b}$ of 0.076 m^2, the SIC will be 5475 €/kW and the VC 4.16 m^3/MJ. Considering sizing of the expander as the main objective, higher SIC and boiler area will be obtained. Therefore, with an optimal value of VC of 2.22 m^3/MJ, the final values will be 0.17 m^2 and 3581 €/kW.

Therefore, in order to select a single-solution from the Pareto frontier, a multiple attribute decision-making method (TOPSIS) is implemented in order to take into account the preferences of the Decision Maker. Considering the weight factors 0.5 for Specific Investment Cost (SIC), 0.3 for the area of boiler area ($A_{tot,b}$) and 0.2 for Volume Coefficient (VC) and the boundaries of this particular application, the result is optimized with values of 0.48 m^2 ($A_{tot,b}$), 2515 €/kW (SIC) and 2.62 m^3/MJ (VC). The condenser area ($A_{tot,c}$) in this case is 0.90 m^2.

The boiler and condenser heat transfer area is in the order of magnitude of the one tested in the mock-up, with a slight reduction in the heat transfer area due to the optimization process using the GA. Taking into account the volume of the heat exchangers tested in the installation and the improvement in size due to the optimization, the approximate volume of the boiler and condenser is around 800 cm^3 and 200 cm^3 respectively. Regarding the expander, the Volume Coefficient optimal value is 2.62 cm^3/J (VC), this means that with this optimal solution it is needed a displacement of at least 55 cm^3 to produce 20 J in the expander. This is consistent with the order of magnitude of the expander prototype tested in the ORC mock-up.

Additionally, two parametric studies are done in order to take into account the uncertainty surrounding cost of fuel and number of ORC operating hours in a year. The cost of fuel is initially estimated to 1 €/l. However, due to ongoing fuel price changes, this parameter fluctuates over time. Rising fuel prices from 0.6 to 2.4 €/l involve a reduction in the Payback parameter from 8 to 2 years and an increase of Net Present Value from -300 € to 11000 €. The negative value implies that with fuel prices lower than 0.65 €/l this system would not be

feasible.

The number of hours for an ORC operating in a year is estimated to 1100 h, which is approximately 3 hour/day. However, due to differences between countries and vehicle users regarding the average time spent in a vehicle, differences are shown within the users. Rising the number of hours per day from 0.5 h (182.5 h/year) to 7.5 h (2737.5 h/year) involves a variation in PB from 18 to 2 years and a NPV variation from -2500 € to 12500 €. The negative value implies that with a number of operating hours lower than 2.2 h per day (780 h/year) this system would not be feasible.

7.2.5 ORC impact on engine performance

The main effects produced by an ORC based energy recovery are as follows:

Increase of net engine power due to the WHRS The highest net power obtained from the ORC system corresponds to approximately 1.8 kW, delivered for the IC engine operating point with 30 kW of heat energy in exhaust gases (boiler power). The highest engine power increase is obtained for the 25 kW of boiler power, with an $\eta_{ORC,eng,mec}$ improvement of 3.9 % (defined in Equation 3.17).

Increase of cooling loads comparing to the original engine Adding a WHR system increases between 20 % and 40% the vehicle need for heat rejection because the condenser of the Rankine cycle needs to be cooled down using the engine cooling water (at 90 °C).

Increase of total engine weight A maximum mechanical power increase of 0.2 kW is needed for working conditions with the vehicle at 126 km/h to compensate the increment in vehicle weight due to the ORC system.

Increase of pumping losses in the engine due to additional pressure drop through the exhaust line Maximum value of 60 mbar is obtained for the engine operating point when boiler power is 30 kW. Regarding the pressure loss maximum power, around 0.55 kW of mechanical power is needed to compensate the increment in pumping losses due to the boiler installed in the exhaust line.

Consequently, the design of the boiler (increment of the exhaust line back pressure), the weight, the compactness of the system and the control of the optimal operating conditions are critical aspects for the implementation and feasibility of these cycles in the ICE.

To sum up, for the low engine operating point (63 km/h) the ORC has no benefit because the power delivered by the expander is not high enough to compensate the loss of power due to the higher back pressure and weight. Above 105 km/h the WHR system provides a net output power increase up to 2% compared to the original system. Therefore, this result confirms that this type of technology is only feasible at high load and/or vehicle speed.

7.3 Future works

Nowadays the heavy duty industry seem to be clear that they will implement the technology of Rankine Cycle on their long haul trucks before 2020 as an answer to future stringent regulation and the still increasing customers request for operating cost reduction. This improvement will save approximately 2700 € per year in each truck, avoiding emitting 6 tons of CO_2 to the atmosphere [100]. Further research is needed in order to achieve an optimal solution in terms of compactness and reliability. A great effort will be needed by manufacturers to improve the system and make it compact to be able to install it in on-road vehicles. Moreover the following aspects will have to be studied:

Experimental future works

- Mixtures evaluation as a path to improve global organic rankine efficiency. The experimental testing of mixtures (water, ethanol) will be an alternative option to the ethanol.
- Experimental evaluation of heat sources in the engine. New experimental tests will have to be done, using the CAC, the EGR and the cooling heat to understand the potential of all the heat sources.
- Experimental evaluation of turboexpanders in order to compare the global performance of the two expander types.

Theoretical future works

- Development of a CFD model of the expander to be able to understand the behaviour of the flow under off-design conditions and to take into account the real conditions of the working fluid and the transient and local effects of the flow.

7.4 References

[100] R. Daccord, A. Darmedru, and J. Melis. “Oil-free axial piston expander for waste heat recovery”. English. In: *SAE International* 1 (2014), pp. 1–12. ISSN: 0148-7191. DOI: 10.4271/2014-01-0675.Copyright. URL: http://papers.sae.org/2014-01-0675/ (cit. on pp. 28, 214).

Bibliography

[1] **Galindo, J., Ruiz, S., Dolz, V., Royo-Pascual, L., Haller, R., Nicolas, B., and Glavatskaya, Y.**
"Experimental and thermodynamic analysis of a bottoming Organic Rankine Cycle (ORC) of gasoline engine using swash-plate expander"
in: *Energy Conversion and Management* 103 (2015), pp. 519–532. ISSN: 01968904. DOI: 10.1016/j.enconman.2015.06.085. URL: http://linkinghub.elsevier.com/retrieve/pii/S0196890415006470
(cit. on pp. vii, 13, 23, 28, 115, 116, 181)

[2] **Galindo, J., Dolz, V., Royo-Pascual, L., Haller, R., and Melis, J.**
"Study of a volumetric expander suitable for waste heat recovery from an automotive IC engine using an ORC with ethanol"
in: *3rd International Seminar on ORC Power Systems* 85 (2015), pp. 1–17 (cit. on p. vii)

[3] **Galindo, J., Ruiz, S., Dolz, V., and Royo-Pascual, L.**
"Advanced exergy analysis for a bottoming organic rankine cycle coupled to an internal combustion engine"
in: *Energy Conversion and Management* 126 (2016), pp. 217–227. ISSN: 01968904. DOI: 10.1016/j.enconman.2016.07.080. URL: http://dx.doi.org/10.1016/j.enconman.2016.07.080 (cit. on p. vii)

[4] **Torregrosa, A., Galindo, J., Dolz, V., Royo-Pascual, L., Haller, R., and Melis, J.**
"Dynamic tests and adaptive control of a bottoming organic Rankine cycle of IC engine using swash-plate expander"
in: *Energy Conversion and Management* 126 (2016), pp. 168–176. ISSN: 01968904. DOI: 10.1016/j.enconman.2016.07.078. URL: http://linkinghub.elsevier.com/retrieve/pii/S0196890416306574
(cit. on p. vii)

[5] **Galindo, J., Dolz, V., Royo-Pascual, L., Haller, R., and Melis, J.**
"Modeling and Experimental Validation of a Volumetric Expander Suitable for Waste Heat Recovery from an Automotive Internal Combustion Engine Using an Organic Rankine"

in: *Energies* 9.279 (2016), pp. 1–18. ISSN: 1996-1073. DOI: 10.3390/en9040279 (cit. on p. vii)

[6] **Galindo, J., Climent, H., Dolz, V., and Royo-Pascual, L.**
"Multi-objective optimization of a bottoming Organic Rankine Cycle (ORC) of gasoline engine using swash-plate expander"
in: *Energy Conversion and Management* 126 (2016), pp. 1054–1065. ISSN: 01968904. DOI: 10.1016/j.enconman.2016.08.053. URL: http://linkinghub.elsevier.com/retrieve/pii/S0196890416307270 (cit. on p. vii)

[7] **Novella, R., Dolz, V., Martín, J., and Royo-Pascual, L.**
"Thermodynamic analysis of an absorption refrigeration system used to cool down the intake air in an Internal Combustion Engine"
in: *Applied Thermal Engineering* 111 (2017), pp. 257–270. ISSN: 13594311. DOI: 10.1016/j.applthermaleng.2016.09.084. URL: http://linkinghub.elsevier.com/retrieve/pii/S1359431116316921 (cit. on pp. viii, 13)

[8] **Payri, F., Luján, J. M., Guardiola, C., and Pla, B.**
"A Challenging Future for the IC Engine: New Technologies and the Control Role"
in: *Oil & Gas Science and Technology – Revue d'IFP Energies nouvelles* 70 (2014), pp. 15–30. ISSN: 1294-4475. DOI: 10.2516/ogst/2014002. URL: http://ogst.ifpenergiesnouvelles.fr/10.2516/ogst/2014002 (cit. on p. 2)

[9] **Berger, R.**
"Trends in ICE-Technologies Besides Electrification , improvements in conventional powertrain technologies will play a major role looking forward"
in: *Automotive megatrends* 2013, pp. 1–13 (cit. on p. 2)

[10] **Heywood, J. B.**
Internal combustion engine fundamentals
1988, pp. 1–930. ISBN: 007028637X. URL: http://books.google.es/books/about/Internal{_}combustion{_}engine{_}fundamentals.html?id=u9FSAAAAMAAJ{\&}pgis=1 (cit. on pp. 2, 15, 126)

[11] **Hossain, S. N. and Bari, S.**
"Waste heat recovery from the exhaust of a diesel generator using Rankine Cycle"
in: *Energy Conversion and Management* 75 (2013), pp. 141–151. ISSN: 01968904. DOI: 10.1016/j.enconman.2013.06.009. URL: http://dx.doi.org/10.1016/j.enconman.2013.06.009 (cit. on p. 2)

[12] **Saidur, R., Rezaei, M., Muzammil, W. K., Hassan, M. H., Paria, S., and Hasanuzzaman, M.**
"Technologies to recover exhaust heat from internal combustion engines"
in: *Renewable and Sustainable Energy Reviews* 16.8 (2012), pp. 5649–5659. ISSN: 13640321. DOI: 10.1016/j.rser.2012.05.018. URL: http://dx.doi.org/10.1016/j.rser.2012.05.018 (cit. on p. 2)

[13] **Bianchi, M. and De Pascale, A.**
"Bottoming cycles for electric energy generation: Parametric investigation of available and innovative solutions for the exploitation of low and medium temperature heat sources"
in: *Applied Energy* 88.5 (2011), pp. 1500–1509. ISSN: 03062619. DOI: 10.1016/j.apenergy.2010.11.013. URL: http://linkinghub.elsevier.com/retrieve/pii/S0306261910004769 (cit. on p. 2)

[14] **Bronicki, L. and Harry, Z.**
Vapor turbines
US Patent 3,040,528 1962. URL: https://www.google.com/patents/US3040528 (cit. on p. 2)

[15] **Hernandez, A., Desideri, A., Ionescu, C., and Quoilin, S.**
"Towards the optimal operation of an Organic Rankine Cycle unit by means of model predictive control"
in: *3rd International Seminar on ORC Power Systems* (2015), pp. 1–10 (cit. on p. 2)

[16] **Robertson, M. C., Costall, A. W., Newton, P. J., and Martinez-botas, R. F.**
"Transient duty cycle analysis for mobile Organic Rankine Cycle applications"
in: *3rd International Seminar on ORC Power Systems* (2015), pp. 1–10 (cit. on p. 2)

[17] **Rodrigue, J. P., Comtois, C., and Slack, B.**
The Geography of Transport Systems
2006, p. 297 (cit. on p. 11)

[18] **Holditch, Stephen**
"Factors That Will Influence Oil and Gas Supply and Demand in the 21st Century"
in: *MRS Bulletin* 33 (2010), pp. 317–323 (cit. on p. 11)

[19] **Eurostat**
Energy, transport and environment indicators
2007. ISBN: 978-92-79-07044-0. DOI: 10.2785/547816 (cit. on p. 11)

[20] **Horst, T. A., Tegethoff, W., Eilts, P., and Koehler, J.**
"Prediction of dynamic Rankine Cycle waste heat recovery performance and fuel saving potential in passenger car applications considering interactions with vehicles' energy management"
in: *Energy Conversion and Management* 78 (2014), pp. 438–451. ISSN: 01968904. DOI: 10.1016/j.enconman.2013.10.074. URL: http://linkinghub.elsevier.com/retrieve/pii/S0196890413007097
(cit. on p. 11)

[21] **Mock, P.**
"EU CO2 standards for passenger cars and light-commercial vehicles"
in: *Policy update* January (2014). URL: http://www.theicct.org/eu-co2-standards-passenger-cars-and-lcvs (cit. on p. 12)

[22] **Eurostat**
Smarter, greener, more inclusive?
2015. ISBN: 9789279400797 (cit. on p. 12)

[23] **Torregrosa, A. J., Broath, A., Olmeda, P., and Romero, C.**
"Assessment of the influence of different cooling system configurations on engine warm-up, emissions and fuel consumption"
in: *International Journal of Automotive Technology* 9.4 (2008), pp. 447–458. DOI: 10.1007/s12239âĹŠ008âĹŠ0054âĹŠ1 (cit. on p. 13)

[24] **Zegenhagen, T. and Ziegler, F.**
"Experimental investigation of the characteristics of a jet-ejector and a jet-ejector cooling system operating with R134a as a refrigerant"
in: *International Journal of Refrigeration* 56 (2015), pp. 173–185. ISSN: 01407007. DOI: 10.1016/j.ijrefrig.2015.01.001. URL: http://linkinghub.elsevier.com/retrieve/pii/S0140700715000031
(cit. on p. 13)

[25] **Zegenhagen, M. and Ziegler, F.**
"Feasibility analysis of an exhaust gas waste heat driven jet-ejector cooling system for charge air cooling of turbocharged gasoline engines"
in: *Applied Energy* 160 (2015), pp. 221–230. ISSN: 03062619. DOI: 10.1016/j.apenergy.2015.09.057. URL: http://linkinghub.elsevier.com/retrieve/pii/S0306261915011629 (cit. on p. 13)

[26] **Rêgo, A., Hanriot, S., Oliveira, A., Brito, P., and Rêgo, T.**
"Automotive exhaust gas flow control for an ammonia–water absorption refrigeration system"
in: *Applied Thermal Engineering* 64.1-2 (2014), pp. 101–107. ISSN: 13594311. DOI: 10.1016/j.applthermaleng.2013.12.018. URL: http://linkinghub.elsevier.com/retrieve/pii/S1359431113008958
(cit. on p. 13)

[27] **Bailey, M.**
"Comparative Evaluation of Three Alternative Power Cycles for Waste Heat Recovery from the Exhaust of Adiabatic Diesel Engines"
in: *DOE NASA, United Technologies Research Center* 86953 (1985). ISSN: 04999320 (cit. on pp. 13, 191)

[28] **Galindo, J., Serrano, J., Dolz, V., and Kleut, P.**
"Brayton cycle for internal combustion engine exhaust gas waste heat recovery"
in: *Advances in Mechanical Engineering* 7.6 (2015), pp. 1–9. ISSN: 1687-8140. DOI: 10.1177/1687814015590314. URL: http://ade.sagepub.com/lookup/doi/10.1177/1687814015590314 (cit. on p. 13)

[29] **Liebl, J., Neugebauer, S., Eder, A., and Linde, M.**
"The Thermoelectric Generator from BMW is Making Use of Waste Heat"
in: *MTZ* 70 (2009), pp. 4–11 (cit. on p. 13)

[30] **Kushch, A., Bass, J., Ghamaty, S., and Eisner, N.**
"Thermoelectric development at Hi-Z technology"
in: *Proceedings ICT2001. 20 International Conference on Thermoelectrics (Cat. No.01TH8589)* (2001), pp. 1–9. ISSN: 1094-2734. DOI: 10.1109/ICT.2001.979922 (cit. on p. 13)

[31] **Aghaali, H. and Ångström, H.-E.**
"A review of turbocompounding as a waste heat recovery system for internal combustion engines"
in: *Renewable and Sustainable Energy Reviews* 49 (2015), pp. 813–824. ISSN: 13640321. DOI: 10.1016/j.rser.2015.04.144. URL: http://linkinghub.elsevier.com/retrieve/pii/S1364032115004141 (cit. on p. 13)

[32] **Weerasinghe, W., Stobart, R., and Hounsham, S.**
"Thermal efficiency improvement in high output diesel engines a comparison of a Rankine cycle with turbo-compounding"
in: *Applied Thermal Engineering* 30.14-15 (2010), pp. 2253–2256. ISSN: 13594311. DOI: 10.1016/j.applthermaleng.2010.04.028. URL: http://linkinghub.elsevier.com/retrieve/pii/S1359431110001912 (cit. on p. 13)

[33] **Stobart, R. and Weerasinghe, R.**
"Heat Recovery and Bottoming Cycles for SI and CI engines"
in: *SAE Technical Paper* 2006.724 (2006). DOI: 10.4271/2006-01-0662. URL: http://sro.sussex.ac.uk/15122/ (cit. on p. 15)

[34] **Duparchy, A., Leduc, P., Bourhis, G., and Ternel, C.**
"Heat Recovery for next Generation of Hybrid Vehicles : Simulation and Design of a Rankine Cycle System"
in: *World Electric Vehicle Journal Vol.3* 3 (2009), pp. 1–17
(cit. on pp. 15, 46)

[35] **Chammas, R. E. and Clodic, D.**
"Combined Cycle for Hybrid Vehicles"
in: *SAE International* 1 (2012), p. 10 (cit. on pp. 15, 21)

[36] **Macián, V., Serrano, J., Dolz, V., and Sánchez, J.**
"Methodology to design a bottoming Rankine cycle, as a waste energy recovering system in vehicles. Study in a HDD engine"
in: *Applied Energy* 104 (2013), pp. 758–771. ISSN: 03062619. DOI: 10.1016/j.apenergy.2012.11.075. URL: http://linkinghub.elsevier.com/retrieve/pii/S0306261912008859 (cit. on p. 15)

[37] **Dolz, V., Novella, R., García, A., and Sánchez, J.**
"HD Diesel engine equipped with a bottoming Rankine cycle as a waste heat recovery system. Part 1: Study and analysis of the waste heat energy"
in: *Applied Thermal Engineering* 36 (2012), pp. 269–278. ISSN: 13594311. DOI: 10.1016/j.applthermaleng.2011.10.025. URL: http://linkinghub.elsevier.com/retrieve/pii/S1359431111005631
(cit. on pp. 15, 16)

[38] **Teng, H. and Regner, G.**
"Improving Fuel Economy for HD Diesel Engines with WHR Rankine Cycle Driven by EGR Cooler Heat Rejection"
English. In: *SAE International* 1 (2009), pp. 1–11. DOI: 10.4271/2009-01-2913. URL: http://papers.sae.org/2009-01-2913/
(cit. on pp. 15, 21)

[39] **Hountalas, D. T., Mavropoulos, G. C., Katsanos, C., and Knecht, W.**
"Improvement of bottoming cycle efficiency and heat rejection for HD truck applications by utilization of EGR and CAC heat"
in: *Energy Conversion and Management* 53.1 (2012), pp. 19–32. ISSN: 01968904. DOI: 10.1016/j.enconman.2011.08.002. URL: http://dx.doi.org/10.1016/j.enconman.2011.08.002 (cit. on p. 15)

[40] **Espinosa, N., Tilman, L., Lemort, V., Quoilin, S., and Lombard, B.**
"Rankine cycle for waste heat recovery on commercial trucks: approach, constraints and modelling"
en. In: *Diesel International Conference and Exhibition* 1 (2010), pp. 1–10. URL: http://orbi.ulg.ac.be/handle/2268/62995 (cit. on p. 15)

[41] **Serrano, J. R., Dolz, V., Novella, R., and García, A.**
"HD Diesel engine equipped with a bottoming Rankine cycle as a waste heat recovery system. Part 2: Evaluation of alternative solutions"
in: *Applied Thermal Engineering* 36.1 (2012), pp. 279–287 (cit. on p. 16)

[42] **Teng, H., Regner, G., and Cowland, C.**
"Achieving High Engine Efficiency for Heavy-Duty Diesel Engines by Waste Heat Recovery Using Supercritical Organic-Fluid Rankine Cycle"
in: 724 (2010) (cit. on p. 16)

[43] **Ringler, J., Seifert, M., Guyotot, V., and Hübner, W.**
"Rankine Cycle for Waste Heat Recovery of IC Engines"
in: *SAE International* 2.1 (2012), pp. 67–76 (cit. on p. 16)

[44] **He, M., Zhang, X., Zeng, K., and Gao, K.**
"A combined thermodynamic cycle used for waste heat recovery of internal combustion engine"
in: *Energy* 36.12 (2011), pp. 6821–6829. ISSN: 03605442. DOI: 10.1016/j.energy.2011.10.014. URL: http://linkinghub.elsevier.com/retrieve/pii/S0360544211006736 (cit. on p. 16)

[45] **El Chammas, R., Clodic, D., and Chammas, R. E.**
"Combined Cycle for Hybrid Vehicles"
English. In: *SAE International* 1.724 (2005), pp. 1–10. ISSN: 0148-7191. DOI: 10.4271/2005-01-1171. URL: http://papers.sae.org/2005-01-1171/ (cit. on p. 16)

[46] **Morgan, D., Patel, P., Doyle, E., Raymond, R., Sakhuja, R., and Barber, K.**
"Laboratory test results low emission rankine-cycle engine with organic-based working fluid and reciprocating expander for automobiles"
in: *Proceedings of the 8th Intersociety energy conversion engineering conference*. Philadelphia, PA, USA 1973 (cit. on p. 17)

[47] **Chen, H., Goswami, D. Y., and Stefanakos, E. K.**
"A review of thermodynamic cycles and working fluids for the conversion of low-grade heat"
in: *Renewable and Sustainable Energy Reviews* 14.9 (2010), pp. 3059–3067. ISSN: 13640321. DOI: 10.1016/j.rser.2010.07.006. URL: http://dx.doi.org/10.1016/j.rser.2010.07.006 (cit. on p. 17)

[48] **Colonna, P., Casati, E., Trapp, C., Mathijssen, T., Larjola, J., Turunen-Saaresti, T., and Uusitalo, A.**
"Organic Rankine Cycle Power Systems: From the Concept to Current Technology, Applications, and an Outlook to the Future"

in: *Journal of Engineering for Gas Turbines and Power* 137.10 (2015), p. 100801. ISSN: 0742-4795. DOI: 10.1115/1.4029884. URL: http://gasturbinespower.asmedigitalcollection.asme.org/article.aspx?doi=10.1115/1.4029884 (cit. on p. 18)

[49] **Tchanche, B. F., Lambrinos, G., Frangoudakis, A., and Papadakis, G.**
"Low-grade heat conversion into power using organic Rankine cycles - A review of various applications"
in: *Renewable and Sustainable Energy Reviews* 15.8 (2011), pp. 3963–3979. ISSN: 13640321. DOI: 10.1016/j.rser.2011.07.024. URL: http://dx.doi.org/10.1016/j.rser.2011.07.024 (cit. on p. 18)

[50] **Brock, W. J., Calm, J. M., and Richard, R. G.**
Designation and Safety Classifications of Refrigerants
2000, pp. 1–15 (cit. on p. 19)

[51] **Rand, I.**
"Considerations for Next Generation HVAC Refrigerants"
in: *Engineers Newsletter* (2015), pp. 1–4 (cit. on p. 19)

[52] **Comission, E.**
The Montreal Protocol
tech. rep. 2005, p. 24. DOI: 10.1093/0199286094.003.0008. URL: http://www.oxfordscholarship.com/view/10.1093/0199286094.001.0001/acprof-9780199286096 (cit. on pp. 19, 21)

[53] **Comission, E.**
Proposal for a Regulation on fluorinated greenhouse gases
tech. rep. 2012, p. 45 (cit. on pp. 19, 21)

[54] **Quoilin, S., Broek, M. V. D., Declaye, S., Dewallef, P., and Lemort, V.**
"Techno-economic survey of Organic Rankine Cycle (ORC) systems"
in: *Renewable and Sustainable Energy Reviews* 22 (2013), pp. 168–186. ISSN: 13640321. DOI: 10.1016/j.rser.2013.01.028. URL: http://linkinghub.elsevier.com/retrieve/pii/S1364032113000592 (cit. on p. 21)

[55] **Pearson, A.**
"Refrigeration with ammonia"
in: *International Journal of Refrigeration* 31.4 (2008), pp. 545–551. ISSN: 01407007. DOI: 10.1016/j.ijrefrig.2007.11.011 (cit. on p. 21)

[56] **Boccardi, G., Calabrese, N., Celata, G. P., Mastrullo, R., Mauro, A. W., Perrone, A., and Trinchieri, R.**
"Experimental performance evaluation for a carbon dioxide light commercial cooling application under transcritical and subcritical conditions"
in: *Applied Thermal Engineering* 54.2 (2013), pp. 528–535. ISSN: 13594311. DOI: 10.1016/j.applthermaleng.2013.02.026. URL: http://dx.doi.org/10.1016/j.applthermaleng.2013.02.026 (cit. on p. 21)

[57] **Ziviani, D. and Beyene, A.**
"Advances and challenges in ORC systems modeling for low grade thermal energy recovery"
in: *Applied Energy* 121 (2014), pp. 79–95 (cit. on p. 21)

[58] **Dai, Y., Wang, J., and Gao, L.**
"Parametric optimization and comparative study of organic Rankine cycle (ORC) for low grade waste heat recovery"
in: *Energy Conversion and Management* 50.3 (2009), pp. 576–582. ISSN: 01968904. DOI: 10.1016/j.enconman.2008.10.018. URL: http://linkinghub.elsevier.com/retrieve/pii/S0196890408004342 (cit. on p. 21)

[59] **Saleh, B., Koglbauer, G., Wendland, M., and Fischer, J.**
"Working fluids for low-temperature organic Rankine cycles"
in: *Energy* 32.7 (2007), pp. 1210–1221. ISSN: 03605442. DOI: 10.1016/j.energy.2006.07.001. URL: http://linkinghub.elsevier.com/retrieve/pii/S0360544206001812 (cit. on p. 21)

[60] **Tian, H., Shu, G., Wei, H., Liang, X., and Liu, L.**
"Fluids and parameters optimization for the organic Rankine cycles (ORCs) used in exhaust heat recovery of Internal Combustion Engine (ICE)"
in: *Energy* 47.1 (2012), pp. 125–136. ISSN: 03605442. DOI: 10.1016/j.energy.2012.09.021. URL: http://linkinghub.elsevier.com/retrieve/pii/S0360544212006998 (cit. on p. 21)

[61] **Wang, E. H., Zhang, H. G., Zhao, Y., Fan, B. Y., Wu, Y. T., and Mu, Q. H.**
"Performance analysis of a novel system combining a dual loop organic Rankine cycle (ORC) with a gasoline engine"
in: *Energy* 43.1 (2012), pp. 385–395. ISSN: 03605442. DOI: 10.1016/j.energy.2012.04.006 (cit. on p. 21)

[62] **Eyerer, S., Wieland, C., Vandersickel, A., and Spliethoff, H.**
"Experimental study of an ORC (Organic Rankine Cycle) and analysis of R1233zd-E as a drop-in replacement for R245fa for low temperature heat utilization"

in: *Energy* 103 (2016), pp. 660–671. ISSN: 03605442. DOI: 10.1016/j.energy.2016.03.034. URL: http://linkinghub.elsevier.com/retrieve/pii/S036054421630278X (cit. on p. 21)

[63] **Mota-Babiloni, A., Navarro-Esbrí, J., Molés, F., Cervera, Á. B., Peris, B., and Verdú, G.**
"A review of refrigerant R1234ze(E) recent investigations"
in: *Applied Thermal Engineering* 95 (2016), pp. 211–222. ISSN: 13594311. DOI: 10.1016/j.applthermaleng.2015.09.055. URL: http://linkinghub.elsevier.com/retrieve/pii/S1359431115009758 (cit. on p. 21)

[64] **Juhasz, J. R. and Simoni, L. D.**
"A Review of Potential Working Fluids for Low Temperature Organic Rankine Cycles in Waste Heat Recovery"
in: *3rd International Seminar on ORC Power Systems* 2015, pp. 1–10 (cit. on p. 21)

[65] **Fernández, F. J., Prieto, M. M., and Suárez, I.**
"Thermodynamic analysis of high-temperature regenerative organic Rankine cycles using siloxanes as working fluids"
in: *Energy* 36.8 (2011), pp. 5239–5249. ISSN: 03605442. DOI: 10.1016/j.energy.2011.06.028. URL: http://dx.doi.org/10.1016/j.energy.2011.06.028 (cit. on p. 22)

[66] **Colonna, P., Nannan, N. R., Guardone, A., and Lemmon, E. W.**
"Multiparameter equations of state for selected siloxanes"
in: *Fluid Phase Equilibria* 244.2 (2006), pp. 193–211. ISSN: 03783812. DOI: 10.1016/j.fluid.2006.04.015 (cit. on p. 22)

[67] **Preißinger, M. and Brüggemann, D.**
"Thermal stability of hexamethyldisiloxane (MM) for high-temperature Organic Rankine Cycle (ORC)"
in: *Energies* 9.3 (2016). ISSN: 19961073. DOI: 10.3390/en9030183 (cit. on p. 22)

[68] **Song, J. and Gu, C. W.**
"Analysis of ORC (Organic Rankine Cycle) systems with pure hydrocarbons and mixtures of hydrocarbon and retardant for engine waste heat recovery"
in: *Applied Thermal Engineering* 89 (2015), pp. 693–702. ISSN: 13594311. DOI: 10.1016/j.applthermaleng.2015.06.055. URL: http://dx.doi.org/10.1016/j.applthermaleng.2015.06.055 (cit. on p. 22)

[69] **Seher, D., Lengenfelder, T., Gerhardt, J., Eisenmenger, N., Hackner, M., and Krinn, I.**
"Waste Heat Recovery for Commercial Vehicles with a Rankine Process"
in: *21 st Aachen Colloquium Automobile and Engine Technology* 2012, pp. 1–15 (cit. on pp. 22, 28)

[70] **Howell, T. and Gibble, J.**
"Development of an ORC system to improve HD truck fuel efficiency"
in: *Deer Conference*. Vol. 1 2011, pp. 1–21 (cit. on p. 22)

[71] **Zhang, Y.-Q., Wu, Y.-T., Xia, G.-D., Ma, C.-F., Ji, W.-N., Liu, S.-W., Yang, K., and Yang, F.-B.**
"Development and experimental study on organic Rankine cycle system with single-screw expander for waste heat recovery from exhaust of diesel engine"
in: *Energy* 77.0 (2014), pp. 499–508. ISSN: 03605442. DOI: http://dx.doi.org/10.1016/j.energy.2014.09.034. URL: http://www.sciencedirect.com/science/article/pii/S0360544214010901 (cit. on pp. 22, 28)

[72] **Latz, G., Andersson, S., and Munch, K.**
"Comparison of Working Fluids in Both Subcritical and Supercritical Rankine Cycles for Waste-Heat Recovery Systems in Heavy-Duty Vehicles"
in: *SAE International* 1 (2012), pp. 1–18. DOI: 10.4271/2012-01-1200. URL: http://www.sae.org/technical/papers/2012-01-1200 (cit. on p. 22)

[73] **Shu, G., Liu, L., Tian, H., Wei, H., and Yu, G.**
"Parametric and working fluid analysis of a dual-loop organic Rankine cycle (DORC) used in engine waste heat recovery"
in: *Applied Energy* 113 (2014), pp. 1188–1198. ISSN: 03062619. DOI: 10.1016/j.apenergy.2013.08.027. URL: http://linkinghub.elsevier.com/retrieve/pii/S0306261913006624 (cit. on p. 22)

[74] **Zhao, L. and Bao, J.**
"The influence of composition shift on organic Rankine cycle (ORC) with zeotropic mixtures"
in: *Energy Conversion and Management* 83 (2014), pp. 203–211. ISSN: 01968904. DOI: 10.1016/j.enconman.2014.03.072. URL: http://linkinghub.elsevier.com/retrieve/pii/S0196890414002830 (cit. on p. 22)

[75] **Teng, H., Regner, G., and Cowland, C.**
"Waste Heat Recovery of Heavy-Duty Diesel Engines by Organic Rankine

Cycle Part II : Working Fluids for WHR-ORC"
in: *SAE Technical Paper* 724 (2012), pp. 1–12 (cit. on p. 22)

[76] **Teng, H., Regner, G., and Cowland, C.**
"Waste Heat Recovery of Heavy-Duty Diesel Engines by Organic Rankine Cycle Part I: Hybrid Energy System of Diesel and Rankine Engines"
English. In: *SAE International* 1.724 (2007), pp. 1–13. DOI: 10.4271/2007-01-0537. URL: http://papers.sae.org/2007-01-0537/
(cit. on pp. 22, 25)

[77] **Shu, G., Liu, L., Tian, H., Wei, H., and Xu, X.**
"Performance comparison and working fluid analysis of subcritical and transcritical dual-loop organic Rankine cycle (DORC) used in engine waste heat recovery"
in: *Energy Conversion and Management* 74 (2013), pp. 35–43. ISSN: 01968904. DOI: 10.1016/j.enconman.2013.04.037. URL: http://linkinghub.elsevier.com/retrieve/pii/S0196890413002343
(cit. on p. 22)

[78] **Wang, T., Zhang, Y., Peng, Z., and Shu, G.**
"A review of researches on thermal exhaust heat recovery with Rankine cycle"
in: *Renewable and Sustainable Energy Reviews* 15.6 (2011), pp. 2862–2871. ISSN: 13640321. DOI: 10.1016/j.rser.2011.03.015. URL: http://linkinghub.elsevier.com/retrieve/pii/S1364032111001158
(cit. on p. 23)

[79] **Bao, J. and Zhao, L.**
"A review of working fluid and expander selections for organic Rankine cycle"
in: *Renewable and Sustainable Energy Reviews* 24 (2013), pp. 325–342. ISSN: 13640321. DOI: 10.1016/j.rser.2013.03.040. URL: http://linkinghub.elsevier.com/retrieve/pii/S1364032113001998
(cit. on p. 24)

[80] **Quoilin, S. and Sart-tilman, C.**
"Expansion Machine and Fluid Selection for the Organic Rankine Cycle"
in: *7th International Conference on Heat Transfer, Fluid Mechanics and Thermodynamics*. July 2010, pp. 1–7 (cit. on p. 24)

[81] **Latz, G., Andersson, S., and Munch, K.**
"Selecting an Expansion Machine for Vehicle Waste-Heat Recovery Systems Based on the Rankine Cycle"
in: *SAE International* 1 (2013), pp. 1–15. DOI: 10.4271/2013-01-0552. URL: http://www.sae.org/technical/papers/2013-01-0552
(cit. on p. 24)

[82] **Declaye, S., Quoilin, S., Guillaume, L., and Lemort, V.**
"Experimental study on an open-drive scroll expander integrated into an ORC (Organic Rankine Cycle) system with R245fa as working fluid"
in: *Energy* 55 (2013), pp. 173–183. ISSN: 03605442. DOI: 10.1016/j.energy.2013.04.003. URL: http://linkinghub.elsevier.com/retrieve/pii/S0360544213003034 (cit. on pp. 24, 81)

[83] **Legros, A., Guillaume, L., Lemort, V., Diny, M., Bell, I., and Quoilin, S.**
"Investigation on a scroll expander for waste heat recovery on internal combustion engines"
in: *International conference on compressors and their systems* 1 (2013), p. 10 (cit. on p. 24)

[84] **Quoilin, S., Lemort, V., and Lebrun, J.**
"Experimental study and modeling of an Organic Rankine Cycle using scroll expander"
in: *Applied Energy* 87.4 (2010), pp. 1260–1268. ISSN: 03062619. DOI: 10.1016/j.apenergy.2009.06.026. URL: http://linkinghub.elsevier.com/retrieve/pii/S030626190900258X (cit. on p. 24)

[85] **Lemort, V., Declaye, S., and Quoilin, S.**
"Experimental characterization of a hermetic scroll expander for use in a micro-scale Rankine cycle"
in: *Proceedings of the Institution of Mechanical Engineers, Part A: Journal of Power and Energy* 226.1 (2011), pp. 126–136. ISSN: 0957-6509. DOI: 10.1177/0957650911413840. URL: http://pia.sagepub.com/lookup/doi/10.1177/0957650911413840 (cit. on p. 24)

[86] **Aoun, B. and Clodic, D. F.**
"Theoretical and Experimental Study of an Oil-Free Scroll Vapor Expander"
in: *International Compressor Engineering Conference* (2008), p. 1925. DOI: http://docs.lib.purdue.edu/icec/1925 (cit. on p. 24)

[87] **Lemort, V., Quoilin, S., Cuevas, C., and Lebrun, J.**
"Testing and modeling a scroll expander integrated into an Organic Rankine Cycle"
in: *Applied Thermal Engineering* 29.14-15 (2009), pp. 3094–3102. ISSN: 13594311. DOI: 10.1016/j.applthermaleng.2009.04.013. URL: http://linkinghub.elsevier.com/retrieve/pii/S1359431109001173 (cit. on p. 24)

[88] **Lopes, J., Douglas, R., McCullough, G., O'Shaughnessy, R., Hanna, A., Rouaud, C., and Seaman, R.**
"Review of Rankine Cycle Systems Components for Hybrid Engines Waste

Heat Recovery"
in: *SAE International* 1 (2012), pp. 1–14. DOI: 10.4271/2012-01-1942. URL: http://www.sae.org/technical/papers/2012-01-1942 (cit. on p. 25)

[89] **Santos, H., Pinheiro, S., and Costa, M.**
"Expander Selection for Internal Combustion Engines Bottoming with steam and Organic Rankine Cycle"
in: 1 (2012), pp. 1–12 (cit. on p. 25)

[90] **Glavatskaya, Y., Podevin, P., Lemort, V., Shonda, O., and Descombes, G.**
"Reciprocating Expander for an Exhaust Heat Recovery Rankine Cycle for a Passenger Car Application"
in: *Energies* 5.12 (2012), pp. 1751–1765. ISSN: 1996-1073. DOI: 10.3390/en5061751. URL: http://www.mdpi.com/1996-1073/5/6/1751/ (cit. on p. 25)

[91] **Kunte, H. and Seume, J.**
"Partial Admission Impulse Turbine for Automotive ORC Application"
in: *SAE Technical Papers* 6 (2013). DOI: 10.4271/2013-24-0092. URL: http://www.scopus.com/inward/record.url?eid=2-s2.0-84890407668{\&}partnerID=tZOtx3y1 (cit. on pp. 25, 152)

[92] **Sauret, E. and Rowlands, A. S.**
"Candidate radial-inflow turbines and high-density working fluids for geothermal power systems"
in: *Energy* 36.7 (2011), pp. 4460–4467. ISSN: 03605442. DOI: 10.1016/j.energy.2011.03.076. URL: http://dx.doi.org/10.1016/j.energy.2011.03.076 (cit. on p. 25)

[93] **Ambros, P.**
"Twin-Round-Tube Evaporator for Waste Heat Recovery"
in: *MTZ* 4 (2014), pp. 44–49 (cit. on p. 27)

[94] **Haller, R., Nicolas, B., Hammi, S., Taklanti, A., and Glavatskaya, Y.**
"Comparison of High and Low Temperature Working Fluids for Automotive Rankine Waste Heat Recovery Systems"
in: (2014), pp. 1–9 (cit. on p. 27)

[95] **Töpfer, T., Dingel, O., Friedrich, I., and Seebode, J.**
"Use of Route Information for Predictive ORC Control"
in: *MTZ* (2015), pp. 14–17 (cit. on p. 27)

[96] **Oomori, H. and Ogino, S.**
"Waste Heat Recovery of Passenger Car Using a Combination of Rankine Bottoming Cycle and Evaporative Engine Cooling System"
in: *SAE International* 930880 (1993). DOI: 10.4271/930880. URL: http://papers.sae.org/930880/ (cit. on p. 28)

[97] **Kosmadakis, G., Manolakos, D., and Papadakis, G.**
"Experimental investigation of a low-temperature organic Rankine cycle (ORC) engine under variable heat input operating at both subcritical and supercritical conditions"
in: *Applied Thermal Engineering* 92 (2016), pp. 1–7. ISSN: 1359-4311. DOI: 10.1016/j.applthermaleng.2015.09.082. URL: http://www.sciencedirect.com/science/article/pii/S1359431115010078$\backslash$nhttp://www.sciencedirect.com/science/article/pii/S1359431115010078/pdfft?md5=07e1aaf4e5a0479ffff5611536d75123{\&}pid=1-s2.0-S1359431115010078-main.pdf (cit. on p. 28)

[98] **Freymann, R.**
"The Turbosteamer : A System Introducing the Principle of Cogeneration in Automotive Applications"
in: *MTZ* 69.5 (2008), pp. 20–27 (cit. on p. 28)

[99] **Endo, T., Kawajiri, S., Kojima, Y., Takahashi, K., Baba, T., Ibaraki, S., Takahashi, T., and Shinohara, M.**
"Study on Maximizing Exergy in Automotive Engines"
in: *SAE International* 1 (2007), pp. 1–12 (cit. on pp. 28, 78)

[100] **Daccord, R., Darmedru, A., and Melis, J.**
"Oil-free axial piston expander for waste heat recovery"
English. In: *SAE International* 1 (2014), pp. 1–12. ISSN: 0148-7191. DOI: 10.4271/2014-01-0675.Copyright. URL: http://papers.sae.org/2014-01-0675/ (cit. on pp. 28, 214)

[101] **Latz, G., Erlandsson, O., Skåre, T., and Contet, A.**
"Water-based Rankine-cycle waste heat recovery systems for engines: challenges and opportunities"
in: *Asme Orc 2015* 2013 (2015), pp. 1–10 (cit. on p. 28)

[102] **Freyman, R., Ringler, J., Seifert, M., and Horst, T.**
"The Second Generation T urbosteamer"
in: *MTZ* 73 (2012), pp. 18–23 (cit. on p. 28)

[103] **Cipollone, R., Di Battista, D., Perosino, A., and Bettoja, F.**
"Waste Heat Recovery by an Organic Rankine Cycle for Heavy Duty Vehicles"
in: *SAE International* 234 (2016), pp. 1–9. DOI: 10.4271/2016-01-0234. URL: http://papers.sae.org/2016-01-0234/ (cit. on p. 28)

[104] **Park, T., Teng, H., Hunter, G. L., Velde, B. van der, and Klaver, J.**
"A Rankine Cycle System for Recovering Waste Heat from HD Diesel Engines - Experimental Results"
in: *SAE International* 1 (2011), pp. 1–9. DOI: 10.4271/2011-01-1337. URL: http://papers.sae.org/2011-01-1337/ (cit. on p. 28)

[105] **Guillaume, L., Legros, A., Desideri, A., and Lemort, V.**
"Performance of a radial-inflow turbine integrated in an ORC system and designed for a WHR on truck application: An experimental comparison between R245fa and R1233zd"
in: *Applied Energy* (2016). ISSN: 03062619. DOI: 10.1016/j.apenergy.2016.03.012. URL: http://linkinghub.elsevier.com/retrieve/pii/S0306261916303233 (cit. on p. 28)

[106] **Neukirchner, H., Semper, T., Lüderitz, D., and Dingel, O.**
"Symbiosis of Energy Recovery and Downsizing"
in: *MTZ* 75.Innovative Engine Systems (2014), pp. 4–9 (cit. on p. 46)

[107] **Moran, M. J., Shapiro, H. N., Boettner, D. D., and Bailey, M.**
Fundamentals of Engineering Thermodynamics
John Wiley & Sons 2010, p. 944. ISBN: 0470495901. URL: http://books.google.com/books?id=oyt8iW6B4aUC{\&}pgis=1 (cit. on p. 65)

[108] **Lapuerta, M, Armas, O, and Herna, J. J.**
"Diagnosis of DI Diesel combustion from in-cylinder pressure signal by estimation of mean thermodynamic properties of the gas"
in: *Applied Thermal Engineering* 19 (1999), pp. 513–529
(cit. on p. 65)

[109] **Taylor, B. N. and Kuyatt, C. E. K.**
"Guidelines for Evaluating and Expressing the Uncertainty of NIST Measurement Results"
in: *NIST Technical Note 1297* 1 (1994), p. 20 (cit. on p. 77)

[110] **Shah, M.**
"A General Correlation for Heat Transfer During Film Condensation inside Pipes"
in: *International Journal of Heat and Mass Transfer* 22 (1979), pp. 547–556. ISSN: 00179310. DOI: 10.1016/0017-9310(79)90058-9
(cit. on p. 110)

[111] **Steiner, D. and Taborek, J.**
"Flow Boiling Heat Transfer in Vertical Tubes Correlated by an Asymptotic Model"
in: *Heat transfer engineering* 13 (2010), pp. 322–329. URL: http://65.54.113.26/Publication/3107655/flow-boiling-heat-transfer-

in-vertical-tubes-correlated-by-an-asymptotic-model
(cit. on p. 110)

[112] **Richardson, E. S.**
"Thermodynamic performance of new thermofluidic feed pumps for Organic Rankine Cycle applications"
in: *Applied Energy* 161 (2016), pp. 75–84. ISSN: 03062619. DOI: 10.1016/j.apenergy.2015.10.004. URL: http://dx.doi.org/10.1016/j.apenergy.2015.10.004 (cit. on pp. 112, 178)

[113] **Churchill, S.**
"Friction-factor equation spans all fluid flow regimes"
in: *Chem. Eng.* (1977), pp. 91–92 (cit. on p. 112)

[114] **McAdams, W.H., Woods, W.K., and Bryan, R.**
"Vaporization inside horizontal tubes -II- Benzene-oil mixtures"
in: *Trans. ASME* 64 (1942), p. 193 (cit. on p. 112)

[115] **Quoilin, S.**
"Sustainable energy conversion through the use of Organic Rankine Cycles for waste heat recovery and solar applications"
PhD thesis 2011, pp. 1–183. ISBN: 0-7803-3213-X. arXiv: 9605103 [cs]. URL: http://orbi.ulg.ac.be/handle/2268/96436 (cit. on p. 120)

[116] **Tsatsaronis, G. and Morosuk, T.**
"A general exergy-based method for combining a cost analysis with an environmental impact analysis. Part I – Theoretical Development"
in: *Asme Imece2008-67218* (2008), p. 10 (cit. on pp. 137, 150)

[117] **Ehyaei, M., Ahmadi, P., Atabi, F., Heibati, M., and Khorshidvand, M.**
"Feasibility study of applying internal combustion engines in residential buildings by exergy, economic and environmental analysis"
in: *Energy and Buildings* 55 (2012), pp. 405–413. ISSN: 03787788. DOI: 10.1016/j.enbuild.2012.09.002. URL: http://linkinghub.elsevier.com/retrieve/pii/S0378778812004501 (cit. on p. 137)

[118] **Özkan, M., Özkan, D. B., Özener, O., and Yılmaz, H.**
"Experimental study on energy and exergy analyses of a diesel engine performed with multiple injection strategies: Effect of pre-injection timing"
in: *Applied Thermal Engineering* 53.1 (2013), pp. 21–30. ISSN: 13594311. DOI: 10.1016/j.applthermaleng.2012.12.034. URL: http://www.sciencedirect.com/science/article/pii/S1359431113000082
(cit. on p. 137)

[119] **Li, Y.-R., Wang, J.-N., and Du, M.-T.**
"Influence of coupled pinch point temperature difference and evaporation temperature on performance of organic Rankine cycle"
in: *Energy* 42.1 (2012), pp. 503–509. ISSN: 03605442. DOI: 10.1016/j.energy.2012.03.018. URL: http://linkinghub.elsevier.com/retrieve/pii/S0360544212002095 (cit. on pp. 140, 152)

[120] **Kelly, S., Tsatsaronis, G., and Morosuk, T.**
"Advanced exergetic analysis: Approaches for splitting the exergy destruction into endogenous and exogenous parts"
in: *Energy* 34.3 (2009), pp. 384–391. ISSN: 03605442. DOI: 10.1016/j.energy.2008.12.007. URL: http://linkinghub.elsevier.com/retrieve/pii/S036054420800323X (cit. on p. 148)

[121] **Wang, L., Yang, Y., Morosuk, T., and Tsatsaronis, G.**
"Advanced thermodynamic analysis and evaluation of a supercritical power plant"
in: *Energies* 5.6 (2012), pp. 1850–1863. ISSN: 19961073. DOI: 10.3390/en5061850 (cit. on p. 151)

[122] **Tsatsaronis, G. and Park, M.**
"On avoidable and unavoidable exergy destructions and investment costs in thermal systems"
in: *Energy Conversion and Management* 43.9-12 (2002), pp. 1259–1270. ISSN: 01968904. DOI: 10.1016/S0196-8904(02)00012-2 (cit. on p. 151)

[123] **Keçebaş, A. and Gökgedik, H.**
"Thermodynamic evaluation of a geothermal power plant for advanced exergy analysis"
in: *Energy* 88 (2015), pp. 746–755. ISSN: 03605442. DOI: 10.1016/j.energy.2015.05.094 (cit. on p. 152)

[124] **Panesar, A. S., Morgan, R. E., Miché, N. D. D., and Heikal, M. R.**
"Working fluid selection for a subcritical bottoming cycle applied to a high exhaust gas recirculation engine"
in: *Energy* 60 (2013), pp. 388–400. ISSN: 03605442. DOI: 10.1016/j.energy.2013.08.015. URL: http://dx.doi.org/10.1016/j.energy.2013.08.015 (cit. on p. 156)

[125] **Morosuk, T. and Tsatsaronis, G.**
"Strengths and Limitations of Advanced Exergetic Analyses"
in: *Volume 6B: Energy* November (2013), V06BT07A026. DOI: 10.1115/IMECE2013-64320. URL: http://proceedings.asmedigitalcollection.asme.org/proceeding.aspx?doi=10.1115/IMECE2013-64320 (cit. on p. 158)

[126] **Thonon, B., Vidil, R., and Marvillet, C.**
"Recent Research and Developments in Plate Heat Exchangers"
English. In: *Journal of Enhanced Heat Transfer* 2.1-2 (1995), pp. 149–155. ISSN: 1065-5131. DOI: 10.1615/JEnhHeatTransf.v2.i1-2.160. URL: http://www.dl.begellhouse.com/journals/4c8f5faa331b09ea,3ad0afe360a3d751,5fffa7650c786752.html (cit. on p. 175)

[127] **Quoilin, S., Declaye, S., Tchanche, B. F., and Lemort, V.**
"Thermo-economic optimization of waste heat recovery Organic Rankine Cycles"
in: *Applied Thermal Engineering* 31.14-15 (2011), pp. 2885–2893. ISSN: 13594311. DOI: 10.1016/j.applthermaleng.2011.05.014. URL: http://dx.doi.org/10.1016/j.applthermaleng.2011.05.014 (cit. on pp. 175, 178, 179)

[128] **Lecompte, S., Huisseune, H., Broek, M. van den, De Schampheleire, S., and De Paepe, M.**
"Part load based thermo-economic optimization of the Organic Rankine Cycle (ORC) applied to a combined heat and power (CHP) system"
in: *Applied Energy* 111 (2013), pp. 871–881. ISSN: 03062619. DOI: 10.1016/j.apenergy.2013.06.043. URL: http://linkinghub.elsevier.com/retrieve/pii/S0306261913005503 (cit. on p. 175)

[129] **Chen, J. C.**
"Correlation for boiling heat transfer to saturated fluids in convective flow"
in: *Industrial & Engineering Chemistry Process Design and development* 5.3 (1966), pp. 322–329. ISSN: 01964305. DOI: 10.1021/i260019a023. URL: http://pubs.acs.org/doi/pdf/10.1021/i260019a023$\backslash$npapers3://publication/uuid/1ABFD2F3-EA32-4B69-BE88-0A22F931A08C (cit. on p. 175)

[130] **Lockhart, R.W., Martinelli, R.**
"Proposed Correlation of Data for Isothermal Two-Phase Two-Component Flow in Pipes"
in: *Chemical Engineering Progress* 45 (1949), pp. 39–48 (cit. on p. 175)

[131] **Hsieh, Y. and Lin, T.**
"Saturated flow boiling heat transfer and pressure drop of refrigerant R-410A in a vertical plate heat exchanger"
in: *International Journal of Heat and Mass Transfer* 45.5 (2002), pp. 1033–1044. ISSN: 00179310. DOI: 10.1016/S0017-9310(01)00219-8. URL: http://www.sciencedirect.com/science/article/pii/S0017931001002198 (cit. on p. 176)

[132] **Kuo, W. S., Lie, Y. M., Hsieh, Y. Y., and Lin, T. F.**
"Condensation heat transfer and pressure drop of refrigerant R-410A flow in a vertical plate heat exchanger"
in: *International Journal of Heat and Mass Transfer* 48.25-26 (2005), pp. 5205–5220. ISSN: 00179310. DOI: 10.1016/j.ijheatmasstransfer.2005.07.023 (cit. on p. 176)

[133] **García-Cascales, J. R., Vera-García, F., Corberán-Salvador, J. M., and Gonzálvez-Maciá, J.**
"Assessment of boiling and condensation heat transfer correlations in the modelling of plate heat exchangers"
in: *International Journal of Refrigeration* 30.6 (2007), pp. 1029–1041. ISSN: 01407007. DOI: 10.1016/j.ijrefrig.2007.01.004 (cit. on p. 176)

[134] **Maraver, D., Royo, J., Lemort, V., and Quoilin, S.**
"Systematic optimization of subcritical and transcritical organic Rankine cycles (ORCs) constrained by technical parameters in multiple applications"
in: *Applied Energy* 117 (2014), pp. 11–29. ISSN: 03062619. DOI: 10.1016/j.apenergy.2013.11.076. URL: http://dx.doi.org/10.1016/j.apenergy.2013.11.076 (cit. on p. 177)

[135] **Lecompte, S., Lemmens, S., Huisseune, H., Van Den Broek, M., and De Paepe, M.**
"Multi-objective thermo-economic optimization strategy for ORCs applied to subcritical and transcritical cycles for waste heat recovery"
in: *Energies* 8.4 (2015), pp. 2714–2741. ISSN: 19961073. DOI: 10.3390/en8042714 (cit. on p. 179)

[136] **Heberle, F. and Brüggemann, D.**
"Thermo-economic analysis of zeotropic mixtures and pure working fluids in organic rankine cycles for waste heat recovery"
in: *3rd International Seminar on ORC Power Systems* 53 (2013), pp. 1689–1699. ISSN: 1098-6596. DOI: 10.1017/CBO9781107415324.004. arXiv: arXiv:1011.1669v3 (cit. on p. 181)

[137] **Holland, J. H.**
Adaptation in natural and artificial systems: An introductory analysis with applications to biology, control, and artificial intelligence.
Masachusetts: MIT Press 1992 (cit. on p. 185)

[138] **Poloni, C.**
"Hybrid GA for multi objective aerodynamic shape optimization"
in: *Genetic algorithms in engineering and computer science* 33 (1995), pp. 397–415 (cit. on p. 185)

[139] **Ferreira, J. C., Fonseca, C. M., and Gaspar-Cunha, A**
"Methodology to select solutions from the pareto-optimal set: A comparative study"
in: *Proceedings of GECCO 2007: Genetic and Evolutionary Computation Conference* (2007), pp. 789–796. DOI: 10.1145/1276958.1277117. URL: http://www.scopus.com/inward/record.url?eid=2-s2.0-34548064369{\&}partnerID=40{\&}md5=54135b3d61ca8d41d13c67384fd5ff92 (cit. on p. 187)

[140] **Yue, Z.**
"A method for group decision-making based on determining weights of decision makers using TOPSIS"
in: *Applied Mathematical Modelling* 35.4 (2011), pp. 1926–1936. ISSN: 0307904X. DOI: 10.1016/j.apm.2010.11.001. URL: http://dx.doi.org/10.1016/j.apm.2010.11.001 (cit. on p. 187)

[141] **Wang, X.-Q., Li, X.-P., Li, Y.-R., and Wu, C.-M.**
"Payback period estimation and parameter optimization of subcritical organic Rankine cycle system for waste heat recovery"
in: *Energy* 88 (2015), pp. 734–745. ISSN: 03605442. DOI: 10.1016/j.energy.2015.05.095. URL: http://www.sciencedirect.com/science/article/pii/S0360544215006970 (cit. on p. 189)

[142] **Energy, U.**
"Waste Heat Recovery: Technology Opportunities in the US Industry"
in: *Waste Heat Recovery: Technology Opportunities in the US Industry* (2008), pp. 1–112. URL: http://www1.eere.energy.gov/manufacturing/intensiveprocesses/pdfs/waste{_}heat{_}recovery.pdf (cit. on p. 191)

[143] **Koffler, C. and Rohde-Brandenburger, K.**
"On the calculation of fuel savings through lightweight design in automotive life cycle assessments"
in: *International Journal of Life Cycle Assessment* 15.1 (2010), pp. 128–135. ISSN: 09483349. DOI: 10.1007/s11367-009-0127-z (cit. on p. 194)

[144] **Payri, F., Guardiola, C., Pla, B., and Blanco-Rodriguez, D.**
"A stochastic method for the energy management in hybrid electric vehicles"
in: *Control Engineering Practice* 29 (2014), pp. 257–265. ISSN: 09670661. DOI: 10.1016/j.conengprac.2014.01.004. URL: http://dx.doi.org/10.1016/j.conengprac.2014.01.004 (cit. on p. 198)